University of Sheffield

Exploring striatal neuron and astrocyte dysfunction in amyotrophic lateral sclerosis and frontotemporal dementia using stem cell technology and patch-clamp electrophysiology

Iris-Stefania Pasniceanu

A thesis submitted in partial fulfilment of the requirements for the degree of Doctor of Philosophy

Division of Neuroscience
School of Medicine and Population Health
Faculty of Health
The University of Sheffield

Submission Date: April 2024

Acknowledgements

I would first like to thank my primary supervisor, Dr Matthew Livesey for his unwavering guidance, support and encouragement throughout my PhD journey. This opportunity of working on exciting projects has been invaluable. Thank you for sharing your passion and enthusiasm for science with me, for all your support and the countless things that I have learnt from you inside and outside of the lab!

Further, I would like to express my sincere gratitude to my secondary supervisors. Prof Laura Ferraiuolo, thank you for your insightful feedback, advice and great discussions. Dr Cleide Dos Santos Souza, I am grateful to have worked alongside such an amazing scientist and supportive friend!

Special thanks go to Emily, Mara and Kriti for their endless support and encouragement but even more for your friendship, spontaneous coffee breaks and long unplanned therapy sessions. I wish you all the best and never forget how great you are! Thank you to everyone at SITraN for making work more enjoyable. It's been a pleasure working with you all!

The biggest and most sincere thanks go to my dear Alex. Your endless support and encouragement have been a constant source of strength throughout this journey. Thank you for putting up with me, especially in the last few months. I couldn't have done this without you!

Special thanks to my parents and family. Dragă mama și tata, vă mulțumesc pentru ajutorul și suportul vostru necondiționat! Vă datorez vouă tot ce sunt eu astăzi și sper că v-am făcut mândri!

I would like to dedicate this thesis entirely to my grandpa, my biggest supporter, who sadly passed away in 2023. Thank you for teaching me patience and kindness.

IT ALWAYS SEEMS IMPOSSIBLE UNTIL IT'S DONE.

Nelson Mandela

Abstract

Amyotrophic lateral sclerosis (ALS) and frontotemporal dementia (FTD) are progressive neurodegenerative diseases, part of a spectrum with overlapping pathology, impacting multiple brain regions and non-neuronal cell types beyond the characteristic motor and cortical neuron degeneration.

The striatum, an important integrative hub in the brain crucial for functions often impaired in FTD (e.g. behavioural and cognitive regulation, speech and language defects), exhibits dysfunction in FTD/ALS patients. Electrophysiological analysis revealed the first evidence of impaired medium spiny neuron (MSN) function. *C9ORF72*^{RE} MSNs, harbouring the most common genetic mutation in FTD/ALS, displayed progressive hypoexcitability, abnormal action potential waveforms, impaired function of slow outwardly rectifying potassium (I_K) channels and a potential shift in axon initial segment (AIS) positioning. MSN dysfunction may disrupt communication in brain networks, potentially explaining cognitive and behavioural symptoms in FTD/ALS patients. Targeting the discovered I_K channel dysfunction and potential AIS changes offers promise for novel pharmaceutical intervention.

Astrocytes, essential for neuronal support, contribute to motor neuron death in ALS through a non-cell autonomous mechanism. The loss-of-protective-function and gain-of-toxic-feature are likely caused by dysfunctional astrocyte membrane properties. Electrophysiological characterisation of *C9ORF72*^{RE} astrocytes reveals membrane dysfunction due to connexin 43 (Cx43) dysregulation, mechanism which leads to astrocyte-mediated motor neuron toxicity, orchestrated in part by DPRs, and enhanced by environmental factors. This dysfunction expands to sporadic ALS, FTD and AD patients. Targeting astrocyte connexin dysfunction serves as a potential therapeutic target and biomarker for ALS and other neurodegenerative diseases.

Table of contents

ACKNOWLEDGEMENTS ERROR! BOOKMARK NOT DEFINED.

ABSTRACT VI

TABLE OF CONTENTS VII

LIST OF TABLES XII

LIST OF FIGURES XVI

DECLARATION XXIII

LIST OF PUBLICATION XXIII

CHAPTER 1: INTRODUCTION 1

1.1. INTRODUCTION TO AMYOTROPHIC LATERAL SCLEROSIS 1

1.2. INTRODUCTION TO FRONTOTEMPORAL DEMENTIA 2

1.3. OVERLAP BETWEEN CLINICAL FEATURES OF ALS AND FTD 3

1.4. GENETIC LANDSCAPE OF ALS AND FTD 4

1.4.1. SOD1 5

1.4.2. C9ORF72^{RE} 6

1.5. NEUROPATHOLOGICAL FEATURES OF ALS AND FTD 7

1.6. PATHOLOGY OF *C9ORF72*^{RE} ALS/FTD 8

1.7. MOLECULAR MECHANISMS BY WHICH *C9ORF72*^{RE} INDUCES NEURODEGENERATION IN ALS/FTD PATIENTS 9

1.7.1. C9ORF72 PROTEIN LOSS-OF-FUNCTION 9

1.7.2. RNA AGGREGATION AND GAIN-OF-FUNCTION 10

1.7.3. RAN TRANSLATION AND DPR TOXICITY 11

1.8. TDP-43 PATHOLOGY 13

1.9. ALS/FTD PATHOLOGICAL MECHANISMS 14

1.9.1. OXIDATIVE STRESS 14

1.9.2. MITOCHONDRIAL DYSFUNCTION 14

1.9.3. AXONAL TRANSPORT IMPAIRMENTS 15

1.9.4. Disrupted protein metabolism 15
1.9.5. Disrupted RNA metabolism 16
1.10. Neurophysiology of ALS/FTD 16
1.10.1. Cortical dysfunction in *C9ORF72*^{RE} ALS/FTD 17
1.10.2. Synaptic dysfunction in *C9ORF72*^{RE} ALS/FTD 18
1.10.3. Network and synaptic plasticity 18
1.10.4. Cortical hyperexcitability 20
1.10.5. Upper motor neuron hyperexcitability and morphological defects 22
1.10.6. Early cortical dysfunction and homeostatic adaptation in *C9ORF72*^{RE} ALS/FTD 22
1.10.7. Lower motor neuron dysfunction in *C9ORF72*^{RE} ALS/FTD 23
1.10.8. The loss of synaptic innervation from upper motor neurons to lower motor neurons 25
1.10.9. Changes in excitability in lower motor neurons 27
1.10.10. Impaired neurotransmitter release due to the neuromuscular junction in ALS 28
1.11. Multiple brain areas are impacted in FTD/ALS 29
1.11.1. The . has been greatly overlooked in FTD/ALS 30
1.11.2. Aims and hypothesis: 31
1.12. Astrocyte toxicity in ALS/FTD 32

2. CHAPTER 2: MATERIALS AND METHODS 35

2.1. Cell Culture Methods 35
2.2. Brief introduction to human stem cell technology 35
2.2.1. The use of iPSCs in neurodegenerative disease modelling 35
2.2.2. Brief introduction to direct reprogramming: induced neuronal progenitor cells (iNPCs) 38
2.2.3. iPSC lines maintenance 39
2.2.4. iPSC to NPC differentiation 41
2.2.5. NPC to medium spiny neuron (MSN) differentiation 44
2.2.6. NPC to motor neuron (MN) differentiation 47
2.2.7. Reagents and cultureware information relevant for the differentiation of iPSC-derived MNs and MSNs 51
2.2.8. Direct conversion of fibroblast to iNPC 52
2.2.9. Differentiation of iNPCs to iNPC-astrocytes (iAstrocytes) 54
2.2.10. SRSF1 lentivirus transduction 55
2.2.11. Reagents and cultureware information relevant for the generation of iAstrocytes 56
2.3. Fluorescence Assays 57

2.3.1. IMMUNOCYTOCHEMISTRY (ICC) 57
2.3.2. IMAGING 59
2.3.3. ANALYSIS 59
2.4. WHOLE-CELL PATCH-CLAMP ELECTROPHYSIOLOGY 60
2.4.1. PATCH-CLAMP TECHNIQUE: A HISTORICAL PERSPECTIVE 60
2.4.2. PATCH-CLAMP CONFIGURATIONS 60
2.4.3. THE CELL MEMBRANE AND ITS ELECTRICAL PROPERTIES 63
2.4.4. RECORDING SETUP 64
2.4.5. ANALYSIS OF APS 65
2.4.6. REAGENTS USED FOR PATCH-CLAMP ELECTROPHYSIOLOGY RECORDINGS 70
2.5. DATA AND STATISTICAL ANALYSIS 71
2.5.1. RECTIFICATION INDICES 71
2.5.2. LIQUID JUNCTION POTENTIAL 72

3. CHAPTER 3: *C9ORF72*^{RE} MEDIUM SPINY NEURONS DISPLAY HYPOEXCITABILITY. 73

3.1. INTRODUCTION 73
3.2. HYPOTHESIS AND AIMS OF THE STUDY: 76
3.3. METHODS 77
3.3.1. IPSC MAINTENANCE (AS DESCRIBED IN METHODS SECTION 2.2.3) 77
3.3.2. MSN DIFFERENTIATION (AS DESCRIBED IN METHODS SECTION 2.2.4 AND 2.2.5) 77
3.3.3. ICC- MSN CHARACTERISATION (AS DESCRIBED IN METHODS SECTION 2.3) 77
3.3.4. ELECTROPHYSIOLOGY (AS DESCRIBED IN METHODS SECTION 2.4) 77
3.4. RESULTS 77
3.4.1. IPSCS FROM *C9ORF72*^{RE} FTD/ALS PATIENTS AND HEALTHY CONTROLS WERE USED TO GENERATE MSN CULTURES. 77
3.4.2. ENRICHED POPULATIONS OF GABAERGIC MSNS WERE GENERATED WHICH PRESENT THE EXPECTED MARKER PROFILE 78
3.4.3. *C9ORF72*^{RE} MSNS DISPLAY HYPOEXCITABILITY 83
3.5. DISCUSSION 105
3.6. CONCLUSIONS 110

4. CHAPTER 4: *IN VITRO* ASTROCYTES DERIVED FROM *C9ORF72*^{RE} PATIENTS DISPLAY ENHANCED MEMBRANE CURRENTS 111

4.1. INTRODUCTION 111

4.2. HYPOTHESIS AND AIMS OF THE STUDY: 116

4.3. METHODS 117

4.3.1. DIRECT CONVERSION OF FIBROBLAST TO INPC (AS DESCRIBED IN METHODS SECTION 2.2.8) 117

4.3.2. DIFFERENTIATION OF INPCS TO INPC-ASTROCYTES (IASTROCYTES; AS DESCRIBED IN METHODS SECTION 2.2.9) 117

4.3.3. ICC – IASTROCYTE CHARACTERISATION (AS DESCRIBED IN METHODS SECTION 2.3) 117

4.3.4. ELECTROPHYSIOLOGY (AS DESCRIBED IN METHODS SECTION 2.4) 117

4.4. RESULTS 117

4.4.1. DIRECTLY DIFFERENTIATING IASTROCYTES FROM *C9ORF72*^{RE} ALS PATIENTS 117

4.4.2. THE ELECTROPHYSIOLOGICAL CHARACTERISATION OF *C9ORF72*^{RE} ALS IASTROCYTES 119

4.5. DISCUSSION 141

4.6. CONCLUSION 144

5. CHAPTER 5: CONNEXIN-MEDIATED DYSFUNCTION IS A CONVERGENT FEATURE OF ALS AND IS INDUCIBLE 145

5.1. INTRODUCTION 145

5.2. METHODS 149

5.2.1. DIRECT CONVERSION OF FIBROBLAST TO INPC (AS DESCRIBED IN METHODS SECTION 2.2.8) 149

5.2.2. DIFFERENTIATION OF INPCS TO INPC-ASTROCYTES (IASTROCYTES; AS DESCRIBED IN METHODS SECTION 2.2.9) 149

5.2.3. ICC – IASTROCYTE CHARACTERISATION (AS DESCRIBED IN METHODS SECTION 2.3) 149

5.2.4. ELECTROPHYSIOLOGY (AS DESCRIBED IN METHODS SECTION 2.4) 149

5.3. RESULTS 149

5.4. DISCUSSION 167

5.5. CONCLUSION 172

6. CHAPTER 6: DISCUSSION AND FUTURE RESEARCH 173

6.1. INTRODUCTION 173

I. INVESTIGATE THE FUNCTIONAL ELECTROPHYSIOLOGICAL PROPERTIES OF HUMAN *IN VITRO*-DERIVED MEDIUM SPINY NEURONS (MSNS) GENERATED FROM *C9ORF72*^{RE} PATIENTS. 173

II. INVESTIGATE THE FUNCTIONAL ELECTROPHYSIOLOGICAL PROPERTIES OF HUMAN *IN VITRO*-DERIVED ASTROCYTES DERIVED FROM *C9ORF72*^{RE} PATIENTS. 173

6.2. IN VITRO-DERIVED *C9ORF72*^{RE} MSNS ARE HYPOEXCITABLE. 173
6.3. FUTURE WORK 174
6.4. WHAT IS THE TRANSLATIONAL RELEVANCE OF THIS STUDY? 178
6.5. SUMMARY 181
6.6. *IN VITRO*-DERIVED ASTROCYTES OBTAINED FROM SYMPTOMATIC ALS PATIENTS DISPLAY CONNEXIN DYSFUNCTION. 182
6.7. FUTURE WORK 183
6.8. IS ASTROCYTE CONNEXIN DYSFUNCTION A THERAPEUTIC TARGET? 187
6.9. SUMMARY 188

7. REFERENCES 189

8. APPENDIX 241

List of Tables

Table 1-1. ***Lower motor neuron dysfunction in C9ORF72^{RE} models.*** _____ *25*

Table 2-1. ***Information on iPSC lines.*** _____ *40*

Table 2-2. ***Basal media composition.*** _____ *42*

Table 2-3. ***iPSC to NPC (day 1-6) media composition.*** _____ *42*

Table 2-4. ***iPSC to NPC (day 7-12) media composition.*** _____ *43*

Table 2-5. ***NPC expansion media composition.*** _____ *43*

Table 2-6. ***GABA 1 media day 13-24 composition.*** _____ *46*

Table 2-7. ***GABA 2 media day 25-72 composition.*** _____ *47*

Table 2-8. ***MN day 13-18 media.*** _____ *48*

Table 2-9. ***MN day 19-28 media.*** _____ *49*

Table 2-10. ***MN day 29-40 media.*** _____ *50*

Table 2-11. ***Cell culture reagents used for the differentiation of MNs and MSNs from iPSCs.*** _____ *51*

Table 2-12. ***Information about cultureware.*** _____ *52*

Table 2-13. ***Information on iNPC lines.*** _____ *53*

Table 2-14. ***iNPC expansion media composition.*** _____ *54*

Table 2-15. ***iAstrocyte differentiation media composition.*** _____ *56*

Table 2-16. ***Cell culture reagents used for the generation of iAstrocytes.*** _____ *56*

Table 2-17. ***Information about cultureware.*** _____ *57*

Table 2-18. ***Primary antibodies information.*** _____ *58*

Table 2-19. ***Secondary antibody information.*** _____ *59*

Table 2-20. ***K-gluconate intracellular solution.*** _____ *65*

Table 2-21. ***Cesium Chloride (CsCl) internal solution.*** _____ *66*

Table 2-22. ***The standard extracellular solution.*** _____ *68*

Table 2-23. ***I_k extracellular solution.*** _____ *69*

Table 2-24. ***Electrophysiology reagents.*** _____ *70*

Table 1-1. ***Lower motor neuron dysfunction in C9ORF72^{RE} models.*** *The table summarizes key physiological findings from various sources, potential link to mechanism of C9ORF72^{RE} pathology and specific disease model used. 25*

Table 2-1. ***Information on iPSC lines.*** *The table highlights the identifying code for each cell lines derived from donors/patients from their respective repository. Included is a brief publicly available clinical description of the patients' and diagnosis relevant to the study (this includes the age of disease onset, site of onset); the specific genetic alteration identified in each patient and repeat expansion length; the sex of the patient (male or female); patient's age at the time the samples were collected and the source from where the cells were acquired. For the latter, the cell lines were provided by the Coriell Institute for Medical Research, The University of Sheffield (TUoS) and the Cedar-Sinai Medical Centre. The tissue source used to create the cell line was skin fibroblast for all line, except for MIFF1 which was sourced from foetal foreskin fibroblasts.....40*

Table 2-2. ***Basal media composition.*** *The basal media provides the basic nutrients and energy needed for cell survival and growth, promoting neural fate and differentiation in stem cells. The table contains information about all constituents of the basal media, their concentration and the purpose of each component. 42*
Table 2-3. ***iPSC to NPC (day 1-6) media composition****. iPSC to NPC (Day 1-6) media provides essential nutrients for cell survival and reagents block pathways that prevent neural differentiation and encourage neural fate...42*
Table 2-4. ***iPSC to NPC (day 7-12) media composition****. iPSC to NPC (Day 7-12) contains same core ingredients as previously described media with added retinoic acid (RA) and purmorphamine (PUR) that promote neuronal differentiation within the NPC population.....43*
Table 2-5. ***NPC expansion media composition****. NPC expansion media promotes proliferation and maintenance of NPCs. NPC expansion media maintains core ingredients to support NPCs with added valproic acid (VA) to increase NPC proliferation and survival.....43*
Table 2-6. ***GABA 1 media day 13-24 composition.*** *A combination of factors was used with basal media to create a controlled environment that favours GABAergic neuron differentiation. Table contains information about the essential components used, the concentration they were used at and the purpose of each reagent. Each reagent provides essential support for neuronal fate commitment, promoting survival and neurite outgrowth. 46*
Table 2-7. ***GABA 2 media day 25-72 composition****. The table contains information about component used for GABAergic neuron maturation media, including concentration and purpose. The combined effect of these reagents fosters a supportive environment for GABAergic neuron maturation. 47*
Table 2-8. ***MN day 13-18 media.*** *This combination of reagents provides a supportive environment for initial motor neuron differentiation. The table highlights the key components, their concentration and purpose.....48*
Table 2-9. ***MN day 19-28 media.*** *The table highlight media composition used in the middle stages of motor neuron differentiation, including each factor and their concentration, alongside with their purpose in the media. This combination of factors aids in the differentiation of motor neurons. 49*
Table 2-10. ***MN day 29-40 media.*** *The table contains information about the media composition used in the final stages of motor neuron differentiation to support motor neuron maturation, including concentration and purpose. The combined effect of all elements supports an environment efficient for maturation of the motor neurons, triggering specific maturation pathways to generate functional neurons and synapses. 50*
Table 2-11. ***Cell culture reagents used for the differentiation of MNs and MSNs from iPSCs.*** *The table includes the specific chemical or reagent used in this study, the commercial supplier form which the reagent was obtained and the manufacturer's identifier for the specific product. 51*
Table 2-12. ***Information about cultureware.*** *The table highlights the specific culture used in this project, the commercial supplier, the manufacturer's identifier for the specific product and purpose of each cell cultureware. The table mentions a selection of cell cultureware, including dishes, multiwell plates used to plate the iNPC-astrocytes (iAstrocytes) and iPSC-derived medium spiny neurons (MSNs) and/or motor neurons (MNs). Optic 96-well plates were used for immunocytochemistry (ICC) and co-culture experiments. 52*
Table 2-13. ***Information on iNPC lines.*** *The table highlights the cell line sample code for the cultured cell lines derived from donors/patients; clinical information which features the patient's known medical condition; the specific genetic alteration identified in each patient and, when appropriate, the sporadic form of disease; the sex*

of the patient (male or female); patient's age at the time the samples were collected and the source from where the cells were acquired. For the latter, the cell lines were provided by the Sheffield Teaching Hospital (STH) (Genomics Department or AMBRoSia, A multicentre Biomarker Resource Strategy in ALS), the Cedar-Sinai Medical Centre and the University of Sheffield (TUoS). Sporadic Alzheimer's Disease and matched control lines were recruited as part of MODEL-AD study. The tissue source used to create all cell lines was skin fibroblast. Note median survival time from onset to death for sporadic ALS lines depicted in two categories: slow (decreased within 2 years after disease onset) and fast (deceased 2-5 years after onset). *53*

Table 2-14. ***iNPC expansion media composition.*** *Media composition of iNPC expansion cells included in table highlights the concentration and purpose of each element. These components provide essential nutrients and energy for the expansion and initial maturation of iNPCs, preventing premature specialization.* *54*

Table 2-15. ***iAstrocyte differentiation media composition.*** *The table illustrates the components of the media, their concentration and their role. The combined effect of these components creates a supportive environment for both survival and proliferation of iNPC-derived astrocytes.* *56*

Table 2-16. ***Cell culture reagents used for the generation of iAstrocytes.*** *The table mentions the specific chemical or reagent used in this part of the study, the commercial supplier and the catalogue number for each product.* *56*

Table 2-17. ***Information about cultureware.*** *The table highlights the specific cultureware used in this project, the commercial supplier, the catalogue number for the specific product and associated role of each component. The table lists a selection of cell cultureware, including dishes, multiwell plates used to plate the iAstrocytes. Optic 96-well plates were used for immunocytochemistry (ICC) of co-culture and astrocyte conditioned media experiments.* *57*

Table 2-18. ***Primary antibodies information.*** *Immunocytochemistry (ICC) experiments employed a variety of primary antibodies targeting specific antigens of interest. Detailed information about each antibody, including the target marker, host species, supplier, catalogue number and concentrations used are provided in the table above.* *58*

Table 2-19. ***Secondary antibody information.*** *Secondary antibodies were used to bind to primary antibodies, above mentioned, to aid the indirect detection of the target antigen. The secondary antibodies have specificity for the antibody species and the isotope of the primary antibody. Secondary antibodies have a detectable tag facilitating detection using imaging or molecular biology technique. The secondary antibodies are generated against a pooled population of immunoglobulin from a target species. The target species, host are highlighted in the above table. All secondary antibodies were purchased from Invitrogen (individual catalogue numbers mentioned) and were used at 1:400 concentration.* *59*

Table 2-20. ***K-gluconate intracellular solution*** *components in mM and their role. The intracellular solution mimics the cell's cytoplasm to maintain cell health and optimize recording quality. The solution was filtered through 0.33 mm filters and snap frozen at -80°C. The solution was aliquoted and stored at -4°C.* *65*

Table 2-21. ***Cesium Chloride (CsCl) internal solution****. This intracellular solution offers advantages for recording K^+ channels in whole-cell patch-clamp experiments, by blocking K^+ currents and providing a stable environment to maintain cellular health and function during recordings.* *66*

Table 2-22. ***The standard extracellular solution****. The specific extracellular solution components provide a balanced environment for whole-cell patch-clamp recordings, supporting cellular function and enabling accurate measurement of ionic currents. The solution mimics physiological levels of key ionic concentrations enabling the study of various ion channels and membrane excitability. 68*

Table 2-23. ***I_K extracellular solution****- equimolar substitution of NaCl with 30mM TEA. The table highlights the components of the media, their concentration and their role. This modified version of the extracellular solution with equimolar TEA substitution for NaCl offers a valuable tool for selectively studying I_K currents from other channels. By reducing K^+ currents, TEA allows the isolation and analysis of I_K channels. 69*

Table 2-24. ***Electrophysiology reagents****. The table includes information about all electrophysiology reagents used in this study, the supplier from which these substances were acquired and their catalogue number. 70*

List of Figures

Figure 2-1. ***From patient to disease model.*** *Somatic cells (e.g. fibroblasts, hematopoietic cells, peripheral blood mononuclear cells, squamous epithelial cells, keratinocytes) are isolated from patients or donors. The cells are reprogrammed into iPSCs via retroviral transduction using pluripotency transcription factors also known as the 'Yamanaka factors' (Oct4, Sox2, c-Myc, Klf4), regaining pluripotency. iPSCs undergo differentiation into specific cell lineages by pharmacologically manipulating signalling pathways and transcription factors, according to defined developmental cellular specification, to progressively drive iPSCs towards the desired cell fate. iPSCs can be induced via the tri-lineage developmental lineages, ectoderm, mesoderm and endoderm. Neural progenitor cells are derived from ectodermal lineage development and are differentiated to neurons. Figure created with BioRender.....36*

Figure 2-2. ***Direct reprogramming protocol of human fibroblasts to iNPCs.*** *Fibroblasts were injected with a mixture of retroviral vectors expressing four reprogramming factors (Sox2, Kfl4, Oct3/4, c-Myc). To generate iNPCs, the culture media was switched to medium containing growth factors, such as fibroblast growth factor 2 (FGF2), epidermal growth factor 2 (EGF2) and heparin. The iNPCs are further differentiated and can give rise to neurons, oligodendrocytes and astrocytes. Figure created with BioRender. 39*

Figure 2-3. ***Multi-step in vitro differentiation protocol of patient-derived MSNs, MNs and astrocytes.*** *This schematic illustrates a multi-step protocol for generating three cell types in the CNS from patient fibroblasts: MSNs, MNs and astrocytes. Fibroblasts are isolated, cultured and exposed to specific media containing a cocktail of four transcription factors, inducing reprogramming into pluripotent iPSCs or straight into induced neuronal progenitor cells (iNPCs), bypassing the pluripotent stem cell stage. The iPSCs undergo neural induction through a dual-SMAD inhibition protocol to form NPCs. NPCs are exposed to MN- or MSN-specific factors to generate precursor cells, which undergo maturation with relevant factors to drive the acquisition of mature MNs or MSNs features. For the direct conversion, the expanded iNPCs are exposed to DMEM, FBS and N-2 to promote astroglial lineage commitment. Differentiating iAstrocytes exhibit mature astrocyte morphology and functionality. Figure created with BioRender. 45*

Figure 2-4. ***Patch-clamp configurations****. Schematic showing the various methods of establishing different patch-clamp configurations. Initially, the electrode is moved close to the cell membrane. Negative pressure is applied so that the pipette attaches to the membrane. The electrode passes nominal current, establishing a 'electrically' tight seal with high resistance, called a GigaOhm seal. This configuration is called 'cell-attached' (top-left). Then, strong acute negative pressure is required to break the cell membrane forming the whole-cell configuration (top-right). The cytoplasm and the pipette interior are continuous and the K^+-gluconate solution floods the cell cytoplasm. It is possible to record single channels via one of two configurations, outside-out or inside-out configurations. inside-out recordings look at single channels, exposing the cytosolic surface of the membrane (bottom-left), while outside-out configuration is used to investigate receptor activated ion channels (bottom-right). Figure created using BioRender. 62*

Figure 2-5. ***Electrophysiology rig setup****. These images highlight some of the important components part of the standard whole-cell patch-clamp electrophysiology setup employed in our laboratory. In the top image, the*

Faraday cage surrounds the entire setup shielding sensitive electronic equipment from external electrical interference, ensuring accurate and reliable recordings. The precise micromanipulator alloys the movement positions for recording pipettes onto the cell of interest under the microscope. The main amplifier further amplifies the signal from the headstage and filters out high-frequency noise, providing a clear representation of the recorded membrane currents. The gravity-fed system continuously delivers fresh extracellular solution to the recording chamber and washes away debris, maintaining stable physiological environment for recordings. The figure below highlights the upright microscope, the recording chamber where the coverslips are placed and the patch electrode. 67

Figure 3-1. ***GABAergic MSNs were generated from iPSCs.*** *The protocol for generating GABAergic MSNs included the differentiation of iPSCs derived from both healthy controls and C9ORF72^{RE} patients, as detailed in the Methods chapter (Sections 2.2.4 and 2.2.5). Dual SMAD inhibition was employed to trigger neural cell formation. A cocktail of BDNF, SHH and DKK-1 generated GABAergic MSN progenitors. BDNF treatment fostered their development into mature MSNs. Timepoints mentioned throughout the thesis refer to period after neuronal differentiation was initiated (Day 0 – 60). Figure created with BioRender.com. 78*

Figure 3-2. NPCs express specific markers (Pax6 and Nestin)*. Representative images highlighting the co-expression of Nestin and Pax6 in NPC at day 2 post neuronal induction. Note the presence of neural rosettes, radially arranged groups of cells surrounding a central lumen. Scale bar set to 50μm. 79*

Figure 3-3. ***MSN progenitors express neuronal markers (β-III-tubulin and MAP2) at day 20.*** *A. Representative images highlighting the expression of MAP2, Nestin and DAPI. Scale bar set to 50μm. B,C,D,E. Graphs showing the mean $\pm$ SEM percentage expression of β-III-tubulin+, MAP2+, GFAP+ and Nestin+ cells, respectively, in the cultures. Note that enriched neuronal populations were generated. Note the lack of immunopositive GFAP+ and Nestin+ markers. Data from individual de-novo preparations are depicted by circles inset into the bar graphs. (β-III-tubulin: Con-1, N=4; Con-2, N=4; C9-1, N=5; C9-2, N=5; C9-3, N=5, C9-Δ1, N=4; MAP2: Con-1, N=2; Con-2, N=3; C9-1, N=4; C9-2, N=4; C9-3, N=3; C9-Δ1, N=2; GFAP: Con-1, N=4; Con-2, N=2; C9-1, N=4; C9-2, N=3; C9-3, N=4; C9-Δ1, N=2; Nestin: Con-1, N=2; Con-2, N=3; C9-1, N=3; C9-2, N=3; C9-3, N=4; C9-Δ1, N=4). 80*

Figure 3-4. ***Increased expression of DARPP32 at day 40.*** *A. Representative images highlight the expression of β-III-tubulin and DARPP32, specific MSN marker. Scale bar, 50μm. B,C,D,E. Graphs showing the mean $\pm$ SEM percentage expression of β-III-tubulin+, MAP2+, DARPP32+ and GFAP+ cells, respectively, in the cultures. Note enriched DARPP32+ neuronal populations were generated. Data, β-III-tubulin: Con-1, N=4; Con-2, N=3; C9-1, N=3; C9-2, N=3; C9-3, N=4, C9-Δ1, N=2; MAP2: Con-1, N=2; Con-2, N=1; C9-1, N=2; C9-2, N=2; C9-3, N=1; C9-Δ1, N=1; DARRP32: Con-1, N=3; Con-2, N=2; C9-1, N=3; C9-2, N=3; C9-3, N=2; C9-Δ1, N=1; GFAP: Con-1, N=2; Con-2, N=1; C9-1, N=2; C9-2, N=3; C9-3, N=2; C9-Δ1, N=1.....81*

Figure 3-5. ***Enriched populations of GABA-ergic MSNs were generated at day 60.*** *Figure caption on the next page. 82*

Figure 3-6. ***Representative AP traces*** *of whole-cell current clamp recordings reveal a loss-of-function phenotype in C9ORF72^{RE} MSNs. Recordings were made from individual MSNs at timepoints day 20, 40 and 60 post neuronal differentiation for healthy control lines (blue), C9ORF72^{RE} MSNs (grey) and the isogenic control line, C9-Δ 1*

(purple). The matrix format displays responses to sequential 500ms current injections from -20pA to 50pA in 10pA increments from a holding potential of -74mV (including liquid junction potential correction [-14mV])......84
Figure 3-7. ***Decreased firing capability in GABAergic MSNs.*** *A. Example traces of the three categories of action potential firing observed; no response (no bona fide AP that either did not reach threshold or cross 0 mV), single AP or multiple APs. B. Percentage of cells exhibiting each firing category throughout the course of differentiation at day 20, 40 and 60 for Con-1, C9-1 and C9-Δ1 MSNs. Note the increase in activity over time for each lines indicating neuronal maturation. Note the lower overall activity of C9-1 with time versus Con-1 and C9-Δ1. C. Percentage of total cells showing firing patterns at day 60. Note the lower overall activity of all C9ORF72^{RE} MSNs compared to healthy controls. D. Comparison at day 60 between C9-1 and its matched isogenic line C9-Δ1. Note the lower overall activity in C9-1 compared to C9-Δ1. Data: Con-1, day 20, n=14, N=7; day 40, n=19, N=6; day 60, n=13, N=5; C9-1, day 20, n=29, N=8; day 40, n=24, N=6; day 60, n=24, N=6; C9-Δ1, day 20, n=18, N=5; day 40, n=13, N=4; day 60, n=9, N=4; Con-2, day 60, n=11,N=4; C9-2, day 60, n=16, N=4; C9-3, n=18, N=4.* 86
Figure 3-8. ***C9ORF72^{RE} MSNs are less responsive to depolarization.*** *Figure caption on the next page.* 88
Figure 3-9. ***Intrinsic membrane properties of C9ORF72^{RE} MSNs are not impacted.*** *A. Mean ± SEM RMP data for Con-1, C9-1 and C9-Δ1 for days 20, 40 and 60. Data from individual cells are depicted by circles inset into the bar graphs. B. Mean ± SEM RMP data for Con-1, Con-2, C9-1, C9-2 and C9-3 for day 60. C. Mean ± SEM RMP data for C9-1 and respective C9-Δ1 for day 60. Note that no consistent changes in RMP are observed. D, E and F. As in A, B, and C, respectively, but for whole-cell capacitance (WCC). Note increasing WCC trend with maturation, as expected, in all lines. G, H and I. As in A, B, and C, respectively, but for membrane input resistance (Rin). Statistical analysis was determined by using One-way ANOVA or Student's t-test (*, p<0.05; **, p<0.01; ****, p<0.0001). Data: Con-1, day 20, n=14, N=7; day 40, n=19, N=6; day 60, n=13, N=5; C9-1, day 20, n=29, N=8; day 40, n=24, N=6; day 60, n=24, N=6; C9-Δ1, day 20, n=18, N=5; day 40, n=13, N=4; day 60, n=9, N=4; Con-2, day 60, n=11,N=4; C9-2, day 60, n=16, N=4; C9-3, n=18, N=4.* 91
Figure 3-10. ***C9ORF72^{RE} MSNs show impaired AP waveform.*** *Caption on the next page.* 93
Figure 3-11. ***Altered AP properties are observed in C9ORF72^{RE} MSN.*** *Caption on the next page.* 95
Figure 3-12. ***Phase plot analysis of AP waveforms shows disturbed C9ORF72^{RE} MSN waveforms.*** *A. Schematic showing the distinct phase plot components corresponding to the AP waveform components, as highlighted in Figure 3-10, including V_{rest} (RMP), V_{thres} (threshold membrane potential), V_{max} (maximal voltage peak of AP or amplitude), V_{repol} (repolarization potential or AHP). B. The mean AP waveforms presented in Figure 3-10 were taken and replotted according to the rate of membrane potential change (dV/dt) versus membrane potential (V) for Con-1, C9-1 and C9-Δ1 MSNs at day 20, 40 and 60. Note the progressive impairment in the 'shape' of the C9-1 AP waveform over time, and that this is notably impacted in the depolarisation and repolarisation phases...98*
Figure 3-13. ***Voltage-gated Na^+-channel current density measurements are consistent in MSNs.*** *Caption on the next page.* 100
Figure 3-14. ***A-type (I_A) voltage-gated K^+ channel activity is not impaired.*** *Caption on the next page.* 102
Figure 3-15. ***Delayed outwardly rectifying K^+ channel (I_K) current density is altered in C9ORF72^{RE} MSNs.*** *A. A two-step depolarizing protocol was utilised to isolate I_K channel activity. First, the I_K channels were activated via a depolarization step of the membrane potential from a holding potential of -70mV to + 30mV (activation). The*

*same step was repeated in the presence of TEA (30 mM). The TEA-sensitive current was yielded by subtracting the current response in the absence of TEA from the TEA-containing trace, to yield TEA-sensitive I_K channel activity. B,C, D. Representative traces at day 40 were selected to highlight each step of the protocol for each line investigated, Con-1 (blue), C9-1 (black) and C9-Δ1 (purple). Current amplitudes were determined from the peak of the IK-sensitive deflections. E. Mean $\pm$SEM I_K current density of Con-1, C9-1 and C9-Δ1 at day 40. Note increase in C9-1 I_K current density compared to C9-Δ1. Statistical analysis was assessed Student's t-test (**, p<0.001). Data: Con-1, n=12, N=3; C9-1, n=11, N=2; C9-Δ1, n=6, N=2.* *104*

Figure 4-1. ***iAstrocytes were generated from fibroblasts via a direct reprogramming protocol and express specific astrocytic markers at day 7.*** *Caption on the next page.* *118*

Figure 4-2. ***Passive membrane properties are impacted in C9ORF72^{RE} ALS iAstrocytes****. Caption on the next page.* *120*

Figure 4-3. ***C9ORF72^{RE} ALS iAstrocytes display enlarged membrane currents****. Individual iAstrocytes were examined using whole-cell patch-clamp in the voltage-clamp configuration. Cells were held at potential of -84 mV (including LJP of -14 mV) and a voltage-step protocol was initiated to investigate the evoked membrane current response. The protocol is depicted in the upper panel and consisted of stepped voltages (from -124 mV to 16 mV) for 200 ms from -84 mV every 10s. The panels below the protocol show representative current traces from individual day 7 and day 14 from Con-1, Con-2, C9-1 and C9-2 iAstrocytes evoked by the described protocol. Note the enhanced current response in the C9-1 and C9-2 lines particularly at day 14.* *123*

Figure 4-4. ***Membrane currents in C9ORF72^{RE} ALS iAstrocytes are enlarged****. A, B. Mean ± SEM current (I) versus voltage (V) plot of day 7 and day 14, respectively, iAstrocytes derived from Con-1 (day 7, n=9, N=3; day 14, n=20, N=4), Con-2 (day 7, n=8, N=3; day 14, n=15, N=5), C9-1 (day 7, n=9, N=3; day 14, n=32, N=7) and C9-2 (day 7, n=6, N=2; day 14, n=19, N=7). Note the increased amount of current evoked by the voltage protocol at each given potential for C9ORF72^{RE} ALS iAstrocytes. C, D. As in A, B, but for current density, which takes into account the WCC data for each individual iAstrocyte. Note that at day 14, C9ORF72^{RE} ALS iAstrocytes show an enhanced passage of current in their membranes. Note that SEM bars are hidden by the mean data points.* *125*

Figure 4-5. ***Rectification of membrane currents are not impaired.*** *A,B. Mean ± SEM normalised current [$II(-104mV)$] versus potential (V) plots of day 7 and day 14, respectively, Con-1, Con-2, C9-1 and C9-2 iAstrocytes. C, Mean ± SEM rectification index for each of the iAstrocyte lines. Rectification was determined by dividing the normalised current data obtained at 16 mV by -124 mV for each cell. Students' t-test was used to determine statistical significance between day 7 to day 14 for each line; *, p<0.05; **, p<0.01; ***, p<0.001.* *126*

Figure 4-6. ***Membrane currents in C9ORF72^{RE} ALS iAstrocytes are not blocked by $BaCl_2$****. Caption on the next page.* *128*

Figure 4-7. ***Membrane currents in C9ORF72^{RE} ALS iAstrocytes are not blocked by CsCl****. A. The panel shows representative voltage-step evoked current traces from individual day 14 healthy control, Con-2, iAstrocytes recorded in the presence of K-gluconate-based and a CsCl-based intracellular patch-pipette solution. B. Mean ± SEM current density (pA.pF) versus voltage (V) plot of day 14 Con-2 iAstrocytes in K^+-gluconate-based intracellular (n=6, N=2) and CsCl-based intracellular (n=6, N=2). C. The panel shows representative current traces from*

individual day 14 C9-2 ALS iAstrocytes in the presence of K^+-gluconate-based intracellular patch-pipette solution and CsCl-based solution. D. Mean ± SEM current density (pA.pF) versus voltage (V) plot of day 14 C9-2 iAstrocytes in K-gluconate-based intracellular (n=3, N=1) and CsCl-based intracellular (n=9, N=2)......130

Figure 4-8. ***Membrane currents in C9ORF72^{RE} ALS iAstrocytes are not blocked by TRPV4 antagonist, HC067047****. A. The panel shows representative voltage-step evoked current traces from an individual day 14 Con-1 Astrocyte before and after the addition of extracellular-applied HC067047. B. As in A, but for C9-1 iAstrocytes. C, Mean ± SEM current density (pA.pF) versus voltage (V) plot of day 14 Con-1 and C9-1 iAstrocytes in the presence and absence of HC067047 (Con-1, n=7, N=2; C9-1, n=9, N=2).*.....131

Figure 4-9. ***Connexin blocker CBX attenuates membrane current dysfunction in C9ORF72^{RE} ALS iAstrocytes****. Caption on the next page.*.....133

Figure 4-10. ***Hemichannel partial blocker Gap19 blocks membrane currents in C9ORF72^{RE} ALS iAstrocytes.*** *Caption on the next page.*.....135

Figure 4-11. ***Membrane current dysfunction in C9ORF72^{RE} ALS iAstrocytes is sensitive to SRSF1 knock down.*** *Caption on the next page.*.....137

Figure 4-12. ***Schematic diagram illustrating the main steps for the co-culture experiment****. MNs were kept in culture until the end of differentiation. At day 37, iAstrocytes were plated on top of the MNs. Treatments were added 6 hours after plating. The co-cultures were fixed with 3.8% PFA after 72 hours of incubation. ICC staining was performed to demonstrate co-culture of MAP2+ motor neurons and Vimentin+ iAstrocytes. Caspase3+ MNs were quantified as a measurement of neuronal death. Imaging was performed using the wide-field In-Cell Analyzer and quantification was done using Columbus Analysis System.* 139

Figure 4-13. ***Preliminary data indicate that CBX causes a reduction in C9ORF72^{RE} ALS iAstrocytes-mediated motor neuron death****. A. Figure shows co-culture of MNs with iAstrocytes. ICC demonstrated cultures displayed Vimentin+ iAstrocytes and MAP2+ MNs. Caspase-3+ immunopositive MNs were quantified to determine percentage of neuronal death. B. Preliminary data depicts reduction in MN death in co-cultures in the presence of CBX. Scale bar set to 100 μm.*.....140

*Figure 5-1.****Passive membrane properties are impacted in sporadic ALS iAstrocytes****. A,B,C, Day 7 and day 14 mean ± SEM data of passive membrane properties, WCC, Rin and RMP, respectively, for Con-2 (day 7, n=10, N=4; day 14, n=15, N=5; Note Con-2 data includes previously presented data in Chapter 4), sALS-1 C9-1 (day 7, n=7, N=2) and sALS-2 (day 7, n=10, N=2; day 14, n=2, N=1). Statistical significance for A,B,C was assessed using One-way ANOVA (*, p<0.05; **, p<0.01; ***; P<0.001; ****, p<0.0001).*.....151

Figure 5-2. ***Membrane currents in sporadic ALS iAstrocytes are abnormally enlarged****. Caption on the next page.* 152

Figure 5-3. ***Passive membrane properties are impacted in C9ORF72^{RE} FTD iAstrocytes****. A,B,C. Day 14 mean ± SEM data of passive membrane properties, WCC, Rin and RMP, respectively, for Con-2 (n=10, N=2), FTD-1 (n=13, N=3), FTD-2 (n=14, N=3) and FTD-3 (n=14, N=3). Statistical significance for A,B,C was assessed using One-way ANOVA (*, p<0.05; **, p<0.01; ***; ****, p<0.0001).* 153

Figure 5-4. ***Membrane currents in C9ORF72^{RE} FTD iAstrocytes are abnormally enlarged****. A. The panels show representative voltage-step evoked current traces from individual day 14 Con-2, FTD-1, FTD-2 and FTD-3*

iAstrocytes. Note the enhanced current response in the C9ORF72^{RE} FTD iAstrocytes. B. Mean ± SEM current density (pA.pF) versus voltage (V) plot of day 14 iAstrocytes derived from Con-2 (n=10, N=2), FTD-1 (n=13, N=3), FTD-2 (n=14, N=3) and FTD-3 (n=14, N=3)......155

Figure 5-5. ***Passive membrane properties are impacted in Alzheimer's Disease iAstrocytes****. A,B,C. Day 14 mean ± SEM data of passive membrane properties, WCC, Rin and RMP, respectively, for Con (n=6, N=2), Alzheimer's disease (n=11, N=3). Statistical significance for A,B,C was assessed using Students' t-test (*, p<0.05; **, p<0.01).*
.....156

Figure 5-6. ***Membrane currents in Alzheimer's Disease iAstrocytes are abnormally enlarged.*** *A. The panels show representative voltage-step evoked current traces from individual day 14 Con and Alzheimer's disease iAstrocytes. Note the enhanced current response in the AD iAstrocytes. B,C. Representative current trace in the same Alzheimer's disease iAstrocyte in A in the presence of CBX. C. Mean ± SEM current density (pA.pF) versus voltage (V) plot of day 14 iAstrocytes derived from Con (n=6, N=2), AD (n=11, N=3) and Alzheimer's disease in the presence of CBX (n=5, N=2).* 157

Figure 5-7. ***C9ORF72^{RE} family iAstrocytes express specific astrocytic markers at day 7****. Figure depicts iAstrocytes at day 7 in culture from a family harbouring C9ORF72^{RE} mutation. ICC staining demonstrates cultures derived from the unaffected father and twin, and the affected twin at two samples points (early and late) are highly enriched for cells harbouring key astrocyte markers CD44 (yellow) and Vimentin (red). DAPI stain is presented in blue. Scale bar set to 50μm. Stainings and images were performed/obtained by members of the Ferraiuolo/Shaw laboratories and presented with permission.* 159

Figure 5-8. ***Passive membrane properties are impacted in C9ORF72^{RE} family iAstrocytes****. A,B,C. Day 14 mean ± SEM data of passive membrane properties, WCC, Rin and RMP, respectively, for unaffected father (n=15, N=5), unaffected twin (n=11, N=5), affected twin (early sample; n=17, N=5) and affected twin (late sample; n=17, N=5). Statistical significance for A,B,C was assessed using Students' t-test (*, p<0.05; **, p<0.01; ***, p<0.001).....160*

Figure 5-9. ***Membrane currents in C9ORF72^{RE} family iAstrocytes are abnormally enlarged in symptomatic patients.*** *A. The panels show representative voltage-step evoked current traces from individual day 14 unaffected father, unaffected twin, symptomatic twin (early sample) and symptomatic twin (late sample) iAstrocytes. Note the enhanced current response in the symptomatic C9ORF72^{RE} ALS iAstrocytes. B. Mean ± SEM current density (pA.pF) versus voltage (V) plot of day 14 iAstrocytes derived from the unaffected father unaffected father (n=15, N=5), unaffected twin (n=11, N=5), affected twin (early sample; n=17, N=5) and affected twin (late sample; n=17, N=5).* 161

Figure 5-10. ***Membrane currents in the symptomatic C9ORF72^{RE} twin iAstrocytes are sensitive to CBX****. A. The panel shows representative voltage-step evoked current traces from individual day 14 symptomatic (late sample) C9ORF72^{RE} twin iAstrocytes. B. The same iAstrocyte in A in the presence of CBX. C. The CBX-sensitive current for the iAstrocyte presented in A. D. Mean ± SEM current density (pA.pF) versus voltage (V) plot of day 14 iAstrocytes derived from the symptomatic C9ORF72^{RE} twin in the presence and absence of CBX (n=4, N=1).* 162

Figure 5-11. ***Passive membrane properties are impacted in pre-symptomatic C9ORF72^{RE} iAstrocytes.*** *A,B,C. Day 14 mean ± SEM data of passive membrane properties, WCC, Rin and RMP, respectively, for Con-2 (n=15, N=5; Note Con-2 as previously presented data in Chapter 4), pre-symptomatic PreSx-1 (n=11, N=3), PreSx-2 (n=11,*

N=3) and PreSx-3 (n=7, N=2). Statistical significance for A,B,C was assessed using One-way ANOVA (, p<0.05; **, p<0.01).*.....163

Figure 5-12. ***Membrane currents in C9ORF72^{RE} pre-symptomatic iAstrocytes are variably impacted.*** *A. The panels show representative voltage-step evoked current traces from individual day 14 Con-2, PreSx-1, PreSx-2 and PreSx-3 iAstrocytes. Note the variable current response in the pre-symptomatic C9 ALS iAstrocytes. B. Mean ± SEM current density (pA.pF) versus voltage (V) plot of day 14 iAstrocytes derived from the unaffected Con-2 (n=15, N=5; Note Con-2 data as previously presented data in Chapter 4), pre-symptomatic PreSx-1 (n=11, N=3), PreSx-2 (n=11, N=3) and PreSx-3 (n=7, N=2).*.....165

Figure 5-13. ***KCl-mediated induction of connexin dysfunction in pre-symptomatic iAstrocytes****. Caption on the next page.*.....166

Declaration

I, the author, confirm that the Thesis is my own work. I am aware of the University's Guidance on the Use of Unfair Means (www.sheffield.ac.uk/ssid/unfair-means). This work has not previously been presented for an award at this, or any other, university.

List of publication

Iris S. Pasniceanu, Manpreet S. Atwal, Cleide D. S. Souza, Laura Ferraiuolo and Matthew R. Livesey*. (2021). Emerging mechanisms underpinning neurophysiological impairments in C9ORF72 repeat expansion-mediated amyotrophic lateral sclerosis/frontotemporal dementia. Frontiers in Cellular Neuroscience, Volume 15, 784833, DOI: 10.3389/fncel.2021.784833.

Sai Zhang, Johnathan Cooper-Knock, Annika K. Weimer, Minyi Shi, Tobias Moll, Jack N.G.Marshall, Calum Harvey, Helia G. Nezhad, John Franklin, Cleide D. S. Souza, Ke Ning, Cheng Wang, Jingjing Li, Allison A. Dilliott, Sali Farhan, Eran Elhaik, **Iris S. Pasniceanu**, Matthew R. Livesey, Chen Eitan, Eran Hornstein, Kevin P. Kenna, Jan H. Veldink, Laura Ferraiuolo, Pamela J. Shaw, Michael P.Snyder (2022). Genome-wide identification of the genetic basis of amyotrophic lateral sclerosis. Neuron, Issue 6, Pages 992-1008.e11, DOI: 10.1016/j.neuron.2021.12.019.

List of abbreviations

Abbreviation	Full name
A	Ampere
AD	Alzheimer's disease
ADA	Adenosine deaminase
AHP	Afterhyperpolarization
AIS	Axon initial segment
ALS	Amyotrophic lateral sclerosis
AMPA	α-amino-3-hydroxy-5-methyl-4-isoxazolepropionic acid
AMPAR	α-amino-3-hydroxy-5-methyl-4-isoxazolepropionic acid receptor
AP	Alanine-proline
AP	Action potential
AP-5	D(-)-2-Amino-7-phosphonoheptanoic acid
ATP	Adenosine triphosphate
Ba	Barium
BBB	Blood-brain-barrier
BDNF	Brain-derived neurotrophic factor
bvFTD	Behavioural variant FTD
C9ORF72	Chromosome 9 open reading frame 72
Ca^{2+}	Calcium
CBX	Carbenoxolone
Cd	Cadmium
Cl^-	Chloride
CNQX	Cyano-7-nitroquinoxaline-2,3-dione
CNS	Central nervous system
CNTF	Ciliary neurotrophic factor
CREB	cAMP response element-binding protein
Cs	Caesium
CSF	Cerebrospinal fluid
Cx	Connexin
DARPP32	Dopamine- and cAMP-regulated phosphoprotein 32 kDa
DKK1	Dickkopf related protein 1
DMSO	Dimethyl sulfoxide
DNA	Deoxyribonucleic acid
DPR	Dipeptide repeat
DS	Donkey serum
EAAT	Excitatory amino acid transporter
ECM	Extracellular matrix
EGTA	ethylene glycol-bis(β-aminoethyl ether)-N,N,N′,N′-tetra acetic acid
E_{rev}	Reversal potential
ESC	Embryonic stem cell
F	Farad
fALS	Familial ALS
FTD	Frontotemporal dementia
FUS	Fused in sarcoma
GA	Glycine-alanine
GABA	Gamma-aminobutyric acid

GAT	Gamma-aminobutyric acid transporter
GLT-1	glutamate transporter 1
Glu	Glutamate ionotropic receptor AMPA type subunit
GNPs	GABA-ergic MSN progenitor
GP	Glycine-proline
GP_e	Globus pallidus externus
GR	Glycine-arginine
GRN	Granulin
GTP	Guanosine-5'-triphosphate
GΩ	Giga-ohms
HBSS	Hanks' Balanced Salt Solution
HD	Huntington’s Disease
HEK	Human embryonic kidney
HeLa	Henrietta Lacks
HEPES	4-(2-hydroxyethyl)-1-piperazineethanesulfonic acid
HSPA	Heat shock protein family A
I	Current
I_A	A-type K channels
iAstrocytes	Induced astrocytes
ICC	Immunocytochemistry
IGF-1	Insulin-like growth factor-1
IgG	Immunoglobulin
I_K	Outwardly rectifying K^+ channels
IL-1	Interleukin-1
IMS	Industrial methylated spirit
iPSC	Induced pluripotent stem cell
K^+	Potassium
Klf4	Kruppel-like factor 4
K_v	Voltage-gated K^+ channels
LCD	Low-complexity domains
LLPS	Liquid-liquid phase separation
LMN	Lower MN
LPJ	Liquid junction potential
LV	Lentivirus
MAP2	Microtubule-associated protein 2
MAPT	Microtubule-associated protein tau
MEG	Magnetencephalography
mEPSCs	Miniature excitatory postsynaptic currents
Mg	Magnesium
MN	Motor neuron
MNP	MN progenitor
MRI	Magnetic resonance imaging
MSN	Medium spiny neuron
mV	Millivolts
Na^+	Sodium
NAD	Nicotinamide adenine dinucleotide
Na_v	Voltage-gated Na^+ channels
NMDA	N-methyl-D-aspartic acid or N-methyl-D-aspartate
NPC	Neuronal progenitor cell
NPY	Neuropeptide Y

PBS	Phosphate buffered saline
PFA	Paraformaldehyde
PNFA	Progressive non-fluent aphasia
PolyP	Inorganic phosphate
PR	Proline-arginine
PTX	Picrotoxin
PUR	Purmorphamine
RA	Retinoic acid
RAN	Repeat-associated non-AUG
RE	Repeat expansion
RI	Rectification index
R_{in}	Input resistance
RMP	Resting membrane potential
RNA	Ribonucleic acid
RNAi	RNA interference
ROCK	Rho-associated protein kinase
ROS	Reactive oxygen species
sALS	Sporadic ALS
SCNT	Somatic cell nuclear transfer
SD	Semantic dementia
SEM	Standard error of the mean
SHH	Sonic hedgehog
SICI	Short-interval intercortical inhibition
SOD1	Cu/Zn Superoxide dismutase 1
SOD1-ALS	ALS patients with a mutation in the SOD1 gene
SOX2	SRY-related HMG-Box Gene 2
SN_{pr}	Substantia nigra pars reticulata
SRSF1	Serine and Arginine Rich Splicing Factor 1
SV2	Synaptic vesicle protein 2
TARDBP	Transactive response DNA binding protein 43 kDa
TDP-43	Transactive response DNA binding protein 43 kDa
TEA	Tetraethylammonium
TMS	Transcranial magnetic stimulation
TNF-α	Tumour necrosis factor alpha
TREM106B	Transmembrane protein 106 B
TTX	Tetrodotoxin
UMN	Upper MN
UPS	Ubiquitin/Proteasome System
V	Voltage
VPA	Valproic acid
WCC	Whole-cell capacitance

CHAPTER 1: Introduction

1.1. Introduction to amyotrophic lateral sclerosis

Amyotrophic lateral sclerosis (ALS) is an incurable and progressive neurodegenerative disease characterised by the loss of upper and lower motor neurons (MNs) within the spinal cord and motor cortex. Degeneration of the motor neurons leads to a disruption of neuromuscular junctions resulting in muscular atrophy, paralysis and death usually by respiratory failure within 2-5 years of first symptoms (Yang et al., 2014, Renton et al., 2014). Age is a major contributor for ALS, as it is for other neurodegenerative diseases like Alzheimer's and Parkinson's diseases. ALS typically affects adults between the ages of 40 and 60 (Kiernan et al., 2011). The incidence of ALS varies significantly across different regions of the world, suggesting a role for both genetic and environmental factors (Xu et al., 2020). The aetiology of ALS is thought to be due to a combination of risk-genotypes that interact with environmental risk factors over time, enhancing the neurodegenerative cascade (reviewed in (Chapman et al., 2023)). Men are at a slightly higher risk of developing ALS compared to women, particularly at younger ages. However, this gender disparity diminishes as people get older (Yamashita et al., 2023). While ALS can affect people from all ethnicities, some studies suggest a higher prevalence among individuals of European descent (Logroscino and Chiò, 2020, Kiernan et al., 2011). Although multiple reports attempted to delineate the environmental risk factors predisposing the development of ALS, no clear delimitation of specific gene-environmental interaction were found (reviewed in (Chapman et al., 2023)). The identification of environmental factors and the predisposition to the development of ALS could play an important role in disease prevention and the future of personalized medicine approaches.

ALS presents with two main subtypes defined by the initial symptom location: spinal-onset (~66%) with extremity weakness and bulbar-onset (~33%) with speech/swallowing difficulties (Al-Chalabi et al., 2012). These reflect the initial site of motor neuron degeneration (spinal cord *versus* corticobulbar tract) (Al-Chalabi et al., 2012). Bulbar-onset patients have worse disease prognosis due to respiratory complications and increased cognitive decline (Chiò et al., 2009, Shellikeri et al., 2017).

Currently there are no beneficial treatments for ALS, with only one available disease modifying drug in Europe, Riluzole, which extends life expectancy by 1-3 months (Hardiman et al., 2017). Other medication has showed promising results in mildly prolonging functional independence in selective patients using Edaravone, an antioxidant drug (Bhandari et al., 2018). More recently, toferson, an antisense oligonucleotide for Cu/Zn Superoxide dismutase 1 gene (SOD1) familial ALS, which was shown to reduce mRNA production from mutated SOD1 genes, effectively reducing the synthesis of toxic SOD1 protein, was approved in the United States of America (Blair, 2023).

1.2. Introduction to frontotemporal dementia

Frontotemporal dementia (FTD) is a group of neurodegenerative diseases defined by atrophy of frontal and temporal lobes often in conjunction with other subcortical brain regions (Englund et al., 1994, Neary et al., 1998, Rascovsky et al., 2011). FTD presents with alteration to behaviour and character, with relative presentation of memory loss in the early phases of the disease. In patients aged 65 and above, FTD is the third most common cause of dementia, and it is second most common cause of early onset dementia (age below 65) and usually ranges from 45 to 65 (Logroscino et al., 2023). Recent studies have indicated that individuals of Black/African American descent may experience higher disease severity in FTD compared to their White and Asian counterparts. However, no significant difference in disease severity was observed between White and Asian individuals (Jin et al., 2023).

Different subtypes of FTD are distinguished by their clinical manifestations (Lashley et al., 2015, Woollacott and Rohrer, 2016). FTD can be defined by three main subtypes: behavioural variant (bvFTD), semantic dementia (SD) and progressive non-fluent aphasia (PNFA). The most common subtype is bvFTD, accounting for 70% of patients, which present with progressive behavioural changes and inappropriate social behaviour, whereas the other two forms are primarily language disorders (Neary et al., 1998, Snowden et al., 2002).

In bvFTD, behavioural changes manifest as a significant shift in character, marked by emotional blunting, apathy, speech and language impairments and social disinhibition (Snowden et al., 2002, Snowden et al., 2012). Patients often lack awareness of these changes, with limited insight being an early indicator (Neary et al., 1998). Dietary modifications are also present with increased craving for sugary and fatty foods (Woolley et

al., 2007a, Woolley et al., 2007b). Disease progression leads to heightened disinhibition. These characteristics are crucial for differentiating FTD from other forms of dementia, particularly Alzheimer's disease (Miller et al., 1997). Psychosis and repetitive behaviours are also observed in these patients, especially with the *C9ORF72*^{RE} mutation (Snowden et al., 2012). Interestingly, sex is a potential factor in determining the clinical phenotype of FTD, with bvFTD being more prevalent in men and PNFA being more common in women. However, sex does not influence survival rates in FTD (Pengo et al., 2022).

Currently, there are no specific drugs or cure for FTD. Treatment usually focuses on improving the quality of life of patients via speech therapy, decreasing behavioural symptoms using antidepressants and antipsychotics (Tsai and Boxer, 2014).

1.3. Overlap between clinical features of ALS and FTD

ALS and FTD were initially characterised as two distinct diseases. However, clinical, genetic and pathological evidence suggests that they belong to a continuous disease spectrum (Kato et al., 1993, Talbot et al., 1995, Lomen-Hoerth et al., 2002).

Although the presentation of ALS varies between individuals, cognitive decline and behavioural disturbances are increasingly recognised are defining characteristics of ALS. ALS has been linked with FTD, as 50% of ALS patients meet the clinical diagnostic criteria for FTD and up to 30% of FTD patients exhibit motor impairments (Christidi et al., 2018). Survival after diagnosis is decreased in patients with distinct onset of ALS/FTD and even more severe in patients which simultaneously develop motor and cognitive symptoms (Hu et al., 2009). A large number of genes have been reported to be implicated in ALS and FTD (section 1.4), but also both diseases share a pathological hallmark: protein misfolding and aggregation (section 1.5). A comprehensive understanding of the clinical and epidemiological factors associated with ALS and FTD can reveal shared pathogenic mechanisms, leading to more targeted treatments and improved patient care.

1.4. Genetic landscape of ALS and FTD

ALS and FTD are primarily sporadic diseases, however disease causing mutations appear *de novo* and with familial history. The genetics of ALS and FTD are highly heterogeneous, mirroring the wide range of clinical and pathological features. Determining genetic origins has facilitated insights into the mechanisms of these diseases thought to underlie neuronal degeneration.

Although the majority of patients diagnosed with ALS (~90%) are sporadic (sALS), a smaller (~10%) of cases have a familial form (fALS), often inherited in a dominant pattern from a parent (Renton et al., 2014). Despite the different origins, the clinical manifestations of sALS and fALS are very similar (Al-Chalabi et al., 2010). The advances in sequencing technologies in the recent years have identified over 50 causative or disease-modifying genes for ALS (Boylan, 2015). Interestingly, around 15% of sALS cases may be caused by genetic mutations. *C9ORF72*^{RE} is the most frequent genetic cause of ALS and accounts for approximately 25-40% of familial cases and about 7% of sALS (Renton et al., 2014). SOD1 was the first ALS-causative mutation identified to have a pathological role in ALS (Rosen et al., 1993) and accounts for 15-20% of fALS and 2% of sporadic cases (Renton et al., 2014). Mutations in *FUS* are responsible for about 5% of inherited cases and 1% of sALS (Renton et al., 2014). Mutations in TAR DNA binding protein (*TARDBP*) gene have been linked to 4% of fALS and 1% of sALS cases (Renton et al., 2014).

FTD exhibits a highly heritability compared with ALS, with 40-50% of cases being familial (Rohrer et al., 2009). Over 50 genes have been linked to FTD (Sirkis et al., 2019). Similar to ALS, *C9ORF72*^{RE} contributes to approximately a third of familial cases and 4-21% of sporadic FTD (Devenney et al., 2014). Mutations in microtubule-associated protein tau (*MAPT)* are responsible for approximately 30% of familial FTD cases around 17% sporadic cases (van Swieten and Spillantini, 2007). Mutations in granulin (*GRN*) account for 20-25 of familial cases and about 10% of sporadic cases (Wang et al., 2021).

A key pathological hallmark found in almost all ALS patients (~98%) of ALS cases and approximately 50% of FTD patients is the presence of neuronal and glial cytoplasmic inclusions containing the 43kDa transactive response DNA binding protein, TDP-43 (Neumann et al., 2006a).

I will discuss in further detail the *SOD1* and *C9ORF72*^{RE} mutations. *SOD1* was the first gene to be associated with ALS (Rosen et al., 1993) and important insight into the pathogenesis of ALS has been drawn from models harbouring this mutation. *C9ORF72* mutation is the most common genetic cause of both ALS and FTD (Renton et al., 2011, DeJesus-Hernandez et al., 2011) and important insight into the mechanisms has been drawn from this mutation. The majority of the cells studied in this project harboured this mutation.

1.4.1. SOD1

SOD1 is an ubiquitously expressed cytosolic and mitochondrial antioxidant enzyme that converts reactive oxidative species (ROS) into oxygen and hydrogen peroxide, but it is also involved in repression of respiration and immunomodulation (Saccon et al., 2013). Early research proposed that *SOD1* mutations mediated ALS through a loss-of-function mechanism, resulting in decreased radical scavenging activity (Rosen et al., 1993). *SOD1* mutations have been shown to destabilize protein folding, leading to the formation of intracellular aggregates (Bendotti et al., 2001). Gain-of-function mechanisms have emerged as an alternative. *SOD1* mutations have been shown to destabilize protein folding, leading to the formation of intracellular aggregates. These protein aggregates are implicated in neurotoxicity through mechanisms potentially involving oxidative stress and mitochondrial dysfunction (Crown et al., 2019, Hadano et al., 2010). It is therefore possible that both loss- and gain-of-function contribute to *SOD1*-ALS, but variation is caused by different mutation types. *SOD1*-ALS accounts for approximately 15-20% of fALS patients and 2% sALS cases harbour the *SOD1* mutation (Renton et al., 2014). *SOD1*-ALS patients often exhibit clinical and pathological features that differ from the broader ALS spectrum, classically lacking the characteristic TDP-43 inclusions and cognitive decline (Robertson et al., 2007). These clinical and pathological differences might explain the limited success in translating findings from *SOD1* animal models to effective clinical therapies for wider ALS populations. However, mouse models harbouring *SOD1* mutations have offered important mechanistic insight for two decades.

The first animal model of ALS was the SOD1^{G93A} mouse (Gurney et al., 1994), which overexpresses human mutant SOD1 randomly inserted into the genome. This transgenic mouse model remains the most widely used animal model of ALS. The SOD1^{G93A} mice presents with hind limb weakness at approximately 90-110 days, neurodegeneration that closely resembles that of ALS patients and death occurs at 135-150 days (Synofzik et al., 2010, Zang and Cheema, 2002).

Studies utilizing the mutant SOD1^{G93A} mouse have significantly advanced our understanding of ALS. This model improved the understanding of various pathological changes and mechanisms in the disease including mitochondrial abnormalities (Kong and Xu, 1998, Méndez-López et al., 2021, Cassina et al., 2008), oxidative stress (Hall et al., 1998, Ferrante et al., 1997b, Mahoney et al., 2006), glutamate toxicity (Bendotti et al., 2001, Howland et al., 2002, Foran and Trotti, 2009), cytoskeletal dysfunction (Wong et al., 1995, Tu et al., 1996, Morrison et al., 1996), defective axonal transport (De Vos et al., 2007) and progressive denervation of the neuromuscular junction (Dupuis et al., 2009).

1.4.2. C9ORF72^{RE}

In 2011, a landmark discovery in ALS/FTD genetics identified a hexanucleotide (GGGGCC) repeat expansion in the *C9ORF72* gene (*C9ORF72*^{RE}) as a critical factor for ALS/FTD pathogenesis (DeJesus-Hernandez et al., 2011, Renton et al., 2011). While pathogenic expansions are typically hundreds to thousands of repeats in length in *C9ORF72*^{RE} ALS/FTD patients, smaller expansions (20-30 repeats) may also increase the risk of ALS (Iacoangeli et al., 2019). The size of the *C9ORF72*^{RE} hexanucleotide expansion has been suggested to correlate with the age and onset of ALS (Gijselinck et al., 2016, Beck et al., 2013), although some studies fail to replicate this (Chen et al., 2016, Dols-Icardo et al., 2014). The disparities may appear due to the somatic instability of the expansion, specifically that the repeat size is highly variable between tissue types, often with a significant increase in size in the CNS in comparison to blood-derived DNA, which most studies are based on (Nordin et al., 2015). A second factor is the variety of testing modalities that make determining the size of the expansion often unreliable or incomparable (Breevoort et al., 2022). Because asymptomatic expansion-positive relatives and asymptomatic expansion carriers are

unlikely to be tested, the frequency if the *C9ORF72*^{RE} is not yet clear (Murphy et al., 2017). The repeat length and somatic repeat instability may contribute to the reduced disease penetrance of *C9ORF72*^{RE} ALS/FTD, differences in age of onset and the wide-range clinical symptoms observed in patients (Chiò et al., 2012, Murphy et al., 2017).

C9ORF72^{RE} is present in around 40% of fALS individuals, 7% of sALS cases, 25% of familial FTD and 6% of sporadic FTD individuals making it the most common genetic cause of ALS/FTD (Majounie et al., 2012). The pathogenic mechanism of *C9ORF72*^{RE} are considered to involve a combination of loss-of-C9ORF72-function (haploinsufficiency) and gain-of-function mechanisms (Balendra and Isaacs, 2018) relating to the formation of RNA foci and the potentially 5 dipeptide repeat proteins (poly GA, GR, PR, AP, GP). The mechanisms by which these act are focused on in section 1.7.

1.5. Neuropathological features of ALS and FTD

ALS is characterized by the degeneration of motor neurons in the motor cortex, corticospinal tract and atrophy of the skeletal muscles (Brooks et al., 2000). Post-mortem macroscopic examination reveals depletion of more than 50% of spinal motor neurons, diffuse astrocytic gliosis and microglia infiltration in both grey and white matter of the spinal cord (Hardiman et al., 2017).

FTD is characterised by bilateral atrophy that primarily affects the frontal and temporal lobes, but other brain areas are also targeted, such as the striatum (Neary et al., 1998). The pattern of atrophy exhibits variability, reflecting the clinical heterogeneity of the disease. Each clinical subtype of FTD is associated with a distinct topographical distribution of atrophy (Neary et al., 1998, Snowden et al., 2002). bvFTD is characterised by symmetrical atrophy in the frontal and anterior temporal lobes (Snowden et al., 2002, Seelaar et al., 2011). In PNFA, the predominant pattern of atrophy involves the left frontotemporal hemisphere, while SD is characterised by selective atrophy of the anterior temporal cortex (Snowden et al., 2002). Additional atrophy is observed in the posterior brain as the disease progresses (Neary et al., 1998).

Both diseases are characterised by the formation, aggregation and accumulation of misfolded proteins within neurons and glial cells. Subtype classification within this

spectrum is based on the predominant protein component found within these inclusions. FTD can be further classified into four main proteinopathies: FTD-tau, which accounts for 40-45% of familial cases; FTD-TDP, the most predominant proteinopathy in familial FTD, accounting for 50-60%; FTD-FUS, present in 5-10% of familial FTD patients; FTD-UPS pathological proteinopathy is observed in 1% of FTD (Mackenzie et al., 2010, Urwin et al., 2010). Similarly, ALS is mainly classified into three sub-categories: ALS-SOD1, present in 2% of familial ALS patients; ALS-TDP proteinopathy, present in almost all (98%) fALS; ALS-FUS, accounting for less than 1% of fALS cases (Al-Chalabi et al., 2012). Mutations in all of the genes that encode these major aggregating proteins in ALS and FTD cause a subset of familial ALS and FTD cases. The discovery of the TDP-43 as a ubiquitin positive protein inclusion in both ALS and FTD provided a clear pathological link between these two diseases (Neumann et al., 2006a).

1.6. Pathology of *C9ORF72*^{RE} ALS/FTD

C9ORF72^{RE} ALS/FTD patients exhibit classical molecular pathology manifestations, which set apart repeat expansion carriers from non-*C9ORF72*^{RE}-related FTD/ALS cases. All *C9ORF72*^{RE} ALS patients exhibit the loss of motor neurons in the motor cortex and spinal cord, ubiquitinated TDP-43 cytoplasmic inclusions in neurons and glia, Bunina bodies and pyramidal tract degeneration (Cooper-Knock et al., 2012). However, a key difference for *C9ORF72*^{RE} ALS lies in the presence of p62-positive inclusions outside motor neurons in *C9ORF72*^{RE} individuals, prominent in the hippocampus (CA3, CA4) (Cooper-Knock et al., 2012). These inclusions were identified in all cortical layers with few dystrophic neurites, corresponding to FTD-TDP type 2 which is associated with *C9ORF72*^{RE}-mediated bvFTD and ALS/FTD (Cooper-Knock et al., 2012, Mackenzie et al., 2011). MRI studies reveal significant atrophy in the thalamus and cerebellum of *C9ORF72*^{RE} FTD carriers compared to non-carriers (Irwin et al., 2013, Mahoney et al., 2012), areas with increased *C9ORF72*^{RE} expression.

Besides TDP-43 pathology and p62-positive inclusions, dipeptide repeat (DPR)-containing cytoplasmic inclusions, rising from non-canonical translation of the GGGGCC repeat, were found in pyramidal cells (hippocampus) and cerebellar layers (Mahoney et al., 2012, Cooper-Knock et al., 2012, Hsiung et al., 2012, Al-Sarraj et al., 2011, Mackenzie et al.,

2014). Importantly, these DPR inclusions have since been found in the frontal and motor cortices (Cooper-Knock et al., 2012, Hsiung et al., 2012, Al-Sarraj et al., 2011, Troakes et al., 2012) and are thought to be involved in proteasomal degradation and autophagy (Brettschneider et al., 2012). DPRs appear in at low levels in glial cells and even skeletal muscle (Schludi et al., 2015, Cykowski et al., 2019).

Beyond DPRs, another pathological hallmark of *C9ORF72*^{RE} ALS/FTD is the presence of RNA foci. These abnormal aggregations of RNA transcripts have been identified in motor neurons (DeJesus-Hernandez et al., 2011) and neurons of the frontal cortex, hippocampus and cerebellum (Mizielinska et al., 2013, Lagier-Tourenne et al., 2013). RNA foci are not exclusive to neurons, with a small number detected in microglia and astrocytes (Mizielinska et al., 2013, Lagier-Tourenne et al., 2013). RNA foci comprise both sense and antisense RNA transcripts derived from the GGGGCC repeat expansion (Lee et al., 2013), but are not equally distributed. Sense transcripts appear more frequently in cerebellar Purkinje neurons and motor neurons compared to antisense transcripts are more prevalent in cerebellar granule neurons in *C9ORF72*^{RE} ALS patients (Cooper-Knock et al., 2015). Despite interacting with similar proteins, mislocalization of TDP-43 in motor neurons was observed in the presence of antisense RNA foci (Cooper-Knock et al., 2015). This suggests that different RNA transcripts arising from the *C9ORF72*^{RE} might have distinct toxicities and play various roles in neurodegeneration.

1.7. Molecular mechanisms by which *C9ORF72*^{RE} induces neurodegeneration in ALS/FTD patients

1.7.1. C9ORF72 protein loss-of-function

Normal physiological function of C9ORF72 has been linked with the autophagy pathway. C9ORF72 depletion leads to impaired autophagosome formation and protein aggregation clearance and impaired lysosomal biogenesis (Farg et al., 2014, Webster et al., 2016, Diab et al., 2023). As such, these pathways have become a central hypothesis in ALS/FTD disease mechanisms. Studies have reported reduced mRNA and protein levels in *C9ORF72*^{RE} ALS/FTD carriers, suggesting a loss-of-function mechanism by haploinsufficiency to cause neurodegeneration (Belzil et al., 2014, Ciura et al., 2013, DeJesus-Hernandez et al., 2011,

Waite et al., 2014). Loss-of-function mouse exhibit inflammatory and autoimmune response, suggesting a role of C9ORF72 in immune homeostasis in microglia (Burberry et al., 2016). However, the *C9ORF72*^{RE} knockout mice lack of neurodegeneration and TDP-43 pathology argues against haploinsufficiency being the primary cause of neurotoxicity (Koppers et al., 2015), but may be acting as a contributing factor, potentially amplifying the toxic effects of RNA foci and DPRs (gain-of-function mechanisms) in a non-cell autonomous manner (Jiang et al., 2016). Emphasising this, no truncation or missense mutations in *C9ORF72* have been found in ALS/FTD patients (Harms et al., 2013).

1.7.2. RNA aggregation and gain-of-function

The *C9ORF72*^{RE} is transcribed bidirectionally in sense and antisense direction producing RNA prone to forming atypical secondary structures- sense RNA (hairpins and G-quadruplexes) and antisense RNA (i-motifs and protonated hairpins) (Fratta et al., 2012, Kovanda et al., 2015). *In vivo,* such secondary structures are likely to mediate the sequestration and, consequently, the depletion of RNA-binding proteins (RBPs) (Fratta et al., 2012), providing the potential route to RNA toxicity (reviewed in (Balendra and Isaacs, 2018, Geng and Cai, 2024)). These accumulations are called RNA foci and represent a hallmark of ALS/FTD pathology and are predominantly observed in the frontal cortex, and to a lesser extent in glial cells (Mizielinska et al., 2013, Lagier-Tourenne et al., 2013). The correlation of sense and antisense RNA foci with other pathological hallmarks of ALS/FTD is unclear (Mizielinska et al., 2013, Peters et al., 2015), however, disparities between the two forms are being identified. The antisense CCCCGG, but not sense GGGGCC repeat expanded RNAs activate PKR/eIF2α-dependent integrated stress response and contributes to neurodegeneration in *C9ORF72*^{RE} ALS/FTD patients (Parameswaran et al., 2023).

In *C9ORF72*^{RE} ALS patients, RNA foci co-localize and interact with hnRNPA1 (heterogeneous nuclear riboprotein) and Pur-α, but not other RNA binding proteins, such as TDP-43 and FUS (Sareen et al., 2013, Xu et al., 2013). However, TDP-43 binds hnRNPA1, therefore, this does not rule out that RNA foci contribute to TDP-43 pathology indirectly (Buratti et al., 2005). RNA foci interact with RNA splicing and transporter proteins disrupting gene regulation, translation and splicing (Sareen et al., 2013, Xu et al., 2013, Buratti et al., 2005). Previously *C9ORF72*^{RE} RNA foci have been reported in repeat expansion diseases, like

myotonic dystrophy type 1 and 2, changing gene expression and disrupting the function of RNA binding proteins (Ranum and Day, 2004).

In order to investigate toxicity caused by RNA foci as an independent mechanism, without the effect of DPRs, the effect of GGGGCC repeat sequences was interspaced with stop codons to prevent translation in every frame (Mizielinska et al., 2014). *Drosophila* models showed drastically reduced lifespan upon expression of $(G_4C_2)_{36}$, $(G_4C_2)_{103}$ and $G_4C_2)_{288}$ repeats was not toxic (Mizielinska et al., 2014, Baldwin et al., 2016).

Sense and antisense RNA foci are pathological hallmarks of *C9ORF72*^{RE} ALS/FTD (DeJesus-Hernandez et al., 2011). These expanded RNAs are unlikely to be the main drives of neurotoxicity but contribute to the sequestration of a variety of RNA binding proteins, which may interrupt RNA metabolism and cellular homeostasis (DeJesus-Hernandez et al., 2017, Mizielinska et al., 2013).

1.7.3. RAN translation and DPR toxicity

Expansion repeat *C9ORF72*^{RE} sense and antisense transcripts are translated in all reading frames via the phenomenon of repeat associated non-AUG (RAN) translation, leading to the production of DPRs. RAN translation is a pathologic mechanism in which repeat expansion sequences are translated into aggregation-prone proteins from multiple reading frames, even without the AUG start codon. The RAN translation of the sense RNA produces two DPRs: glycine-alanine (GA) and glycine-arginine (GR), whilst the antisense produces proline-arginine (PR), alanine-proline (AP), and both produce glycine-proline (GP) (Mori et al., 2013a, Zu et al., 2013).

Studies employing *Drosophila* models expressing codon-optimised DPR constructs reveal that arginine-rich DPRs (poly-GR and poly-PR) induce several retinal degeneration and reduced lifespan, suggesting their potential neurotoxic potential, while poly-GA displayed moderate neurotoxic effect and no toxicity was associated with poly-PA (Mizielinska et al., 2014). GA, PR and GR have been widely reported to have toxic effects in various models, including mice, zebrafish, *Drosophila* primary neurons and iPSC-derive neurons (Kwon et al., 2014, Bennion Callister et al., 2016, Liu et al., 2016, Mizielinska et al., 2017, Tao et al., 2015). However, these DPRs can potentially interact with each other and

act synergistically to contribute to the neurotoxic effects. Studies suggest that DPR species compared to RNA foci are a greater source of toxicity (Tran et al., 2015). However, this mechanism by which DPRs exert toxicity are still investigated, but may involve nucleolar dysfunction, altered splicing, impaired protein homeostasis and DNA damage (Freibaum and Taylor, 2017). Importantly, DPRs can be transmitted intercellularly, potentially propagating pathology (Westergard et al., 2016).

Arginine-rich DPRs interact with proteins containing low-complexity domains (LCDs). These interactions disrupt the formation and function of membranelles organelles like nucleoli and stress granules, impairing RNA processing and homeostasis (Bennion Callister et al., 2016, Kwon et al., 2014, Mizielinska et al., 2017, Tao et al., 2015). Poly-GR and poly-PR can aggregate and interact with LCD proteins in nucleoli and stress granules, interfering with liquid-liquid phase separation (LLPS) and sequester RNA at high concentrations, further disrupting RNA metabolism (Lee et al., 2016, Lin et al., 2016, Zhang et al., 2018, Boeynaems et al., 2017) providing another mechanism by which arginine-rich DPRs cause neurodegeneration. DPRs interact with translation initiation and elongation factors inhibiting global protein synthesis *in vitro* and *in vivo* (Green et al., 2017, Moens et al., 2019). Moreover, poly-GR and poly- PR DPRs contribute to DNA damage, vesicle trafficking and mitochondrial dysfunction, neuronal excitability and axonal outgrowth (Bennion Callister et al., 2016, Dafinca et al., 2016, Farg et al., 2014, Freibaum et al., 2015b, Lopez-Gonzalez et al., 2016, Selvaraj et al., 2018). Importantly a sequential interacting set of phenotypes might contribute to *C9ORF72*^{RE} ALS/FTD.

Interestingly, limited immunohistochemical evidence of DPR pathology in affected brain regions in ALS/FTD patients (Sakae et al., 2018, Saberi et al., 2018), but more recently, soluble and insoluble DPRs have been quantified and poly-GR levels are associated with clinical parameters of disease and highlight the potential role not only in disease models, but in human patients (Quaegebeur et al., 2020).

In conclusion, DPRs are important players in *C9ORF72*^{RE} ALS/FTD with various potential disease mechanisms, some of which include impaired RNA metabolism, translation and DNA damage. DPR pathology precedes TDP-43 pathology (Proudfoot et al., 2014, Baborie et al., 2015, Vatsavayai et al., 2016a), suggesting DPRs act upstream in the

disease cascade. This spatial disconnect may rise because DPRs initiate the neurodegenerative process, but other factors are necessary.

1.8. TDP-43 pathology

Mislocalization of hyperphosphorylated and ubiquitinated TDP-43 in the cytoplasm is a common hallmark of ALS and FTD (Neumann et al., 2006b). Almost all ALS post-mortem brain tissue exhibits TDP-43 pathology, while half are present in FTD cases in neurons and glia (Neumann et al., 2006a, Arai et al., 2006). TDP-43 is a ubiquitously expressed ribonucleoprotein that is predominantly located in the nucleus, where it is involved in functions linked to RNA metabolism including transcription, mRNA splicing, RNA transport, stress granule dynamics (Buratti and Baralle, 2012). The mislocalization of TDP-43 from the nucleus to the cytoplasm and formation of TDP-43 cytoplasmic inclusions is recognised as a pathological hallmark in almost all ALS cases and half of FTD patients (Sreedharan et al., 2008, Neumann et al., 2006a). TDP-43 is present in most of ALS/FTD spectrum, including sporadic and *C9ORF72*^{RE} form, indicating that either different disease mechanisms converge on TDP-43 pathology or that TDP-43 pathology is a generally important mechanisms contributing to neurodegeneration (Neumann et al., 2006a). it is unclear whether TDP-43 causes toxicity though a gain- and/or loss-of function mechanism, but several groups have reported loss of nuclear TDP-43 causes splicing deficits in cellular and animal models, as well as in motor neurons from *TARDBP*-ALS patients (De Conti et al., 2015, Highley et al., 2014). Additionally, other suggest that the pathological effect is due to loss of autoregulation leading to TDP-43 overexpression (White et al., 2018).

TDP-43 pathology correlates with clinical degeneration independent of *C9ORF72* DPRs and RNA foci localization (Davidson et al., 2016). Post-mortem studies indicate that *C9ORF72* pathology precedes TDP-43 mislocalization, implying a cascade of events (Vatsavayai et al., 2016a). DPR expression caused cytoplasmic accumulation of TDP-43 in a *Drosophila* model (Solomon et al., 2018). Further, TDP-43-related pathology can cause downstream events. TDP-43 regulates a cryptic exon-splicing event in the ALS/FTD gene *UNC13A*, one of the strongest genetic risk factors for ALS and ALS/FTD (Ma et al., 2022). The

loss of TDP-43 from the nucleus results in inclusion of a cryptic exon in *UNC13A* mRNA, leading to decreased UNC13A protein production (Ma et al., 2022).

1.9. ALS/FTD pathological mechanisms

1.9.1. Oxidative stress

Oxidative stress occurs due to an increased production of reactive oxidative species (ROS) and decrease in the body's inability to remove or repair oxidative damage through effective antioxidant defences (Sies, 2015). Although ROS may not be the triggering factor, this imbalance can promote tissue damage and interact with other disease mechanisms, ultimately leading to motor neuron degeneration (Liu and Wang, 2017). High levels of radical damage and abnormal free radical metabolism have been observed in the spinal cord (Shaw et al., 1995) and motor cortex (Ferrante et al., 1997a) of ALS patients. Increased levels of oxidative stress markers have been reported in early disease stages in CSF samples from ALS patients (Ihara et al., 2005, Simpson et al., 2004). These markers indicate various downstream effects of oxidative stress including axonal health, DNA oxidation and lipid peroxidation (Devos et al., 2019). Also, ROS inhibits the release of neurotransmitters and an increase in ROS levels leads to inhibition in the neuromuscular junction function (Naumenko et al., 2011). In response to oxidative stress, cells with the *C9ORF72*^{RE} increase levels of RAN translation of DPRs (Westergard et al., 2019), which can lead to increased pathology and accelerating neurodegeneration. Stress granules are form as a response to the exposure to oxidative stress. In *C9ORF72*^{RE} ALS, pathological TDP-43 aggregates are recruited to stress granules, potentially contributing to the disease (Kim et al., 2014).

1.9.2. Mitochondrial dysfunction

Mitochondria primarily acts as a source of energy for the majority of cellular processes. Mitochondrial defects in ALS are linked to impaired ATP production, calcium buffering, redox balance, respiratory complexes and mitochondria-dependent apoptosis (Cozzolino and Carrì, 2012). *C9ORF72*^{RE} patient fibroblasts exhibit altered mitochondrial morphology compared to healthy controls (Onesto et al., 2016). *C9ORF72*^{RE} motor neurons exhibit

reduced mitochondrial Ca^{2+} buffering (Dafinca et al., 2020) and the loss of mitochondrial function leads to axonal dysfunction (Mehta et al., 2021). Impaired mitochondrial function increases ROS production, leading to a positive feedback loop defined by enhanced oxidative stress due to mitochondrial component and greater mitochondrial impairments (Zhao et al., 2022a). These pathways play a significant role in the onset and development of ALS.

1.9.3. Axonal transport impairments

Axonal transport maintains neuronal homeostasis by ensuring long-range delivery of several cargos, including cytoskeletal components, organelles, signalling molecules and RNA between proximal and distal neuronal components (Vargas et al., 2022). Therefore, defects in axonal transport are associated with impaired neuronal homeostasis and function (Sleigh et al., 2019). Deficits in *in vivo* axonal transport have been proposed in several different ALS backgrounds (Sleigh et al., 2019, Bilsland et al., 2010, Sleigh et al., 2020, Tosolini et al., 2022) and is proposed to represent one of the first pathological signs of motor neuron dysfunction and have been reported in $SOD1^{G93A}$ presymptomatic mice (Bilsland et al., 2010). In *C9ORF72*^{RE} ALS/FTD, DPRs have been linked with the axonal transport machinery. Single molecule tracking revealed that arginine-rich DPRs associated with the C-terminal tubulin tails of microtubules caused reduced axonal transport (Fumagalli et al., 2021).

1.9.4. Disrupted protein metabolism

The presence of insoluble protein aggregates within degenerating neurons and glial cells across various brain regions, including the brainstem, spinal cord, cerebellum hippocampus, and frontal and temporal lobes have been defining pathological features of ALS (Ramesh and Pandey, 2017, Montibeller et al., 2020). Intracellular protein aggregates are hallmark pathological features of ALS. Several studies indicate ER stress in ALS pathology, suggesting an inability properly manage misfolded proteins (Parakh and Atkin, 2016). Numerous genes associated with ALS, such as *SOD1*, *TARDBP*, *FUS* and *C9ORF72,* are

associated with protein trafficking and degradation via the ubiquitin-proteasome and autophagy (Webster et al., 2017).

1.9.5. Disrupted RNA metabolism

Aberrant RNA metabolism is a key player in the pathophysiology of ALS. The main ALS genes (*SOD1*, *TARDBP*, *FUS* and *C9ORF72*) have functional roles in multiple features of RNA metabolism including mRNA transcription, alternative splicing, RNA transport, mRNA stabilization and miRNA biogenesis (Butti and Patten, 2019). As mentioned before, the *C9ORF72*^{RE} mutation leads to the accumulation of RNA foci which directly exert RNA toxicity by disrupting RNA metabolism (Konopka et al., 2020). RNA foci facilitate the recruitment, mislocalization and impaired function of RNA binding proteins (Donnelly et al., 2013, Lee et al., 2013). The sequestration of RNA binding proteins to *C9ORF72* RNA foci permits nuclear export, allowing the pathological transcripts to escape to the cytoplasmic ribosomal machinery, resulting in the production of DPRs (Hautbergue et al., 2017). Current advances led to the potential therapeutic intervention by inhibiting the nuclear export protein adaptor SRSF1 (Castelli et al., 2021, Hautbergue et al., 2017).

1.10. Neurophysiology of ALS/FTD

Neurophysiological impairment is a well-established and prominent hallmark of ALS/FTD (reviewed by Pasniceanu et al., 2021). These impairments are though to contribute to the pathological progression and the systematic loss of function through a complex interplay of neuronal and synaptic loss. These perturbations are core contributors to disease pathogenesis through excitotoxicity and impaired neurotransmission. Further, studies on pre-symptomatic non-degenerative patients, including *C9ORF72*^{RE} ALS/FTD, suggest that neurophysiological perturbations may be detectable even before the emergence of notable clinical symptoms (Benussi et al., 2016, Geevasinga et al., 2016b, Styr and Slutsky, 2018). This early detection of neurophysiological dysfunction presents a potential target intervention to slow or prevent disease progression based early drivers of disease. Understanding the origins of neurophysiological dysfunction and the mechanisms directly linking these features to molecular pathogenesis of *C9ORF72*^{RE} is important for advancing

our understanding of ALS/FTD. Neuronal physiology is considered to be underpinned by their general excitability, which is dependent on a complex interplay of factors such as synaptic function, morphology and intrinsic excitability. The latter, is, in turn, contingent on the functional expression of ion channels associated with action potential generation. To date, ALS/FTD research, to which study of the *C9ORF72*^{RE} has been central, has focused on cortical and motor neurons, the key sites of degeneration.

1.10.1. Cortical dysfunction in *C9ORF72*^{RE} ALS/FTD

Cortical dysfunction in both sALS and fALS, including those with *C9ORF72*^{RE}, is a well-recognised clinical pathophysiological hallmark (Geevasinga et al., 2016b, Williams et al., 2013, Benussi et al., 2016, Schanz et al., 2016, Nasseroleslami et al., 2019). Transcranial magnetic stimulation (TMS) and magnetoencephalography (MEG) studies consistently demonstrate early cortical network dysfunction in ALS (Govaarts et al., 2022, Vucic et al., 2013, Eisen et al., 2017, Proudfoot et al., 2017) and FTD patients (Lindau et al., 2003, Nishida et al., 2011), potentially preceding lower motor neuron degeneration. This suggests a staged progression of pathology with cortical dysfunction potentially driving neurodegeneration in a feed-forward manner (Geevasinga et al., 2016b, Menon et al., 2015). Similar to other neurodegenerative diseases (Styr and Slutsky, 2018), early-stage functional synaptic perturbations are thought to contribute to cortical synapse loss (Henstridge et al., 2018), potentially explaining the severe cognitive impairments observed in *C9ORF72*^{RE} ALS/FTD patients. Structural and functional magnetic resonance imaging (MRI) studies in ALS/FTD further support this notion, demonstrating correlations between cortical changes/atrophy and behavioural/cognitive impairments (Agosta et al., 2016, Consonni et al., 2018, Ahmed et al., 2021). Collectively, these findings suggest a pivotal role for cortical dysfunction in the early pathogenesis of ALS/FTD. Several physiological studies have investigated the implications of *C9ORF72*^{RE} in cortical dysfunction using various experimental models and techniques.

1.10.2. Synaptic dysfunction in *C9ORF72*^{RE} ALS/FTD

An emerging body of literature appears to converge on abnormalities in synaptic function and structure associated with *C9ORF72*^{RE}. For instance, altered gene expression in synaptic signalling pathways was observed in *C9ORF72*^{RE} post-mortem cortical tissue (Prudencio et al., 2015). Similarly, electron microscopy and array tomography revealed a decrease in synaptic density in *C9ORF72*^{RE} post-mortem material, potentially linking this to the cognitive decline observed in patients (Henstridge et al., 2018). Additionally, using patch-clamp electrophysiology in a DPR mouse model, a reduction in the frequency of miniature excitatory postsynaptic currents (mEPSCs) was revealed, indicative of impaired synaptic function (Choi et al., 2019). Furthermore, studies employing calcium imaging and vesicular staining techniques in primary rat cortical neurons and *C9ORF72*^{RE} patient-derived iPSC cortical neurons demonstrated reduced levels of synaptic vesicle protein 2 (SV2), disrupted calcium homeostasis, and impaired vesicle release, all potential contributors to cortical dysfunction in *C9ORF72*^{RE} pathology (Jensen et al., 2020). In contrast, Perkins et al. (2021) reported increased network burst activity and synaptic density in *C9ORF72*^{RE} patient-derived iPSC cortical neurons, alongside impaired synaptic potentiation and reduced vesicular pools (Perkins et al., 2021). A decrease in SV2 and synaptophysin levels in *C9ORF72*^{RE} post-mortem cortex was observed, suggesting a disease modifier-mediated effect on these synaptic proteins (Barbier et al., 2021b). *C9ORF72*^{RE} haploinsufficiency plays a central role in the regulation of neurotransmission at excitatory synapses by interaction with pre-synaptic vesicle localisation protein synapsin and modulation of synaptic vesicle pools (Bauer et al., 2022a).

1.10.3. Network and synaptic plasticity

Homeostatic network and synaptic plasticity, serve as a modulator of synaptic strength in order to prevent excessive potentiation or depression of synapses within a network, maintain the efficient signalling and neuronal function (Li et al., 2019). Synaptic plasticity, the process by which synapses modify their strength based on activity, is crucial for learning and memory. Functional impairments in network and synaptic plasticity are recognized as prominent early features of neurodegenerative diseases, including ALS/FTD (Styr and

Slutsky, 2018, Starr and Sattler, 2018). Severe impairments are thought to reflect altered cellular homeostasis that precedes and potentially contributes to further neuronal dysfunction and death (Styr and Slutsky, 2018, Starr and Sattler, 2018). Studies using paired associative stimulation with TMS have revealed deficits in LTP-like network plasticity in asymptomatic *C9ORF72*^{RE} individuals, suggesting early and widespread cortical dysfunction with potential synaptic origins (Benussi et al., 2016). It is proposed that synaptic/network plasticity impairments may occur 15 years before symptom onset, making them some of the earliest detectable pathological changes in ALS/FTD. Further evidence for impaired synaptic plasticity comes from studies using iPSC-derived cortical neurons from *C9ORF72*^{RE} patients, which exhibited impaired potentiation of miniature excitatory postsynaptic currents (mEPSCs), a feature that was restored in gene-corrected lines (Perkins et al., 2021).

Similar findings of impaired synaptic plasticity have been observed in various animal models of ALS/FTD, including SOD1^{G93A}, UBQLN2^{P497H}, TDP-43 transgenic mice, MAPT and GRN knockout mice (Rei et al., 2020, Koza et al., 2019, Wu et al., 2019, Spalloni et al., 2011, Petkau et al., 2012, Biundo et al., 2018, Ho et al., 2021, Handley et al., 2022, Liu et al., 2022). *Drosophila* overexpressing *C9ORF72*^{RE} and *FUS* mutations also exhibit impaired synaptic plasticity (Perry et al., 2017b, Sahadevan et al., 2021).

Broader cellular disruptions affecting molecules and signalling pathways essential for synaptic plasticity are evident from transcriptional disturbances observed in both *C9ORF72*^{RE} patient-derived cortical neurons and post-mortem cortical tissue (Perkins et al., 2021, Prudencio et al., 2015). However, the precise molecular mechanisms underlying altered cortical synaptic plasticity in ALS/FTD remain unclear. However, studies using a *C9ORF72* knockout mouse model have demonstrated reduced LTP and LTD in cortico-hippocampal connections, suggesting a role for the C9ORF72 protein in synaptic plasticity mechanisms within the hippocampus. These findings also raise the possibility that haploinsufficiency of *C9ORF72* may contribute to synaptic plasticity deficits (Ho et al., 2020).

The close association between plasticity and neuronal homeostasis suggests that impairments in plasticity may represent very early markers of disease onset. These impairments may reflect the inability of neurons to adapt to chronic disease-mediated changes (Benussi et al., 2016, Starr and Sattler, 2018, Styr and Slutsky, 2018).

1.10.4. Cortical hyperexcitability

A plethora of studies using TMS suggest a reduction of short-interval intercortical inhibition (SICI) in ALS patients (Geevasinga et al., 2016b, Vucic et al., 2008), including *C9ORF72*^{RE} patients (Wainger and Cudkowicz, 2015, Schanz et al., 2016, Nasseroleslami et al., 2019). SICI reflects decreased inhibitory activity that appears pre-symptomatically preceding lower motor neuron degeneration (Menon et al., 2015, Geevasinga et al., 2016b), worsening with disease progression (Menon et al., 2020). This suggests a potential role for reduced inhibition in the development and course of ALS/FTD. Cortical hyperexcitability is thought to be a pathogenic driver of motor neuron dysfunction in ALS/FTD because cortical circuits control upper motor neurons within the cortico-spinal tract. Increased excitability is associated with excitotoxicity, which can damage motor neurons (Khademullah et al., 2020, Timmins et al., 2023). This link is further supported by the observation that the degree of cortical hyperexcitability in ALS patients correlates with their disease progression (Shibuya et al., 2016). Cognitive dysfunction associated more intense SICI (Higashihara et al., 2021, Agarwal et al., 2021). Further, hyperexcitability in FTD is subtly different to that of other neurodegenerative diseases, suggesting it can be used as a biomarker (Wang et al., 2016).

Understanding the physiological mechanism behind cortical hyperexcitability centre on the interplay between excitatory and inhibitory neurons. Studies suggest a loss of function of the inhibitory input mediated by inhibitory neurotransmitter GABA. However, to date, no observations have been reported in *C9ORF72*^{RE} disease models and our knowledge comes from other genetic models of ALS. This dysfunction may be particularly pronounced for parvalbumin interneurons, a vulnerable class reduced in *TDP-43*^{Q331K} model of ALS/FTD and *C9ORF72*^{RE} ALS patient post-mortem (Lin et al., 2021). Cortical interneuron dysfunction might occur early to cortical hyperexcitability, and subsequent interneuron degeneration contributes to an increase in excitability as the disease progresses. Impaired inhibitory neuron function has been reported in pre-symptomatic SOD1^{G93A} mouse model, where layer 5 parvalbumin interneurons were hypoactive and increasing their activity was effective in delaying the onset of ALS-mediated motor deficits, slowing symptom progression and increasing the lifespan of these animals (Khademullah et al., 2020). However, anatomical differences between primates and rodents should be carefully

considerate as rodent models lack the direct cortico-motor neuron connection observed in humans (Lemon, 2008). Other studies report increased intrinsic excitability of parvalbumin interneurons in neonatal and symptomatic $SOD1^{G93A}$ model (Kim et al., 2017a), while hypoexcitability in parvalbumin neurons and hyperexcitability of somatostatin interneurons was observed in a *TDP-43*^{A315T} mouse model (Zhang et al., 2016b). Also, pronounced decrease of inhibitory synapses was reported in *FUS*$^{\Delta NLS/+}$ mouse model (Sahadevan et al., 2021, Scekic-Zahirovic et al., 2021). Selective dysfunction of inhibitory synapses occurs in early pathological stages in *tau* mouse model, leading to neuronal loss, hyperexcitability and excitotoxicity (Shimojo et al., 2020).

Studies suggest that *C9ORF72*^{RE} ALS/FTD patient-derived cortical neurons exhibit early increase in excitatory synaptic activity, possibly due to enhanced synaptic density (Perkins et al., 2021). This finding aligns with observations in pre-symptomatic *TDP-43*^{Q331K} mice and *SOD*^{G93A} mice, showing increased excitatory synaptic activity of cortical neurons (van Zundert et al., 2008, Fogarty et al., 2016a, Saba et al., 2016). These findings suggest an increased excitatory synaptic activity may be an early feature of cortical hyperexcitability in ALS/FTD patients. However, this effect seems to be transient as later stages showing a shift towards synaptic loss in *TDP-43*^{A315T} mice (Handley et al., 2017). While the mechanisms underlying increased cortical synaptic density in *C9ORF72*^{RE} ALS/FTD remain elusive, evidence suggests involvement of transcriptional dysregulation affecting synaptic architecture proteins (Prudencio et al., 2015, Perkins et al., 2021). In contrast, mechanisms for later-stage synaptic loss use aged *C9ORF72*^{RE} (GR_{80}) mice prefrontal cortical synaptic loss (Choi et al., 2019). (GR_{400}) and (PR_{400}) knock-in mice recapitulate cortical hyperexcitability and spinal motor neuron loss which was associated with a decrease in synapse proteins and increase in extracellular matrix, potentially offering neuroprotective properties (Milioto et al., 2024). Moreover, C9ORF72 knockout mice display reduced synaptic density in the hippocampus, potentially due to the effects of haploinsufficiency on synaptic health (Frick et al., 2018; Xiao et al., 2019). In line with these observations, *C9ORF72*^{RE} plays a role in the regulation of synaptic vesicle pools through the interaction with Synapsin via a loss-of-function mechanism, impacting on synaptic function, vesicle trafficking and neuronal function (Bauer et al., 2022a). Microglia might play a central role in dysfunctional synaptic pruning and synaptic loss. Microglia specific C9ORF72 knockout

mice indicates decreased synaptic branching, loss and cognitive decline (Lall et al., 2021). More recently, a significant increase in neuropeptide Y (NPY) expression in the ALS post-mortem cortex was reported. In vitro and in vivo experiments using SOD1^{G93A} mouse demonstrated that NPY can improve motor function and survival specifically during the symptomatic phase of ALS, suggesting NPY Y1 receptor antagonist as a promising therapeutic target (Clark et al., 2023).

1.10.5. Upper motor neuron hyperexcitability and morphological defects

Layer V cortical projection neurons (or upper motor neurons) represent the main efferent pathway of the cortex to the spinal cord, and their role in propagating pathophysiology in ALS is fundamental. Early intrinsic hyperexcitability of these neurons has been observed in TDP-43^{A135T} and TDP$^{\Delta NLS}$ mouse models (Zhang et al., 2016b, Dyer et al., 2021). Chronic chemogenetically driven hyperexcitability of upper motor neurons induces motor symptoms and neurophysiological hallmarks of ALS, including upper and motor neuron degeneration, reactive gliosis and TDP-43 pathology (Haidar et al., 2021). No data is available on *C9ORF72*^{RE}, but observations in ALS patient post-mortem tissue (Genç et al., 2017) and *TDP-43*^{A315T} (Handley et al., 2017), *SOD1*^{G93A} (Fogarty et al., 2016b, Fogarty et al., 2017), and *FUS*^{R521G} (Sephton et al., 2014) indicate that upper motor neuron hyperexcitability may drive functional synaptic degeneration, dendritic spine loss and pathology in these neurons. Upstream changes to upper motor neurons likely play an important role in disease pathology, but more information is needed to understand their activity in ALS/FTD.

1.10.6. Early cortical dysfunction and homeostatic adaptation in *C9ORF72*^{RE} ALS/FTD

Early cortical dysfunction in ALS/FTD likely reflects a preclinical ‘homeostatic adaptation’ phase, where disease-induced network changes are initially tolerated before ultimately leading to network failure (Frere and Slutsky, 2018). Studies in SOD1^{G93A} mouse suggest a pre-symptomatic, fluctuating pattern of altered intrinsic excitability and synaptic input in upper motor neurons. This dynamic shift may reflect the functional adaptation at prodromal stages of disease. Similarly, although *C9ORF72*^{RE} ALS/FTD cortical neurons

exhibit increased synaptic density, consistent with increased excitability, neurons display a reduced readily releasable pool of synaptic vesicles, hindering sustained synaptic transmission (Perkins et al., 2021). This suggests a potential homeostatic response to counter the initial increase in synaptic density. The C9ORF72 protein is involved in vesicular trafficking and reduced protein function may contribute to the limited vesicular pool release (Aoki et al., 2017, Frick et al., 2018). Supporting this notion, mice engineered to express (GA_{149}) DPRs indicate reduced expression of synaptic vesicle protein and impaired vesicle release (Jensen et al., 2020). Early cortical dysfunction in *C9ORF72*^{RE} ALS/FTD thus appears to involve a multifaceted interplay between potentially pathological increases in synaptic density, homeostatic responses to dampen excitability, and underlying vesicular trafficking dysfunction driven by *C9ORF72*^{RE}-mediated mechanism. Interestingly, genetic modifiers influencing disease onset seem linked to synaptic vesicle function (Barbier et al., 2021a), further highlighting this intricate interplay. Since cortical function can be monitored in patients, identifying the earliest physiological disruptions in *C9ORF72*^{RE} holds immense value for understanding disease progression and potentially developing earlier interventions.

1.10.7. Lower motor neuron dysfunction in *C9ORF72*^{RE} ALS/FTD

Lower motor neuron, receiving monosynaptic input from upper motor neurons, represent the final pathway for controlling skeletal muscle. Their dysfunction is detected in patients by electromyogram (EMG) and nerve conduction studies, serving as a diagnostic tool for ALS (Joyce and Carter, 2013). Lower motor neuron dysfunction follows cortical dysfunction, mirroring clinical progression of muscle weakness, atrophy, fasciculations and cramps . Interestingly, lower motor neurons initially experience a phase of hyperexcitability, potentially contributing to early symptoms like fasciculations and cramps (Bae et al., 2013). This is followed by a progressive decline in function (hypoexcitability) before concluding in degeneration and death. The mechanisms underlying these changes in lower motor neurons and the neurophysiological processes leading to excitotoxicity and cell death are summarized in Table 1-1.

Study	Physiological finding	Mechanism?	Model
(Donnelly et al., 2013)	Increased susceptibility to glutamate-mediated excitotoxicity	Toxic RNA gain-of-function	*C9ORF72*^{RE} iPSC motor neurons
(Shi et al., 2018)	Increased susceptibility to glutamate-mediated excitotoxicity Increased functional expression of Ca^{2+} permeable AMPAR Upregulation of NMDA receptor subunit GluN1	C9ORF72 haploinsufficiency	*C9ORF72*^{RE} iPSC motor neurons
(Selvaraj et al., 2018)	Increased susceptibility to glutamate-mediated excitotoxicity Increased GluA1 AMPA subunit expression Increased functional expression of Ca^{2+} permeable AMPAR		*C9ORF72*^{RE} iPSC motor neurons *C9ORF72* post-mortem
(Gregory et al., 2020)	Increased susceptibility to glutamate-mediated excitotoxicity Increased GluA1 AMPA subunit expression Increased functional expression of Ca^{2+} permeable AMPAR		*C9ORF72*^{RE} post-mortem
(Bursch et al., 2019)	Increased susceptibility to glutamate-mediated excitotoxicity Increased GluA1 AMPA subunit expression		*C9ORF72*^{RE} iPSC motor neurons
(Xu and Xu, 2018)	Increased extracellular glutamate and intracellular Ca^{2+} levels Increased in NMDA receptor mediated signalling Increase of synaptic boutons and active zones in larval neuromuscular junctions	Poly GR/PR (36 repeat) DPRs	*C9ORF72*^{RE} *Drosophila* model
(Sareen et al., 2013)	Hypoexcitability		*C9ORF72*^{RE} iPSC motor neurons
(Devlin et al., 2015)	Transition from hyper- to hypo-excitability; loss of synaptic activity		*C9ORF72*^{RE} iPSC motor neurons
(Burley et al., 2022)	Transition from hyper- to hypo-excitability; increased intracellular Ca^{2+} release at early stages, followed by mitochondrial Ca^{2+} dysfunction at later stages		*C9ORF72*^{RE} iPSC motor neurons
(Zhao et al., 2020)	Hypoexcitability Loss of voltage-activated sodium and potassium currents in MNs		*C9ORF72* iPSC astrocytes
(Wainger et al., 2014)	Hyperexcitability		*C9ORF72*^{RE} iPSC motor neurons

(Catanese et al., 2021)	Loss of excitatory synapses		*C9ORF72*^{RE} iPSC motor neurons
(Zhang et al., 2015)	Impaired synaptic release at the neuromuscular junction Reduction in active zones number	Disruption of normal RNA processing	*C9ORF72*^{RE} iPSC motor neurons $(C_4G_2)_{30}$ *Drosophila* model
(Freibaum et al., 2015a)	Impaired synaptic release at the neuromuscular junction Reduction in active zones number	Disruption of normal RNA processing	$(C_4G_2)_{58}$ *Drosophila*
(Perry et al., 2017b)	Impaired synaptic plasticity at the neuromuscular junction	Poly-GR (100 repeat) DPRs	*C9ORF72*^{RE} *Drosophila*
(Castelli et al., 2021)	Manipulating SK ion channel activity improves C9ORF72-ALS motor neuron death and Drosophila locomotor deficits		*C9ORF72*^{RE} iPSC motor neurons *C9ORF72*^{RE} *Drosophila*
(Butti et al., 2021)	Reduction in the number of presynaptic and postsynaptic structures at the NMJ	C9ORF72 haploinsufficiency	*C9ORF72*^{RE}-related zebrafish

Table 1-1. ***Lower motor neuron dysfunction in C9ORF72^{RE} models.*** *The table summarizes key physiological findings from various sources, potential link to mechanism of C9ORF72^{RE} pathology and specific disease model used.*

1.10.8. The loss of synaptic innervation from upper motor neurons to lower motor neurons

Glutamate excitotoxicity is considered a key pathogenic mechanism that contributes to motor neuron degeneration in ALS/FTD (Cleveland and Rothstein, 2001). The established observation of synaptic loss in lower motor neurons during later stages of ALS aligns with the hypothesis that this loss disrupts motor neuron function . This aligns with findings in *C9ORF72*^{RE} patient-derived iPSC motor neurons, where prolonged culture resulted in synaptic loss accompanied by changes in gene expression regulated by CREB (cAMP response element-binding protein) (Catanese et al., 2021). In line with the notion that disruptions in glutamate signalling and altered excitability significantly contribute to synaptic loss and other lower motor neuron injury.

Lower motor neurons respond to glutamate through AMPA and NMDA receptors (Van Den Bosch et al., 2006). Early studies pointed toward a potential intrinsic vulnerability of LMNs to AMPA receptor-mediated excitotoxicity (Rothstein et al., 1996, Rothstein et al., 1992, Rothstein et al., 1995, Cleveland and Rothstein, 2001). This vulnerability is likely enhanced by elevated synaptic glutamate levels predicted due to increased excitability of upper motor neurons in ALS/FTD. However, the presence of pre-synaptic deficits in glutamate release from upper motor neurons remains unclear. Astrocytes play a crucial role in clearing glutamate from the synaptic cleft via the glutamate transporter EAAT2. Reduced expression of EAAT2 has been observed in various ALS models, suggesting a potential reduction in glutamate uptake (Rosenblum and Trotti, 2017). However, this observation appears inconsistent with *C9ORF72*^{RE} ALS/FTD, where patient-derived astrocytes do not consistently show reduced EAAT2 expression or function (Allen et al., 2019b, Zhao et al., 2020).

iPSC-derived motor neurons from *C9ORF72*^{RE} ALS/FTD patients exhibit enhanced vulnerability to glutamate excitotoxicity (Donnelly et al., 2013, Selvaraj et al., 2018, Shi et al., 2018, Bursch et al., 2019), which can be potentially rescued by specific drugs and antisense oligonucleotides (Shi et al., 2018, Donnelly et al., 2013). The underlying mechanism seems linked to increased expression of calcium-permeable AMPA receptors due to higher levels of the GluA1 subunit in *C9ORF72*^{RE} lower motor neurons compared to the cortex (Selvaraj et al., 2018, Gregory et al., 2020). Furthermore, C9ORF72 protein haploinsufficiency is proposed as a potential mechanism for GluA1 upregulation (Shi et al., 2018, Xiao et al., 2019) and the knockout of Rab39b-C9ORF72 protein interactor in primary cultures results in increased GluA1 trafficking to dendrites (Mignogna et al., 2021).The observed dysregulation of GluA1 appears in other ALS subtypes, including those associated with TDP-43 and FUS proteinopathies, as well as in sporadic ALS patients (Bursch et al., 2019, Udagawa et al., 2015, Gregory et al., 2020). Interestingly, upregulation of the NMDA receptor subunit GluN1 is also observed in *C9ORF72*^{RE} lower motor neurons (Shi et al., 2018). Recently, *C9ORF72*^{RE} FTD mouse primary neurons show susceptibility of neurons to glutamate-induced excitotoxicity, morphological changes at dendritic spines and hyperexcitation phenotype mediated by increased activity of extrasynaptic GluN2B NMDA receptors (Huber et al., 2022).

1.10.9. Changes in excitability in lower motor neurons

Altered neuronal excitability in *C9ORF72*^{RE} ALS/FTD patients is linked to changes in intrinsic expression of ion channel function that impact on the generation of action potentials (Geevasinga et al., 2015). *In vitro* investigations utilizing iPSC-derived motor neurons from *C9ORF72*^{RE} ALS/FTD patient fibroblasts have extensively explored the physiological mechanisms underlying lower motor neuron excitability (summarised in Table 1.1). Patch-clamp recordings revealed hyperexcitability during early stages of motor neuron differentiation (2-6 weeks in culture) (Devlin et al., 2015, Wainger et al., 2014, Burley et al., 2022). Extended culture periods (7-10 weeks) allowed neurons to transition to a state of hypoexcitability (Sareen et al., 2013, Zhang et al., 2013, Devlin et al., 2015, Naujock et al., 2016, Guo et al., 2017). Notably, no significant changes in cell survival were observed throughout this excitability shift. This finding strengthens the hypothesis that altered excitability represents an early marker of lower motor neuron functional decline preceding overt neurodegeneration, a notion further supported by clinical studies of motor function decline in ALS patients (Iwai et al., 2016). Moreover, these in vitro observations align with the established pattern of shifting excitability observed in motor neurons of mutant SOD1 mice models of ALS (Leroy and Zytnicki, 2015). These mice also exhibit an initial phase of hyperexcitability followed by hypoexcitability, ultimately leading to motor neuron denervation (Martínez-Silva et al., 2018). This shared pattern across models suggests potential convergence of disease mechanisms in different ALS subtypes.

Key mechanisms driving these changes in excitability are starting to emerge. Studies suggest that early-stage hyperexcitability in lower motor neurons may be driven, at least partially, by upstream cortical and upper motor neuron dysfunction. Selective modulation of cortical inhibition in SOD1^{G93A} mice, aimed at reducing potential cortical hyperexcitability, demonstrated a protective effect on lower motor neurons (Khademullah et al., 2020). This suggests a potential causal link between cortical dysfunction and altered excitability in lower motor neurons. Further, multiple studies show progressive loss of glycinergic inputs to lower motor neurons (Allodi et al., 2021, Chang and Martin, 2009, Sunico et al., 2011), which is thought to appear before motor neuron death and is paralleled

by the development of locomotor deficits in SOD1^{G93A} mice (Allodi et al., 2021, Cavarsan et al., 2023).

Furthermore, increased depolarization of motor neurons, has been shown to promote the formation of pathological TDP-43 aggregates (Weskamp et al., 2020) and the production of DPRs (Westergard et al., 2019). These findings suggest a vicious cycle where hyperexcitability can contribute to the development of *C9ORF72*^{RE} ALS/FTD pathology, potentially leading to further excitotoxicity and neurodegeneration.

The use of improved protocols for generating enriched motor neuron cultures from iPSCs has not consistently observed altered excitability in these models (Selvaraj et al., 2018; Zhao et al., 2020). This seemingly contradicts earlier studies. However, Zhao et al. (2020) suggest that the presence of astrocytes in previous studies, due to heterogeneous cellular differentiation protocols, may have influenced the observed hyperexcitability. Their research demonstrates that co-cultures of motor neurons with *C9ORF72*^{RE} astrocytes exhibit hypoexcitability. This highlights the critical non-cell autonomous roles astrocytes play in modulating motor neuron excitability. The influence of astrocytes will be discussed further in section 1.12.

1.10.10. Impaired neurotransmitter release due to the neuromuscular junction in ALS

Motor neuron denervation from the neuromuscular junction occurs before motor neuron loss. Reduced motor unit activity is a hallmark of symptomatic ALS patients and consistent with pre-synaptic dysfunction of motor neurons (Maselli et al., 1993). This dysfunction appears to affect neuromuscular junctions innervating fast-twitch motor neurons in SOD1^{G93A} mice (Cappello and Francolini, 2017). Similar observations of reduced synaptic function have been extended to *Drosophila* and zebrafish models (Cappello and Francolini, 2017, Butti et al., 2021).

Studies in *Drosophila* model overexpressing *C9ORF72* hexanucleotide repeats (58/30 repeats) demonstrate impaired neurotransmitter release and a reduction in active zones at the neuromuscular junction (Freibaum et al., 2015a, Zhang et al., 2015). Furthermore, *C9ORF72*^{RE} iPSC-derived motor neurons exhibit a progressive decrease in spontaneous post-synaptic current activity, directly linked to hypoexcitability rather than motor neuron

loss (Devlin et al., 2015). This suggests a potential inability of these neurons to generate sufficient action potential activity for proper synaptic release. Recently, the presence of poly-GA DPRs at the neuromuscular junction causes muscle weakness, impaired synaptic transmission and altered synaptic function (Tu et al., 2023), highlighting potential early therapeutic intervention for ALS.

Jensen et al. (2020) implicate aberrant vesicle dynamics in ALS pathogenesis. They observed a loss of the synaptic vesicle protein SV2 preceding motor neuron loss in both a poly-GA transgenic mice and *C9ORF72*^{RE} motor neurons. Interestingly, these observations extend beyond motor neurons, with similar reductions in vesicular dynamics observed in cortical neurons, suggesting a potential shared mechanism (Jensen et al., 2020). Coyne et al. (2017) reported that synaptic vesicle cycling defects due to deficits in the post-transcriptional inhibition of Hsc70-4/HSPA8 expression are common to *C9ORF72*^{RE} and mTDP-43 Drosophila models, suggesting a role for vesicle depletion at the neuromuscular junction. Importantly, this mechanism is linked to dynamin function, a key player in axonal transport, potentially connecting synaptic vesicle impairments with established axonal transport deficits in ALS (Gunes et al., 2020).

1.11. Multiple brain areas are impacted in FTD/ALS

As described in Section 1.5, ALS and FTD are characterised by selective structural and functional alterations. However, it has been widely accepted that ALS impacts upon cerebral extra-motor parts of the brain, such as the frontotemporal region, which are equivalently pathologically and degenerative impacted leading to behavioural and/or cognitive deficits (Agosta et al., 2016, Turner and Verstraete, 2015). Cognitive and behavioural manifestations are observed in 65% of ALS patients, while 15% exhibit dementia in early stages of disease manifestation (Goldstein and Abrahams, 2013, Rusina et al., 2021).

Despite substantial progress that has been made in understanding the molecular and genetic pathways involved in FTD/ALS disease spectrum, the precise mechanisms of disease progression and degeneration remain unknown. Immunohistological studies propose the pattern of degeneration in FTD/ALS is initiated in the motor cortex, then

advances to the motor neuron circuitry and subsequently to other sub-cortical nuclei including the striatum (Brettschneider et al., 2013, Riku et al., 2016).

1.11.1. The striatum has been greatly overlooked in FTD/ALS

Importantly, the striatum is an important integrative hub, that has central roles in selecting, planning and executing motor functions, but is involved in higher cognitive functions such as social behaviour, cognition, language generation, receiving inputs from cerebral cortices (Crinion et al., 2006, Crittenden and Graybiel, 2011). These roles strikingly overlap with the cognitive impairments observed in FTD/ALS patients (Pauli et al., 2016). Therefore, impairments of the striatum might be involved in the aberrant cognitive and behavioural perturbations associated with FTD/ALS.

Post-mortem examinations in FTD/ALS patients consistently reveal significant neuronal loss within the striatum (Kato et al., 1994). *In vivo* neuroimaging using MRI and diffusion tensor imaging corroborate these observations. Striatal atrophy and altered diffusivity are observed in ALS patients, including those harbouring the *C9ORF72*^{RE} mutations (Bede et al., 2013b, Lee and Huang, 2017). MRI and vertex analysis reveal a critical role of the striatum, demonstrating a strong correlation between striatal dysfunction and disrupted frontostriatal networks in *C9ORF72*^{RE} patients (Bede et al., 2013b, Bertoux et al., 2015). The presence of severe TDP-43 pathology expands to the striatum of FTD/ALS patients, affecting medium spiny neurons (MSNs), the most abundant neuronal cell type in the striatum, making up to 90% of the total neuronal population (Graveland and DiFiglia, 1985, Gerfen et al., 1990a, Gerfen and Surmeier, 2011). These neurons reduce the striatal input to the behavioural motor system by hampering an adequate response to external stimuli linked to emotionally mediated motor responses (Brettschneider et al., 2013). TDP-43 accumulations are evident in axon terminals of striatal neurons and their projections in substrantia nigra and globus pallidus, supporting the idea that neurotoxic inclusions extend to the targets of striatal neurons in FTD/ALS (Riku et al., 2016).

It is important to note, striatal degeneration represents the main neuropathological feature of Huntington's Disease (HD). However, FTD/ALS patients present degeneration in the ventral striatum (nucleus accumbens) (Vatsavayai et al., 2016a, Pauli et al., 2016),

responsible for behavioural cognitive functions, such as decision making, reward-related behaviour and fluidity of language (Báez-Mendoza and Schultz, 2013), while in HD the degeneration of the dorsal striatum (caudate nucleus and putamen) is favoured, which is involved predominantly in motor function (executive function) (Morigaki and Goto, 2017, Balleine et al., 2007). Despite the strong link of atrophy, TDP-43 pathology and physiology to the cognitive impairments identified in FTD/ALS, the striatum has been greatly overlooked as a contributor to FTD/ALS and functional evidence of striatal contribution in FTD/ALS disease spectrum remains limited.

Neurodegenerative diseases, including ALS and FTD, are characterised by neuronal dysfunction that precedes neuronal loss (Geevasinga et al., 2016b). In this regard, neurophysiological impairments in FTD/ALS represent hallmarks of the disease thought to be prominent early in the disease contributing to pathological mechanisms and underpinning disease symptoms (as described in section 1.10). However, given the rationale of striatal involvement, there remains no direct evidence that striatal neurons are dysfunctional in FTD/ALS. Striatal function likely leads to impaired cognitive function, commonly seen in FTD/ALS patients. This project will address this unmet need.

1.11.2. Aims and hypothesis:

Hypothesis: I hypothesise that striatal neurons – medium spiny neurons – are dysfunctional in the context of FTD/ALS.

To address this hypothesis, I will generate in vitro MSNs from induced pluripotent stem cells (iPSC) obtained from *C9ORF72*^{RE} patients using an established methodology. The usage of iPSC-derived neurons is discussed in detail in Methods section 2.2.1, but in short, this methodology enables the routine generation of enriched populations of human MSNs to be examined in detail. Importantly, I have chosen the *C9ORF72*^{RE} mutation because this mutation is the most common mutation giving rise to FTD/ALS. To examine MSN function, I will use patch-clamp electrophysiology. Its usage is highly appropriate to the assessment of neuronal function, as discussed in detail in Methods section 2.4, however, here I highlight its powerful use in being able to directly examine the excitability of individual neurons. A key objective therefore is to demonstrate whether other neuronal types in other brain

regions away from the cortex and spinal cord also demonstrate neurophysiological dysfunction. This is critical for two reasons; FTD/ALS is increasingly described as a multisystem disorder (Zago et al., 2022), however only limited evidence is around to show that neuronal physiology is impacted beyond cortical and motor neurons in FTD/ALS. Further, as demonstrated by research into motor neuron's function (Wainger et al., 2014, Wainger et al., 2021), electrophysiological studies have the ability to highlight future therapeutic targets. If FTD/ALS is a multisystem disorder, then it must be treated as such.

1.12. Astrocyte toxicity in ALS/FTD

ALS and FTD share disrupted pathways involving oxidative stress, excitotoxicity, RNA processing problems, as above mentioned. This impairment may extend beyond neurons, potentially affecting glial cells as well. The contribution of glial cells to disease progression in ALS has been widely investigated (Vahsen et al., 2021) and is an emerging concept in FTD research as well (Ghasemi et al., 2021). Glial cells are classified into four types: astrocytes, oligodendrocytes, microglia and ependymal cells, of which astrocytes are the most abundant population (Verkhratsky et al., 2019). Here, I focus on astrocytes. Astrocytes in ALS typically exhibit a pathological burden similar to that of neurons. ALS pathology triggers significant morphological changes in astrocytes (Rossi et al., 2008). These changes represent hallmark observations in ALS post-mortem tissue, transgenic models and human cell cultures and include enlargement, increase proliferation and a reactive state (Peng et al., 2020, Haidet-Phillips et al., 2011, Rossi et al., 2008). Some of these changes may precede symptom onset (Howland et al., 2002), while others might be specific to later stages (Haidet-Phillips et al., 2011). Astrocytes can also harbour pathological protein inclusions linked to ALS pathology, like TDP-43 and FUS (Nishihira et al., 2008, Kia et al., 2018), DPRs and RNA foci (Zhao et al., 2020, Varcianna et al., 2019).

Astrocytes are crucial for brain function and are versatile cells in the nervous system, regulating ion balance, clear neurotransmitters, supply energy to neurons, regulate blood flow, and contribute to the blood-brain barrier (Verkhratsky et al., 2019). However, in ALS they play a pathogenic role.

Multiple studies have established the non-cell autonomous contribution of ALS astrocytes to motor neuron degeneration (Taha et al., 2022, Van Harten et al., 2021). Initially, *in vitro* co-culture of mouse embryonic stem cell-derived motor neurons and purified astrocytes from human mutant SOD1 transgenic mice demonstrated a significant detrimental effect of ALS astrocytes on motor neuron viability (Nagai et al., 2007). Subsequent *in vitro* experiments have replicated the toxic effect of ALS astrocytes on motor neuron survival in the context of sporadic ALS and other ALS-linked genetic mutations, including *C9ORF72*^{RE}, *TDP-43*, and *FUS*, utilising both transgenic mice and patient derived motor neurons and astrocytes (Nagai et al., 2007, Di Giorgio et al., 2007, Bilsland et al., 2008, Ferraiuolo et al., 2011, Phatnani et al., 2013, Kia et al., 2018, Provenzano et al., 2022, Meyer et al., 2014, Gatto et al., 2021, Haidet-Phillips et al., 2011, Re et al., 2014). This proposes a broad spectrum of ALS astrocyte-mediated motor neuron toxicity, specific towards motor neurons (Di Giorgio et al., 2008, Haidet-Phillips et al., 2011, Nagai et al., 2007, Re et al., 2014). Importantly, the conditional removal of the SOD1 mutation from astrocytes in SOD1^{G93A} animal model demonstrated a delay in disease progression without affecting disease onset (Yamanaka et al., 2008), while the deletion of mutant SOD1 from SOD1^{G85R} mice delayed disease onset (Lino et al., 2002, Wang et al., 2011). ALS astrocytes promote disease progression and possibly the onset of symptoms.

Several lines of evidence point towards the loss of supportive function and gain of toxic properties that have a detrimental role in ALS and, at the centre of these changes, is the astrocyte membrane, which potentially impacts on ion channel functions and signalling pathways (Verkhratsky et al., 2019). The critical loss of support of astrocytes towards motor neurons is evidenced by the reduced expression of membrane glutamate transporter EAAT2 in ALS (Rosenblum and Trotti, 2017), leading to elevated levels of glutamate and excitotoxicity, established hallmarks of ALS (Van Den Bosch et al., 2006). Beyond glutamate clearance, astrocytes show impaired metabolic support to motor neurons in ALS. Impaired lactate release from ALS astrocytes deprived motor neurons of essential energy substrates (Allen et al., 2019a, Ferraiuolo et al., 2011). ALS astrocytes acquire toxic function that have detrimental effects on motor neurons. These astrocytes release soluble toxic factors (Nagai et al., 2007, Di Giorgio et al., 2008), pro-inflammatory molecules (TNF-α, IL-1α, IL-6) (Haidet-Phillips et al., 2011), through their membranes that are damaging motor neurons.

Contributing to their neurotoxic effect is the disruption of ATP signalling, increased production of reactive oxidative species (Birger et al., 2019) and electrical activity of motor neurons by increased polyphosphate release and leading to excitotoxic cell death (Arredondo et al., 2022). Toxic microRNAs and *C9ORF72*^{RE} DPRs are released from extracellular membrane vesicles and cause motor neuron death (Varcianna et al., 2019, Marchi et al., 2022). The release of toxic factors through the astrocyte membrane, disrupts critical cellular processes and causes motor neuron toxicity, contributing significantly to ALS disease progression. The function of the astrocyte membrane therefore is a critical component in mediating non-cell autonomous astrocyte-induced motor neuron toxicity in ALS. Astrocyte dysfunction is therefore a major therapeutic target in ALS (Pehar et al., 2017, Barbeito, 2018). However, a major obstacle to the development of new therapeutic strategies targeting astrocyte dysfunction is knowing which mechanistic features are pathophysiologically altered and how they contribute to disease.

1.12.1. Aims and hypothesis:

Hypothesis: I hypothesise that astrocyte membrane function is severely disrupted in ALS in order to cause astrocyte dysfunction which ultimately leads to mechanisms of non-cell autonomous mechanisms of toxicity.

To address this, I will generate *in vitro* ALS patient-derived astrocytes using established directed differentiation protocols (Meyer et al., 2014), which is discussed in detail in Methods section 2.2.8. In short, this methodology allows me to generate enriched populations of astrocytes rapidly (~30 days from patient fibroblasts or ~ 2 weeks from iNPC stage) and directly from patient derived fibroblasts. Beyond neuronal physiology, patch-clamp electrophysiology offers a powerful tool to investigate the membrane physiology of other cell types, including astrocytes (Zhou et al., 2021a). Remarkably, despite the dysfunction associated with astrocytes and the level of electrophysiological evidence to implicate electrophysiological motor neuron dysfunction in ALS, there has been no electrophysiological characterisation of the astrocyte membrane physiology in the context of ALS/FTD. By doing this, I expect to extend our understanding of astrocyte dysfunction in ALS/FTD and, in doing so, this information may lead to new therapeutic strategies.

2. CHAPTER 2: Materials and methods

2.1. Cell Culture Methods

This work will use human stem cell technology to generate *in vitro* neurons - medium spiny neurons (MSNs), motor neurons (MNs) and astrocytes from ALS/FTD patients. In the first part, I will describe the *in vitro* human models that I employed in my work. Later, the patch-clamp electrophysiological technique will be introduced.

2.2. Brief introduction to human stem cell technology

For decades, neurological research faced limitations that hindered our understanding of human brain function and disease due to reduced access to relevant human tissues, scarce and end of life post-mortem samples and the limited availability of adequate non-human transgenic models. Furthermore, whilst human, convenient and widely used, non-specialised clonal cells (e.g. human embryonic kidney cells- HEK, and Henrietta Lacks- HeLa cell lines), lack the specificity required for studying cell types present in different brain regions, hindering the ability to investigate region-specific diseases. The emergence of human stem cell technology has revolutionised this landscape, offering a readily available source of human-derived, region-specific cell populations. This technology therefore allows the study of human brain physiology, neurological diseases and generation of human specific platforms to establish new therapeutic strategies (Gage and Temple, 2013, Zhao and Moore, 2018).

This research will incorporate two well-established human stem cell technology approaches – induced pluripotent stem cell technology (iPSC) and directly-induced differentiation to generate iPSC-derived striatal, medium spiny neurons (2.2.5), iPSC-derived motor neurons (2.2.6) and directly-differentiated astrocytes (2.2.9).

2.2.1. The use of iPSCs in neurodegenerative disease modelling

The emergence of iPSC technology has revolutionized the generation of patient-specific cell populations, reflecting the unique genetic landscape of each individual, enabling disease modelling and translational research. iPSCs are specialised cells that indefinitely self-

renew, meaning that they have a (theoretically) unlimited supply. They are generated from adult somatic cells, such as skin and blood cells, and reprogrammed into a pluripotent state, described as the ability to differentiate into all three developmental germ layers and their derived cell lineages (Figure 2-1). To introduce the model further, I will review the historical journey of iPSC generation, emphasizing key conceptual and practical advances leading to their current, widespread use in research.

iPSC technology builds on significant pioneering work related to the concept of pluripotency. Key proof that stem cells could differentiate into new cells of a defined fate was generated by Till and McCulloch, when bone marrow (hematopoietic) cells were

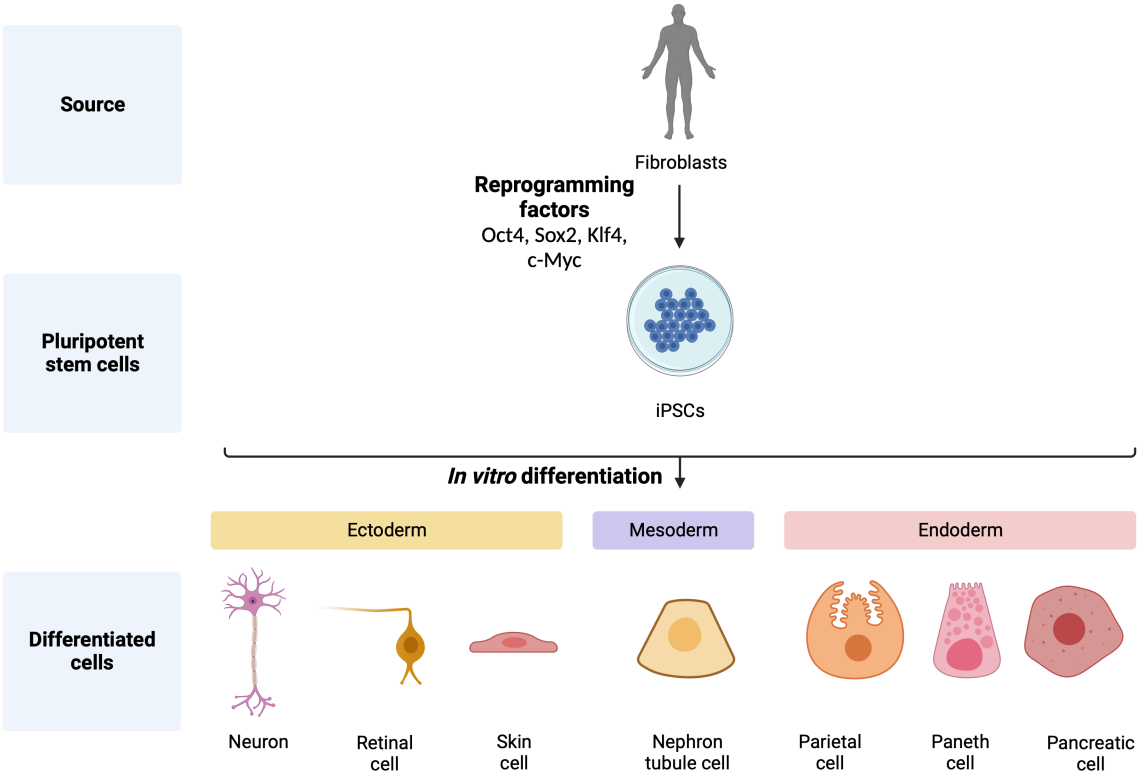

Figure 2-1. ***From patient to disease model.*** *Somatic cells (e.g. fibroblasts, hematopoietic cells, peripheral blood mononuclear cells, squamous epithelial cells, keratinocytes) are isolated from patients or donors. The cells are reprogrammed into iPSCs via retroviral transduction using pluripotency transcription factors also known as the 'Yamanaka factors' (Oct4, Sox2, c-Myc, Klf4), regaining pluripotency. iPSCs undergo differentiation into specific cell lineages by pharmacologically manipulating signalling pathways and transcription factors, according to defined developmental cellular specification, to progressively drive iPSCs towards the desired cell fate. iPSCs can be induced via the tri-lineage developmental lineages, ectoderm, mesoderm and endoderm. Neural progenitor cells are derived from ectodermal lineage development and are differentiated to neurons. Figure created with BioRender.*

transplanted into irradiated mice, which removed endogenous mesenchymal stem cells, and subsequently observed colonies of cells forming in the spleen. They concluded that these colonies originated from a single cell, which was capable of self-renewal and differentiation, called a stem cell (Becker et al., 1963, Siminovitch et al., 1963). However, it was only until 1981, with the establishment of the first mouse embryonic stem cell (mESC) lines, the stem cell field had a laboratory resource which could be employed to theoretically generate cells types of interest, and alongside, introduced the pluripotency concept (Evans and Kaufman, 1981). In 1998, Thompson successfully isolated human embryonic stem cells (hESCs). These hESCs are developed from pre-implantation embryos and can generate any cell in the body (Thomson et al., 1998). However, the use of ESCs was fraught with strong ethical concerns related to embryo destruction and this hindered its clinical applications. Due to its source from the embryo, ESCs are limited in supply, restricting broader therapeutic applications. Hence there was an urgent need for a new source of human stem cells from already differentiated human cells to bypass the drawbacks of embryonic sources of stem cells.

Induced pluripotency, a concept by which a differentiated cell could be evoked back to a stem cell fate, offered a solution to many of the challenges of ESC-based methodologies. It was Gurdon in the 1960s who hinted that differentiated cells might retain their potential to revert to a pluripotent state (Gurdon, 1962). This was the first example of cellular reprogramming by reporting the generation of tadpoles from enucleated unfertilized frog egg cells that had been transplanted with the nucleus from already specialized cells. This remarkable method of reprogramming somatic cells to the pluripotent embryonic state with the same genetic background was termed somatic cell nuclear transfer (SCNT). This method led to the birth of cloning. Three decades later, Ian Wilmut and his team used the same SCNT strategy of cellular reprogramming in the cloning of Dolly the sheep, the first mammalian generated by somatic cloning (Wilmut et al., 1997). These two scientific breakthroughs in somatic cloning proved that the nuclei of differentiated cells contain all the necessary genetic information to generate a whole organism and that the egg cell contains the necessary factors to bring about such reprogramming. Substantially refining these concepts at the experimental level, Yamanaka and colleagues demonstrated the

ability to reprogram adult fibroblasts into iPSCs by introducing just four transcription factors, the 'Yamanaka factors', Oct3/4, KIf4, Sox2, and c-Myc (Takahashi and Yamanaka, 2006, Takahashi et al., 2007). Subsequently, Yamanaka and Gurdon jointly received the Nobel Prize in Physiology or Medicine in 2012 for their discovery that mature cells can be reprogrammed into a pluripotent state. This innovative method, with its non-invasive nature, opened the path for generating theoretically unlimited cell populations from patients, providing a new, easily accessible human disease model, offering an alternative to animal models in research.

2.2.2. Brief introduction to direct reprogramming: induced neuronal progenitor cells (iNPCs)

Direct lineage reprogramming offers a rapid and reproducible approach to generate clinically relevant cell types by bypassing the pluripotent stage of iPSC generation. Direct reprogramming of human somatic cells, such as fibroblasts into differentiated cells in the central nervous system has several advantages (as well as disadvantages) over human iPSC technology for disease modelling. First, the direct conversion does not require the generation of iPSCs, which can cause chromosomal aberrations (Araki et al., 2020) and resets the entire epigenetic and aging signature (Yang et al., 2015). Direct reprogramming maintains many hallmarks of aging, such as epigenetic marks and mitochondrial dysfunction (reviewed in (Aversano et al., 2022)). Second, the availability of fibroblasts or blood cells from individuals carrying specific mutations allows the generation, in a relatively short time, of neurons, astrocytes or oligodendrocytes and studying their phenotypes. Directly reprogrammed neurons, however, remain post-mitotic, limiting their expansion. A solution was developed by converting fibroblasts to expandable neuronal progenitor cells (Meyer et al., 2014). These iNPCs, while retain donor aging features, can be differentiated into various cell types, including induced astrocytes (iAstrocytes) (Gatto et al., 2021) as illustrated in Figure 2-2.

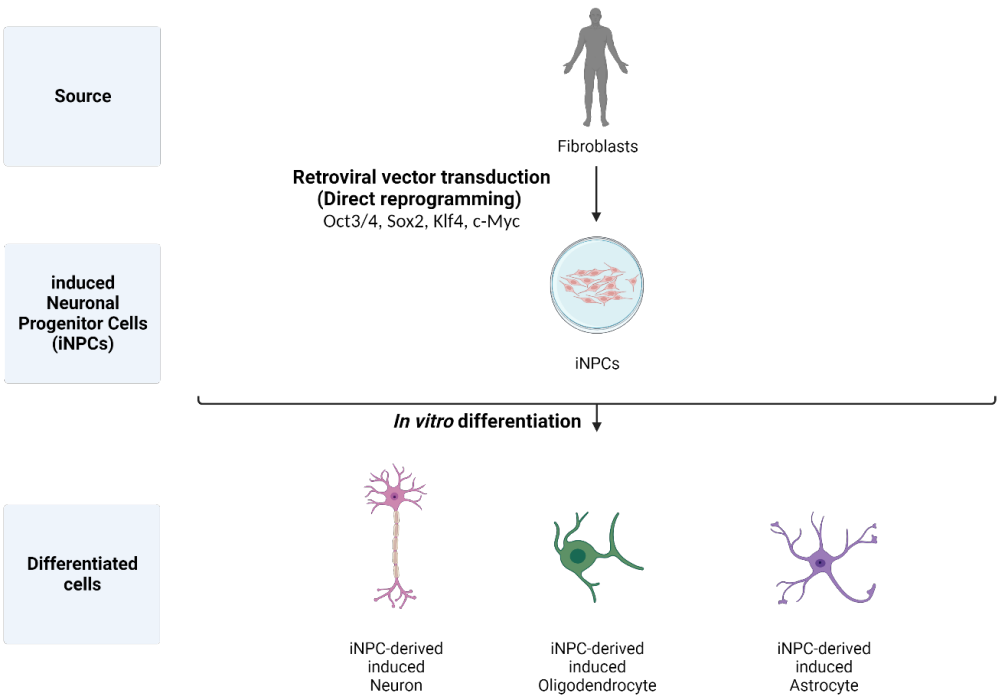

Figure 2-2. ***Direct reprogramming protocol of human fibroblasts to iNPCs.*** *Fibroblasts were injected with a mixture of retroviral vectors expressing four reprogramming factors (Sox2, Kfl4, Oct3/4, c-Myc). To generate iNPCs, the culture media was switched to medium containing growth factors, such as fibroblast growth factor 2 (FGF2), epidermal growth factor 2 (EGF2) and heparin. The iNPCs are further differentiated and can give rise to neurons, oligodendrocytes and astrocytes. Figure created with BioRender.*

2.2.3. iPSC lines maintenance

Human iPSCs were obtained from either the Cedai-Sinai biorepository or Coriell, or prior generated 'in house' under full ethical guidelines and clearance (Table 2-1). All the cultureware and reagents used for the differentiation of iPSC-derived MSNs and MNs with their associated supplier, catalogue number are listed in section 2.2.7. 6-well culture plates were coated with Matrigel (diluted to 0.1 µg.mL in cold KnockOut DMEM medium) for one hour at room temperature prior to seeding. Matrigel was used as it mimics the natural extracellular matrix (ECM) and provides an optimal environment for cell growth, survival and differentiation. iPSCs were maintained on 6-well plates containing mTeSR™ medium, a serum-free widely used medium for maintaining human pluripotent stem cells in culture. Media was replaced every 2 days. Every 4-6 days, the cells were passaged as clumps using ReLeSR™, an enzyme-free reagent that minimizes the stress of cells, thus, improving viability and pluripotency, according to manufacturer's instructions.

Cell line	In text abbreviation	Clinical information	Mutation	Gender	Age at sampling (years)	Source
GM23338	Con-1	Healthy	Unknown	M	55	Coriell
MIFF1	Con-2	Healthy	Unknown	M	Foetal/neonatal	TUoS
CS28iALS-C9nxx	C9-2	Age of onset: 46; Site of onset: left upper extremity.	C9orf72 hexanucleotide repeat expansion (6-8 kb)	M	47	Cedars-Sinai
CS29iALS-C9nxx	C9-3	Age of onset: 46; Site of onset: left upper extremity.	C9orf72 hexanucleotide repeat expansion (6-8 kb)	M	47	Cedars-Sinai
CS52iALS-C9nxx	C9-1	ALS, Age of onset: 57; months disease duration, 48; Site of onset: Left upper extremity	C9orf72 hexanucleotide repeat expansion (6-8 kb)	M	49	Cedars-Sinai
CS52iALS-C9n6.ISOxx	C9-Δ1	ALS, Age of onset: 57; months disease duration, 48; Site of onset: Left upper extremity	Isogenic control line of CS52iALS-nxx (C9orf72 HRE Corrected)	M	49	Cedars-Sinai

Table 2-1. ***Information on iPSC lines.*** *The table highlights the identifying code for each cell lines derived from donors/patients from their respective repository and in text abbreviation. Included is a brief publicly available clinical description of the patients' and diagnosis relevant to the study (this includes the age of disease onset, site of onset); the specific genetic alteration identified in each patient and repeat expansion length; the sex of the patient (male or female); patient's age at the time the samples were collected and the source from where the cells were acquired. For the latter, the cell lines were provided by the Coriell Institute for Medical Research, The University of Sheffield (TUoS) and the Cedar-Sinai Medical Centre. The tissue source used to create the cell line was skin fibroblast for all line, except for MIFF1 which was sourced from foetal foreskin fibroblasts. These iPSCs have been chosen as they have been already mentioned in publications and have been established in the labs. Note ALS-52 also available as iNPC (Table 2-13).*

2.2.4. iPSC to NPC differentiation

iPSC to NPC differentiation was performed by adapting an already established protocol (Du et al., 2015). Small molecules were added at controlled times to guide iPSC differentiation into NPCs and then promote their expansion. iPSC lines at 100% confluency were washed with PBS to remove debris and neutralised by switching to iPSC-NPC day 1-6 media (Table 2-3) to promote neural fate commitment. Media was replaced daily. On day 7, cells were switched to day 7-12 iPSC to NPC differentiation media (Table 2-4) supplemented with retinoic acid and puromorphamine for further neuronal differentiation. Media changes continued every 24 hours. Between day 7-9, cells were lifted from plate and passaged. For passaging, cells were washed with warm HBSS, followed by incubation with 1mL Accutase, a commonly used gentle enzyme that cleaves cell surface adhesion molecules and extracellular matrix components, for 7 minutes at 37°C. Accutase was neutralised with an equal volume of medium and the cell suspension was centrifuged at 200g for 4 minutes. The cell pellet was resuspended in medium containing 10 µM Y27632 Rho-associated protein kinase (ROCK) inhibitor for enhanced survival until the next day's media change. ROCK inhibition with Y27632 enhances cell survival by reducing apoptosis (Rock signalling stimulates cell death pathways), maintains cytoskeletal integrity (Rock regulates actin and myosin activity, crucial for cell shape and adhesion. Y27632 prevents excessive cytoskeletal contraction, reducing cell damage and detachment) and enhances cell attachment (ROCK inhibition promotes cell adhesion to the culture substrate after plating). Cells were replated onto fresh Matrigel-coated 6-well plates and differentiation followed. By day 12, the cells display neural rosettes, characteristic for NPCs and lack iPSC morphology. Immunofluorescence confirm the expression of characteristic NPC markers (Nestin and Pax6 – as shown in Figure 3-2). Following day 12, cells were passaged with Accutase and replated onto new Matrigel-coated 6-well plates. The cells were maintained in NPC expansion media (Table 2-5), which was changed every 48 hours. The NPCs were frozen with 10% DMSO and stored at -80°C until needed, or differentiation into MNs or MSNs was started.

Component	Concentration	Purpose
KnockOut DMEM/F12	48% (v/v)	Serum-free media specially formulated for stem cell cultures.
Neurobasal media	48% (v/v)	Serum-free media formulated for culturing neural cells.
B-27 supplement	1% (v/v)	Serum-free mixture of antioxidants, vitamins, hormones that support the differentiation and maturation of neural cell, promoting neurite outgrowth and neuronal function.
GlutaMax™	1% (v/v)	L-glutamine supplement, essential for energy metabolism, protein synthesis and cell proliferation.
N-2 supplement	0.5% (v/v)	Serum-free mixture of hormones and growth factors that support cell survival, proliferation and metabolic functions of neural cells.
Penicillin/Streptomycin	1% (v/v)	Combination antibiotic used to prevent bacterial contamination, essential for maintaining sterile conditions.

Table 2-2. ***Basal media composition.*** *The basal media provides the basic nutrients and energy needed for cell survival and growth, promoting neural fate and differentiation in stem cells. The table contains information about all constituents of the basal media, their concentration and the purpose of each component.*

Component	Concentration	Purpose
Basal media (Table 2-2)		
CHIR99021	3 µM	GSK3-β (neural differentiation suppressor) inhibitor. Activation of neural fate decisions.
DMH-1	2 µM	TGF-β (neural differentiation inhibitor) inhibitor. Activation of neural commitment.
SB431542	2 µM	BMP receptor (promotes non-neuronal lineages, i.e. mesodermal and endodermal) inhibitor. Encourages neural fate.

Table 2-3. ***iPSC to NPC (day 1-6) media composition****. iPSC to NPC (Day 1-6) media provides essential nutrients for cell survival and reagents block pathways that prevent neural differentiation and encourage neural fate.*

Component	Concentration	Purpose
Basal media (Table 2-2)		Provides basic nutrients like vitamins, aminoacids and glucose for cell survival and growth. No growth factors added to reduce proliferation and promote differentiation by limiting cell fate options.
CHIR99021	1 μM	GSK3-β (neural differentiation suppressor) inhibitor. Activation of neural fate decisions.
DMH-1	2 μM	TGF-β (neural differentiation inhibitor) inhibitor. Activation of neural commitment.
SB431542	2 μM	BMP receptor (promotes non-neuronal lineages, i.e. mesodermal and endodermal) inhibitor. Encourages neural fate.
Retinoic acid (RA)	0.1 μM	Member of vitamin A family involved with development and cell signalling. Potent neural induces, promotes neurite outgrowth, enhances neural fate commitment.
Purmorphamine (PUR)	0.5 μM	Small molecule that activates Sonic hedgehog (Shh) signalling and promotes neural fate commitment.

Table 2-4. ***iPSC to NPC (day 7-12) media composition****. iPSC to NPC (Day 7-12) contains same core ingredients as previously described media with added retinoic acid (RA) and purmorphamine (PUR) that promote neuronal differentiation within the NPC population.*

Component	Concentration	Purpose
Basal media (Table 2-2)		Provides basic nutrients like vitamins, aminoacids and glucose for cell survival and growth. No growth factors added to reduce proliferation and promote differentiation by limiting cell fate options.
CHIR99021	3 μM	GSK3-β (neural differentiation suppressor) inhibitor. Activation of neural fate decisions.
DMH-1	2 μM	TGF-β (neural differentiation inhibitor) inhibitor. Activation of neural commitment.
SB431542	2 μM	BMP receptor (promotes non-neuronal lineages, i.e. mesodermal and endodermal) inhibitor. Encourages neural fate.
Retinoic acid (RA)	0.1 μM	Member of vitamin A family involved with development and cell signalling. Promotes neuronal differentiation, neurite outgrowth, enhances neural fate commitment.
Purmorphamine (PUR)	0.5 μM	Small molecule that activates Sonic hedgehog (Shh) signalling and promotes neural fate commitment.
Valproic acid (VPA)	0.5 μM	Histone deacetylase inhibitor, modifying chromatin structure and gene expression patterns in NPCs. Promotes NPC expansion by regulating cell cycle and cell death pathways.

Table 2-5. ***NPC expansion media composition****. NPC expansion media promotes proliferation and maintenance of NPCs. NPC expansion media maintains core ingredients to support NPCs with added valproic acid (VA) to increase NPC proliferation and survival.*

2.2.5. NPC to medium spiny neuron (MSN) differentiation

The differentiation of MSNs from NPCs (Figure 2-3) was adapted from a previously established protocol (Lin et al., 2015). NPCs were cultured in NPC expansion media (Table 2-5) until they reached 100% confluency. Then the media was switched to GABA 1 day 13-24 media (Table 2-6) which was changed every 48h to create a controlled environment that favours GABAergic MSN differentiation. On day 20-21, cells were gently dissociated with Accutase and cell counts were determined using haemocytometer (0.1 mm depth, Marienfield). For electrophysiological recordings, 13mm coverslips were sterilised in 70% industrial methylated spirit (IMS) for at least 1h. The coverslips were delicately transferred to 24-well plates using sterilised forceps. The coverslips were incubated overnight with 0.1 mg.mL polyornithine in distilled water to enhance cell attachment and adhesion to glass coverslips, then washed 3 times with PBS before a one-hour incubation with Matrigel. For electrophysiology recordings, 120,000-150,000 cells were replated per well, while 30,000 cells were replated per well on optical 96-well plates for immunocytochemistry (Table 2-12). On the day of plating, the medium was supplemented with 10 μM Y-27632 ROCK inhibitor to promote survival. Cells were switched to fresh medium the next day. The media was changed every 48h and differentiation continued. On day 25, the medium was switched to GABA 2 media day 25-72 media (Table 2-7) to promote neuronal maturation. This media was changed every 48 hours until day 72. Cells were characterised at day 32, day 52 and 72 of differentiation, and expressed neuronal (β3-tubulin and MAP2) and, at later stages of differentiation, mature GABAergic medium spiny neuron markers (GABA, DARPP32).

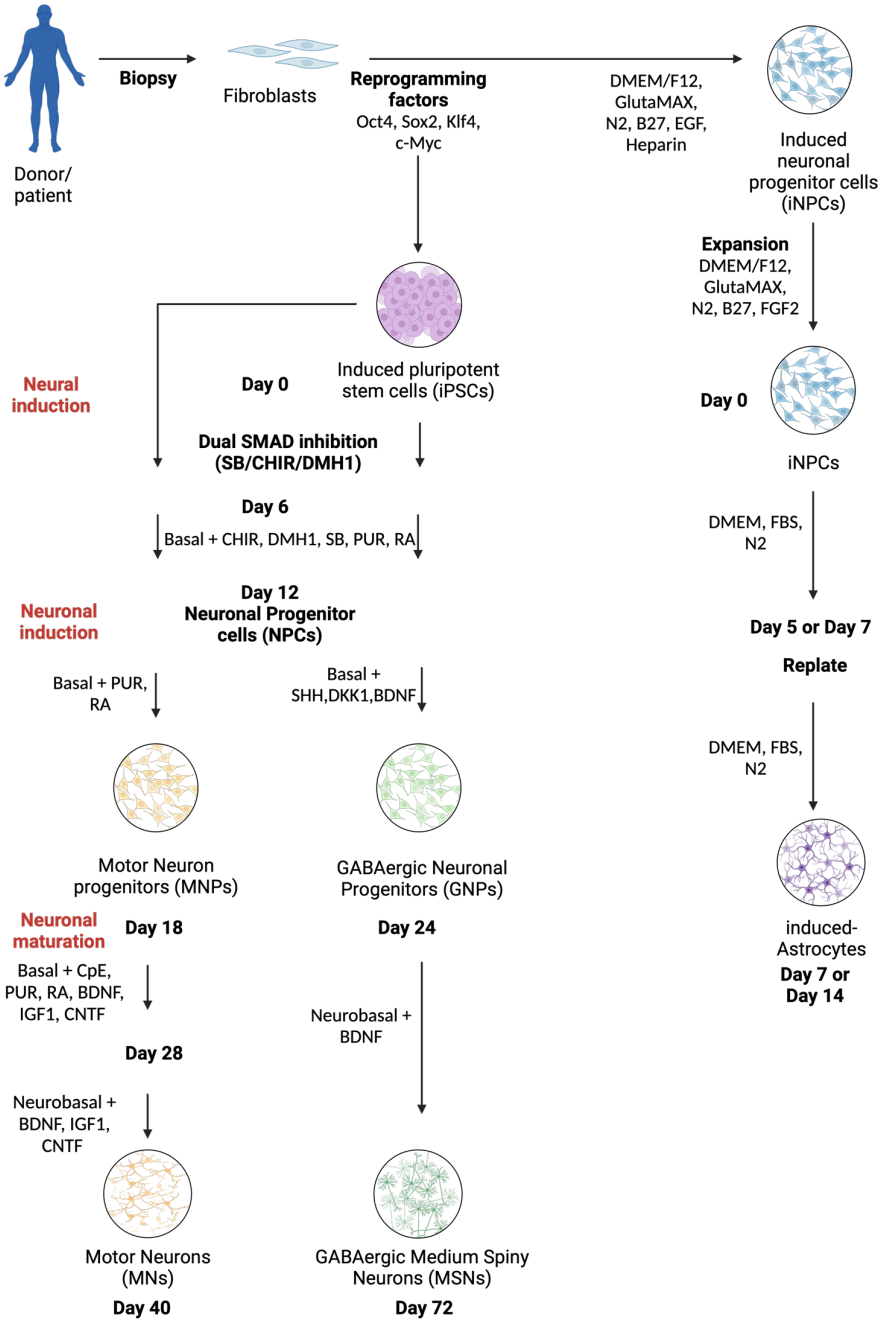

Figure 2-3. ***Multi-step in vitro differentiation protocol of patient-derived MSNs, MNs and astrocytes.*** *This schematic illustrates a multi-step protocol for generating three cell types in the CNS from patient fibroblasts: MSNs, MNs and astrocytes. Fibroblasts are isolated, cultured and exposed to specific media containing a cocktail of four transcription factors, inducing reprogramming into pluripotent iPSCs or straight into induced neuronal progenitor cells (iNPCs), bypassing the pluripotent stem cell stage. The iPSCs undergo neural induction through a dual-SMAD inhibition protocol to form NPCs. NPCs are exposed to MN- or MSN-specific factors to generate precursor cells, which undergo maturation with relevant factors to drive the acquisition of mature MNs or MSNs features. For the direct conversion, the expanded iNPCs are exposed to DMEM, FBS and N-2 to promote astroglial lineage commitment. Differentiating iAstrocytes exhibit mature astrocyte morphology and functionality. Figure created with BioRender.*

Component	Concentration	Purpose
Basal media (Table 2-2)	Media base	Provides basic nutrients like vitamins, aminoacids and glucose for cell survival and growth. No growth factors added to reduce proliferation and promote differentiation by limiting cell fate options.
Brain-derived neurotrophic factor (BDNF)	30 ng/mL	TrkB receptors activator, triggering signalling pathways that promote neuronal survival and neurite outgrowth. GABAergic marker (GAD67 and GAT-1) enhancer, contributing to GABA synthesis and uptake. Increases synaptic formation and connectivity between GABAergic neurons.
DKK-1	100 ng/mL	Secreted protein that inhibits Wnt signalling (Wnt can suppress neuronal differentiation and favour other cell fates) DKK-1 binds to Wnt receptors and blocks their activity by preventing the inhibition of GABAergic differentiation. Allows pro-differentiation factors like SHH to exert their function more effectively.
SHH	200 ng/mL	Signalling molecule that promotes neural development. Promotes patterning of the ventral neural tube, where GABAergic neurons originate. SHH induces ventral identity in neuronal progenitors to enhance GABAergic neuronal fate commitment. Upregulates expression of Pax6 and Nkx2.1, essential for GABA neuron development.

Table 2-6. ***GABA 1 media day 13-24 composition.*** *A combination of factors was used with basal media to create a controlled environment that favours GABAergic neuron differentiation. Table contains information about the essential components used, the concentration they were used at and the purpose of each reagent. Each reagent provides essential support for neuronal fate commitment, promoting survival and neurite outgrowth.*

Component	Concentration	Purpose
Neurobasal media	Media base	Provides basic nutrients like vitamins, aminoacids and glucose for cell survival and growth, optimised for neuronal cells. No growth factors added to reduce proliferation and promote differentiation by limiting cell fate options. Specialized support for mature neuronal function.
B-27 supplement	2% (v/v)	Rich source of antioxidants that reduce reactive oxidative species, protecting neurons and facilitating healthy development. Contains nutrients (selenium, iron) important for neurite growth and synaptic formation. Promotes cell survival and neurite outgrowth by supporting protein synthesis and iron transport.
Penicillin/Streptomycin	1% (v/v)	Antibiotic combination that prevents bacterial contamination and ensures sterile environment, minimizing stress or damage to differentiating neurons.
Brain-derived neurotrophic factor (BDNF)	50 ng/mL	TrkB receptors activator, triggering signalling pathways that promote neuronal survival and neurite outgrowth. Enhances GABAergic neuron maturation by increasing expression of GABAergic markers like GAD67 and GAT-1, facilitating GABA synthesis and uptake for mature neuronal function. Stimulates neurite growth and branching and promotes long-term survival and maintenance of GABAergic neurons.

Table 2-7. ***GABA 2 media day 25-72 composition****. The table contains information about component used for GABAergic neuron maturation media, including concentration and purpose. The combined effect of these reagents fosters a supportive environment for GABAergic neuron maturation.*

2.2.6. NPC to motor neuron (MN) differentiation

NPC differentiation into motor neurons (Figure 2-3) was adapted from Du et al. (2015). At 100% confluence, NPCs were transitioned from NPC expansion media (Table 2-5) to motor neuron day 13-18 differentiation media (Table 2-8), changed every 48 hours. At day 19 of differentiation, the cells were switched to motor neuron day 19-28 differentiation media (Table 2-9), also changed every 48 hours. On days 20-21, cells underwent gentle enzymatic dissociation with Accutase, followed by cell counting using a haemocytometer. The cells were resuspended and replated onto Matrigel-coated plates supplemented with 10µM Y27632 ROCK inhibitor to promote survival and adhesion. 20,000-30,000 cells per well were

plate on optic 96-well plate for co-culture experiments, followed by immunofluorescence staining assays. Fresh medium was added 24h after replating and differentiation continued. Media was changed every 48 hours. On day 29 of differentiation, the media was swapped to day 29-40 media (Table 2-10), which was replaced every 48h, with differentiation continuing until or beyond day 40.

Component	Concentration	Purpose
Basal media (Table 2-2)	Media base	Provides basic nutrients like vitamins, aminoacids and glucose for cell survival and growth. No growth factors added to reduce proliferation and promote differentiation by limiting cell fate options.
All-trans retinoic acid (RA)	0.5 µM	Promotes neural fate commitment by suppressing alternative lineages, enhancing motor neuron specification within the neutralized population. Upregulates key neural progenitor genes, like SOX1 and PAX6, essential for obtaining neural identity. Patterns the ventral neural tube, where motor neurons originate, providing spatial cues for motor neuron specification.
Puromorphamine (PUR)	0.1 µM	SHH signalling agonist that induces ventral identity, a prerequisite for motor neuron specification. Upregulates motor neuron-specific genes, like HB9 and Islet1/2, key transcription factors for establishing motor neuron fate and identity. Promotes survival and proliferation of early motor neuron precursors.

Table 2-8. ***MN day 13-18 media.*** *This combination of reagents provides a supportive environment for initial motor neuron differentiation. The table highlights the key components, their concentration and purpose.*

Component	Concentration	Purpose
Basal media (Table 2-2)	Media base	Provides basic nutrients like vitamins, aminoacids and glucose for cell survival and growth. No growth factors to reduce proliferation, promoting differentiation by limiting cell fate options.
All-trans retinoic acid (RA)	0.5 µM	Promotes neural fate commitment by suppressing other lineages, enhancing motor neuron specification. Upregulates key neural progenitor genes, like SOX1 and PAX6, essential for obtaining neural identity. Patterns the ventral neural tube, the origin of motor neurons.
Puromorphamine (PUR)	0.1 µM	SHH signalling agonist that induces ventral identity, a prerequisite for motor neuron specification. Upregulates ventral motor neuron-specific genes, like HB9 and Islet1/2, key for establishing motor neuron fate. Promotes survival and proliferation of early motor neuron precursors.
Compound-E	0.1 µM	Bone morphogenic protein (BMP) signalling inhibitor (BMP can suppress motor neuron differentiation in favour of other lineages) preventing this inhibitory effect. Enhances motor neuron specification, allowing SHH and RA signalling to promote motor neuron commitment. Potentiates SHH signalling, further promoting motor neuron specification.
Brain-derived neurotrophic factor (BDNF)	10 ng.ml	Neurotrophic factor providing essential support for survival, growth, and maturation of differentiating motor neurons. TrkB and LIF receptors activator, triggering pathways that protect against cell death and promote survival of motor neuron precursors.
Ciliary neurotrophic factor (CNTF)	10 ng.ml	Neurotrophic factor providing essential support for survival, growth, and maturation of differentiating motor neurons. TrkB and LIF receptors activator, triggering pathways that protect against cell death and promote survival of motor neuron precursors. Promotes neurite outgrowth and connectivity.
Insulin-like growth factor-1 (IGF-1)	10 ng.ml	Neurotrophic factor providing essential support for survival, growth, and maturation of differentiating motor neurons. Promotes neurite outgrowth and connectivity.

Table 2-9. ***MN day 19-28 media.*** *The table highlight media composition used in the middle stages of motor neuron differentiation, including each factor and their concentration, alongside with their purpose in the media. This combination of factors aids in the differentiation of motor neurons.*

Component	Concentration	Purpose
Neurobasal media	Media base	Provides basic nutrients like vitamins, aminoacids and glucose for cell survival and growth, optimised for neuronal cells. Specialized support for mature neuronal function.
B-27 supplement	2% (v/v)	Rich source of antioxidants that reduce reactive oxidative species, protecting neurons and facilitating healthy development. Contains nutrients (selenium, iron) important for neurite growth and synaptic formation. Promotes cell survival and neurite outgrowth by supporting protein synthesis and iron transport.
Penicillin/ Streptomycin	1% (v/v)	Antibiotic combination that prevents bacterial contamination and ensures sterile environment, minimizing stress or damage to differentiating neurons.
Brain-derived neurotrophic factor (BDNF)	10 ng.ml	Neurotrophic factor providing essential targeted support for motor neuron maturation. TrkB receptors activator, promoting survival, axonal outgrowth and expression of mature motor neuron markers like ChAT and MAP2.
Ciliary neurotrophic factor (CNTF)	10 ng.ml	Neurotrophic factor providing essential targeted support for motor neuron maturation. GP130 receptor modulator, enhancing neuronal survival, axonal branching and neuromuscular junction formation.
Insulin-like growth factor-1 (IGF-1)	10 ng.ml	Neurotrophic factor providing essential targeted support for motor neuron maturation. PI3K/Akt pathway activator, promoting survival, axonal transport and synaptic refinement.

Table 2-10. ***MN day 29-40 media.*** *The table contains information about the media composition used in the final stages of motor neuron differentiation to support motor neuron maturation, including concentration and purpose. The combined effect of all elements supports an environment efficient for maturation of the motor neurons, triggering specific maturation pathways to generate functional neurons and synapses.*

2.2.7. Reagents and cultureware information relevant for the differentiation of iPSC-derived MNs and MSNs

Reagent	Supplier	Catalogue Number
Accutase	Sigma-Aldrich	A6964-100ML
B-27 supplement	Gibco	11530536
CHIR99021	Merck Millipore	SML1046-25MG
Dickkopf related protein 1 (DKK1)	Peprotech	120-30
DMEM	Gibco	11520416
DMH-1	Merck Millipore	D8946-25MG
Glutamax™	Gibco	35050061
HBSS	Thermo Fisher Scientific	14170112
Human Recombinant Brain derived neurotrophic factor (BDNF)	Peprotech	AF-450-02
Knockout DMEM	Gibco	10829018
KnockOut DMEM/F12	Gibco	12660012
Matrigel	Corning	356230
N-2 supplement	Gibco	15410294
Neurobasal media	Gibco	11570556
Penicillin/Streptomycin	Lonza	DE17-603E
Polyornithine	Sigma-Aldrich	P3655-100MG
Purmorphamine (PUR)	Merck Millipore	SML0868-25MG
ReLeSR	StemCell Technologies	05872
Retinoic acid (RA)	StemCell Technologies	72264
SB431542	Peprotech	3014193
Sonic hedgehog (SHH)	Peprotech	100-45
Valproic acid (VPA)	Merck Millipore	PHR1061-1G
Y27632 Rock inhibitor	Peprotech	1293823

Table 2-11. ***Cell culture reagents used for the differentiation of MNs and MSNs from iPSCs.*** *The table includes the specific chemical or reagent used in this study, the commercial supplier form which the reagent was obtained and the manufacturer's identifier for the specific product.*

Reagent	Supplier	Catalogue Number	Purpose
Corning 6-well plate	Corning	3506	iPSC/MSN plating
24-well plate	Greiner	662 160	MSN/iA plating
Optic 96-well plate	Greiner	G655090	Plating for ICC
13mm coverslips	Scientific Laboratory Supplies	MIC3336	MSN plating

Table 2-12. ***Information about cultureware.*** *The table highlights the specific culture used in this project, the commercial supplier, the manufacturer's identifier for the specific product and purpose of each cell cultureware. The table mentions a selection of cell cultureware, including dishes, multiwell plates used to plate the iNPC-astrocytes (iAstrocytes) and iPSC-derived medium spiny neurons (MSNs) and/or motor neurons (MNs). Optic 96-well plates were used for immunocytochemistry (ICC) and co-culture experiments.*

2.2.8. Direct conversion of fibroblast to iNPC

Induced neuronal progenitor cell (iNPC) lines (Table 2-13) were previously reprogrammed from control and patient fibroblasts obtained from skin biopsies according to an already established protocol (Meyer et al., 2014). Patient fibroblasts were obtained under full ethical guidelines and clearance. All skin biopsy donors provided informed consent before sample collection (University of Sheffield, Study number STH16573, Research Committee reference 12/YH/0330; MODEL-AD study, Yorkshire and Humber Research and Ethics committee number: 16/YH/0155). Cultureware and reagents mentioned in this section are listed in 2.2.11. The transduction of skin fibroblasts with four reprogramming retroviral vectors expressing Kruppel-like factor 4 (Klf4), POU transcription factor *Oct-3/4,* SRY-related HMG-Box Gene 2 (*Sox2*), and *c-Myc* (Takahashi and Yamanaka, 2006) and growth factors FGF2, EGF and heparin to generate iNPC was done by the Shaw/Ferraiuolo laboratories. After 48 hours, iNPCs were cultured into iNPC expansion culturing media (Table 2-14). The morphological changes were apparent after 48 to 72h from fibroblast-like to a sphere-like form or proliferation in rosettes characteristic to NPCs. Cell proliferation occurred quickly, and cells were split at 100% confluency. iNPCs were lifted and cells collected using Accutase and, depending on the rate of growth, they were transferred to 10 cm dishes coated with human plasma fibronectin over a period of 18-21 days. Above 95% of cells express neuronal progenitor cells specific markers, such as Nestin and PAX6 (already established in the Ferraiuolo lab/SITraN). These iNPC populations are expanded and stored multiple passages. These lines are thought to retain aging properties of donors (Gatto et al., 2021).

Cell line	In text abbreviation	Clinical information	Mutation	Gender	Age at sampling	Source
155v2	Con-2	Healthy	-	M	40	STH/Genomics
CS142	Con-1	Healthy	-	F	30-35	Cedars
ALS52	C9-1	ALS	C9ORF72	M	49	TUoS
78	C9-2	ALS	C9ORF72	M	66	TUoS
SHF-077	sALS-1	ALS	Sporadic (slow)	F	58	STH/Ambrosia
SHF-196	sALS-2	ALS	Sporadic (fast)	F	83	STH/Ambrosia
SHF-142	FTD-1	FTD	C9ORF72	F	64	STH/Ambrosia
3009	FTD-2	FTD	C9ORF72	F	60	STH
3682	FTD-3	FTD/MND	C9ORF72	M	? (~72)	STH
M8	AD	AD	Sporadic	F	63	MODEL-AD Study
M12	Con	Healthy	-	F	100	MODEL-AD Study
3410v1	Affected Twin Early	ALS	C9ORF72	M	37	STH
3410v2	Affected Twin Late	ALS	C9ORF72	M	43	STH
3441	Father		C9-Carrier	M	69	STH
3475	Unaffected Twin		C9-Carrier	M	37	STH
3679	PreSx-1		C9-carrier	F	50	STH
3797	PreSx-2		C9-carrier	M	31	STH
3763	PreSx-3		C9-carrier	F	36	STH

Table 2-13. ***Information on iNPC lines.*** *The table highlights the cell line sample code for the cultured cell lines derived from donors/patients and in text abbreviation; clinical information which features the patient's known medical condition; the specific genetic alteration identified in each patient and, when appropriate, the sporadic form of disease; the sex of the patient (male or female); patient's age at the time the samples were collected and the source from where the cells were acquired. For the latter, the cell lines were provided by the Sheffield Teaching Hospital (STH) (Genomics Department or AMBRoSia, A multicentre Biomarker Resource Strategy in ALS), the Cedar-Sinai Medical Centre and the University of Sheffield (TUoS). Sporadic Alzheimer's Disease and matched control lines were recruited as part of MODEL-AD study. The tissue source used to create all cell lines was skin fibroblast. These iNPCs have been chosen as they have been already mentioned in publications and have been established in the labs. Note Con-1, Con-2, C9-1, C9-2 different from iPSC lines mentioned above. Note ALS52 also available as iPSC (Table 2-1). Note median survival time from onset to death for sporadic ALS lines depicted in two categories: slow (decreased within 2 years after disease onset) and fast (deceased 2-5 years after onset).*

Component	Concentration	Purpose
DMEM/F12 Glutamax™	Base media	Serum-free nutrient base that provides vitamins, aminoacids, and glucose to ensure survival and energy supply for iNPCs. Glutamax supplementation fuels the TCA cycle for energy production, important for metabolically active iNPCs undergoing reorganisation and growth.
B-27 supplement	1% (v/v)	Rich source of antioxidants that reduce reactive oxidative species, protecting neurons and facilitating healthy development. Contains nutrients (selenium, iron) important for neurite growth and synaptic formation. Promotes cell survival and neurite outgrowth by supporting protein synthesis and iron transport.
N-2 supplement	1% (v/v)	Inhibitory effect of fibroblast growth factors (FGFs) and platelet-derived growth factors (PDGF) found in DMEM/F12 medium which could alter iNPCs towards unwanted lineages. Allows activation of signalling pathways specific for neuronal differentiation.
FGF-2	40 ng/mL	Stimulates proliferation and early neuronal differentiation by activating pathways like MAPK/ERK for early neuronal network formation
Penicillin/Streptomycin	1% (v/v)	Antibiotic combination that prevents bacterial contamination and ensures sterile environment, minimizing stress or damage to iNPCs.

Table 2-14. ***iNPC expansion media composition.*** *Media composition of iNPC expansion cells included in table highlights the concentration and purpose of each element. These components provide essential nutrients and energy for the expansion and initial maturation of iNPCs, preventing premature specialization.*

2.2.9. Differentiation of iNPCs to iNPC-astrocytes (iAstrocytes)

iNPC lines were expanded and maintained on 10-cm dishes or 6-well plates for 5 minutes at room temperature with 5 µg.mL fibronectin diluted in phosphate-buffered saline (PBS). To generate differentiated astrocytes, iNPCs were differentiated as previously described (Meyer et al., 2014) by switching the medium composition (Table 2-14) to astrocyte differentiation media (Table 2-15). Astrocytes were allowed to differentiate for 7 or 14 days. Cells were inspected for confluence and morphology. Cells were previously characterised at day 7 for differentiation by Ferraiuolo lab and were found to express typical astrocytic

markers (Vimentin and CD44 – Figure 4-1B). For experiments performed at day 7, iAstrocytes were replated onto Thermanox plastic coverslips at day 5 (unless otherwise stated). For recordings at day 14, iAstrocytes were plated on coverslips in 24-well plates at day 7. iAstrocytes were lifted from the plates using Accutase, which was inactivated by adding PBS. Cells were then centrifuged for 4 minutes at 200g. The supernatant was discarded, and the pellet was resuspended in a volume of astrocyte differentiation medium appropriate for counting using haemocytometer. Cells were plated at 30,000 cells/well onto 24-well plate containing Thermanox coverslips coated for 5 minutes at room temperature with 2.5 µg/mL fibronectin diluted in PBS. Media changes were performed at day 3 and 10.

2.2.10. SRSF1 lentivirus transduction

RNA sequestration of the splicing factor and nuclear export factor SRSF1 (serine/arginine-rich splicing factor 1) initiates the nuclear export of intron-1-retaining C9ORF72 repeat expansion which leads to the cytoplasmic RAN translation of DPRs (Hautbergue et al., 2017). The splicing process itself appears to play a key role, as it induces transfer of the mRNA through remodelling of NXF1 to adopt a high RNA-binding conformation. The depletion of SRSF1 or prevention of its interaction with NXF1 specifically inhibits the nuclear export of pathological *C9ORF72* transcripts, the production of DPRs and alleviates neurotoxicity in *Drosophila*, patient-derived neurons and neuronal cell models. Astrocytes were transduced with lentivirus expressing control lentivirus (LV) expressing GFP or human LV-SRSF1 expressing GFP. Multiplicity of infection (MOI) represents the number of virus particles to the number of host cells. MOI was 5 at 30,000 cells. For experiments performed at day 7, the cells were replated onto coverslips at day 4 in the morning and treatment was added the same day after approximately 6 hours. For recordings performed at day 14, the cells were replated at day 7 as normal and lentivirus treatment was added at day 11. The astrocytes were transduced with the control-LV or SRSF1-LV overnight. The next day, the media was changed with fresh Astrocyte media (Table 2-15) and patch-clamp electrophysiology was performed after 72 hours from initial incubation.

Component	Concentration	Purpose
DMEM		Balanced nutrient base providing essential nutrients like vitamins, aminoacids and glucose for basic cellular function. Supportive role for neural cell types.
N-2 supplement	0.2% (v/v)	Offers essential nutrients with reduced complexity (no complex growth factors or hormones as seen in other supplements like B-27) which could interfere with desired astrocyte differentiation signals. Contains selenium and iron important for cellular processes in astrocytes.
Foetal bovine serum (FBS)	10% (v/v)	Complex mixture of growth factors, hormones and attachment proteins that support initial survival and enhance astrocyte differentiation. Mimic extracellular milieu encouraged by astrocytes in the brain. Fine tune cell growth and differentiation
Penicillin/Streptomycin	1% (v/v)	Antibiotic combination that prevents bacterial contamination and ensures sterile environment, minimizing stress or damage to iNPCs.

Table 2-15. ***iAstrocyte differentiation media composition.*** *The table illustrates the components of the media, their concentration and their role. The combined effect of these components creates a supportive environment for both survival and proliferation of iNPC-derived astrocytes.*

2.2.11. Reagents and cultureware information relevant for the generation of iAstrocytes

Reagent	Supplier	Catalogue Number
Accutase	Sigma-Aldrich	A6964-100ML
B-27 supplement	Gibco	11530536
Fibronectin[1]	Merck Millipore	FC010-10MG
Fibronectin[2]	R&D Systems	1918-FN-02M
Foetal bovine serum (FBS)	Life Science Production	5-001A-H1-BR
KnockOut DMEM/F12	Gibco	12660012
N-2 supplement	Gibco	15410294
Penicillin/Streptomycin	Lonza	DE17-603E

Table 2-16. ***Cell culture reagents used for the generation of iAstrocytes.*** *The table mentions the specific chemical or reagent used in this part of the study, the commercial supplier and the catalogue number for each product.*

Reagent	Supplier	Catalogue Number	Purpose
10 cm dishes	Thermo Fischer Scientific	172931	iAstrocyte plating
Greiner 6-well plate	Greiner	657 160	iAstrocyte plating
24-well plate	Greiner	662 160	MSN/iA plating
Optic 96-well plate	Greiner	G655090	Plating for immunocytochemistry co-cultures and astrocyte conditioned media experiments
Optic 96-well plate	Perkin Elmer	6055308	Plating for immunocytochemistry of co-cultures and astrocyte conditioned media experiments
13mm Thermanox Coverslips	Thermo Fischer Scientific	150067	iAstrocyte plating

Table 2-17. ***Information about cultureware.*** *The table highlights the specific cultureware used in this project, the commercial supplier, the catalogue number for the specific product and associated role of each component. The table lists a selection of cell cultureware, including dishes, multiwell plates used to plate the iAstrocytes. Optic 96-well plates were used for immunocytochemistry (ICC) of co-culture and astrocyte conditioned media experiments.*

2.3. Fluorescence Assays

2.3.1. Immunocytochemistry (ICC)

Primary and secondary antibodies were used for immunocytochemistry experiments. Primary antibodies (Table 2-18) were chosen for different target antigens or proteins of interest. Primary antibody concentration, dilution, incubation time and temperature were optimised for each antibody and sample to achieve specific staining and low background. Secondary antibodies (Table 2-19) can detect the immunoglobulin (IgG) domain of the primary antibodies, increase the signal and create a more sensitive assay. A secondary antibody is usually conjugated to a molecule (chromogenic or fluorescent) that allows for the antibody to be detected.

Cell fixation was initiated by removing culture media and incubating the plates with warm 3.8% paraformaldehyde (PFA) for 10 minutes at room temperature, ensuring complete fixation of cells and preservation of cellular architecture. Three subsequent washes with PBS for 5 minutes followed and the plates were stored at 4°C until staining was performed.

To permeabilize cell membranes and access intracellular epitopes, cells were incubated with 0.3% Triton X-100 in PBS solution for 5 minutes at room temperature. Non-specific antibody binding was blocked by incubating the cells with 5% donkey serum (DS) for one hour. Both primary and secondary antibodies were diluted in 5% DS to further minimize non-specific interactions. Primary antibody incubation occurred overnight, followed by three washes with PBS for 5 minutes. Cells were incubated with Alexa Fluor secondary antibodies for 1h at room temperature in the dark, minimizing photobleaching of fluorescent probes. Three subsequent washes were performed. Nuclear counterstaining was achieved by incubating the cells with Hoechst (1:10,000) for 5 minutes in the dark at room temperature, permitting overall nuclear morphology. Three final washes with PBS were performed and the plates were kept in PBS at 4°C until fluorescent imaging was performed.

Marker	Species	Supplier	Catalogue Number	Concentration
Tubulin β 3 (TUBB3)	Mouse	BioLegend	801201	1:500
Cleaved Caspase-3	Rabbit	Cell Signalling	9664	1:400
Active Caspase-3	Rabbit	Merck Millipore	AB3623	1:200
DARPP-32	Rabbit	Abcam	Ab40801	1:100
GABA	Guinea Pig	Abcam	Ab17413	1:1000
GFAP	Rabbit	Invitrogen	13-0300	1:500
MAP2	Rabbit	Synaptic Systems	188 003	1:1000
Pax6	Rabbit	Abcam	Ab5790	1:500
Nestin	Mouse	Abcam	Ab18102	1:200
Vimentin	Chicken	Merck Millipore	AB5733	1:2500

Table 2-18. ***Primary antibodies information.*** *Immunocytochemistry (ICC) experiments employed a variety of primary antibodies targeting specific antigens of interest. Detailed information about each antibody, including the target marker, host species, supplier, catalogue number and concentrations used are provided in the table above.*

Target species	Host	Supplier	Catalogue Number	Concentration
Anti-rabbit	Donkey	Invitrogen	A21206	1:400
Anti-rabbit	Goat	Invitrogen	A11036	1:400
Anti-mouse	Donkey	Invitrogen	A10037	1:400
Anti-guinea pig	Goat	Invitrogen	A21450	1:400
Anti-chicken	Goat	Invitrogen	A11039	1:400

Table 2-19. ***Secondary antibody information.*** *Secondary antibodies were used to bind to primary antibodies, above mentioned, to aid the indirect detection of the target antigen. The secondary antibodies have specificity for the antibody species and the isotope of the primary antibody. Secondary antibodies have a detectable tag facilitating detection using imaging or molecular biology technique. The secondary antibodies are generated against a pooled population of immunoglobulin from a target species. The target species, host are highlighted in the above table. All secondary antibodies were purchased from Invitrogen (individual catalogue numbers mentioned) and were used at 1:400 concentration.*

2.3.2. Imaging

Cells were imaged using the Opera Phenix™ High Content Screening System (Perkin Elmer) at x40 magnification. Z-stacks of 7 or more planes were separated by 0.5 µm were obtained from a minimum of 7 fields per well from at least three technical replicates per experiment (unless otherwise stated). The widefield In Cell Analyzer was used at x20 magnification for co-culture experiments and quantification. A minimum of 7 field per well were analysed from at least three technical replicates per experiment, unless otherwise stated. Different lasers were used (488, 594 and 647 nm) along with appropriate excitation and emission filters. Same settings were used for all wells investigated.

2.3.3. Analysis

Images captured on Opera Phenix or InCell are automatically stored on Harmony server, from which assay files can be uploaded onto Columbus Data Storage and Analysis System (Perkin Elmer) to allow high throughput analysis without experimental bias. For each immunofluorescence staining plate, three technical repeat weeks, containing 7 random fields per experimental condition at 20x or 40x magnification, were imaged and analysed.

2.4. Whole-cell patch-clamp electrophysiology

Here, the whole-cell patch-clamp method used to characterise the electrophysiological profile of the iPSC-derived neurons and directly converted astrocytes will be described.

2.4.1. Patch-clamp technique: a historical perspective

Patch-clamp electrophysiology is a powerful biophysical technique, granting researchers unparalleled access to the ionic flux driving communication and function across cell membranes. Founded on the principle of forming a high-resistance seal between a glass micropipette and the cell membrane, the technique allows precise measurement of ionic current across various scales, from individual ion channels conducting picoampere (pA, pico=10^{-12}) currents to the integrative activity of the entire cell. This resolution revolutionized the field of electrophysiology, enabling direct observation of single-channel behaviour for the first time. While reconstructed membrane bilayers had previously hinted the existence of single channels, patch-clamp opened the door to studying them within the native complexity of living cells. Beyond visualizing the individual activities of ion channels, the real-time nature of data acquisition coupled with various patch-clamp configurations permits various aspects of cellular and sub-cellular physiology to be directly investigated. The advancement profoundly impacted electrophysiological research, leading to Erwin Neher and Bert Sakmann's Nobel Prize in Physiology or Medicine in 1991.

My research uses the patch-clamp technique to investigate the ionic currents underlying the function and dysfunction of various cell lines, including MSNs, MNs and astrocytes.

2.4.2. Patch-clamp configurations

Following the initial innovation, Neher, Sakmann and colleagues soon improved the technique by modifying the pipette properties, using 'fire-polished' tips in filtered solutions and applied slight pressure in the pipette. This enabled the formation of high-resistance seals exceeding gigaohms (GΩ, 10^9 ohms). This configuration is called cell-attached (Figure 2-4), allowing the recording of single channels while maintaining cell integrity (Hamill et al., 1981). Three other measurement configurations were developed. The whole-cell configuration (Figure 2-4), utilized in this study, involves rupturing the membrane patch

under negative pressure while maintaining the gigaseal. A continuous electrical connection between the pipette solution and the cell cytoplasm is created. By applying voltages through the pipette, researchers can precisely control the transmembrane potential, manipulating the driving force for ion movement through specific channels. This is called the voltage-clamp configuration. This allows detailed investigation of voltage-gated channel behaviour and voltage-dependent cellular processes. Alternatively, the current-clamp configuration involves injecting current through the pipette enables researchers to analyse the response to the current input, studying the voltage response. This provides valuable insight into cellular excitability and network function. Further, the direct connection to the cytoplasm allows for manipulation of the intracellular environment via internal pipette solution composition or pharmacological agents, revealing the influence of internal factors on channel activity and cellular signalling pathways.

Another excision can be employed, from whole-cell configuration by pulling a small patch of membrane away from the cell (inside-out patch) to isolate specific channel populations and their regulation by intracellular factors (Figure 2-4). The outside-out patch can be created by gently detaching the whole-cell configuration revealing a single membrane vesicle attached to the pipette tip (Figure 2-4). This allows rapid solution exchange and facilitates the study of small channel populations or single channels with high temporal resolution. The choice of patch-clamp configuration depends on the specific research question and the desired level of control over the cellular environment.

In this study, the whole-cell configuration with current-clamp recordings was employed to investigate neuronal excitability and voltage-clamp to interrogate different ion channel behaviours.

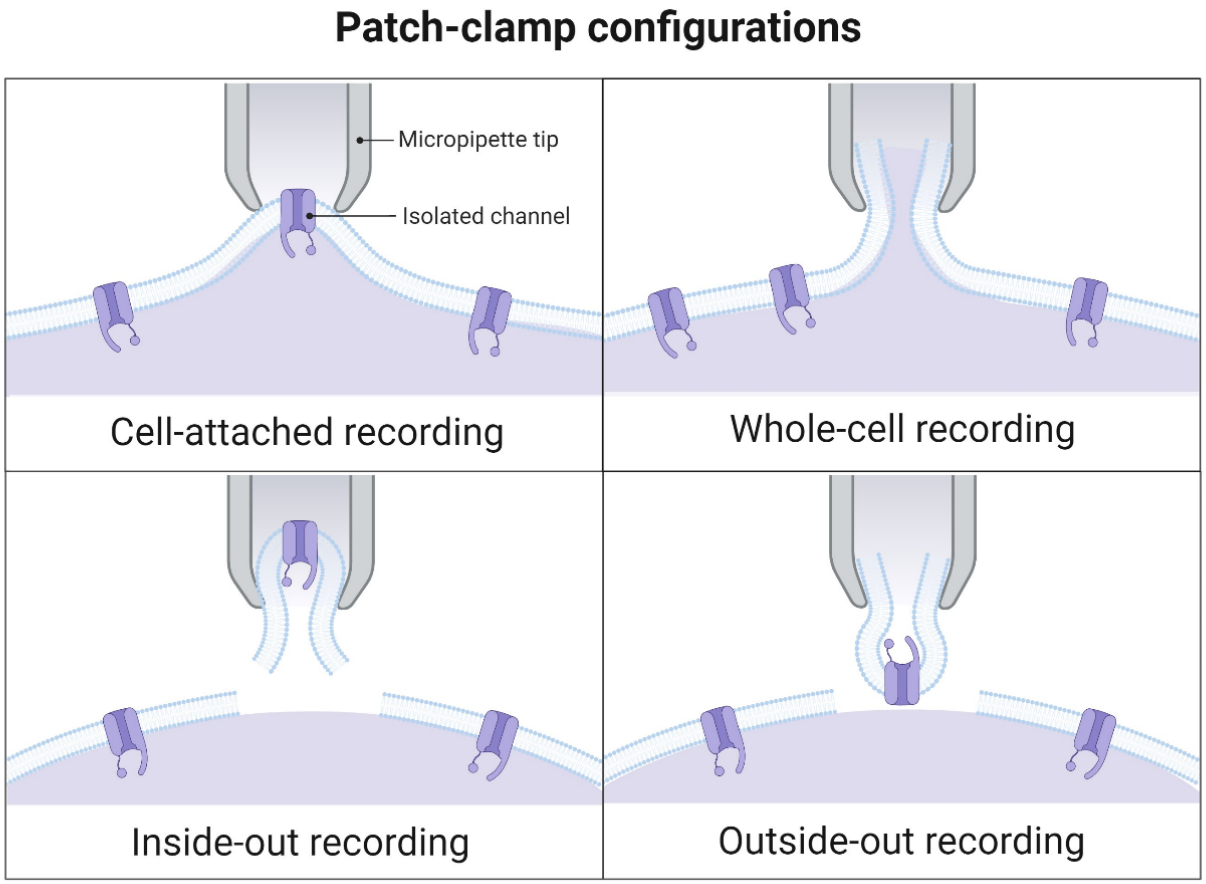

Figure 2-4. ***Patch-clamp configurations****. Schematic showing the various methods of establishing different patch-clamp configurations. Initially, the electrode is moved close to the cell membrane. Negative pressure is applied so that the pipette attaches to the membrane. The electrode passes nominal current, establishing a 'electrically' tight seal with high resistance, called a GigaOhm seal. This configuration is called 'cell-attached' (top-left). Then, strong acute negative pressure is required to break the cell membrane forming the whole-cell configuration (top-right). The cytoplasm and the pipette interior are continuous and the K^+-gluconate solution floods the cell cytoplasm. It is possible to record single channels via one of two configurations, outside-out or inside-out configurations. inside-out recordings look at single channels, exposing the cytosolic surface of the membrane (bottom-left), while outside-out configuration is used to investigate receptor activated ion channels (bottom-right). Figure created using BioRender.*

2.4.3. The cell membrane and its electrical properties

The cell membrane acts as a thin insulating layer that regulates the osmolarity between the intracellular milieu and extracellular environment. It acts as a selectively permeable barrier, regulated by the flow of ions and creating an uneven distribution of charged particles between its compartments. This differential ion distribution, primarily involving sodium (Na^+), potassium (K^+), chloride (Cl^-) and calcium (Ca^{2+}) establishes a membrane potential, a voltage difference across the membrane measured in millivolts (mV). The Nernst equation, based on ionic concentration and permeabilities, predicts the equilibrium potential for each ion, contributing to the overall resting membrane potential.

Beyond its role in ion selectivity, the membrane also exhibits capacitive properties. Its phospholipid bilayer acts as an electric insulator, accumulating and storing electrical charge across its thickness. This capacitive property contributes to the membrane potential changes.

While the cell membrane itself is largely impermeable to charged particles, specialized ion channels and transporters facilitate targeted ion movement. These transmembrane proteins exhibit ion selectivity and regulate the opening and closing of their pores in response to environmental cues, including voltage changes, ligands binding, and phosphorylation. The flow and size of ions through these channels and transporters depend on the driving force (voltage gradient) and the opposition (ionic conductance) offered by the membrane. Ohm's law, a fundamental principle in physiology, relates to these parameters:

$$I = \frac{V}{R},$$

where I is the current (measured in Amperes, A), V is the voltage (measured in Volts, V), and R is the resistance (measured in ohms, Ω). This equation states that the current flowing through the membrane is directly proportional to the voltage difference across it and inversely proportional to the membrane resistance.

By investigating and understanding these membrane properties and the governing principles of ion transport, researchers can interpret changes in voltage and current to gain insight into cellular function, signalling mechanisms, and ultimately, the complex processes underlying health and disease.

2.4.4. Recording setup

Whole-cell patch-clamp recordings were made using borosilicate glass pipettes (Harvard Apparatus) with 1.5 mm outer diameter, 0.86mm inner diameter and 75 mm length, pulled to a resistance of 4-7 MΩ using a Sutter P-97 Horizontal Pipette Puller (Sutter Instruments, Sarasota, FL, USA). Patch electrodes were filled with internal recording solutions as described in the text, with the appropriate composition described in following tables (Table 2-20, Table 2-21). The liquid junction potential was calculated to be +14 mV, and holding potentials were adjusted accordingly (JPCalc, Clampex). The micromanipulator (Scientifica) positioned the recording pipette into the cell, controlled by a headstage (Axon Instruments) connected to an Olympus upright microscope with a 40x submersion lens (Figure 2-5). Recorded signals were low-pass filtered at 2 kHz, digitised at 10 kHz via a BNC-2090A (National Instruments) interface, and acquired using WinWCP v5.7.7 Electrophysiology Data Recorder (J. Dempster, University of Strathclyde, UK).

Coverslips containing the iPSC-derived striatal neurons or NPC-derived astrocytes were placed in the recording chamber (Figure 2-5) and perfused with extracellular solution, also known as artificial cerebrospinal fluid (aCSF) solution (Table 2-22, Table 2-23) using a gravity fed system at room temperature (20-23^{o}C). Pharmacological agents were applied using a bath-exchange system with multiple extracellular aCSF sources ('barrels') containing the appropriate concentration of experimental reagent. The barrels are changed accordingly to deliver appropriate treatment with the liquid aCSF contents to be continuously replaced.

Whole-cell recordings were acquired at a holding potential of -70mV using Axon Multiclamp 700B amplifier (Molecular Devices, Union City, CA, USA). Current-clamp recordings at -74mV with bridge balance and pipette capacitance neutralisation were employed to investigate cell membrane properties. Specific pharmacological manipulation, holding potential, and voltage-ramp protocols are described in detail within dedicated chapters and figure legends. The main components of the electrophysiology rig are highlighted in Figure 2-5. Series resistance stayed below 25MΩ throughout each experiment. Recordings with R_S exceeding 20% of initial value were discarded.

2.4.5. Analysis of action potentials (APs)

Measurements of AP number were stopped at the point of AP accommodation, which was observed at higher current stimulation likely to be pushing the neuron into non-physiological ranges. Datapoints corresponding to the period of stable firing (prior to decline) were included in the analysis for all cell lines. This approach ensures only physiologically relevant responses were measured.

Component	Concentration (mM)	Purpose
K-gluconate	155	Maintains physiological [K^+], ensuring stable membrane potential and normal cell function. Minimizes Cl^- contamination (Gluconate is a non-chloride organic anion) by limiting Cl^- influx (high Cl^- alters excitability and activates Cl^- currents). Gluconate maintains ionic equilibrium cellular energy levels.
$MgCl_2$	2	Mimics $[Mg^{2+}]_i$, supporting protein function and cellular processes. Co-factor for ATPase enzymes, vital for energy production and function. Stabilizes protein structures (ion channels and enzymes).
Na-HEPES	10	Buffer that maintains physiological pH within the pipette and the cell, important for cell survival during recordings. Stabilizes membrane potential.
Na-PiCreatine	10	Energy substrate and antioxidant. Phosphocreatine acts as a high-energy phosphate donor, supplying ATP for cellular processes like ion pumps and maintaining membrane potential.
Mg_2-ATP	2	Direct energy source that maintains ion gradients, neurotransmitter release, protein synthesis. Maintains membrane pumps (ATP fuels the Na^+/K^+/ATPases, responsible for maintaining K^+ gradient and cellular ionic balance.
Na_3-GTP	0.3	G-protein signalling activity regulator, important in signalling pathways in neurons. Low concentration minimises its influence on the RMP.
pH 7.3, 320-330mOsm		

Table 2-20. ***K-gluconate intracellular solution*** *components in mM and their role. The intracellular solution mimics the cell's cytoplasm to maintain cell health and optimize recording quality. The solution was filtered through 0.33 mm filters and snap frozen at -80°C. The solution was aliquoted and stored at -4°C.*

Component	Concentration (mM)	Purpose
CsCl	145	Cs^+ ions are large and mimic K^+ ions, readily replacing it in K^+ channel pores, blocking most voltage-gated K^+ channels. Contributes to the primary cationic charge carrier to the internal solution.
$MgCl_2$	1	Direct energy source that maintains ion gradients, neurotransmitter release, protein synthesis Maintains membrane pumps. ATP fuels the Na^+/K^+/ATPases, responsible for maintaining K^+ gradient and cellular ionic balance.
Na-HEPES	10	Buffer that effectively maintains physiological pH within the pipette and the cell, important for cell survival during recordings. Stabilizes membrane potential.
EGTA	1.1	Ca^{2+} chelator, binds free intercellular Ca^{2+} ions, diminishing their influence on recorded current (important when studying Ca^{2+}-activated K^+ channels)
Mg_2-ATP	2	Direct energy source that maintains ion gradients, neurotransmitter release, protein synthesis. Maintains membrane pumps (ATP fuels the Na^+/K^+/ATPases, responsible for maintaining K^+ gradient and cellular ionic balance
$CaCl_2$	0.1	Low Ca^{2+} concentrations allow for recording of Ca^{2+}-independent K^+ channels while retaining some basal Ca^{2+} signalling capability for channels indirectly modulated by Ca^{2+} pathways (useful for looking at specific activation mechanisms of different K^+ channel types).
pH 7.3, 320-330mOsm		

Table 2-21. ***Cesium Chloride (CsCl) internal solution****. This intracellular solution offers advantages for recording K^+ channels in whole-cell patch-clamp experiments, by blocking K^+ currents and providing a stable environment to maintain cellular health and function during recordings.*

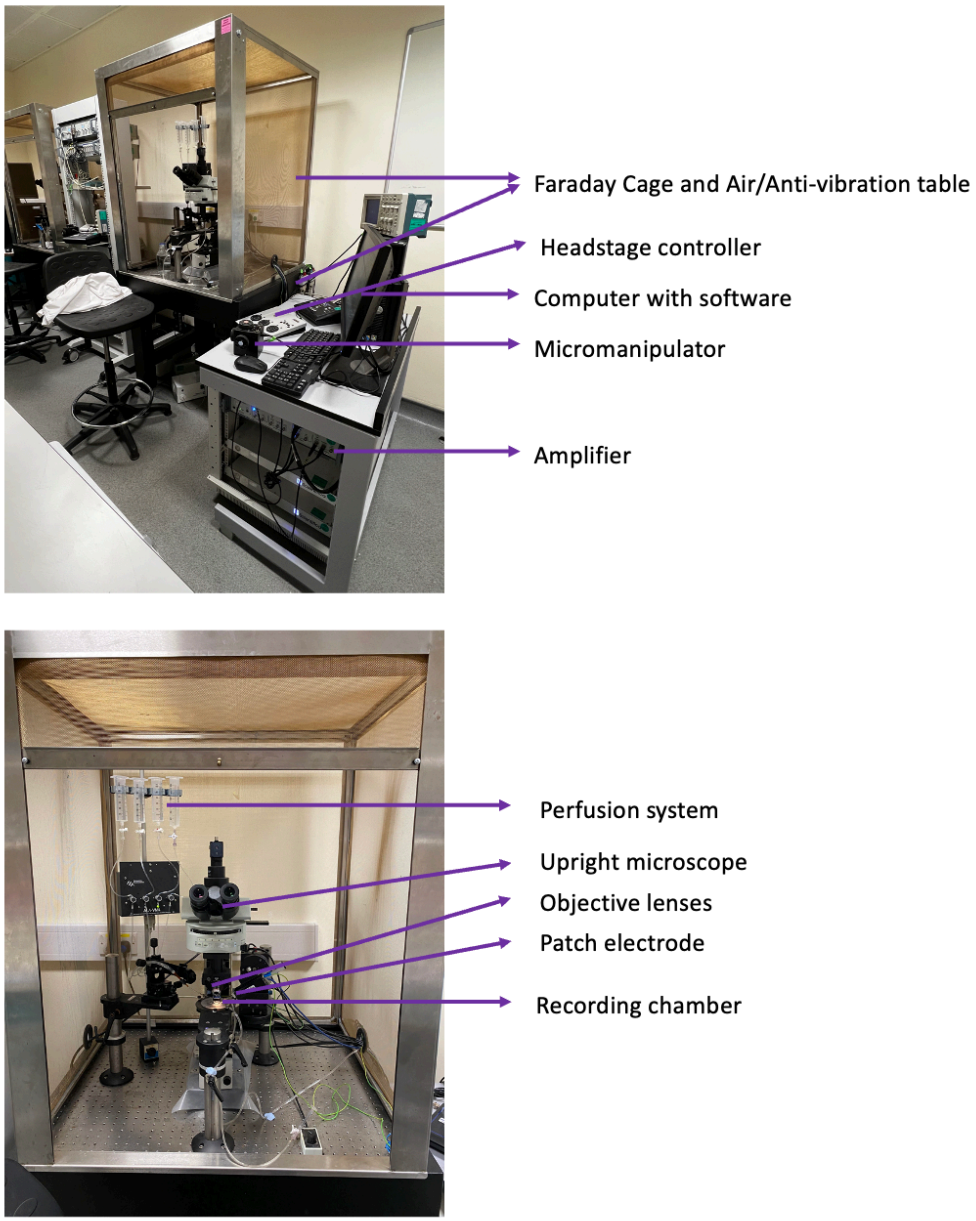

Figure 2-5. ***Electrophysiology rig setup****. These images highlight some of the important components part of the standard whole-cell patch-clamp electrophysiology setup employed in our laboratory. In the top image, the Faraday cage surrounds the entire setup shielding sensitive electronic equipment from external electrical interference, ensuring accurate and reliable recordings. The precise micromanipulator alloys the movement positions for recording pipettes onto the cell of interest under the microscope. The main amplifier further amplifies the signal from the headstage and filters out high-frequency noise, providing a clear representation of the recorded membrane currents. The gravity-fed system continuously delivers fresh extracellular solution to the recording chamber and washes away debris, maintaining stable physiological environment for recordings. The figure below highlights the upright microscope, the recording chamber where the coverslips are placed and the patch electrode.*

Component	Concentration (mM)	Purpose
NaCl	152	Mimics physiological ionic environment (high Na^+ concentration in the extracellular milieu), providing driving force for Na^+ influx. Na^+ is the primary extracellular cationic charger carrier, maintaining adequate current flow in the bath and recorded cell, minimizing voltage artifacts.
KCl	2.8	Balances K^+ equilibrium potential (low K^+ concentration). Maintains cell survival and membrane stability.
HEPES	10	Buffer that effectively maintains physiological pH within the pipette and the cell, important for cell survival during recordings. Stabilizes membrane potential.
$CaCl_2$	2	Supports sufficient extracellular Ca^{2+} for activation of Ca^{2+}-dependent channels. Prevents saturating Ca^{2+} entry pathways at this concentration.
$MgCl_2$	1.5	Maintains Mg^{2+} physiological levels in the extracellular space, facilitating cell health and stability.
Glucose	10	Energy source that promotes cell viability and ongoing cellular processes. Maintains normal metabolic state for recorded cells.
pH 7.3, 320-330mOsm		

Table 2-22. ***The standard extracellular solution****. The specific extracellular solution components provide a balanced environment for whole-cell patch-clamp recordings, supporting cellular function and enabling accurate measurement of ionic currents. The solution mimics physiological levels of key ionic concentrations enabling the study of various ion channels and membrane excitability.*

Component	Concentration (mM)	Purpose
NaCl	122	Maintains Na^+ gradient. Controls membrane potential, contributes to action potential generation.
TEA-Cl	30	Blocks outward K^+ channels, including Kv_3 and Kv_4 subfamilies, which contribute to I_K currents. Although blocking K^+ channels, TEA exhibits affinity for different channel subtypes, advantageous for studying specific I_K channel populations within a cell by observing their differential sensitivity to TEA.
KCl	2.8	Low K^+ concentration minimizes outward leak currents, ensuring K^+ availability for essential cellular functions. Similar to normal extracellular solution, KCl contributes to resting membrane potential.
HEPES	10	Buffer that effectively maintains physiological pH within the pipette and the cell, important for cell survival during recordings. Stabilizes membrane potential.
$CaCl_2$	2	Supports sufficient extracellular Ca^{2+} for activation of Ca^{2+}-dependent channels. Prevents saturating Ca^{2+} entry pathways at this concentration.
$MgCl_2$	1.5	Maintains Mg^{2+} physiological levels in the extracellular space, facilitating cell health and stability. Acts as non-competitive NMDA blocker.
Glucose	10	Energy source that promotes cell viability and cellular processes. Maintains normal metabolic state for recorded cells.
pH 7.3, 320-330mOsm		

*Table 2-23. **I_K extracellular solution**- equimolar substitution of NaCl with 30mM TEA. The table highlights the components of the media, their concentration and their role. This modified version of the extracellular solution with equimolar TEA substitution for NaCl offers a valuable tool for selectively studying I_K currents from other channels. By reducing K^+ currents, TEA allows the isolation and analysis of I_K channels.*

2.4.6. Reagents used for patch-clamp electrophysiology recordings

All electrophysiology reagents used in this study for whole-cell patch-clamp recordings, including for the preparation of extracellular and intracellular solutions, specific antagonists and modulators for blocking or activating specific ion channels, were prepared using commercially available reagents from various vendors (Table 2-24).

Reagent	Supplier	Catalogue Number
KCl	TCI Chemicals	7447-40-7
D-(+)-Glucose	Sigma-Aldrich	G5767
HEPES	Sigma-Aldrich	H337
NaCl	Sigma-Aldrich	793566
$MgCl_2$	SERVA	39772.02
$CaCl_2$	Thermo Scientific Solutions	J63122
K-Gluconate	Sigma-Aldrich	P1847
$BaCl_2$	J.T.Baker	0045
CsCl	ACROS Organics	7647-17-8
Na-HEPES	Sigma-Aldrich	H3375
Sodium creatine phosphate dibasic tetrahydrate	Sigma-Aldrich	27920
Mg-ATP	Sigma-Aldrich	A9187
Na-GTP	Sigma-Aldrich	G8877
Tetrodotoxin Citrate	LKT Labs	18660-81-6
$CdCl_2$	Jena Bioscience	CSS-157
TEA-Cl	Merck	T2265
HC067047	Tocris	4100
Carbenoxolone (CBX) disodium	Tocris	3069
Gap19	Tocris	5353

*Table 2-24. **Electrophysiology reagents**. The table includes information about all electrophysiology reagents used in this study, the supplier from which these substances were acquired and their catalogue number.*

2.5. Data and statistical analysis

Data are presented as mean ± standard error of the mean (SEM). The number of experimental replicates is indicated as 'n' and the number of *de novo* preparations of batches from which n is obtained is called 'N'. The decision to designate individual cells as 'n' and the number of experimental replicates as 'N' was driven by the aim to ensure that any observed cellular phenotype in stem cell-derived material grown *in vitro* was not attributed to potential 'batch to batch' variation. Alternatively, this approach aimed to account for such variations detected, allowing more accurate interpretation of the effects of any experimental intervention.

Data throughout the thesis is presented from individual cell lines to account for variability, identify outliers and determine trends, enhancing transparency based on the specific research questions investigated in this study and allowing more accurate interpretation of the pathogenic disease mechanism underlying ALS/FTD.

Statistical analysis was calculated using Student's t-tests (paired or unpaired), ANOVA (one-way or two-way) on GraphPad Prism and specific post-hoc tests were used as appropriate.

2.5.1. Rectification indices

Ion channel rectification quantifies the directional bias of ion flux across the cell membrane. This property is characterised by the rectification index (RI), calculated as the ratio of outward to inward conductance at specific voltages. An RI of 1 reflects no bias (Ohmic behaviour), while values <1 or >1 denote inward or outward rectification, respectively. The equation:

$$RI = \frac{I/(16-E_{rev})}{I/(124-E_{rev})},$$

Where *I* is the current amplitude and *Erev* is the reversal potential of currents investigated at voltages favouring opposite current directions (inward current at 16mv; outward current at 124mV). This ratio reflects the relative ease of ionic flow in each direction, providing a quantitative measure of rectification.

2.5.2. Liquid junction potential

All data presented includes liquid junction potential (LJP), unless otherwise stated. LJP occurs when two solutions of different composition and concentration are in contact with each other, and it is generated by the different flow of ions in the two solutions.

3. CHAPTER 3: *C9ORF72*^{RE} medium spiny neurons display hypoexcitability.

3.1. Introduction

The degeneration of motor neurons and neurons of the pre-frontal cortex and temporal lobes are well-established key pathological hallmarks of FTD/ALS. In FTD, degeneration of these areas leads to behavioural and cognitive deficits, with cognitive impairments associated with FTD often additionally impacting ALS patients (Strong et al., 2017). These impairments include mainly behavioural and/or dramatic personality changes like increase in apathy, self-awareness deficits, loss of energy and motivation, language difficulties, emotional withdrawal and executive function (Kumfor and Piguet, 2012, Adenzato et al., 2010). However, such functions are not controlled solely by the pre-frontal cortex and temporal regions. One area that appears to be overlooked in its role in FTD/ALS is the striatum.

The striatum is the largest part of the basal ganglia and comprises two distinct regions: the dorsal striatum (caudate and putamen) associated with sensorimotor functions, and ventral striatum (nucleus accumbens) which is part of the limbic circuit, modulating behaviour and memory (Alexander et al., 1986). The striatum is an important integrative hub in the brain. Most striatal functions are mediated by inhibitory GABAergic medium-spiny neurons (MSNs), which encompass 95% of neurons in the striatum (Graveland and DiFiglia, 1985, Gerfen and Surmeier, 2011) with the remaining being interneurons (Tepper and Bolam, 2004). MSNs in the dorsal part of the striatum receive information from dopamine-producing neurons in substantia nigra pars compacta to program motor movements, and encode cognitive behaviours (Tritsch and Sabatini, 2012), while another set of dopaminergic neurons from the ventral tegmental area and prefrontal cortex innervate the ventral striatum via the mesolimbic pathway to programme behaviours (Patton et al., 2013), reward reinforcement (Delgado, 2007, Han et al., 2017, Sharot et al., 2009) and decision-making (Hiebert et al., 2014). Excitatory glutamatergic neurons from the cortex and thalamus project to the striatum from frontal and parietal association areas through the dorsolateral prefrontal circuit (executive function), lateral orbitofrontal circuit

(inhibition and impulses) and the anterior cingulate circuit (motivation) (Looi and Walterfang, 2013, Alexander et al., 1986). Also, the amygdala receives inputs from the thalamus and the sensory cortex and projects to the ventral tegmental area, prefrontal cortex and ventral striatum to produce emotion-based behaviours (Phelps and LeDoux, 2005). These morphological arrangements offer the ventral striatum remarkable importance as it regulates motivation, fear, emotional stability, cognition and other cognitive functions (McGinty et al., 2013, Mavridis and Pyrgelis, 2022, Voorn et al., 2004, Redgrave et al., 2010) and plays a central role in the mechanism of addiction (Volkow et al., 2007, Mitchell et al., 2012). The ventral striatum was also associated with broader function of assessing the value of different stimuli and actions, suggesting a crucial role not only in experiencing reward, but also in guiding behaviour by assigning value to potential outcomes (Pauli et al., 2016). Strikingly, the cognitive roles of the striatum appear to overlap with the cognitive impairments exhibited by FTD/ALS patients, therefore studying the striatum is crucial to understand the disease.

Beyond these correlative observations, multiple lines of evidence implicate the striatum in FTD, and many studies refer to FTD as a frontostriatal disorder (Bocchetta et al., 2021a). Magnetic resonance imaging (MRI) scanning and voxel-based morphometry correlate striatal dysfunction in FTD patients with apathy and response disinhibition (Möller et al., 2015a, Rosen et al., 2005), binge eating (Perry et al., 2014, Woolley et al., 2007a), and long-term memory deficits (Bertoux et al., 2018). Also, progressive atrophy in the ventral striatum is evident in behavioural variant FTD (bvFTD) patients, with volumes ranging from 30% to 50% smaller compared to healthy control (Möller et al., 2015a, Möller et al., 2015b, Garibotto et al., 2011, Halabi et al., 2013, Landin-Romero et al., 2017). Given the striking crossover of striatal roles in cognitive function, cognitive functions impacted in FTD and evidence of striatal dysfunction in FTD patients, I believe that the striatum could be implicated in FTD/ALS.

Anatomical pathology studies have identified frequent neuronal loss within the striatum of patients with FTD/ALS. The loss of neurons in the nucleus accumbens, amongst other areas in the limbic system was reported in ALS patients (Kato et al., 1994). Riku et al. (2016) studied the striatal efferent system in post-mortem tissue revealing reduced striatal MSNs in the caudate nucleus across all patients. ALS patients, notably, exhibited milder

striatal loss compared to FTD patients. Immunohistochemical analysis of axon terminals from striatal efferent neurons in the striatum revealed marked depletion in all FTD patients, regardless of disease duration (Riku et al., 2016), suggesting that striatal loss is primarily associated with FTD. Numerous neuroimaging studies also reveal the striatum appear to be vulnerable in FTD/ALS. In vivo studies using MRI and diffusion tensor imaging have consistently revealed striatal atrophy and altered diffusivity (volumetric changes) in ALS patients, including patients harbouring the *C9ORF72*^{RE} mutation (Bede et al., 2013b, Lee and Huang, 2017). These findings suggest microstructural changes within the striatum, potentially contributing to the motor and cognitive deficits observed in FTD/ALS. MRI and vertex analysis have demonstrated a strong correlation between striatal dysfunction and the disruption of frontostriatal networks in *C9ORF72*^{RE} patients, potentially highlighting a critical role of the striatum in FTD/ALS pathophysiology (Bede et al., 2013b, Bertoux et al., 2015, Machts et al., 2015a). Striatal grey matter deficits have been described previously in asymptomatic *C9ORF72*^{RE} cohorts (Lee et al., 2017b). The nucleus accumbens (ventral striatum) specifically displays significant atrophy and pathological changes in FTD/ALS patients (Tae et al., 2020, Bede et al., 2013b, Machts et al., 2015b). Interestingly, it is believed that these alterations might precede the onset of neuropsychiatric symptoms commonly associated with the FTD/ALS, such as apathy, executive dysfunction and social cognitive impairments (Bede et al., 2013b). Collectively, the weight of evidence indicates that the ventral striatum is a substrate in FTD/ALS and is primarily impacted in FTD cases (Möller et al., 2015a, Garibotto et al., 2011, Halabi et al., 2013, Landin-Romero et al., 2017, Möller et al., 2015b, Bocchetta et al., 2021b). Interestingly, the striatum is a degenerative substrate in other diseases, such as Huntington's Disease (HD) (Waldvogel et al., 2015). However, HD causes primary degeneration to the dorsal striatum (Rüb et al., 2015) which is separated from the ventral region by the internal capsule.

The presence of severe TDP-43 pathology, the hallmark pathology of bvFTD and ALS (Kabashi et al., 2008, Sreedharan et al., 2008, Van Deerlin et al., 2008, Lee et al., 2017a), also expands to the ventral striatum of FTD/ALS patients and is heavily present in MSNs in post-mortem (Brettschneider et al., 2013). TDP-43 accumulations have been evident in axon terminals of striatal neurons and their projections to substantia nigra and globus pallidus, supporting the idea of neurotoxic inclusions extend to the targets of striatal neurons in

FTD/ALS patients (Riku et al., 2016). These findings suggest a strong association between the severity of striatal efferent system degeneration and pathology and the development of clinical FTD. This implies that changes in the striatal MSN pathway may impact the decline in socio-cognitive function observed in FTD/ALS patients.

Altered neuronal excitability is a well-established hallmark of the FTD/ALS disease spectrum and can be detected in FTD/ALS patients before the onset of clinical symptoms and any apparent degeneration (Benussi et al., 2016, Geevasinga et al., 2016b). These perturbations are considered core contributors to disease pathogenesis either via neuronal injury through excitotoxicity and/or reduced function by way of impaired neurotransmission. To date, electrophysiological research has determined that both cortical and motor neuron function in FTD/ALS are disturbed early in disease (reviewed in (Pasniceanu et al., 2021)). Critically, the only current licensed treatment in the UK that extends the life span of ALS patients also targets neuronal function(Bensimon et al., 1994, Zoccolella et al., 2007). Beyond altered excitability being an important disease hallmark that requires to be better understood, it also a tractable therapeutic target. One area that requires to be better understood is our detailed understanding of neuronal dysfunction that extends beyond cortical and motor neurons into other brain regions. Here I focus on the striatum.

3.2. Hypothesis and aims of the study:

Given strong evidence of the loss-of-function phenotype described previously in the striatum, evidenced by 1) the involvement of the ventral striatum in cognitive impairments, strongly affected in FTD/ALS; 2) major atrophy of the ventral, not dorsal, striatum, in bvFTD in MRI brain imaging (Bertoux et al., 2015); 3) major TDP-43 pathology in MSNs, the most prominent neuronal population of the striatum (Brettschneider et al., 2013), and 4) that altered neuronal excitability is a major contributor to FTD/ALS, I hypothesize that FTD/ALS striatal MSNs display excitability impairments.

To address this hypothesis, I investigated neuronal function using patch-clamp electrophysiology in *in vitro* human MSNs derived from FTD/ALS patient-iPSCs. The main

aims were to a) derive enriched populations of striatal MSNs, from unaffected controls, FTD/ALS patients harbouring *C9ORF72*^{RE} mutation, the most common causal mutation giving rise to FTD/ALS (DeJesus-Hernandez et al., 2011, Renton et al., 2011); b) characterise the intrinsic electrophysiological excitability profile of striatal MSNs derived from *C9ORF72*^{RE} patients using whole-cell patch-clamp technique.

3.3. Methods

3.3.1. iPSC maintenance (As described in Methods Section 2.2.3)

3.3.2. MSN differentiation (As described in Methods Section 2.2.4 and 2.2.5)

3.3.3. ICC- MSN characterisation (As described in Methods Section 2.3)

3.3.4. Electrophysiology (As described in Methods Section 2.4)

3.4. Results

3.4.1. iPSCs from *C9ORF72*^{RE} FTD/ALS patients and healthy controls were used to generate MSN cultures.

This study derived *in vitro* MSNs from human iPSC lines that included two iPSC lines previously reprogrammed from two unrelated healthy individuals (Con-1, Con-2), three iPSC lines from FTD/ALS patients carrying the *C9ORF72*^{RE} mutation (C9-1, C9-2, C9-3) and one gene-edited line was generated from C9-1 using CRISPR-Cas9 technology to remove the GGGGCC repeat expansion mutation, named C9-Δ1. These iPSCs have been previously characterised in previous publications (Castelli et al., 2021, Zhang et al., 2022b, Palminha et al., 2022). Further details of the backgrounds of the patients from which the iPSCs have been derived can be found in Methods section 2.2.3, Table 2-1.

To generate MSNs from iPSCs I used an established and previously reported protocol (Lin et al., 2015), summarised in Figure 3-1. A full description of the protocol employed to convert iPSCs to MSNs can be found in the section 2.2.4 and 2.2.5. However, in summary, a dual SMAD inhibition protocol was employed to efficiently induce neurogenesis. Neuronal progenitor cells (NPCs) were differentiated towards GABAergic MSN progenitors using a cocktail of factors including BDNF, SHH and DKK-1. Subsequent maturation into enriched populations of mature MSNs was achieved through BDNF supplementation.

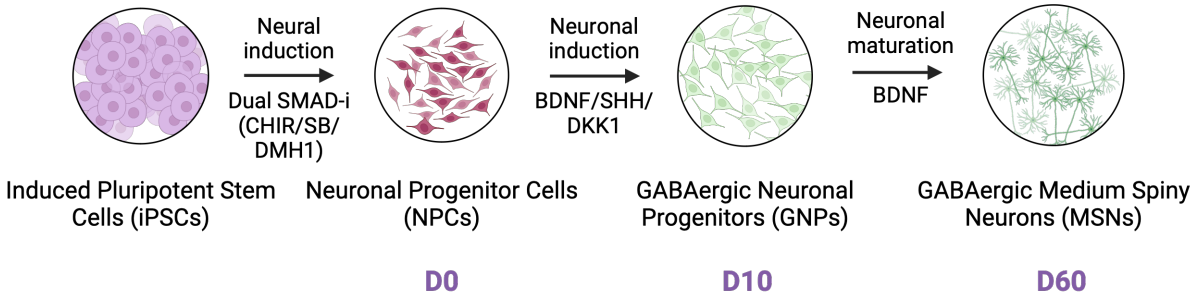

Figure 3-1. ***GABAergic MSNs were generated from iPSCs.*** *The protocol for generating GABAergic MSNs included the differentiation of iPSCs derived from both healthy controls and C9ORF72^{RE} patients, as detailed in the Methods chapter (Sections 2.2.4 and 2.2.5). Dual SMAD inhibition was employed to trigger neural cell formation. A cocktail of BDNF, SHH and DKK-1 generated GABAergic MSN progenitors. BDNF treatment fostered their development into mature MSNs. Timepoints mentioned throughout the thesis refer to period after neuronal differentiation was initiated (Day 0 – 60). Figure created with BioRender.com.*

3.4.2. Enriched populations of GABAergic MSNs were generated which present the expected marker profile

To longitudinally characterize the cellular specification of the cultures, ICC was performed at the NPC stage and at three subsequent timepoints throughout MSN differentiation (day 20, 40 and 60). NPCs were characterised at day 2. At this stage, cells no longer exhibited the characteristic rounded iPSC morphology and cells assembled into neural rosettes. Cultures were highly enriched for NPCs as assessed by specific antibodies against Pax6, critical in specifying neural lineage, promoting the renewal and self-differentiation of NPCs, and Nestin, well-established marker for immature neural cells involved in the formation of neuronal processes (Figure 3-2). At day 20, I observed neuronal-like morphology with 80% of the cells immunopositive for β-III-tubulin, a well-characterized marker for early neuronal differentiation (Mariani et al., 2015) and almost half of them expressed MAP2, a marker typically associated with more mature neurons (Soltani et al., 2005). Negligible expression (<5%) of Nestin and GFAP at day 20 revealed the successful neuronal differentiation and that enriched neuronal populations were generated (Figure 3-3). At day 40, around the same proportion of neurons expressed β-III-tubulin (82%) and MAP2 (>50%). Importantly, these cells now started to express DARPP32, a specific marker for MSNs in the striatum (Ivkovic and Ehrlich, 1999). Over 66% of neurons exhibited DARRP32 at day 40 (Figure 3-4).

At day 60, ICC confirmed the expression of neuronal markers - β-III-tubulin, in over 85% of cells, and MAP2, in 87% of cell populations. Striatal MSN marker, DARPP32 was expressed in more than 77% of neuronal populations. Further, since GABA is the main neurotransmitter in MSNs, ICC against GABA neurons and GABA transporter (vGAT) determined that above 81% of cells were GABAergic. Consistent differentiation efficiency of cultures to DARPP32+ and GABA+ MSNs across all the lines employed was observed (Figure 3-5). Neuronal cell death was assessed using Caspase-3 (Figure 3-5F), a neuronal apoptotic marker (Jelínek et al., 2015), and *C9ORF72*^{RE} MSNs showed a modest, but insignificant, increase in Caspase-3 staining compared to healthy and isogenic MSNs. However, overall Caspase-3 staining was less than 10% of the cell culture and indicates that viability of MSNs from all lines is maintained up to day 60.

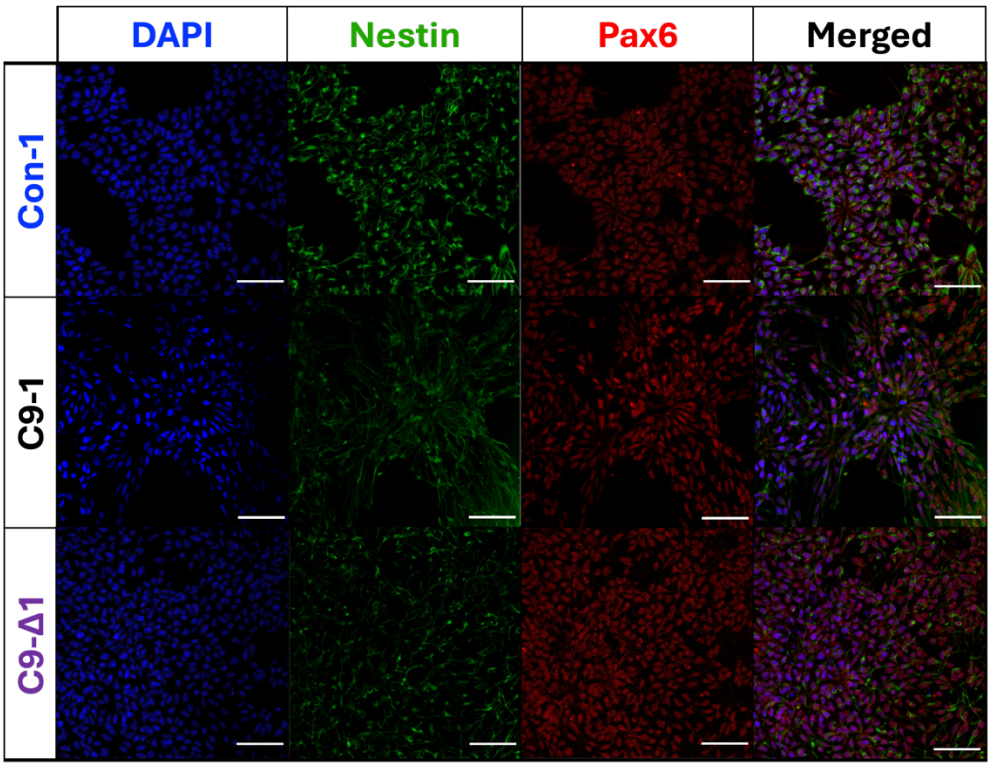

***Figure 3-2. NPCs express specific markers (Pax6 and Nestin)**. Representative images highlighting the co-expression of Nestin and Pax6 in NPC at day 2 post neuronal induction. Note the presence of neural rosettes, radially arranged groups of cells surrounding a central lumen. Scale bar set to 50μm.*

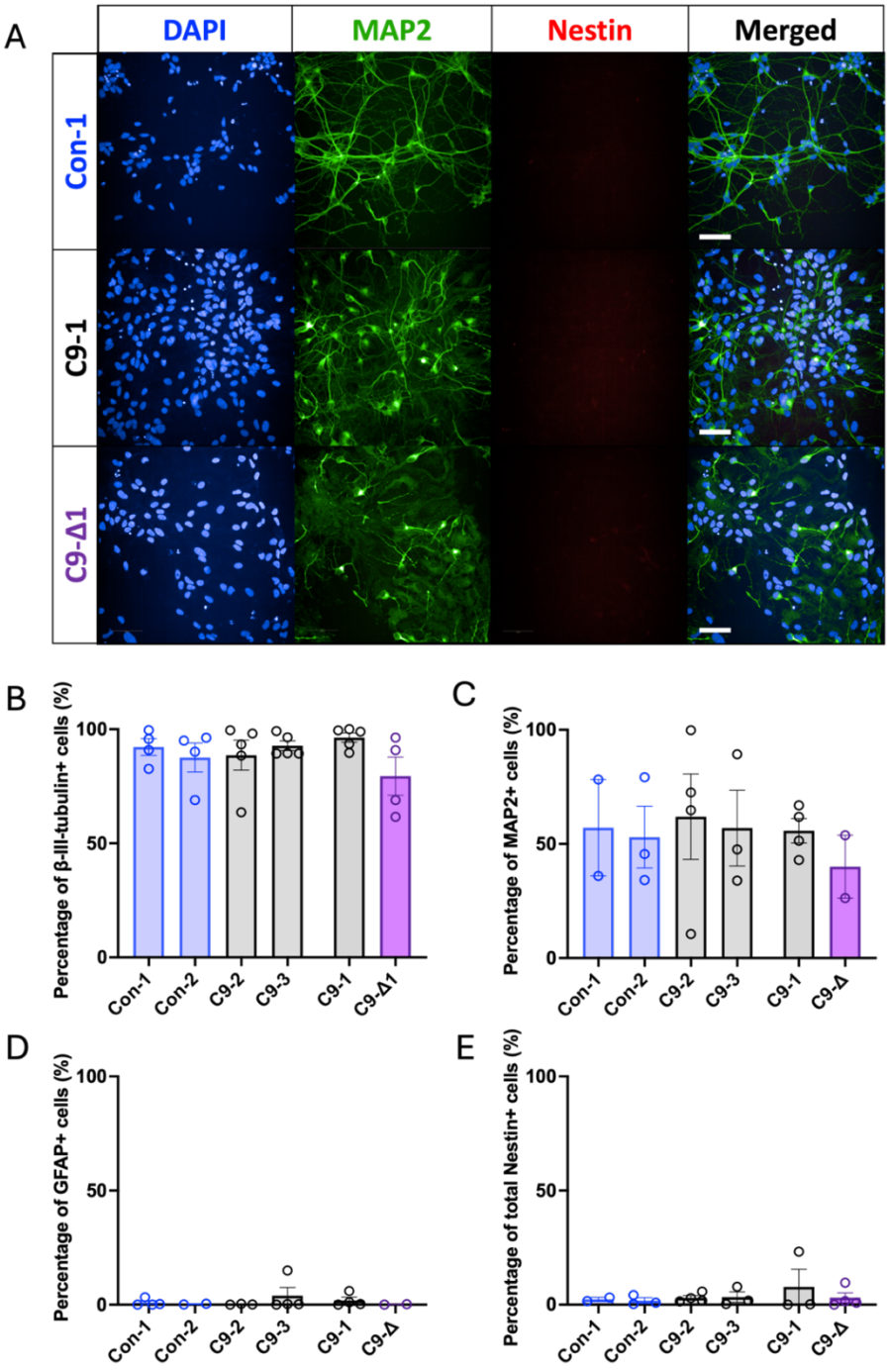

Figure 3-3. ***MSN progenitors express neuronal markers (β-III-tubulin and MAP2) at day 20.*** *A. Representative images highlighting the expression of MAP2, Nestin and DAPI. Scale bar set to 50μm. B,C,D,E. Graphs showing the mean ± SEM percentage expression of β-III-tubulin+, MAP2+, GFAP+ and Nestin+ cells, respectively, in the cultures. Note that enriched neuronal populations were generated. Note the lack of immunopositive GFAP+ and Nestin+ markers. Data from individual de-novo preparations are depicted by circles inset into the bar graphs. Data, β-III-tubulin: Con-1, N=4; Con-2, N=4; C9-1, N=5; C9-2, N=5; C9-3, N=5, C9-Δ1, N=4; MAP2: Con-1, N=2; Con-2, N=3; C9-1, N=4; C9-2, N=4; C9-3, N=3; C9-Δ1, N=2; GFAP: Con-1, N=4; Con-2, N=2; C9-1, N=4; C9-2, N=3; C9-3, N=4; C9-Δ1, N=2; Nestin: Con-1, N=2; Con-2, N=3; C9-1, N=3; C9-2, N=3; C9-3, N=4; C9-Δ1, N=4).*

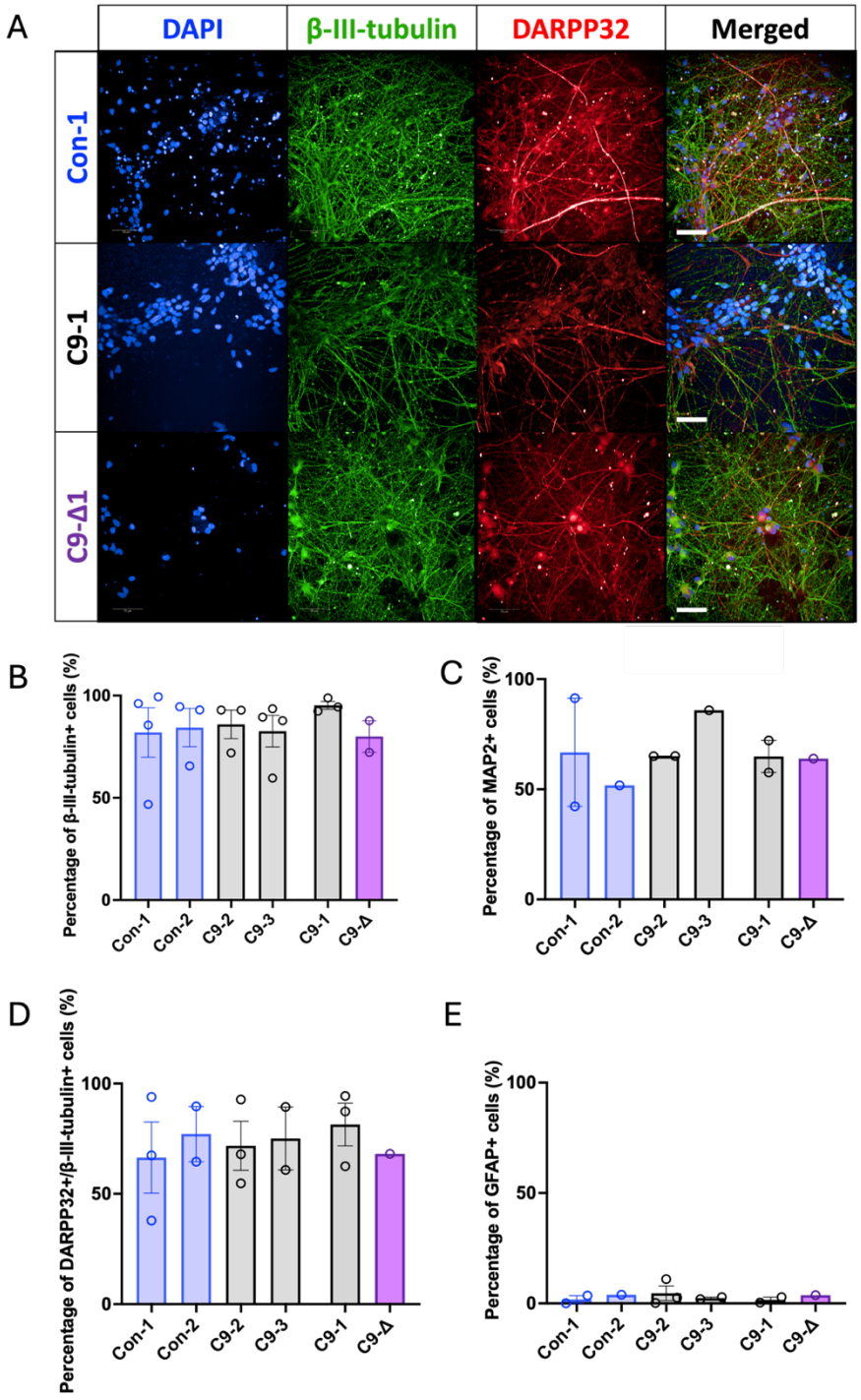

Figure 3-4. ***Increased expression of DARPP32 at day 40.*** *A. Representative images highlight the expression of β-III-tubulin and DARPP32, specific MSN marker. Scale bar, 50μm. B,C,D,E. Graphs showing the mean ± SEM percentage expression of β-III-tubulin+, MAP2+, DARPP32+ and GFAP+ cells, respectively, in the cultures. Note enriched DARPP32+ neuronal populations were generated. Data, β-III-tubulin: Con-1, N=4; Con-2, N=3; C9-1, N=3; C9-2, N=3; C9-3, N=4, C9-Δ1, N=2; MAP2: Con-1, N=2; Con-2, N=1; C9-1, N=2; C9-2, N=2; C9-3, N=1; C9-Δ1, N=1; DARRP32: Con-1, N=3; Con-2, N=2; C9-1, N=3; C9-2, N=3; C9-3, N=2; C9-Δ1, N=1; GFAP: Con-1, N=2; Con-2, N=1; C9-1, N=2; C9-2, N=3; C9-3, N=2; C9-Δ1, N=1.*

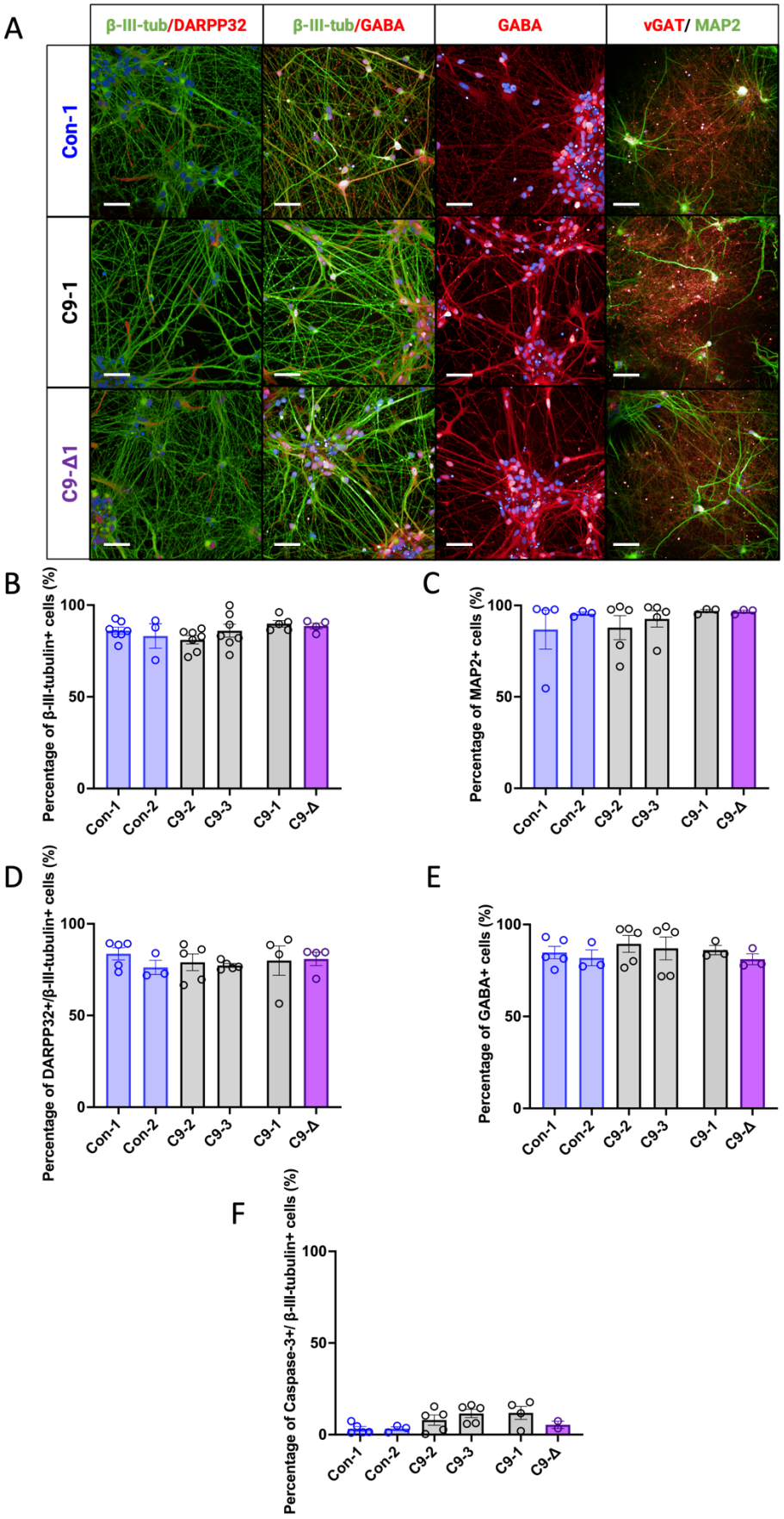

Figure 3-5. ***Enriched populations of GABA-ergic MSNs were generated at day 60.*** *Figure caption on the next page.*

Figure 3-5. ***Enriched populations of GABA-ergic MSNs were generated at day 60.*** *A. Representative images highlight the expression of β-III-tubulin and DARPP32, β-III-tubulin and GABA, GABA alone, and vGAT and MAP2 in day 60 Con-1, C9-1 and C9-Δ1 MSNs. Scale bar set to 50μm. B,C,D,E,F. Graphs showing mean ±SEM percentage expression of β-III-tubulin+, MAP2+, DARPP32+ and GABA+ cells, respectively, at day 60. Note enriched DARPP32+, GABA+ neuronal populations were generated. Note that representative images and quantification data generated by Dr Cleide DS Souza were added to my own data sets. Data, β-III-tubulin: Con-1, N=7; Con-2, N=3; C9-1, N=5; C9-2, N=7; C9-3, N=7, C9-Δ1, N=4; MAP2: Con-1, N=4; Con-2, N=3; C9-1, N=3; C9-2, N=5; C9-3, N=5; C9-Δ1, N=3; DARRP32: Con-1, N=5; Con-2, N=3; C9-1, N=4; C9-2, N=5; C9-3, N=5; C9-Δ1, N=4; GABA: Con-1, N=5; Con-2, N=3; C9-1, N=3; C9-2, N=5; C9-3, N=5; C9-Δ1, N=3; Caspase-3: Con-1, N=5; Con-2, N=3; C9-1, N=4; C9-2, N=5; C9-3, N=5; C9-Δ1, N=2.*

3.4.3. *C9ORF72*^{RE} MSNs display hypoexcitability

To characterise the excitability of MSNs I performed whole-cell patch-clamp electrophysiology in the current-clamp configuration. Specifically, I measured the intrinsic excitability of MSNs, which relates to their inherent ability to generate action potentials in response to stimulation. It encompasses the neuron's membrane properties, including ion channel composition and distribution, membrane potential dynamics, and firing threshold independent of extrinsic influence, such as neurotransmitters. To measure this I therefore performed recordings utilising a cocktail of synaptic transmitter blockers including 6-Cyano-7-nitroquinoxaline-2,3-dione (CNQX, 5 μM), a potent antagonist of glutamate-gated α-amino-3-hydroxy-5-methyl-4-isoxazolepropionic acid (AMPA) receptors, D(-)-2-Amino-7-phosphonoheptanoic acid (AP-5, 50 μM), a selective antagonist of N-Methyl-D-aspartic acid (NMDA) receptors, and picrotoxin (PTX, 50 μM) a competitive antagonist of gamma-aminobutyric acid type A ($GABA_A$) receptors. Whole-cell patch-clamp recordings were performed at a holding potential of -74mV (a value that is corrected for liquid junction potential error offset) and sequential current injections ranging from -20 to +50 pA were applied to evoke voltage responses from individual MSNs. Individual MSNs were investigated at day 20, 40 and 60 post-neuronal differentiation. Representative voltage responses for individual MSNs from each line investigated across days 20, 40 and 60 are shown in Figure 3-6. Due to time constraints, longitudinal comparisons were limited to one control (Con-1), one *C9ORF72*^{RE} MSN (C9-1), and its matched isogenic control (C9-Δ1). This analysis provided valuable insights into electrophysiological changes over time.

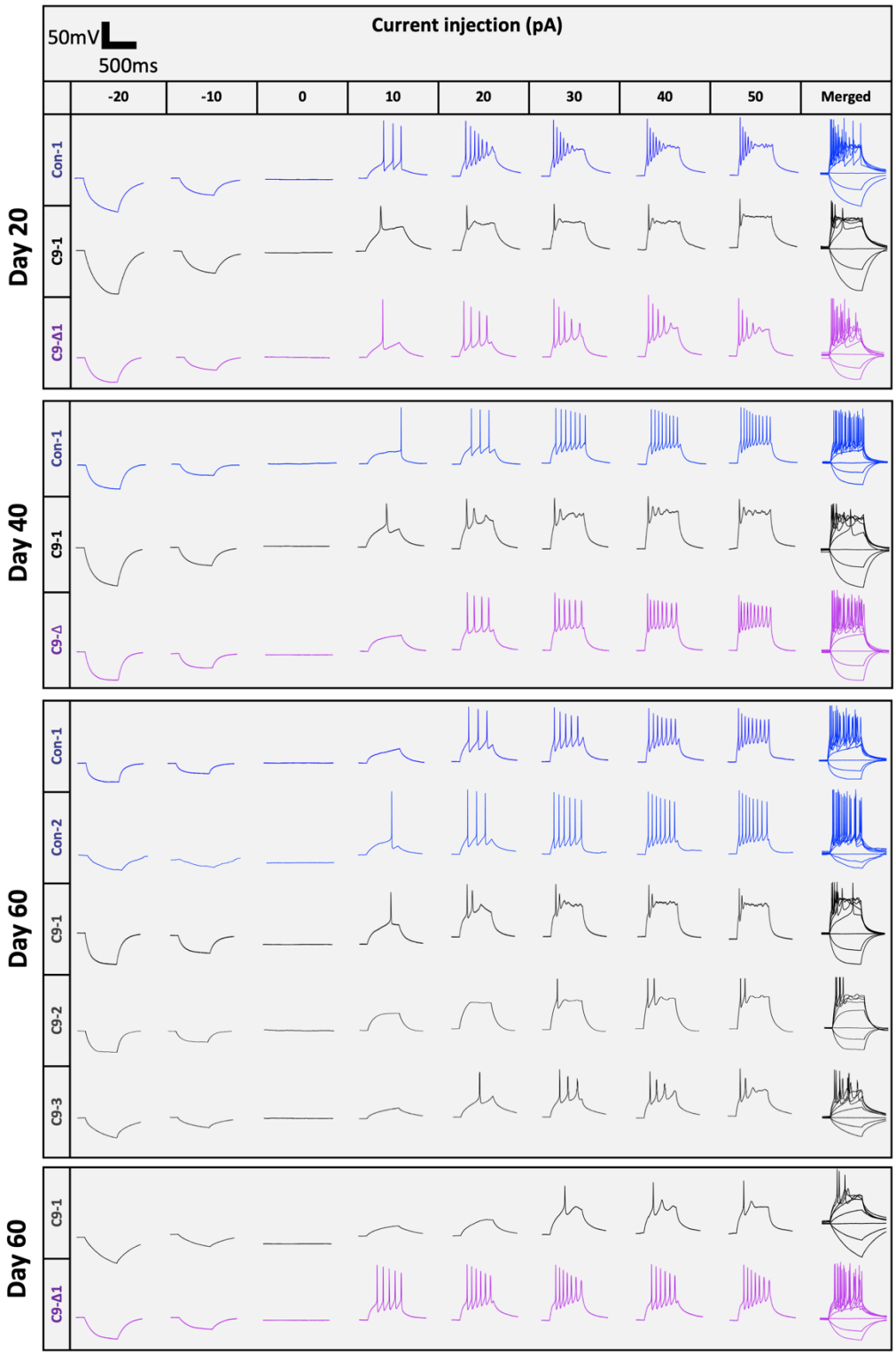

Figure 3-6. ***Representative AP traces*** *of whole-cell current clamp recordings reveal a loss-of-function phenotype in C9ORF72^{RE} MSNs. Recordings were made from individual MSNs at timepoints day 20, 40 and 60 post neuronal differentiation for healthy control lines (blue), C9ORF72^{RE} MSNs (grey) and the isogenic control line, C9-Δ 1 (purple). The matrix format displays responses to sequential 500ms current injections from -20pA to 50pA in 10pA increments from a holding potential of -74mV (including liquid junction potential correction [-14mV]).*

Depolarising current injections were observed to evoke action potential activity in most cells. The C9-1 line was observed to evoke less APs compared to Con-1 and C9-Δ1 line at day 20 and 40. Further, the comparison of representative traces at day 60 for all control lines used in this study (Con-1, Con-2) and all *C9ORF72*^{RE} MSNs (C9-1, C9-2, C9-3) reveal an apparent difference in voltage responses in the latter, evidenced by weaker AP firing. C9-1 was compared to its matched isogenic control, C9-Δ1, at day 60 and appeared to evoke less APs. *C9ORF72*^{RE} MSNs lines therefore appeared hypoexcitable.

To characterise this more formally, I detailed the action potential properties in greater detail. In response to the current injection protocol, MSNs displayed three distinct response behaviours: multiple APs (≥ 2), single AP and no response (Figure 3-7A). An AP was defined as a voltage response exceeded 0 mV. At day 20, 30% of control Con-1 MSNs fired no APs, 20% fired one AP, and 50% fired multiple APs. This progressively shifted with culture time with all lines exhibiting multiple APs firing by day 60 (Figure 3-7B), demonstrating progressive maturation of intrinsic excitability (Le Cann et al., 2021). *C9ORF72*^{RE} MSNs showed an increase in multiple AP firing with maturation (27% at day 20 to 60% at day 60). However, it did not reach the same levels as the control and a larger proportion of *C9ORF72*^{RE} MSNs consistently fired only one AP (47% at day 20, 33% at day 60; Figure 3-7B). Contrastingly, the isogenic control, C9-Δ1, largely mirrored control Con-1 MSN development, suggesting that the *C9ORF72*^{RE} directly impacts MSN excitability (Figure 3-7B). To verify this finding, I extended my data set to include more iPSC lines derived from more healthy individuals and *C9ORF72*^{RE} patients and examined them at day 60. MSNs derived from two healthy individual iPSC lines (Con-1, Con-2) exhibited only multiple APs, while the *C9ORF72*^{RE} patient-derived MSN lines (C9-1, C9-2, C9-3) exhibited diverse firing patterns in response to current injection. The majority of *C9ORF72*^{RE} MSN cells (> 58% of cells) showed multiple APs, while the rest exhibited either single or no APs (Figure 3-7C). The isogenic C9-Δ1 line demonstrated an increase in AP firing compared to C9-1 (Figure 3-7D). These data provided indication of a compromised intrinsic excitability profile in *C9ORF72*^{RE} MSNs compared to healthy controls that further suggests an impaired ability to fire APs.

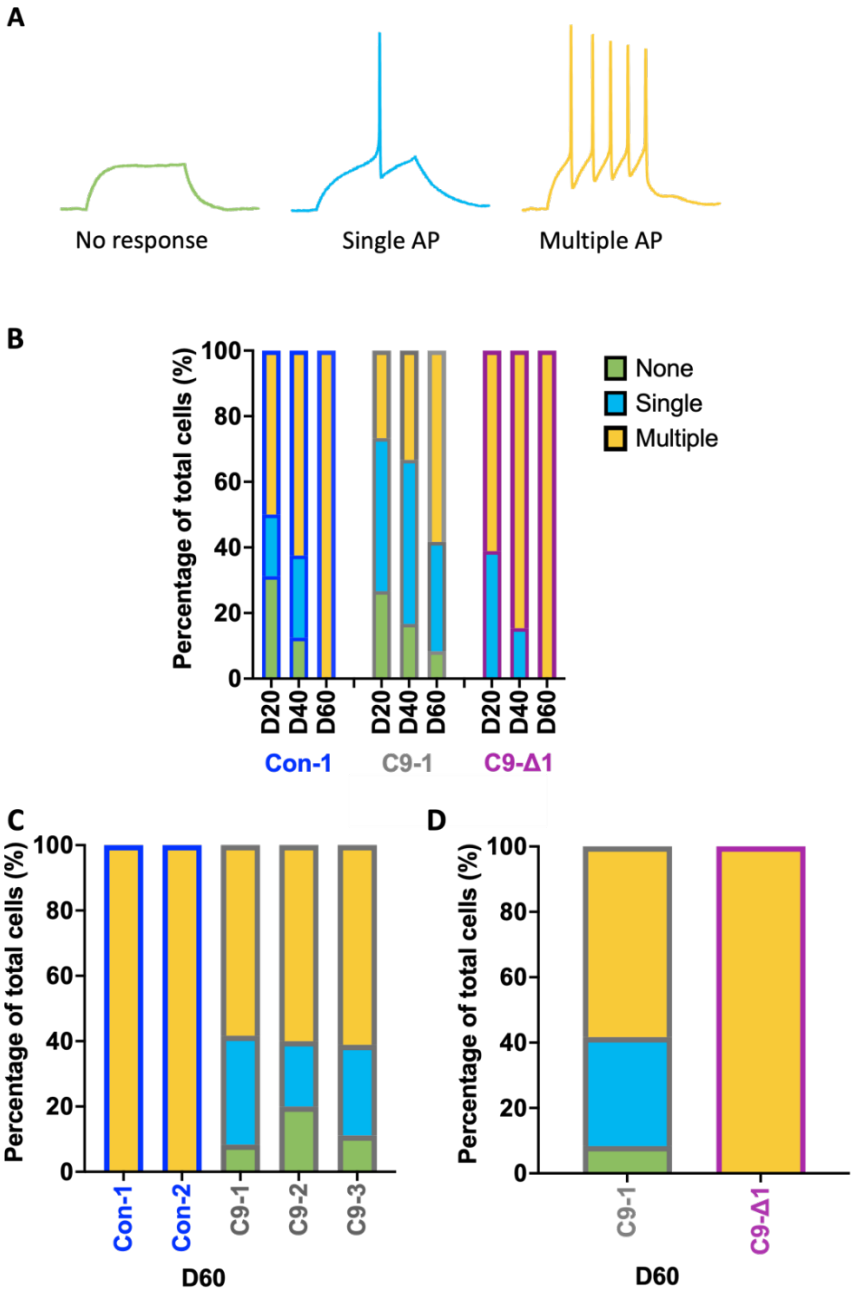

Figure 3-7. ***Decreased firing capability in GABAergic MSNs.*** *A. Example traces of the three categories of action potential firing observed; no response (no bona fide AP that either did not reach threshold or cross 0 mV), single AP or multiple APs. B. Percentage of cells exhibiting each firing category throughout the course of differentiation at day 20, 40 and 60 for Con-1, C9-1 and C9-Δ1 MSNs. Note the increase in activity over time for each lines indicating neuronal maturation. Note the lower overall activity of C9-1 with time versus Con-1 and C9-Δ1. C. Percentage of total cells showing firing patterns at day 60. Note the lower overall activity of all C90RF72^{RE} MSNs compared to healthy controls. D. Comparison at day 60 between C9-1 and its matched isogenic line C9-Δ1. Note the lower overall activity in C9-1 compared to C9-Δ1. Data: Con-1, day 20, n=14, N=7; day 40, n=19, N=6; day 60, n=16, N=5; C9-1, day 20, n=29, N=8; day 40, n=24, N=6; day 60, n=24, N=6; C9-Δ1, day 20, n=18, N=5; day 40, n=13, N=4; day 60, n=9, N=4; Con-2, day 60, n=11,N=4; C9-2, day 60, n=16, N=4; C9-3, n=18, N=4..*

To investigate a potential reduction in capability of *C9ORF72*^{RE} MSNs to fire APs, I next examined the ability of MSNs to respond to depolarising current stimulation (500ms) from 0 pA to 50 pA in 5 pA increments. Specifically, the AP number, if any, was measured for each current stimulation and plotted. Initially, plots for Con-1, C9-1 and C9-Δ1 were obtained at day 20, 40 and 60 to investigate the shift in responsiveness of MSNs over time (Figure 3-8A,B,C). The Con-1 line showed a statistically significant ($F(10, 367)=324.7$, $p<0.0001$, Two-way ANOVA) increase in AP firing to current stimulation as maturation progresses from 20 to 60 days, demonstrating normal development of intrinsic excitability (Figure 3-8A). However, whilst AP firing increased significantly ($F(10,595)=154.5$, $p<0.0001$, Two-way ANOVA) with time from day 20 to 60, C9-1 cells maintained low AP firing number to current stimulation regardless of maturation stage (Figure 3-8B). Notably, the C9-Δ1 data revealed a significant ($F(10, 303)=221.8$, $p<0.0001$, Two-way ANOVA) increase in AP number to current stimulation over time, resembling the behaviour of Con-1 line (Figure 3-8C). Full statistical analysis (Sidak's multiple comparison test) can be found in Appendix 1. MSNs derived from C9-1 patient iPSCs show a hypoexcitable phenotype.

To validate these findings, I extended my analysis to additional cell lines at day 60. Both Con-1 and Con-2 lines displayed equivalent AP number profiles in response current injection ($p=0.99$, Two-way ANOVA, Sidak's multiple comparison test available in Appendix 2). These cells consistently fired multiple action potentials across the current injection protocol, indicating robust intrinsic excitability. In contrast, all three *C9ORF72*^{RE} MSN lines (C9-1, C9-2, C9-3) showed significant ($F(70, 1165)= 24.81$, $p<0.0001$, Two-way ANOVA, Sidak's multiple comparison results available in Appendix 2.) reductions in AP number elicited by current stimulation compared to controls (Figure 3-8D). Further, I compared the gene-edited isogenic line C9-Δ1 to C9-1. C9-Δ1 MSNs lacking the *C9ORF72*^{RE} mutation displayed a significantly improved excitability profile compared to C9-1 ($F(10, 238)= 135.0$, $p<0.0001$,Two-way ANOVA, Sidak's multiple comparison analysis detailed in Appendix 3). The C9-Δ1 MSNs fired significantly more APs across the whole current injection protocol, indicating a restored intrinsic excitability (Figure 3-8E). These data show that *C9ORF72*^{RE} MSNs demonstrate intrinsic hypoexcitability.

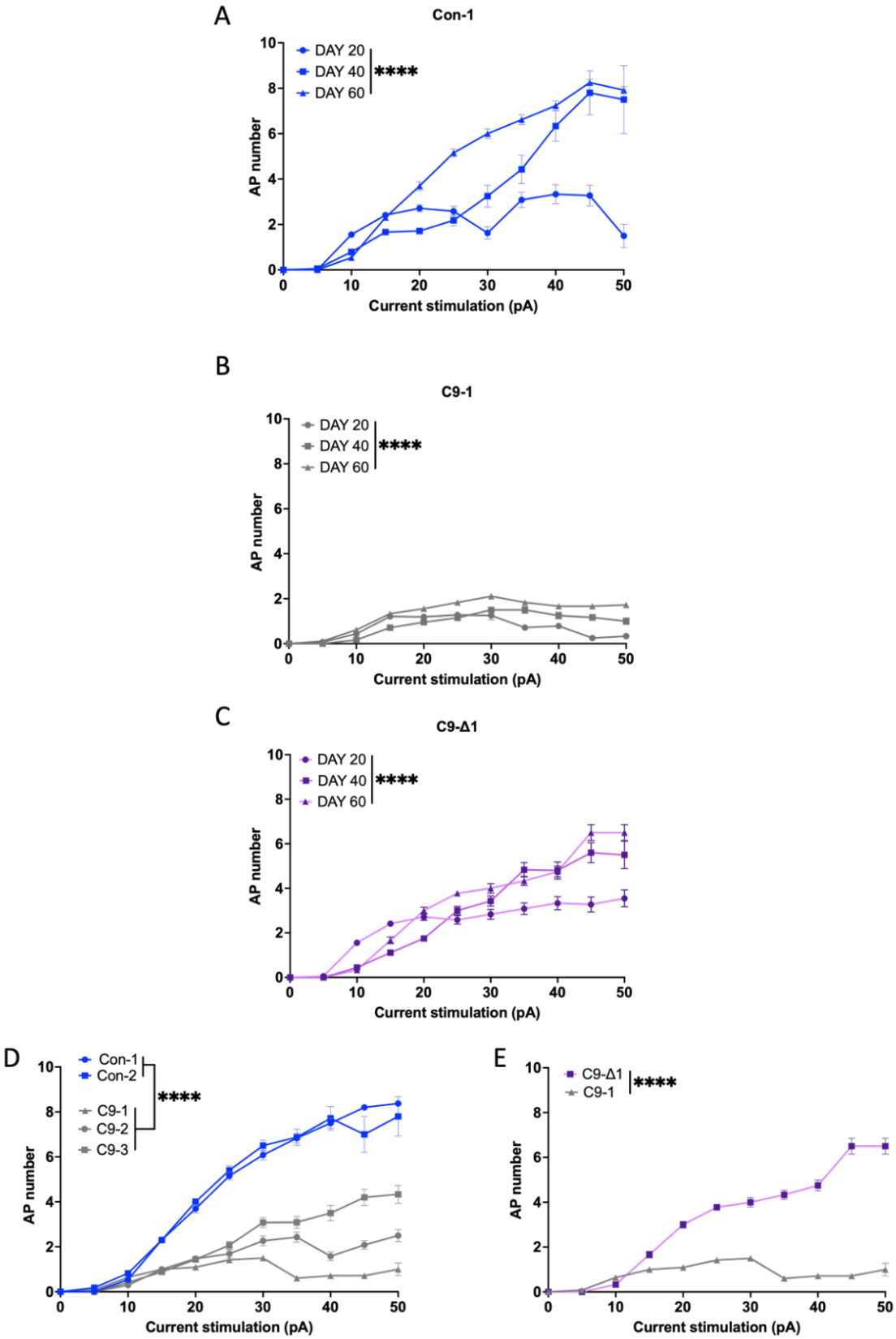

Figure 3-8. ***C9ORF72^{RE} MSNs are less responsive to depolarization.*** *Figure caption on the next page.*

Figure 3-8. ***C9ORF72^{RE} MSNs are less responsive to depolarization.*** *A, B and C. The mean ± SEM AP number in response to increasing current stimulation for days 20, 40 and 60 are presented for Con-1 (blue), C9-1 (grey) and C9-Δ1 (purple), respectively. Note the impaired responsiveness of AP generation in C9-1 from Day 20 to day 60 compared to Con-1 and C9-Δ1. D. Graph illustrates comparison between all three C9ORF72^{RE} lines (C9-1, C9-2, C9-3, grey) and control lines (Con-1 and Con-2, blue) at day 60. AP generation is impaired in all C9ORF72^{RE} lines. E. The mean ± SEM AP number against current stimulation plot of C9-1 and its matched isogenic line C9-Δ1 at day 60 shows C9-1 is impaired. Statistical analysis was determined using Two-tailed ANOVA with Sidak's multiple comparison test (****, p<0001). Data: Con-1, day 20, n=14, N=7; day 40, n=19, N=6; day 60, n=16, N=5; C9-1, day 20, n=29, N=8; day 40, n=24, N=6; day 60, n=24, N=6; C9-Δ1, day 20, n=18, N=5; day 40, n=13, N=4; day 60, n=9, N=4; Con-2, day 60, n=11,N=4; C9-2, day 60, n=16, N=4; C9-3, n=18, N=4.*

To further explore the intrinsic excitability properties of iPSC-derived MSNs I also measured the passive membrane properties of individual MSNs. The resting membrane potential (RMP), whole-cell capacitance (WCC) and input resistance (R_{in}) are important parameters in membrane physiology, reflecting the overall developmental status, viability and excitability of the cell's membrane. RMP is crucial for the regulation of cell excitability. The RMP arises from a dynamic equilibrium between ion concentrations and selective permeability of the cell membrane. This potential difference is maintained by ion pumps like Na^+/K^+-ATPase, which actively use ATP to establish appropriate Na^+/K^+ concentration gradients. In essence, the RMP reflects proper cellular function and establishes the foundation for the generation of APs, which underlie neuronal excitability. RMP was measured by placing the patch-clamp amplifier so that it was not introducing any current (I = 0), therefore allowing the MSN to dictate its natural RMP. The RMP was measured for Con-1, C9-1 and C9-Δ1 at day 20, 40 and 60. Unlike, AP number vs current stimulation, these longitudinal analyses revealed no significant changes (p>0.8, One-way ANOVA) with time for each line (Figure 3-9A). Both Con-1 and Con-2 were compared to all three *C9ORF72*^{RE} MSN lines at day 60 (Figure 3-9B). Only one significant difference was observed between Con-2 and C9-1 in terms of RMP (p=0.0019, One-way ANOVA), but it was not consistent across all the lines. No statistical differences (p=0.3210, Student's t-test) were observed when comparing C9-1 and C9-Δ1 (Figure 3-9C). The RMPs measured for all the lines lie within the expected range for in vitro iPSC-derived MSNs (Le Cann et al., 2021). These data indicate that the RMP of MSNs remained stable across conditions and timepoints, suggesting that

the loss-of-function phenotype observed in terms of AP number is not linked to the overall health and RMP of MSNs. These data are consistent with the other markers of viability (Caspase-3) described previously (Figure 3-5F).

The cell membrane's phospholipid bilayer acts as a capacitator. The WCC is directly proportional to cell surface area and makes the WCC a tool for estimating cell size and is a key marker of health and integrity of the cell membrane. The longitudinal analysis showed a consistent increase in WCC in all lines across maturation, as expected (Gertler et al., 2008), revealing healthy membrane development (Figure 3-9D,E,F). Only C9-1 showed statistically different values between day 20, 40 and 60 (day 20 vs day 40, p=0.0179; day 20 vs day 60, p=0.0001; One-way ANOVA; Figure 3-9D), suggesting the development of the WCC maybe more advanced in C9-1. However, comparative analysis of WCC at day 60 between *C9ORF72*^{RE} MSNs (C9-1, C9-2, C9-3) and control (Con-1, Con-2) lines showed one significant difference between Con-1 and C9-1 (p=0.0498, One-way ANOVA), but further data from other lines, including C9-1 and C9-Δ1 were not impacted. These data indicate that the development of WCC across all lines was not impacted.

The R_{in} reflects the membrane's opposition to the flow of ions via channels and pumps. Higher R_{in} generally indicate less conductive membranes, leading to increased excitability as smaller current can induce larger potential changes. Conversely, lower R_{in} suggests greater membrane conductance, potentially damping excitability. R_{in} can also reflect the morphology of the cell. Larger cells or processes with higher surface area (higher WCC) tend to have lower R_{in}, while smaller neurons or processes with limited surface area (lower WCC) exhibit higher R_{in} values. The R_{in} was established from the mean passive membrane current amplitude generated at a -20pA current injection to minimize (depolarising) voltage-gated channel activation and isolate passive membrane properties. The R_{in} was measured for Con-1 and C9-1 revealed consistent values across from day 20 to 60, but a significant decrease from day 20 to day 60 (p=0.0468, One-way ANOVA) was observed in C9-Δ1 (Figure 3-9G), which correlates with an increase in WCC at day 60. Comparison of both controls (Con-1, Con-2) and *C9ORF72*^{RE} MSNs revealed no consistent changes at day 60 (Figure 3-9I). Same behavioural was observed between C9-1 and C9-Δ1 (Figure 3-9J). Immature neurons are known to display high values of R_{in} that decrease as they reach mature developmental stages (Mongiat et al., 2009). My data confirms this

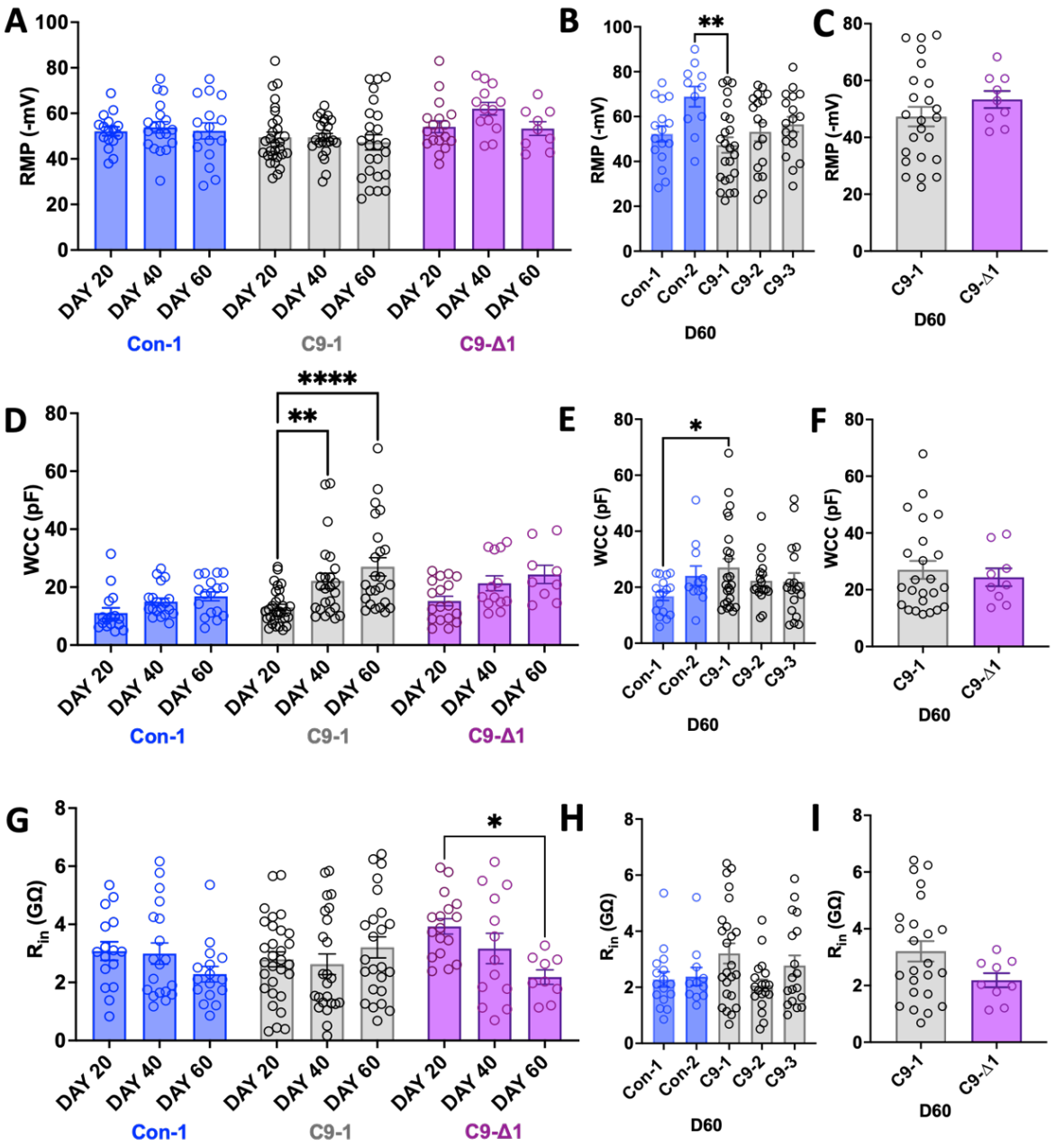

Figure 3-9. ***Intrinsic membrane properties of C9ORF72^{RE} MSNs are not impacted.*** *A. Mean ± SEM RMP data for Con-1, C9-1 and C9-Δ1 for days 20, 40 and 60. Data from individual cells are depicted by circles inset into the bar graphs. B. Mean ± SEM RMP data for Con-1, Con-2, C9-1, C9-2 and C9-3 for day 60. C. Mean ± SEM RMP data for C9-1 and respective C9-Δ1 for day 60. Note that no consistent changes in RMP are observed. D, E and F. As in A, B, and C, respectively, but for whole-cell capacitance (WCC). Note increasing WCC trend with maturation, as expected, in all lines. G, H and I. As in A, B, and C, respectively, but for membrane input resistance (Rin). Statistical analysis was determined by using One-way ANOVA or Student's t-test (*, p<0.05; **, p<0.01; ****, p<0.0001). Data: Con-1, day 20, n=14, N=7; day 40, n=19, N=6; day 60, n=16, N=5; C9-1, day 20, n=29, N=8; day 40, n=24, N=6; day 60, n=24, N=6; C9-Δ1, day 20, n=18, N=5; day 40, n=13, N=4; day 60, n=9, N=4; Con-2, day 60, n=11,N=4; C9-2, day 60, n=16, N=4; C9-3, n=18, N=4.*

maturation feature, and the significant changes observed are unlikely to contribute to the loss-of-function phenotype observed in *C9ORF72*^{RE} MSNs. Overall, these observations suggest that the passive membrane properties remain largely unaltered in *C9ORF72*^{RE} MSNs compared to healthy and isogenic controls, suggesting that the hypoexcitability phenotype observed in terms of their AP number is not due to altered passive membrane properties. Furthermore, given that passive membrane properties are linked MSN development; we can rule out that *C9ORF72*^{RE} MSNs are hypoexcitable due to them being more immature. Collectively, the data presented so far are indicative that *C9ORF72*^{RE} MSNs may exhibit hypoexcitability due to altered induced AP properties, i.e., basal excitability appears unimpacted.

Action potential waveforms form the fundamental basis for neuronal firing and feature distinct phases, which are orchestrated by numerous voltage-gated ion channels and transporters. A summary of the different waveform phases is provided in Figure 3-10A. The waveform of MSNs was investigated for each line over day 20, 40 and 60 by investigating the first AP elicited by a 30 pA depolarising current injection. This 30 pA current depolarisation elicited APs in most cells (Con-1, day 20: 71%, day 40: 89%, day 60: 92%; C9-1, day 20: 60%, day 40: 70%, day 60: 68%; C9-Δ1, day 20: 100%, day 40: 92%, day 60: 100%). Non-responder cells were not used for this analysis. The waveform was taken up to 15 ms before and after the peak amplitude was determined. Each plot was aligned to point at which it crossed 0 mV. The mean AP waveform (bold trace; Figure 3-10B,C,D) was determined from individual recordings from the Con-1 and C9-Δ1 lines (Figure 3-10B,C,D). Longitudinal analysis of the Con-1, C9-1 and its matched isogenic line C9-Δ1 revealed progressively sharper and higher amplitude values over time in accordance with an expected maturation of the AP waveform over time (Lam et al., 2017). However, the AP waveform for the C9-1 line, best observed at day 60, shows a reduced amplitude and a 'stunted' appearance compared to Con-1 and C9-Δ1. The C9-1 AP waveform appears disturbed and because AP waveforms directly underpin neuronal excitability, likely underpin the hypoexcitability in *C9ORF72*^{RE} MSNs.

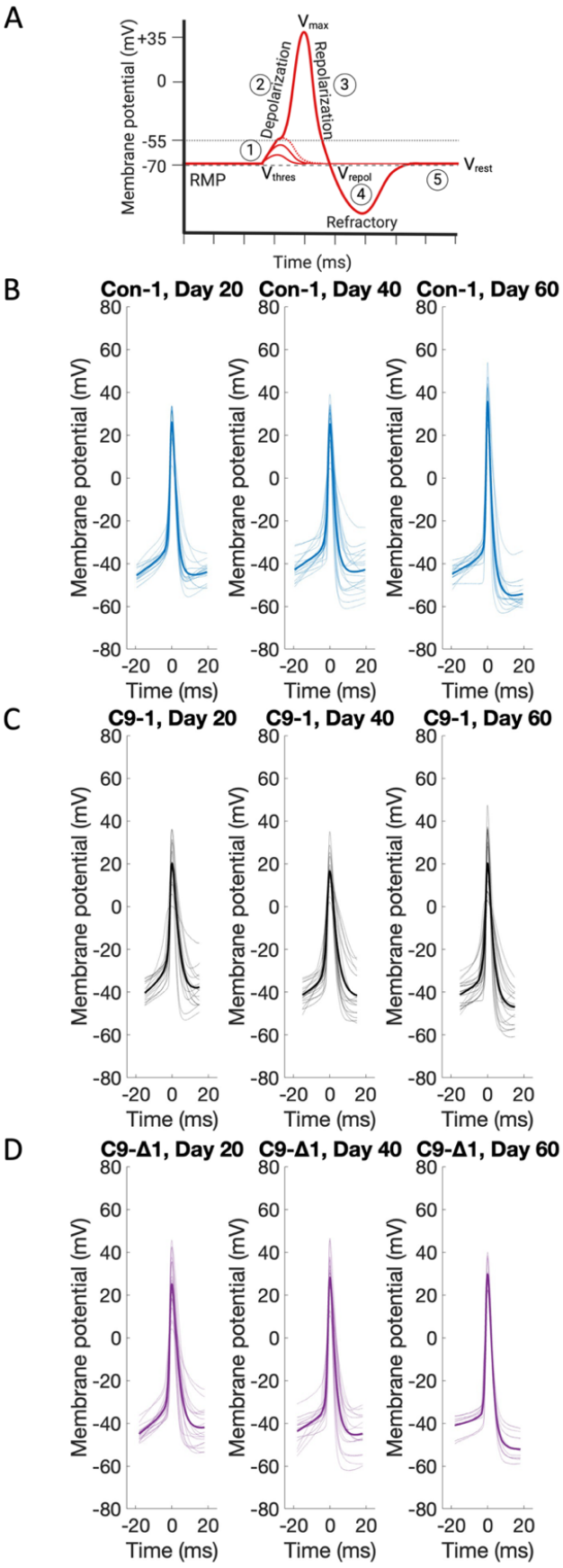

Figure 3-10. ***C9ORF72^{RE} MSNs show impaired AP waveform.*** *Caption on the next page.*

Figure 3-10. ***C9ORF72^{RE} MSNs show impaired AP waveform.*** *A. Schematic representation of the stages of the action potential waveform. 1. Local potential depolarisation. 2. Depolarization: opening of voltage-gated Na^+ channels. 3. Repolarization: closure of voltage-gated Na^+ channels and opening of voltage-gated K^+ channels. 4. Hyperpolarization: voltage-gated K^* channels remain open after the potential reaches resting level. The schematic also shows the potentials at rest (V_{rest}), threshold (V_{thres}), peak amplitude (V_{max}) and repolarization (V_{repol}). B,C and D. The first AP evoked by 30 pA current injection was extracted from all recordings performed for Con-1 (blue), C9-1 (black) and C9-Δ1 (purple). The mean AP waveform for each group of recordings are shown in the bold colour, while individual AP traces are in a lighter colour shade (Con-1, day 20: n = 14, day 40: n = 17, day 60: n = 12; C9-1, day 20: n =18, day 40: n = 17, day 60: n = 17; C9-Δ1, day 20: n = 15, day 40: n = 17, day 60: n = 9). The traces are aligned to 0 mV-crossing time. Note the increase in 'sharpness' (dV/dt) and amplitude (V_{max}) of the AP waveform for each line, as expected of maturation. Note the C9-1 waveform exhibits reduced 'sharpness' compared to Con-1 and C9-Δ1.*

To explore the waveform perturbations in *C9ORF72*^{RE} MSNs, I conducted more detailed AP waveform analysis. First, I investigated the AP recruitment current; the minimum current depolarisation required to evoke an AP. Altered recruitment current can indicate altered excitability. When comparing the lines longitudinally, there is a trend for each line for the recruitment current to increase, though no significant differences were identified between the time points for the Con-1, C9-1 and C9-Δ1 MSNs (p>0.99, One-way ANOVA; Figure 3-11A). Comparison of the recruitment current between the control and *C9ORF72*^{RE} MSNs at day 60 showed no significant differences (p>0.063, One-way ANOVA; Figure 3-11B), nor between the C9-1 line and isogenic control, C9-Δ1 (p=0.219, Student's t-test; Figure 3-11C). *C9ORF72*^{RE} MSNs hypoexcitability appears not to be explained by altered recruitment current.

The recruitment current data suggests that AP threshold is unlikely to be impacted, i.e. a change in recruitment current can reflect an altered threshold of AP initiation. To verify this, I examined the first AP of the rheobasic current for Con-1, C9-1 and C9-Δ1 MSNs from day 20 to 60. For C9-1, the threshold potential revealed one statistically significant change from day 20 to day 60 (p=0.0423, One-way ANOVA), becoming more hyperpolarised with time. However, the change in threshold is modest and doesn't appear to be majorly different from other lines. To compare between lines, I examined the threshold at day 60 and found that only a single significant difference was identified between Con-1 and C9-3

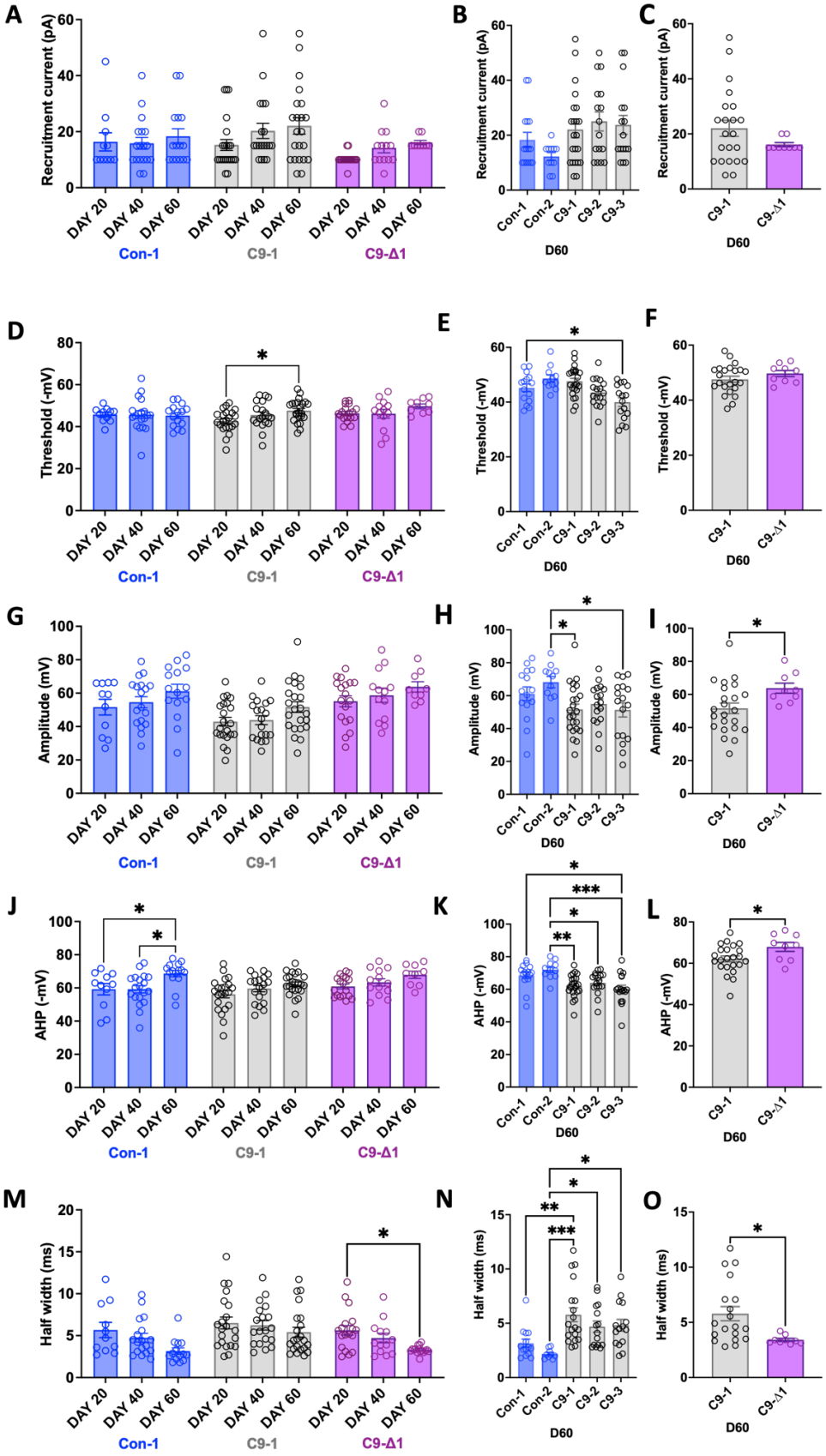

Figure 3-11. ***Altered AP properties are observed in C9ORF72^{RE} MSN***. *Caption on the next page.*

Figure 3-11. ***Altered AP properties are observed in C9ORF72^{RE} MSN****. A, Mean ± SEM recruitment current data for Con-1, C9-1 and C9-Δ1 for days 20, 40 and 60. Data from individual cells are depicted by circles inset into the bar graphs. B. Mean ± SEM recruitment current data for Con-1, Con-2, C9-1, C9-2 and C9-3 for day 60. C. Mean ± SEM recruitment current data for C9-1 and respective C9-Δ1 for day 60. D, E and F, As for A, B and C, but for AP threshold potential. G, H and I, As for A, B and C, but for AP amplitude. J, K and L, As for A, B and C, but for AP AHP. Note the modest depolarisation of the AHP in C9ORF72^{RE} MSN lines versus controls and C9-Δ1 lines. M, N and O, As for A, B and C, but for AP half-width. Note the slower half-width of C9ORF72^{RE} MSN lines versus controls and isogenic line. Statistical significance was determined using One-way ANOVA or Student's t-test (*, p<0.05; **, p<0.01; ***, p<0.001). Data: Con-1, day 20, n=14, N=7; day 40, n=19, N=6; day 60, n=16, N=5; C9-1, day 20, n=29, N=8; day 40, n=24, N=6; day 60, n=24, N=6; C9-Δ1, day 20, n=18, N=5; day 40, n=13, N=4; day 60, n=9, N=4; Con-2, day 60, n=11,N=4; C9-2, day 60, n=16, N=4; C9-3, n=18, N=4.*

(p=0.0404, One-way ANOVA; Figure 3-11C). The data remained non-significantly different across all other comparisons between lines. Threshold data align with the rheobase data, suggesting that alterations in AP threshold are unlikely to underpin the hypoexcitability in *C9ORF72*^{RE} MSNs.

Next, I investigated the AP amplitude (V_{max}- V_{thres}), which forms a key determinant of excitability, i.e. the greater the amplitude the greater the depolarization of the MSN membrane. I observed a gradual increase in AP amplitude from day 20 to 60 in Con-1, C9-1 and C9-Δ1 (Figure 3-11G), which is expected with maturation (Lam et al., 2017). However, it is clear that the C9-1 line appears to have reduced AP amplitude. I therefore extended the amplitude dataset at day 60 to compare between other lines. Control line Con-2, but not Con-1, exhibited significantly higher AP amplitude compared to two *C9ORF72*^{RE} MSN lines (Con-2 vs C9-1, p=0.0216; Con2 vs C9-3, p=0.0291, One-way ANOVA; Figure 3-11E). At day 60, I found statistically higher (p=0.0344, Student's t-test) amplitudes in C9-Δ1 compared to C9-1 line. The data appear consistent with a modest reduction in AP amplitude in *C9ORF72*^{RE} MSNs, however this cannot explain the hypoexcitability displayed by *C9ORF72*^{RE} MSNs.

The afterhyperpolarization (AHP) is the hyperpolarizing phase of the AP when the neuron's membrane potential falls below the standard RMP (V_{repol}). I examined the AHP from day 20 to day 60 for the Con-1, C9-1 and C9-Δ1 MSNs and each line showed a more hyperpolarising trend, significantly changed in Con-1 MSNs (Day 20 vs Day 60, p=0.0488; Day 40 vs day 60, p= 0.0134, One-way ANOVA; Figure 3-11J) as expected as the MSNs become more mature (Larsson, 2013). Comparative analysis at day 60 across all lines shows the AHP

data reveals more hyperpolarizing values in Con-2 compared to all *C9ORF72*^{RE} MSNs (Con-2 vs C9-1, p=0.0030; Con-2 vs C9-2, p=0.0373, Con-2 vs C9-3, p=0.0006, One-way ANOVA, Figure 3-11K). Con-1 MSNs were also significantly different to C9-1 (One-way ANOVA; Figure 3-11K). Furthermore, a statistically significant change (p=0.0376, Student's t-test) was observed between C9-1 and C9-Δ1 (Figure 3-11L). Whilst the data values are relatively modest, the AHP appears to be more depolarised in *C9ORF72*^{RE} MSNs suggesting impaired repolarization dynamics. Similar to amplitude, this AP feature is not consistent across all lines, but could be suggested to contribute to the observed phenotype, but not substantial enough to explain the hypoexcitability in *C9ORF72*^{RE} MSNs.

The speed of the AP was next investigated by measuring the AP half-width. The half-width was defined as the time interval (measured in ms) between the upstroke and downstroke of the AP at half its defined amplitude. Physiologically, the half-width shortens as the cells become more mature (Le Cann et al., 2021), which was observed to be a trend in the longitudinal analysis from day 20 to 60 in Con-1 and C9-1 MSNs and significantly in C9-Δ1 MSNs (p=0.0493, One-way ANOVA; Figure 3-10M). However, the longitudinal decrease in half-width in C9-1 MSNs appears to be notably altered. To explore this further, comparative analysis at day 60 between all lines demonstrated that the half-width was approximately double that in *C9ORF72*^{RE} MSNs versus control lines and significant in the majority of the comparisons (Con-1 vs C9-1, p=0.0033; Con-2 vs C9-1, p=0.0003; Con-2 vs C9-2, p=0.0300; Con-2 vs C9-3, p=0.0200, One-way ANOVA; Figure 3-10N). Further, a statistically shorter half-width was evidenced in C9-Δ1 MSNs when compared to the C9-1 line (p=0.0186, Student's t-test; Figure 3-10O) that is comparable to control lines. Importantly, these findings suggest a significantly longer-lasting action potentials in *C9ORF72*^{RE} MSNs at day 60 compared to healthy controls.

Since the AP waveform half-width is impaired in *C9ORF72*^{RE} MSNs, I generated phase plots from the mean AP waveforms in Figure 3-10B,C,D to depict the rate of change in membrane potential (dV/dt) against the membrane potential of the cell (V). As illustrated in Figure 3-12A, the phase plot allows a greater resolution of waveform dynamics, particularly that of the AP upstroke (depolarisation) and downstroke (repolarisation), which determine the AP

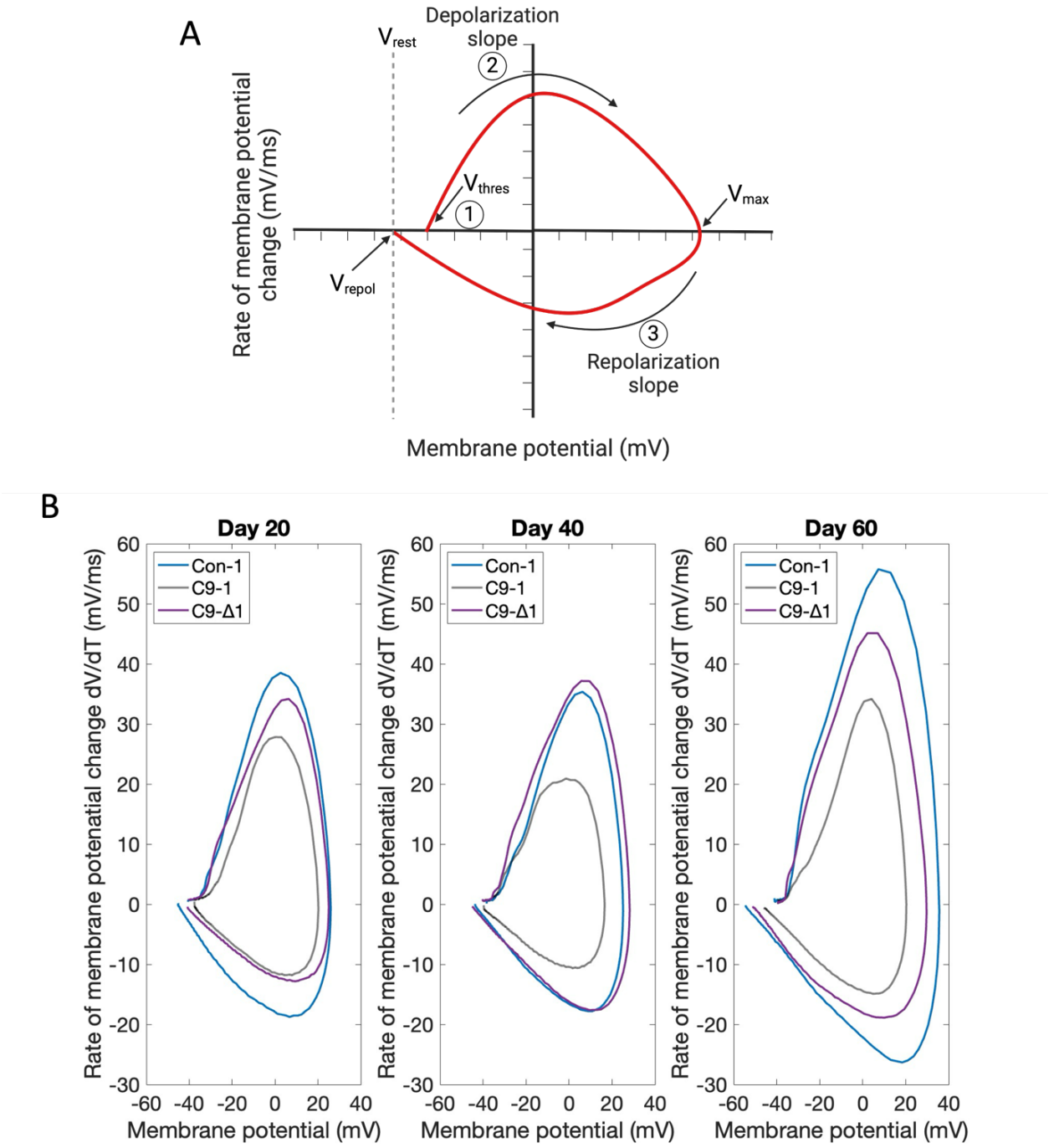

Figure 3-12. ***Phase plot analysis of AP waveforms shows disturbed C9ORF72^{RE} MSN waveforms****. A. Schematic showing the distinct phase plot components corresponding to the AP waveform components, as highlighted in Figure 3-10, including V_{rest} (RMP), V_{thres} (threshold membrane potential), V_{max} (maximal voltage peak of AP or amplitude), V_{repol} (repolarization potential or AHP). B. The mean AP waveforms presented in Figure 3-10 were taken and replotted according to the rate of membrane potential change (dV/dt) versus membrane potential (V) for Con-1, C9-1 and C9-⊿1 MSNs at day 20, 40 and 60. Note the progressive impairment in the 'shape' of the C9-1 AP waveform over time, and that this is notably impacted in the depolarisation and repolarisation phases.*

half-width properties. Phase plots were constructed for Con-1, C9-1 and C9-Δ1 MSNs for day 20, 40 and 60 (Figure 3-12B), which reveals C9-1 AP waveforms to be substantially disturbed from that Con-1 and C9-Δ1. Specifically, both the depolarisation and repolarisation slopes show marked disturbance as time progresses. Because the depolarisation phase is controlled by voltage-gated Na^+ (Na_v) channels, these data indicate Na_v function is disturbed either by impairments in function and/or by having a different cellular position in *C9ORF72*^{RE} MSNs versus Con-1 and C9-Δ1. Equally, the repolarisation phase is controlled by voltage-gated K^+ (K_v) channels, and the disturbance in *C9ORF72*^{RE} MSNs indicates either a disturbed in function and/or positioning in the MSN. The data further show that the Con-1 and C9-Δ1 are largely similar, particularly at day 40, indicating that the waveform disturbances are unlikely to be substantially impacted by line-dependent mechanisms. Day 60 C9-Δ1 MSNs show a modest deviation away from that of Con-1 in terms of kinetics but are clearly disparate from that of C9-1. I also note that the phase plots are in agreement with the raw waveform properties in indicating that the AP threshold (V_{thres}) is not impacted, and, amplitude and AHP (V_{repol}) appear to be modestly disturbed in C9-1 versus Con-1 and C9-Δ1. These data are highly consistent with ion channel (Na_v and K_v channels) disturbances that control the depolarisation and repolarisation phases as being disturbed in *C9ORF72*^{RE} MSNs.

The depolarisation phase is controlled by Na_v channels; therefore, I used protocols (Livesey et al., 2016) to directly investigate Na_v activity. To do this, I examined MSNs in the whole-cell voltage-clamp configuration, which allows the MSN to be kept at constant voltage (-70 mV, not including LJP). To activate Na_v channels, I performed a substantial depolarising voltage-step protocol to 0 mV (detailed in Figure 3-13A) to activate Na_v channels. To isolate Na_v channel-specific activity I then repeated the experiment in the presence of maximally effective concentration of tetrodotoxin (TTX, 300nM), a selective Na_v channel blocker. The TTX-sensitive current was subtracted from the initial evoked current to yield the TTX-(Na_v)-specific current. Experiments were performed in the presence of synaptic blockers, as described for APs. Evoked Na_v currents were fast-activating and de-activating, as expected (Figure 3-13B,C,D). Three recordings were taken for each MSN and averaged to obtain individual MSN current data. To examine the functional expression of

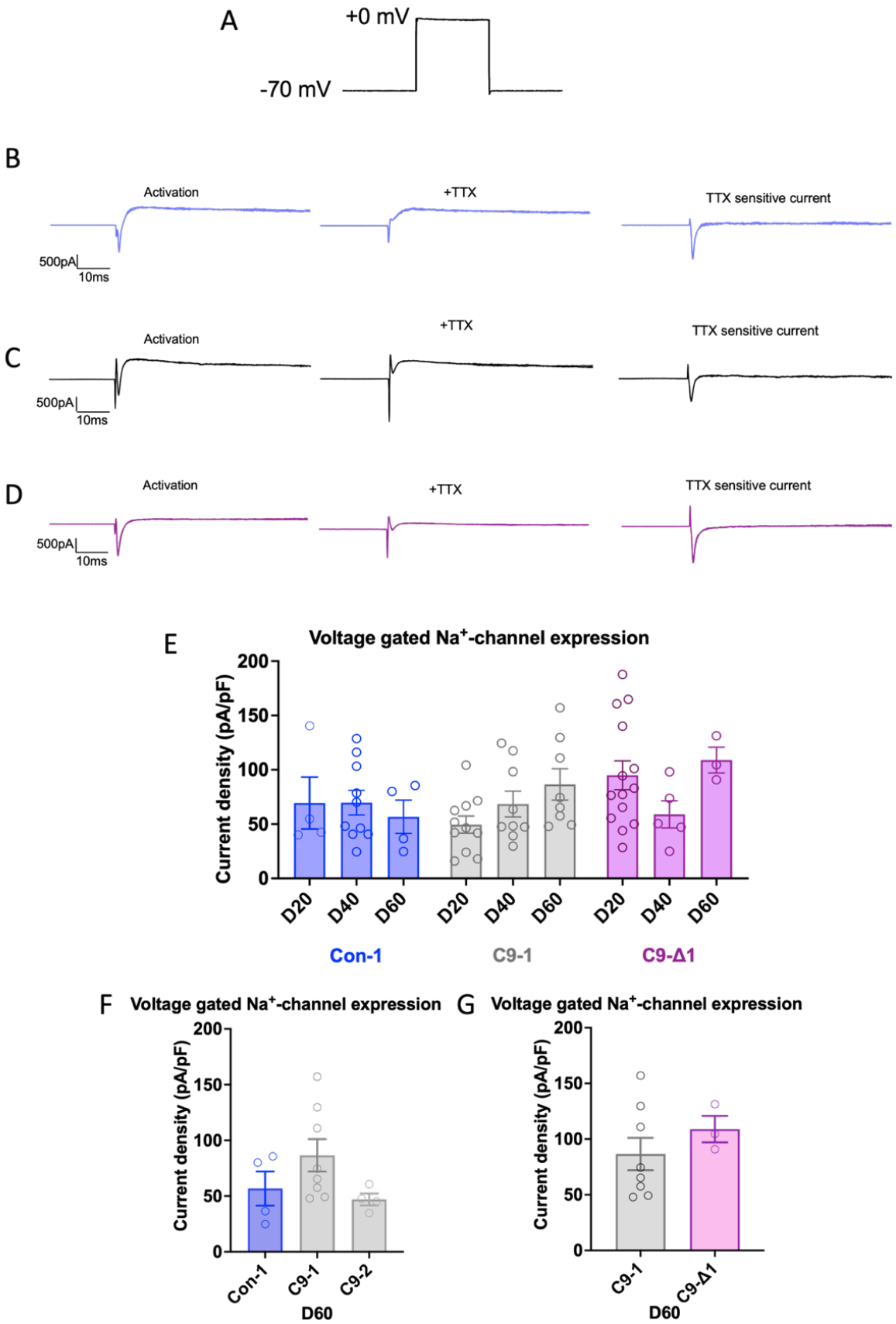

Figure 3-13. ***Voltage-gated Na⁺-channel current density measurements are consistent in MSNs****. Caption on the next page.*

Figure 3-13. ***Voltage-gated Na^+-channel current density measurements are consistent in MSNs****. A. A two-step depolarizing protocol was utilised to isolate Na_v channel activity. First, the Na_v channels were activated via a depolarization step of the membrane potential from a holding potential of -70mV to 0mV (activation). The same step was repeated in the presence of TTX, a specific Na_v channel blocker. The TTX-sensitive current was yielded by subtracting the current response in the absence of TTX from the TTX-containing trace, to yield TTX-sensitive Na_v channel activity. B,C,D. Representative traces at day 60 were selected to highlight each step of the protocol for each line investigated, Con-1 (blue), C9-1 (black) and C9-Δ1 (purple). Current amplitudes were determined from the peak of the Na_v -sensitive deflections. E. Mean ± SEM Na_v current density of Con-1, C9-1 and C9-Δ1 MSNs over days 20, 40 and 60. F. Mean ± SEM Na_v current density of Con-1, C9-1, C9-2 MSNs at day 60. G. As in F, for C9-1 and C9-ISO. Statistical significance was tested using One-way ANOVA or Student's t-test. Data: Con-1, day 20, n=4, N=3; day 40, n=10, N=3; day 60, n=4, N=1; C9-1, day 20, n=11, N=4; day 40, n=9, N=3; day 60, n=8, N=3; C9-Δ1, day 20, n=14, N=4; day 40, n=5, N=2; day 60, n=3, N=1; C9-2, day 60, n=4,N=1.*

Na_v channels I measured the current density, which normalises for differences in WCC between individual MSNs. This is determined by the current measurement divided by WCC for each MSN. Longitudinal analysis did not reveal significant differences in the peak Na_v current density across timepoints across any of the lines (Con-1, C9-1 and C9-Δ1) on days 20, 40 and 60, suggesting stable Na_v-channel expression over time. Comparative analysis of Na_v current density at day 60 between lines revealed that no significant ($p \geq 0.4$, One-way ANOVA and Student's t-test; Figure 3-13F,G) and no consistent changes in current density between MSNs derived from different lines. These data are consistent with the fact that the depolarising phase disturbance is unlikely to be caused by reduced total functional Na_v expression.

Next, to investigate the repolarisation phase disturbance, I examined the properties of K_v channels, which control the repolarisation phase. Two key types of K_v channels determine the repolarisation phase; A-type K channels (I_A) rapidly activate upon depolarisation and contribute to the initial, fast repolarization phase, shaping the AP duration and influencing subsequent AHP. Outwardly rectifying K^+ channels (I_K) slowly activate upon depolarisation and contribute to the sustained and slow repolarization following the rapid drop mediated by I_A channels. Although they activate slower than I_A they maintain K^+ efflux and stabilize the membrane potential towards resting state, influencing the total AP duration. I investigated the properties of these K_v channels.

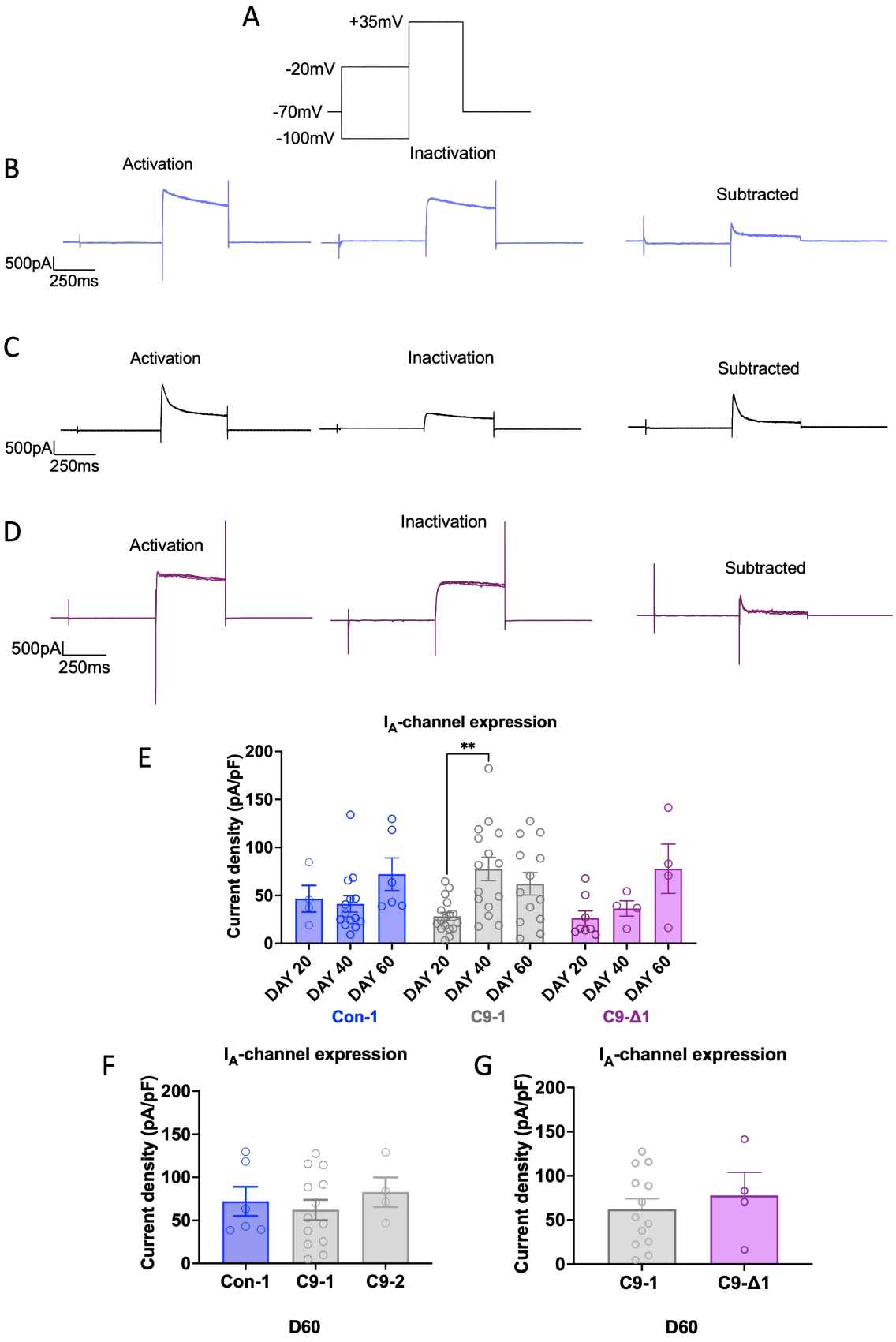

Figure 3-14. ***A-type (I_A) voltage-gated K^+ channel activity is not impaired.*** *Caption on the next page.*

Figure 3-14. ***A-type (I_A) voltage-gated K^+ channel activity is not impaired.*** *A. A two-step depolarizing protocol was utilised to isolate I_A channel activity. First, the current was stepped from -70 mV to -100 mV for 500 ms to 'prime' the I_A-type K_v channels. Then stepped to +35 mV for 400 ms ensuring a robust activation of I_A. To isolate I_A, I_A channels were inactivated by stepping the membrane potential to -20 mV for 500 ms before stepping to +35 mV for 400 ms. The inactivated I_A current was subtracted from the activation current to yield the isolated I_A current. B,C,D. Representative traces at day 60 were selected to highlight each step of the protocol for each line investigated, Con-1 (blue), C9-1 (black) and C9-Δ1 (purple). Current amplitudes were determined from the peak of the I_A-sensitive currents. E, Mean ± SEM I_A current density of Con-1, C9-1 and C9-Δ1 MSNs over days 20, 40 and 60. F. Mean ±SEM I_A current density of Con-1, C9-1, C9-2 MSNs at day 60. G. As in F, for C9-1 and C9-Δ1. Statistical analysis was determined by using One-way ANOVA or Student's t-test (**, p<0.01). Data: Con-1, day 20, n=4, N=2; day 40, n=14, N=6; day 60, n=6, N=2; C9-1, day 20, n=17, N=5; day 40, n=13, N=5; day 60, n=13, N=4; C9-Δ1, day 20, n=8, N=3; day 40, n=6, N=2; day 60, n=4, N=2; C9-2, day 60, n=4,N=1.*

To investigate I_A, I used a voltage-step protocol (Livesey et al., 2016); summarised in Figure 3-14A) that introduced a 500 ms hyperpolarizing pulse (-100mV) from a holding potential of -70 mV to facilitate complete recovery of I_A-channels from inactivation, followed by a 400 ms depolarising pulse to +35mV to activate them (activation). To isolate I_A currents, another protocol used a -20mV conditioning pulse to inactivate I_A-type K_v current, which takes advantage of the rapid inactivation kinetics. The I_A-mediated current was isolated by subtracting the inactivated-I_A current from the initial evoked voltage-step current protocol. TTX and $CdCl_2$ were present in the solution to block Na_v channels and voltage-gated Ca^{2+} channels (Ca^{2+} modulates I_A), respectively, ensuring the isolation of I_A-channel activity. I_A current amplitude was determined by taking the peak current amplitude and the current density determined, as described previously. Current density measurements revealed a trending gradual increase in I_A channel density from day 20 to day 60 in Con-1 and C9-Δ1 MSNs, and significantly in C9-1 MSNs (p=0.0014, One-way ANOVA; Figure 3-14), suggesting progressive maturation of the repolarization mechanism. Comparative analysis between lines at day 60 revealed the I_A channel current density was statistically indistinguishable between all lines investigated and no differences were observed. These data are not consistent with impaired functional I_A expression driving the altered repolarisation phase in *C9ORF72^{RE}* MSNs.

Next I investigated I_K function. To isolate I_K currents, I used an established voltage-clamp protocol (Livesey et al., 2016) that stepped from -70 mV to +30 mV to activate the

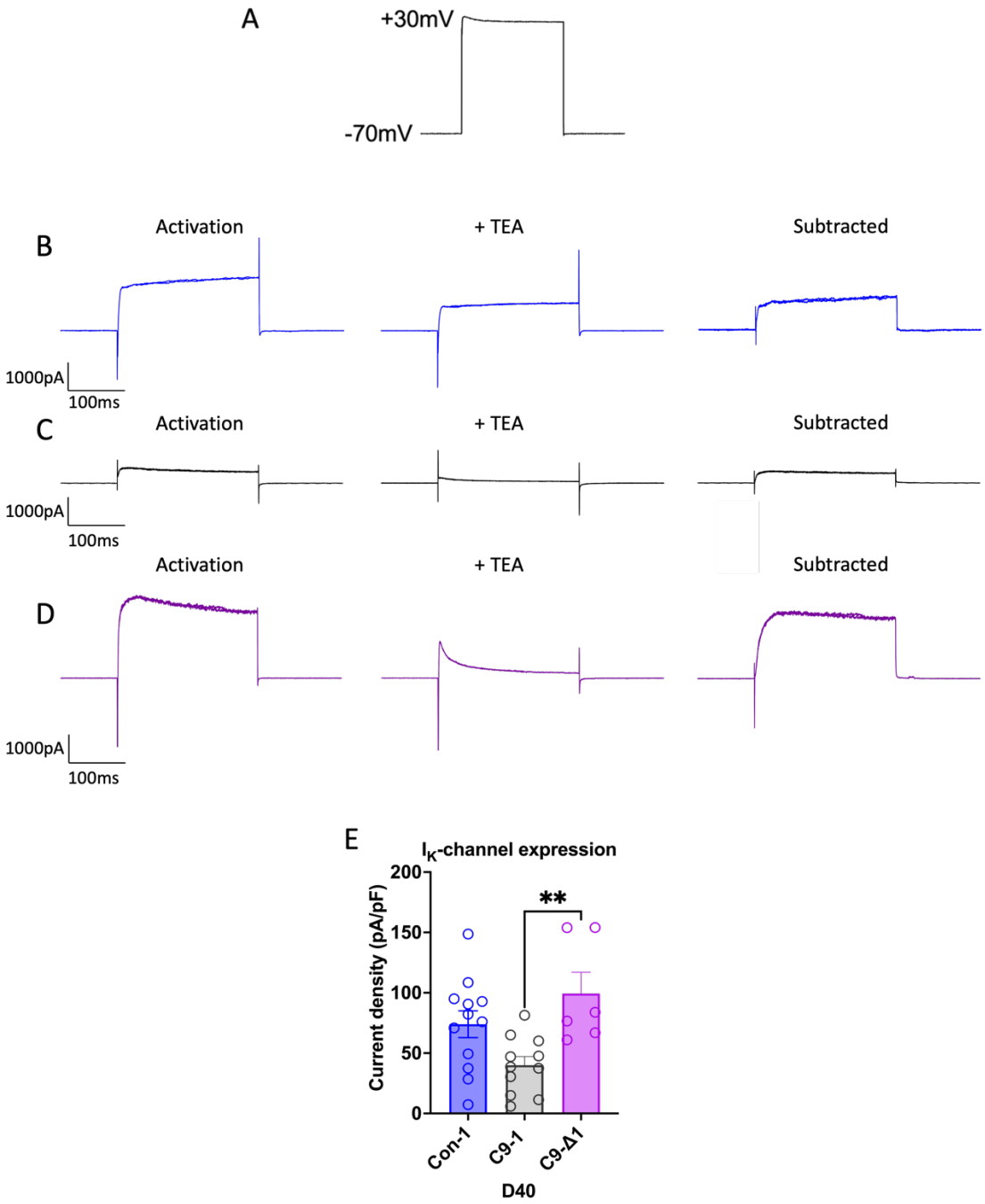

Figure 3-15. ***Delayed outwardly rectifying K⁺ channel (I_K) current density is altered in C9ORF72^{RE} MSNs.*** *A. A two-step depolarizing protocol was utilised to isolate I_K channel activity. First, the I_K channels were activated via a depolarization step of the membrane potential from a holding potential of -70mV to + 30mV (activation). The same step was repeated in the presence of TEA (30 mM). The TEA-sensitive current was yielded by subtracting the current response in the absence of TEA from the TEA-containing trace, to yield TEA-sensitive I_K channel activity. B,C, D. Representative traces at day 40 were selected to highlight each step of the protocol for each line investigated, Con-1 (blue), C9-1 (black) and C9-Δ1 (purple). Current amplitudes were determined from the peak of the IK-sensitive deflections. E. Mean ± SEM I_K current density of Con-1, C9-1 and C9-Δ1 at day 40. Note increase in C9-1 I_K current density compared to C9-Δ1. Statistical analysis was assessed Student's t-test (**, p<0.001). Data: Con-1, n=12, N=3; C9-1, n=11, N=2; C9-Δ1, n=6, N=2.*

voltage-gated I_K channels. Then I performed this protocol in the presence of tetraethyl ammonium (TEA, 30 mM), which blocks I_K channels. I subtracted the TEA-blocked current from the activation current to yield the TEA-sensitive current (Figure 3-15). This was performed in the presence of TTX to block Na_v channels. Peak current amplitude was measured at 225ms after protocol initiation for analysis and the current density was determined as described previously. At day 40, C9-1 MSNs displayed a trend towards decreased I_K current density compared to Con-1 MSNs and a significant difference in I_K current density was observed between C9-1 and C9-Δ1 ($p=0.0063$, Student's t-test; Figure 3-15E). These findings collectively suggest altered functional I_K-channel expression in C9-1 compared to Con-1 and C9-Δ1. While the observed changes require further investigation at day 60, they indicate dysregulation of I_K in the context of *C9ORF72*^{RE} which may contribute to the observed hypoexcitability profile of *C9ORF72*^{RE} MSNs.

3.5. Discussion

Here I exploited the tractability of induced pluripotent human stem cell technology and whole-cell patch-clamp electrophysiology to study the excitability of *in vitro* medium spiny neurons (MSNs) derived from *C9ORF72*^{RE} patients. I demonstrated that *C9ORF72*^{RE} MSNs become progressively more hypoexcitable with time (from day 20 – day 60), whilst maintaining viability, compared to control MSNs and an isogenic control line. All *C9ORF72*^{RE} MSNs derived from all patients (C9-1, C9-2, C9-3) displayed a consistently lower AP number against current injection at day 60 compared to both control MSNs (Con-1 and Con-2). Collectively, these data indicate that *C9ORF72*^{RE} MSN hypoexcitability is a persistent and progressive feature in our *in vitro* system and precedes degeneration. Our experimental assays using an isogenic line (C9-Δ1) gives further confidence that hypoexcitability is being driven by the *C9ORF72*^{RE} mutation. The limited level of cell death observed in the *C9ORF72*^{RE} MSNs aligns with the recognition that neuronal dysfunction often precedes neuronal death in FTD/ALS (Iwai et al., 2016), where neurophysiological impairments are considered hallmarks of the disease, contributing to pathological mechanisms and symptoms even before overt neuronal loss. It is expected that prolonged incubation time would lead to neuronal cell death. However, in my study, I focused on the importance of neuronal

dysfunction as an early marker of disease progression. It is also important to note that neuronal cell death can be influenced by cell autonomous and non-cell autonomous mechanisms that are not fully recapitulated fully in this *in vitro* model. My data indicates that *C9ORF72*^{RE} MSNs hypoexcitability is a persistent and progressive feature in this *in vitro* model and precedes neurodegeneration.

These data broaden our knowledge of the impact of FTD/ALS mutations upon neuronal excitability, providing the first direct electrophysiological evidence of impaired function in other regional-specific neurons beyond the cortex and spinal cord. These functional data provide additional support to the emerging research that other brain regions are involved in the pathophysiology of FTD/ALS, particularly that of the striatum. These data provide strong supportive evidence for observation of prominent frontostriatal dysfunction in FTD/ALS in neuroimaging studies (Möller et al., 2015a, Möller et al., 2015b, Rosen et al., 2005, Garibotto et al., 2011, Halabi et al., 2013, Landin-Romero et al., 2017), which suggest a loss-of-function within these networks. Here, this study shows a loss-of-function in the form of hypoexcitability in MSNs, the most prominent neuronal type in the striatum. Specifically, MSNs are GABA-ergic, and I propose that MSN hypoexcitability is consistent with a reduction of GABAergic inhibition at striatal MSN projection targets, including the basal ganglia's output nuclei, specifically the substantia nigra pars reticulata (SN_{pr}) and globus pallidus externus (GP_e). Because these output nuclei are excitatory and project to the prefrontal cortex (Lanciego et al., 2012), I hypothesise that with less GABA inhibition, the SN_{pr} and GP_e become more active and send excessive excitatory signals to their targets in the prefrontal cortex, possibly contributing to increased overall excitation in the prefrontal cortex of FTD/ALS patients. This increased excitation may manifest in the cognitive disturbances presented by FTD/ALS patients and furthermore, contribute to the process of neuronal injury and loss via excitotoxicity.

Investigation into the source of the hypoexcitability indicated that the passive membrane properties (RMP, R_{in} and WCC) were not associated to the generation of hypoexcitability. However, using such measurements as proxy indicators of neuronal development and maturation, these data broadly indicated *C9ORF72*^{RE} MSNs matured equivalently with respect to the healthy and isogenic control data sets. The hypoexcitability phenotype observed in *C9ORF72*^{RE} MSNs is therefore not due to an impaired maturation. I

investigated the action potentials in greater detail. Through assessment of the AP waveform, I discovered that *C9ORF72*^{RE} MSNs hypoexcitability manifests in the evoked AP waveform properties, predominately in the half-width, and thus a slowing of the waveform. Supporting this, I observed that the phase plots highlighted that the depolarising and repolarising phase of the *C9ORF72*^{RE} MSNs action potentials were impacted, indicating potential functional impairment in ion channels that control these aspects of the action potential. Minor reductions in AP amplitude and modestly more depolarised AHP, which were consistent with hypoexcitability, were also observed in *C9ORF72*^{RE} MSNs. However, these are unlikely to solely account for the hypoexcitability phenotype in *C9ORF72*^{RE} MSNs.

Impaired excitability in MSNs can disrupt information coding within the frontostriatal circuitry in several ways. Beyond a slower action potential waveform being highly compatible with reduced excitability, physiologically altered APs waveforms have considerable implications for both neuronal and circuit function. The conversion of synaptic transmission to action potential driven activity is likely impaired, particularly for high fidelity signalling, i.e., hypoexcitable MSNs are unable to process rapid synaptic input into high fidelity action potential firing (Gjorgjieva et al., 2014). Importantly, MSNs are known to mediate high fidelity signalling which is thought to drive specific cognitive behaviours (Tritsch and Sabatini, 2012). Further, impaired high-fidelity transmission can lead to imprecise pre-synaptic release, in addition to a reduction of GABA release. Studies in multiple system atrophy suggest a potential feedback loop caused by hypoexcitability and downregulation of both $GABA_A$ and $GABA_B$ receptors in patient MSNs (Henkel et al., 2023). Altered postsynaptic responsiveness due to reduced functional $GABA_A$ receptor signalling could disinhibit presynaptic terminals, leading to altered glutamate release and downregulation of $GABA_B$ receptors that could further disrupt presynaptic terminal excitability (Henkel et al., 2023). This disrupted striatal balance may contribute to cognitive dysfunction (Jiménez-Balado and Eich, 2021).

Because the waveform analysis suggested ion channel dysfunction, I further investigated the ion channel profile of MSNs by analysing voltage-gated Na^+ channels (Na_v) expression, transient K^+ (I_A) current density and delayed outwardly rectifying K channels (I_K). Notably the data demonstrate that *C9ORF72*^{RE} MSNs express lower I_K current densities when compared to the isogenic and healthy control MSNs, indicating a reduced function of I_K

channels. Critically, I_K channels contribute to the later stages of repolarization phase of the AP. However, no significant changes were detected in functional I_A expression, which controls the fast component of the repolarisation phase, across timepoints between healthy and isogenic controls and *C9ORF72*^{RE} MSNs and are unlikely to be a contributing factor to the hypoexcitability of *C9ORF72*^{RE} MSNs. Strikingly, pharmacological blockade of I_K channels using tetra-ethyl ammonium (TEA), thus mimicking a reduction in I_K function, is long established to pro-long and slow the AP waveform (Hille, 1978). Importantly, acute block of the I_K mediated current is associate with increased neuronal excitability (Tasaki and Hagiwar, 1957). However, chronic blockade with TEA is associated with reduced intrinsic excitability (Dirkx et al., 2020), which is more consistent with the observation of hypoexcitability in *C9ORF72*^{RE} MSNs and a reduction in I_K channels. Interestingly, reduced mRNA levels of *KNCA1* and *KNCA2* encoding K_V1.1 and K_V1.2 were reported in spinal motor neurons of ALS patients (Jiang et al., 2005). Further, mSOD1 ALS iPSC-derived motor neurons have been found to have a reduction in delayed rectifier K^+ currents (Wainger et al., 2014), analogous to the observation made in *C9ORF72*^{RE} MSNs. However, quite different to what is observed and proposed in my study, it proposed that this change in I_K currents in MNs contributes to hyperexcitability (Wainger et al., 2014), a hallmark feature of the locomotor circuit in early disease (reviewed in (Pasniceanu et al., 2021)). Further, loss of function mutations to I_K channel subunits (e.g., K_V1.1, K_V1.2, K_V7.2, K_V7.3; reviewed in (Gao et al., 2022)) are linked to epilepsy, neurologic disease characterised by hyperexcitability and seizures (Greene and Hoshi, 2017). In this regard, Ezogabine (also known as retigabine) is an anti-convulsant drug used to treat seizures, pharmacologically reduces hyperexcitability in ALS MNs by activating K_V7.2 channel, a delayed rectifier channel (Wainger et al., 2021, Wainger et al., 2014). These strongly indicates that the lower expression of I_K channels contributes to hyperexcitability in MNs. Whilst I_K appears to be lower in ALS MNs and MSNs, there is an apparent contradiction in that lower I_K appears to cause an increase in excitability in ALS MNs, but a reduction in *C9ORF72*^{RE} MSNs.

This potentially could be explained by the site and composition of the axon initial segment (AIS). The AIS has the remarkable capacity of regulating neuronal excitability by changing its length and diameter- a homeostatic mechanism that helps maintain balanced network activity by either dampening or enhancing intrinsic excitability (Kuba et al., 2010,

Evans et al., 2015, Jamann et al., 2021, Galliano et al., 2021). The AIS is a specialized microdomain located at the proximal interface between the axon and the cell body, responsible for initiating and shaping APs. The AIS is characterized by a high density of Na_v and K_v channels, that are anchored to the membrane by a cytoskeletal arrangement of scaffolding proteins, among these, ankyrin-G. Experimental and computational studies illustrated that the length and diameter of the AIS are important for Na_V activation, therefore impacting on the depolarization phase of the AP depolarization (Kole et al., 2008, Kuba et al., 2010, Gulledge and Bravo, 2016, Goethals and Brette, 2020). While my data revealed no significant changes in functional Na_V channel expression across timepoints in *C9ORF72*^{RE} MSNs compared to controls, the impaired depolarization phase of the AP waveform suggests altered AIS dynamics may be at play. AIS disturbances are a major feature of numerous neurological diseases (Nascimento et al., 2022, Smolin et al., 2012, Page et al., 2022a, Kaphzan et al., 2011, Booker et al., 2020) and have been reported in ALS and FTD (Harley et al., 2023, Sasaki and Maruyama, 1992, Bonnevie et al., 2020, Sohn et al., 2019). In light of these findings, I highlight that the chronic pharmacological block of I_K channels such as K_V7.2 induces a compensatory distal shift of the AIS and a relocation away from the soma to reduce firing excitability (Lezmy et al., 2017). Therefore, the most parsimonious explanation for the data in my study is that the observed reduction in I_K in *C9ORF72*^{RE} MSNs may be a reflection of more distally located I_K channels, due to an abnormal physiological AIS state. Critically, this change in AIS dynamics may reflect the converging hypothesis that axonal biology is heavily disrupted in ALS, including the fact that many ALS-causing mutations are related to axon trafficking (Coleman, 2022, Zhang et al., 2022b). It is therefore possible that these processes impact I_K channels in ALS, but do so in a manner that is dependent upon the identity of the neuron.

This study presented some limitations, such as the sex ratio of the *C9ORF72*^{RE} MSNs samples due to limited availability of female samples. While this study provides valuable insights into the impact of *C9ORF72*^{RE} mutation on neuronal excitability in male individuals, it is crucial to recognise the potential sex-specific differences in the disease progression and underlying mechanisms. Given the disparity in ALS prevalence between men and women (Dharmadasa et al., 2022), future research should prioritize the inclusion of female-derived *C9ORF72*^{RE} MSNs to comprehensively understand the full spectrum of FTD/ALS.

3.6. Conclusions

In conclusion, I provide novel electrophysiological evidence of impaired function in the striatum of ALS patients, evidenced by progressive hypoexcitability in *C9ORF72*^{RE} MSNs with a slowed AP waveform, particularly during repolarization. *C9ORF72*^{RE} MSNs exhibit a reduction in I_K channel current density compared to controls. These findings reveal that the *C9ORF72*^{RE} mutation disrupts ion channel function, particularly I_K channels. This dysregulation may be linked to alterations in the AIS, potentially contributing to the observed changes in AP waveform and hypoexcitability in *C9ORF72*^{RE} MSNs. Here I have discussed my core findings and I discuss the translational implications and opportunities for future study in the Chapter 6.

4. CHAPTER 4: *In vitro* astrocytes derived from *C9ORF72*^{RE} patients display enhanced membrane currents

4.1. Introduction

Motor and cortical neuron degeneration remain the defining disease hallmarks of ALS and FTD. Though, it is now understood that ALS/FTD has a broad impact on the nervous system and other neuronal subtypes and glial cells, particularly astrocytes, have been found to significantly contribute to the disease pathology. Indeed, the previous Results chapter has detailed a novel impairment in *C9ORF72*^{RE} patient iPSC-derived striatal neurons. Here, I now focus on *C9ORF72*^{RE} astrocytes.

Astrocytes are the most abundant glial cell type population in the nervous system, constituting 20-40% of the glial population (Allen and Lyons, 2018, Verkhratsky and Nedergaard, 2018). They possess remarkable functional complexity, providing neurons with trophic support, play key roles in modulating their function, maintain optimal CNS environment homeostasis through the regulation of the blood-brain-barrier (BBB), water flux, ion and pH homeostasis, and removal of reactive oxygen species (ROS). Moreover, they play important roles in immunity and inflammation, as they secrete cytokines, phagocytize and facilitate border formation after injury (Verkhratsky et al., 2019).

Astrocytes extend their terminal processes called perisynaptic astrocytic processes (PAPs) that wrap around the synaptic cleft, forming the tripartite synapse. Remarkably, estimates suggest that half of all synapses are enwrapped by these astrocytic processes (Verkhratsky et al., 2019), which tightly regulate the extracellular space surrounding synapses and play key roles in modulating neurotransmitter signalling and synaptic plasticity. For example, astrocytes uptake and recycle neurotransmitters, such as glutamate (Araque et al., 2014), thus preventing neurotransmitter accumulation, which can otherwise have the potential to lead to glutamate-mediated excitotoxicity, which is a key pathogenic mechanism for numerous brain conditions, including ALS and FTD (Allen and Eroglu, 2017).

Further, astrocytes have a fundamental role to maintain ion homeostasis within the nervous system (Walz, 2000). A critical role is their ability to regulate the K^+ concentration

surrounding the extracellular space of neurons via a multitude of ion channels and transporters that are selective for K^+ permeation (Walz, 2000), thereby both accommodating and maintaining the ability of neurons to fire action potentials. This 'K^+ syphoning' mechanism is critical to the functioning of the nervous system and is part of the 'glial syncytium,' involving large, networks of glia, including oligodendrocytes that spans from the neuronal-glial interface to the endothelial cells of blood vessels (Allen and Lyons, 2018). Beyond ion homeostasis, astrocytes also closely regulate osmosis via aquaporin-4 (AQP4) water channels, actively participating in the removal of excess fluid and metabolic water products (Verkhratsky et al., 2019).

Beyond their supportive role to neurons, it is established that astrocytes play a pathogenic role in ALS disease progression. Astrocytes undergo major pathological changes leading to astrogliosis and, instead of being supportive, drive non-cell autonomous toxicity towards MNs, contributing significantly to MN dysfunction and loss.

In ALS, astrocyte morphology undergoes significant 'hallmark' alterations, as evidenced in ALS post-mortem, transgenic ALS models (Peng et al., 2020, Rossi et al., 2008) and *in vitro* human models of ALS (Haidet-Phillips et al., 2011). Hypertrophy, where astrocytes become enlarged, and become more proliferative are typical abnormalities reported by such studies (Gomes et al., 2020, Lino et al., 2002). ALS astrocytes also appear to notably shift towards a more reactive-like astrogliosis state characterised by increased expression of glial fibrillary acidic protein (GFAP), a marker of astrocyte (Guttenplan et al., 2020, Benninger et al., 2016, Gatto et al., 2021). Reactive astrocyte states are typically associated with pathogenic impacts (Escartin et al., 2021). Importantly, many of these traits appear before the disease symptoms manifestation and MN degeneration (Howland et al., 2002), however, many of the aforementioned hallmarks appear specific to the symptomatic stages of disease (Díaz-Amarilla et al., 2011, Haidet-Phillips et al., 2011, Qian et al., 2017). Pre-symptomatic stages of disease are conversely associated with a loss of GFAP and reduced proliferative capacity (Gomes et al., 2019, Gomes et al., 2020). Additional to these changes, astrocytes have also been shown evidence of pathological inclusions such as TDP-43 inclusions in the cytoplasm and processes (Nishihira et al., 2008, Cooper-Knock et al., 2012, Peng et al., 2020, Velebit et al., 2020), FUS inclusions in the cytoplasm and nucleus

(Kia et al., 2018), SOD1 nuclear accumulation in the ventral horn of spinal cord (Nagai et al., 2007, Yamanaka et al., 2008, Guttenplan et al., 2020), C9ORF72 repeat expansion-mediated generation of DPRs and RNA foci (Zhao et al., 2020, Varcianna et al., 2019). Collectively, these studies highlight considerable pathological changes across the disease course of ALS to astrocytes, which remain to be fully understood.

The non-cell autonomous role of ALS astrocytes to MNs is established (Taha et al., 2022, Van Harten et al., 2021). A seminal study by Nagai et al., (2007) performed *in vitro* co-culture experiments using mouse embryonic stem cell-derived motor neurons and purified astrocytes obtained from a transgenic mouse expressing the human mutant SOD1 demonstrated that ALS astrocytes have a considerable toxic influence on motor neuron viability (Nagai et al., 2007). *In vitro* experiments demonstrating astrocyte toxicity to MNs have been conducted in the context of other ALS genetic impairments, including sporadic ALS and *C9ORF72*^{RE}, *TDP-43*, and *FUS* mutations, using both transgenic mouse and patient-derived motor neurons and astrocytes (Nagai et al., 2007, Di Giorgio et al., 2007, Bilsland et al., 2008, Ferraiuolo et al., 2011, Phatnani et al., 2013, Kia et al., 2018, Provenzano et al., 2022, Meyer et al., 2014, Gatto et al., 2021, Haidet-Phillips et al., 2011, Re et al., 2014). ALS astrocyte-mediated motor neuron toxicity is therefore a broad spectrum. Critically, this toxic effect appears to be selective to MNs, as co-cultures with other neuronal populations, such as cortical neurons, GABAergic interneurons or dorsal root ganglia neurons, have not shown similar cell death (Di Giorgio et al., 2008, Haidet-Phillips et al., 2011, Nagai et al., 2007, Re et al., 2014). To understand the impact of ALS astrocytes in disease progression, conditional removal of SOD1 mutation from astrocytes of SOD1^{G93A} ALS mouse model slows disease progression but does not impact on disease onset (Yamanaka et al., 2008). However, the deletion of mutant SOD1 from the SOD1^{G85R} mouse model delays onset and progression (Lino et al., 2002, Wang et al., 2011). Moreover, chimeric SOD1^{G93A} mouse model that are mixtures of normal and SOD1 mutant-expressing cells, toxicity to motor neurons is shown to require damage from mutant SOD1 acting within non-neuronal cells and extend the survival of SOD1 MNs (Clement et al., 2003). It is clear that ALS astrocytes advance disease progression after the onset of symptomatic disease. However, critically there is important debate and open questions regarding the early role of astrocytes in the initiation of disease.

Given this role of astrocytes in ALS, there has been intensive research into the mechanisms by which ALS astrocytes impact toxicity to MNs. These can be classified into two mechanistic areas; loss-of-supportive function and gain-of-toxic function.

ALS leads to compromised, astrocyte loss-of-function preventing their specific roles that are considered critical for nervous system homeostasis. Astrocyte processes that extend into the synapse express the glutamate transporter EAAT2/GLT1, which provides a key regulatory mechanism for the uptake of neurotransmitter glutamate (Zhou and Danbolt, 2013). Astrocyte EAAT2/GLT1 expression is long established to be reduced in ALS (Bruijn et al., 1997, Rosenblum and Trotti, 2017), leading to elevated synaptic glutamate levels and subsequent glutamate-gated receptor ion channel-mediated excitotoxicity, a key mechanism of motor neuron injury and death in ALS (Van Den Bosch et al., 2006). Astrocytes critically support neurons metabolically by providing essential energy substrates, such as lactate, derived from glucose metabolism (Allen and Barres, 2009). Metabolic dysfunction in ALS involves diminished astrocytic intracellular and extracellular lactate levels, attributed to downregulation of Slc16a4 and decreased NAD+ levels, depriving MNs of essential energy substrates (Ferraiuolo et al., 2011, Madji Hounoum et al., 2017). Additionally, decreased adenosine deaminase (ADA) activity contributes to compromised purine metabolism, further reducing astrocytic bioenergetic output (Allen et al., 2019a). Astrocytes support neurons via by releasing a complex mixture of factors that influencing neuronal survival and function (Allen and Barres, 2009). For example, dysfunctional astrocyte secretome exacerbates neuronal damage through increased oxidative stress from impaired secretion of antioxidants (Birger et al., 2019, Cassina et al., 2008). Further, loss of miRNA vesicle formation in ALS astrocytes disrupts miRNA-mediated modulation of neuronal survival and differentiation, with specific miRNAs like miR-494-3p implicated in MN survival and neurite maturation (Varcianna et al., 2019). Overall, these mechanisms highlight the multifaceted role of astrocyte dysfunction in ALS pathogenesis, involving excitotoxicity, metabolic disruption, and impaired secretion of neuroprotective factors.

Beyond their diminishing supportive role, ALS astrocytes acquire pathogenic properties towards MNs, characterised broadly by 'gain-of-function' mechanisms. Seminal experiments demonstrated that ALS astrocyte-conditioned medium was sufficient to cause

MN toxicity, indicating that astrocytes release soluble toxic factors (Nagai et al., 2007, Di Giorgio et al., 2008). Numerous toxic factors have been proposed to be released by astrocytes. Consistent with a reactive-like state, ALS astrocytes release of pro-inflammatory cytokines such as TNF-α, IL-6, IL-1β and upregulation of these genes have been reported in both fALS and sALS patients (Di Giorgio et al., 2008, Haidet-Phillips et al., 2011). FUS-ALS astrocytes release TNF-α, which partially mediates their toxic effects on motor neurons (Kia et al., 2018). Interestingly, knockout of these pro-inflammatory cytokines (TNF-α, IL-1α) was found to significantly delay the death of motor neurons in $SOD1^{G93A}$ mice (Guttenplan et al., 2020). Coupled with the loss of the healthy metabolic status of ALS astrocytes, ALS astrocytes are proposed to contribute to neurotoxicity via dysregulation of ATP signalling, leading to increased production of ROS, exacerbating oxidative stress within their microenvironment and contributing to neuronal injury and loss (Birger et al., 2019, Cassina et al., 2008). Astrocytes possess the ability to store and release polyphosphate, which serves various essential functions in cells including acting as a phosphate reserve for energy metabolism (Arredondo et al., 2022). Excessive secretion of polyphosphate by *in vitro SOD1, TARDBP* and *C9ORF72*^{RE} ALS astrocytes dysregulates neuronal excitability by modulating ion channels, leading to excessive calcium influx and ultimately excitotoxic cell death in MNs independent of glutamate levels (Arredondo et al., 2022).

Extracellular vesicles, particularly exosomes, released by astrocytes play key roles in the transport of various biomolecules such as proteins, lipids, and nucleic acids, allowing astrocytes to modulate neuronal function, synaptic activity, and neuroinflammatory responses (Upadhya et al., 2020). Exosomes, containing toxic agents such microRNA-containing extracellular vesicles, derived from *C9ORF72*^{RE} ALS astrocytes conditioned medium exhibit toxicity towards healthy MNs (Varcianna et al., 2019). Interestingly, exosomes released by ALS astrocytes also allow transmission of ALS-associated proteinopathy. Recent work showed *C9ORF72*^{RE} ALS astrocytes promote propagation of DPRs (poly-GA) to neurons (Marchi et al., 2022). Autophagy plays an important role in regulating inflammation and autophagy regulation in astrocytes can regulate neuronal viability after harmful stimuli (Ortiz-Rodriguez and Arevalo, 2020). Astrocyte-induced autophagy in ALS causes accumulation of an autophagy receptor protein, P62, indicating impaired autophagic flux, a concomitant increase in expression of SOD1 and decreasing the

viability of motor neurons (Madill et al., 2017). In summary astrocytes, acquire a gain-of-function role by mediating the generation of agents that are toxic to MNs.

Importantly, astrocytes can actively uptake the microRNA miR-218, leading to downregulation of the astrocytic glutamate transporter EAAT2 (Hoye et al., 2018). This reduction in EAAT2 expression, observed in ALS post-mortem brain tissue, is linked to neuronal excitotoxicity. Overexpressing EAAT2 in $SOD1^{G93A}$ mice has protective effects against glutamate-induced cytotoxicity and delays disease progression. These findings suggest a neurotoxic feedback loop, wherein ALS astrocytes contribute to motor neuron death, and dying motor neurons release factors that further exacerbate astrocytic dysfunction, ultimately contributing to disease progression.

Though astrocytes undergo a significant loss of supportive functions and, in certain scenarios, exhibit a toxic gain-of-function leading to adverse effects on MNs and the development of a disease-specific astrocytic phenotype, the precise mechanisms governing this transition from a neuro-supportive to a pathogenic role remain, overall, poorly understood. Given that many of the supportive and pathogenic roles of ALS astrocyte involve membrane physiology, i.e., loss of function of specific physiological functions (e.g., EAAT2/GLT2 reduction) or that toxic agents must pass through the membrane to MNs, this shift is likely to involve alterations in astrocyte cell membrane function.

4.2. Hypothesis and aims of the study:

The astrocyte cell membrane is a crucial interface through which astrocytes mediate their physiological roles, containing a myriad of receptors, transporters and channels that enable neuronal-astrocytic signalling, including metabolic support, ion homeostasis, neurotrophic factor provision, neurotransmitter modulation, and participation in neuroinflammatory processes (Verkhratsky et al., 2019). Many of these key processes are implicated in the pathogenic mechanisms of non-cell autonomous astrocyte-mediated MN toxicity.

Hypothesis: I hypothesize that astrocyte function may be linked to alterations in the astrocytic membrane, potentially impacting ion channel activity and signalling pathways.

Electrophysiological impairments in astrocyte membrane physiology have not been investigated previously in the context of ALS. Electrophysiological analysis offers a powerful tool to characterise the membrane physiology in detail (Methods Section 2.4). This aspect of the project therefore aims to characterize the astrocyte membrane current in *C9ORF72*^{RE} ALS astrocytes using voltage-clamp patch-clamp electrophysiology to better understand the underlying mechanism mediating astrocytic dysfunction and identify potential targets that could restore a supportive astrocytic environment for MNs in ALS.

4.3. Methods

The Methods employed in this Chapter are described in the following sections:

4.3.1. Direct conversion of fibroblast to iNPC (As described in Methods Section 2.2.8)

4.3.2. Differentiation of iNPCs to iNPC-astrocytes (iAstrocytes; As described in Methods Section 2.2.9)

4.3.3. ICC – iAstrocyte characterisation (As described in Methods Section 2.3)

4.3.4. Electrophysiology (As described in Methods Section 2.4)

4.4. Results

4.4.1. Directly differentiating iAstrocytes from *C9ORF72*^{RE} ALS patients

To study the electrophysiological properties of *in vitro* human astrocytes, a previous protocol was employed enabling the generation of astrocytes derived from induced neuronal progenitor cells (iNPCs), which were directly converted from fibroblasts obtained from ALS patients and healthy individuals (Meyer et al., 2014). This protocol is summarised in Figure 4-1A and described in detail in Methods section 2.2.9. For this chapter, I have generated astrocytes from fibroblasts obtained from two healthy individuals (Con-1, 30-35 years old female; Con-2, 40 years old male) and two ALS patients that harbour the *C9ORF72*^{RE} mutation (C9-1, 49 years old male; C9-2, 66 years old male). Full patient details can be found in Table 2-13 of the Methods. It is important to distinguish that the patients denoted in this chapter as Con-1, Con-2, C9-1 and C9-2 are different to those from which patient-derived MSNs have been generated (Chapter 3). iNPC-derived astrocytes (iAstrocytes) were differentiated for 7 and 14 days, as detailed in Figure 4-1A. Previously,

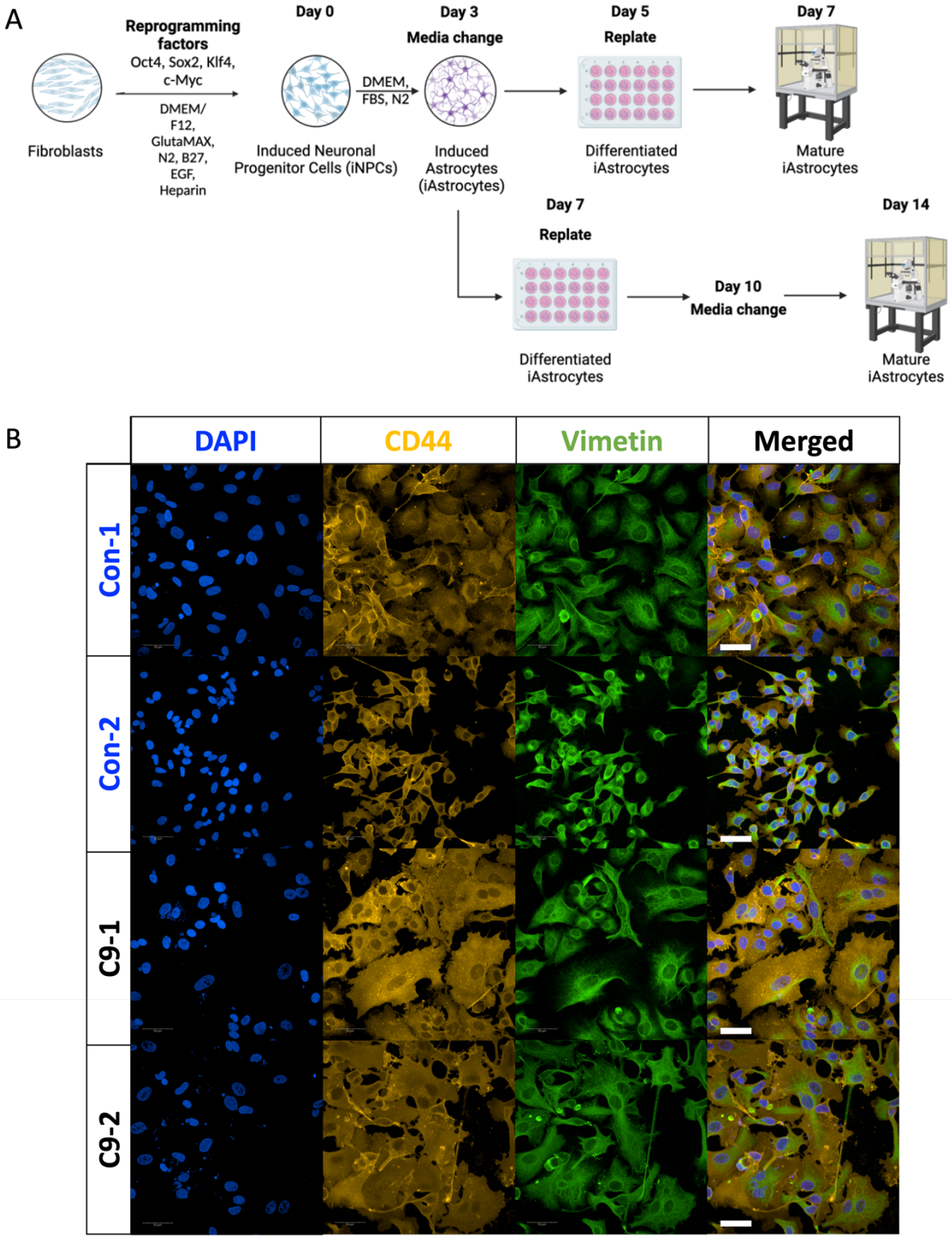

Figure 4-1. ***iAstrocytes were generated from fibroblasts via a direct reprogramming protocol and express specific astrocytic markers at day 7.*** *Caption on the next page.*

Figure 4-1. ***iAstrocytes were generated from fibroblasts via a direct reprogramming protocol and express specific astrocytic markers at day 7.*** *A. A multi-step direct reprogramming protocol for generating mature iAstrocytes included the isolation, culturing and exposure of donor fibroblasts to a cocktail of transcription factors (Oct4, Sox2, Klf4, c-Myc) and growth factors (FGF2, EGF and heparin) to induce differentiation to neuronal progenitor cells (iNPCs). iNPCs were exposed to DMEM, FBS and N-2 to differentiate to astrocytes and promote glial morphology and functionality. For electrophysiological recordings at day 7 or 14, iAstrocytes were replated onto Therminox coverslips at day 5 or 7, respectively. Media was changed every 72 hours. B. Figure depicts iAstrocytes at day 7 in culture. ICC staining demonstrates cultures derived from two healthy individuals (Con-1, Con-2) and two C9ORF72^{RE} ALS patients (C9-1, C9-2) are highly enriched for cells harbouring key astrocyte markers CD44 (yellow) and Vimentin (green). DAPI stain is presented in blue. Scale bar, 50μm. Stainings and images were performed/obtained by members of the Ferraiuolo/Shaw laboratories and presented with permission.*

these lines were found to efficiently differentiate into enriched cultures of astrocytes by day 7 (iAstrocytes derived from the patients denoted Con-1, Con-2 and C9-2 have been published in (Hautbergue et al., 2017, Varcianna et al., 2019, Allen et al., 2019a, Gatto et al., 2021, Bauer et al., 2022b, Marchi et al., 2022)). iAstrocytes express typical astrocytic markers, including vimentin and CD44 (Figure 4-1B).

4.4.2. The electrophysiological characterisation of *C9ORF72*^{RE} ALS iAstrocytes

The membrane physiology of astrocytes differs considerably from that of neurons and is commonly termed as electrically 'non-excitable' or 'passive'. Previously iAstrocytes have not been examined electrophysiologically. Using whole-cell patch-clamp, I investigated the intrinsic membrane properties (WCC, R_{in} and RMP) of iAstrocytes Con-1, Con-2, C9-1 and C9-2 at days 7 and 14. As development and maturation progresses, astrocytes are expected to become more morphologically ramified, increasing their WCC, and increase their expression of channels and transporters leading to decreased R_{in} and more hyperpolarised RMPs (Zhou et al., 2006). Whilst non-significant, whole-cell measurements of WCC of iAstrocytes were overall consistent with a trending increase in WCC (Figure 4-2A). A consistent decreasing trend in R_{in} was observed across differentiation for both control and *C9ORF72*^{RE} ALS iAstrocyte lines, with a decrease in R_{in} from day 7 to day 14, as expected with maturation. However, both Con-1 and Con-2, but not C9-1 and C9-2, exhibited a statistically

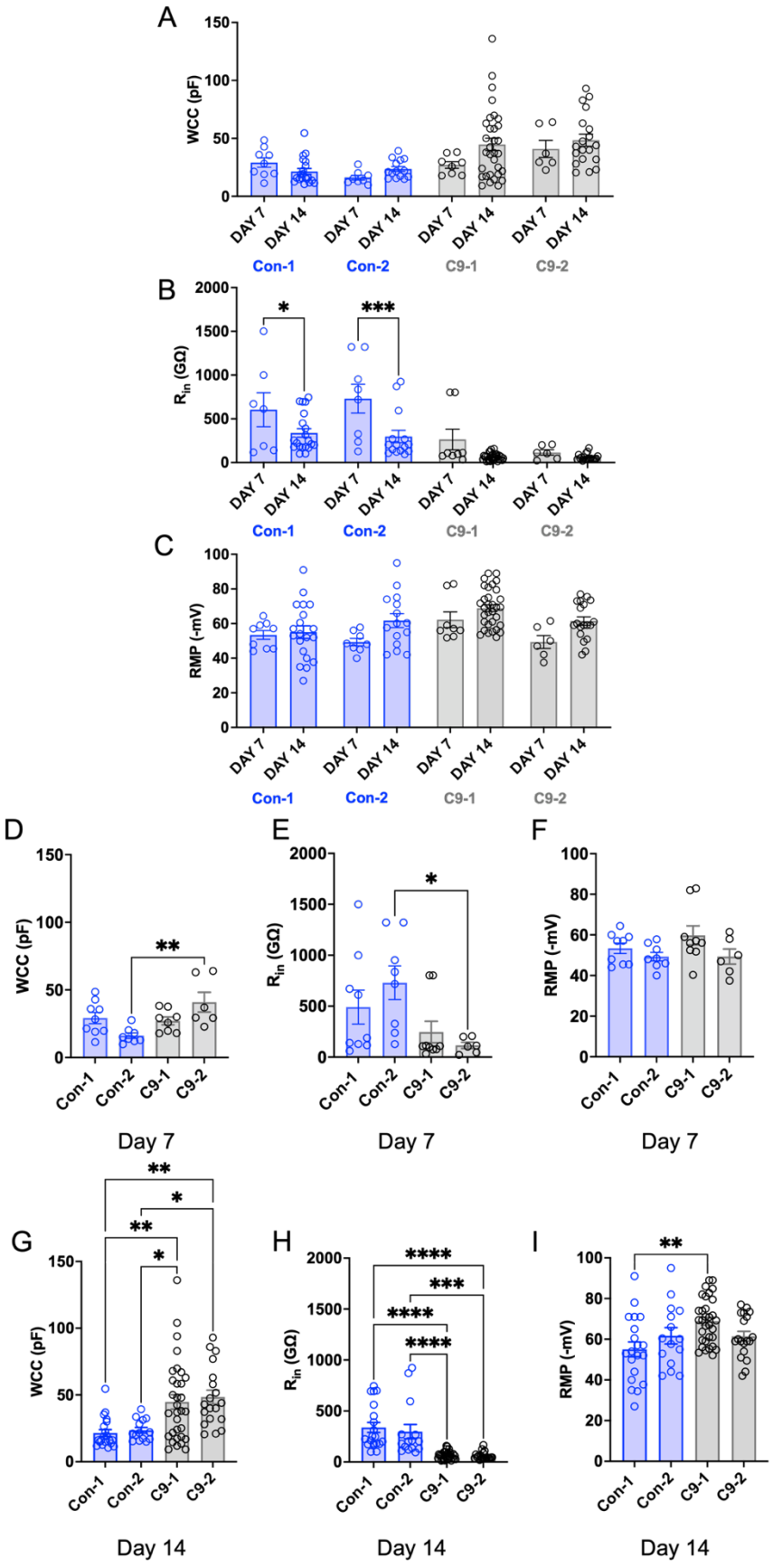

Figure 4-2. ***Passive membrane properties are impacted in C9ORF72^{RE} ALS iAstrocytes.*** *Caption on the next page.*

Figure 4-2. Passive membrane properties are impacted in C9ORF72^{RE} ALS iAstrocytes*. A,B,C. Mean ± SEM data of passive membrane properties WCC, Rin and RMP, respectively, at day 7 and day 14 for Con-1 (day 7, n=9, N=3; day 14, n=20, N=4), Con-2 (day 7, n=8, N=3; day 14, n=15, N=5), C9-1 (day 7, n=9, N=3; day 14, n=32, N=7) and C9-2 (day 7, n=6, N=2; day 14, n=19, N=7). Statistical significance for A,B,C was assessed using Students' t-test. D, E, F. Comparative data for WCC, Rin and RMP, respectively, between each line at day 7. G, H, I. As previous, but for day 14. Statistical tests for D-I; One-way ANOVA with Bonferroni's multiple comparison test (*, p<0.05; **, p<0.01; ***, P<0.001; ****, p<0.0001).*

significant decrease in R_{in} over from day 7 to day 14 (Con-1, day 7 vs day 14, p=0.0462; Con-2, day 7 vs 14, p=0.0002, Student's t-test; Figure 4-2B). However, the non-significant difference in R_{in} in C9-1 and C9-2 iAstrocytes does not appear to be related to impaired maturation, since the R_{in} values for these lines are much lower than that of the control iAstrocytes. The RMP of iAstrocytes was found to show a more hyperpolarising trend with time, as expected during cell maturation (Figure 4-2C). I compared the intrinsic properties between healthy and *C9ORF72*^{RE} ALS iAstrocytes on days 7 (Figure 4-2D,E,F) and 14 (Figure 4-2G,H,I). At day 7, a significant difference in WCC was only observed between Con-2 and C9-2 (p=0.0027, One-way ANOVA). However, the WCC parameter became significantly elevated at day 14 for both *C9ORF72*^{RE} ALS iAstrocyte lines compared to controls (Con-1 vs C9-1, p=0.0029; Con-1 vs C9-2, p=0.0020; Con-2 vs C9-1, p=0.0251; Con-2 vs C9-2, p=0.0141, One-way ANOVA; Figure 4-2G). An elevated WCC in *C9ORF72*^{RE} ALS iAstrocytes compared to controls indicates an increased membrane surface area in these cells, which allows the incorporation of more ion channels and transporters. Our findings on WCC are consistent with previously published data that reported that iAstrocytes derived from older patients displayed larger cell morphology (Gatto et al., 2021). For R_{in}, a day 7 comparison across iAstrocytes highlighted a significant reduction in R_{in} between Con-2 and C9-2 (p=0.0369, One-way ANOVA; Figure 4-2E). However, by day 14 the *C9ORF72*^{RE} ALS iAstrocytes demonstrated a clear and highly significant reduction in R_{in} *versus* controls (Con-1 vs C9-1, p<0.0001; Con-1 vs C9-2, p<0.0001; Con-2 vs C9-1, p=0.0002; Con-2 vs C9-2, p<0.0001, One-way ANOVA; Figure 4-2H). As R_{in} reflects membrane current (ion) flow, a larger membrane surface area, as mentioned above, can accommodate more ion channels, potentially increasing overall channel conductance, thus lowering R_{in}. This indicates that *C9ORF72*^{RE} ALS iAstrocytes display significant membrane disturbances. For RMP, no significant

differences were observed between control and *C9ORF72*^{RE} ALS iAstrocytes at day 7 and only one significant difference (Con-1 vs C9-1; p=0.0025,One-way ANOVA; Figure 4-2I) at day 14, indicating a largely unaffected RMP between healthy patient *versus* *C9ORF72*^{RE} ALS iAstrocytes. Given that RMP is a proxy measure of cellular viability, i.e., unhealthy cells lose RMP and become depolarised (McKhann et al., 1997), these data show that *C9ORF72*^{RE} ALS iAstrocytes retain their functional membrane integrity whilst displaying WCC and R_{in} abnormalities relative to control iAstrocytes.

Next, to explore these membrane defects, I investigated the passive membrane currents in iAstrocytes. Astrocytes present a membrane conductance that is characterised by linear passive current responses to a voltage command (Zhou et al., 2021b). To do this, I performed whole-cell voltage-clamp recordings and employed a voltage-step protocol that enables 'passive' membrane currents to be evoked in other glia and astrocytes (Livesey et al., 2016, Zhou et al., 2009). The depolarizing voltage-step protocol (Figure 4-3, top) involved incremental 20mV voltage steps (200ms) from a holding potential of -84mV ranging from -124 mV to +16 mV (including liquid junction potential correction). Recordings were performed at day 7 and day 14 post-differentiation for the Con-1, Con-2, C9-1 and C9-2 iAstrocytes. Representative current traces were selected to characterise each cell population at day 7 and day 14 (Figure 4-3, day 7-left, day 14-right). Both controls (Con-1 and Con-2) displayed highly comparable current responses at both timepoints. Notably, *C9ORF72*^{RE} ALS iAstrocytes demonstrated large membrane currents compared to controls by day 14 (Figure 4-3). These data suggested major membrane dysfunction in *C9ORF72*^{RE} ALS iAstrocytes.

To quantify membrane current dysfunction, I constructed mean current–voltage (I–V) relationships from currents evoked from the voltage-step protocol. I-V relationships enable the visualisation and quantification of the relationship between applied voltage and the resulting current flow across the astrocyte membrane, where the slope of an I-V plot represents the membrane conductance, i.e., a steeper slope reflects higher conductance, indicating a greater ease with which ions can flow across the membrane. At day 7, both *C9ORF72*^{RE} ALS iAstrocytes displayed increased current responses compared to controls

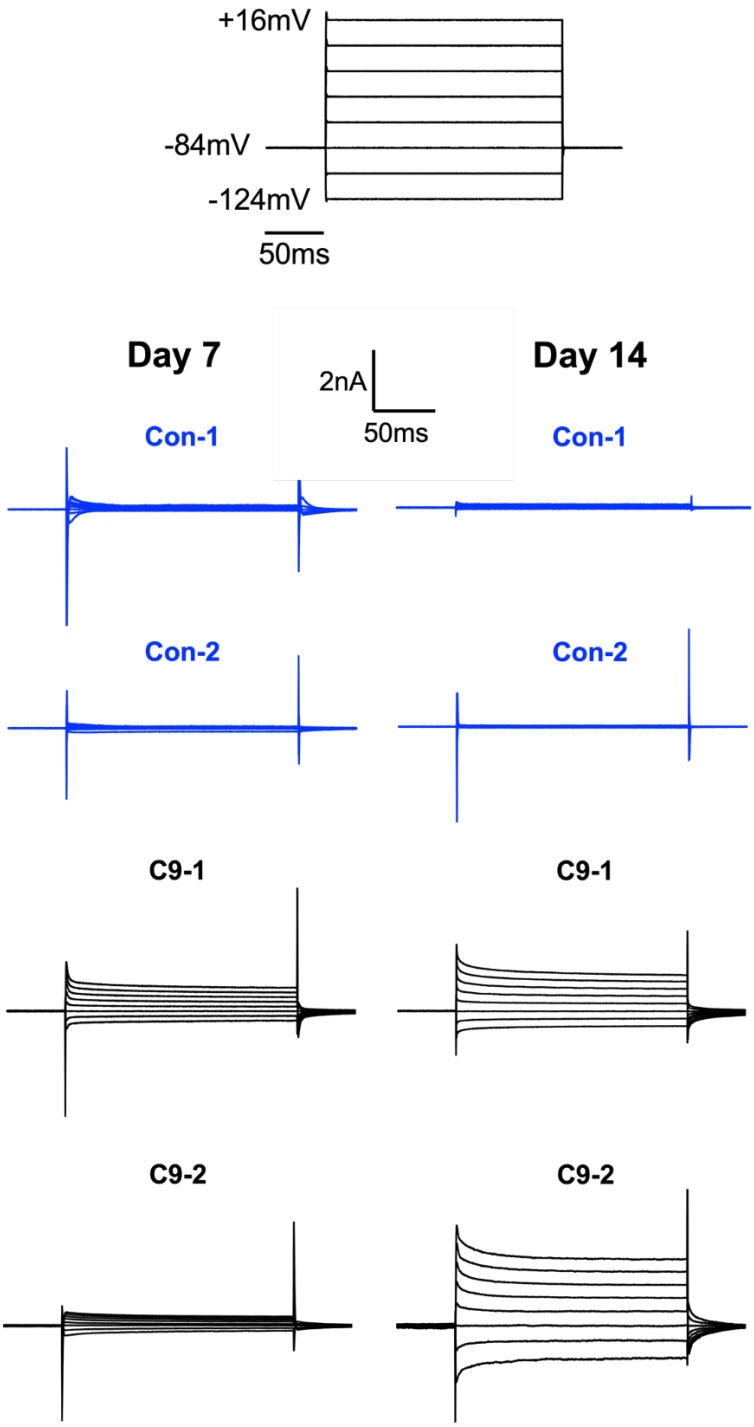

Figure 4-3. ***C9ORF72^{RE} ALS iAstrocytes display enlarged membrane currents****. Individual iAstrocytes were examined using whole-cell patch-clamp in the voltage-clamp configuration. Cells were held at potential of -84 mV (including LJP of -14 mV) and a voltage-step protocol was initiated to investigate the evoked membrane current response. The protocol is depicted in the upper panel and consisted of stepped voltages (from -124 mV to 16 mV) for 200 ms from -84 mV every 10s. The panels below the protocol show representative current traces from individual day 7 and day 14 from Con-1, Con-2, C9-1 and C9-2 iAstrocytes evoked by the described protocol. Note the enhanced current response in the C9-1 and C9-2 lines particularly at day 14.*

(Figure 4-4A), indicating a higher passage of current through the membrane, as expected from the R_{in} data. Control lines exhibited similar and relatively low current amplitudes. By day 14, the *C9ORF72*^{RE} ALS iAstrocytes I-V relationships become more pronounced in their passage of current compared to control iAstrocytes (Figure 4-4B). However, the WCC data indicate that the *C9ORF72*^{RE} ALS iAstrocytes display a much larger membrane surface area than controls. A simple explanation for the increase in current size in response to the voltage protocol could therefore be that the iAstrocytes are simply larger and, thereby, have more membrane channels/transporters to pass current. For each individual iAstrocyte recording I therefore measured current density (current divided by the WCC), thus normalising between iAstrocytes with different WCC properties. Taking this approach, the plot of current density *versus* voltage revealed that the differences between day 7 healthy and *C9ORF72*^{RE} ALS iAstrocytes were not substantial (Figure 4-4C). However, at day 14, both *C9ORF72*^{RE} ALS iAstrocytes showed a clear increase in current density compared to controls (Figure 4-4D). These data directly demonstrate that *C9ORF72*^{RE} ALS iAstrocytes possess a higher membrane current passivity compared to controls, which is developed with culture time. Since membrane currents are generated by ion channels and transporters, this suggests an abnormal dysregulation of ion channels/transporter in the *C9ORF72*^{RE} ALS iAstrocytes.

I next investigated the source of the membrane current dysfunction. First, I examined the rectification of the membrane currents. Rectification refers to the phenomenon where the current flowing through a membrane ion channel exhibits a directional preference, meaning its conductance is higher for one direction of current flow compared to the other for an equal driving force. Notably, the property of rectification is a major hallmark of specific ion channels (for example, delayed-rectifier K^+ channels) and is ideally investigated using I-V relationships. The rectification of the membrane currents was used therefore to determine whether this would yield an indication to a differentially expressed ion channel. To investigate rectification of membrane currents, I normalised each individual iAstrocyte current data set to the current data obtained at -104 mV to inspect the rectification of membrane currents. This normalised current data was then plotted against the voltage. These data do not highlight any notable deviation at day 7 between Con-1, Con-2, C9-1 and

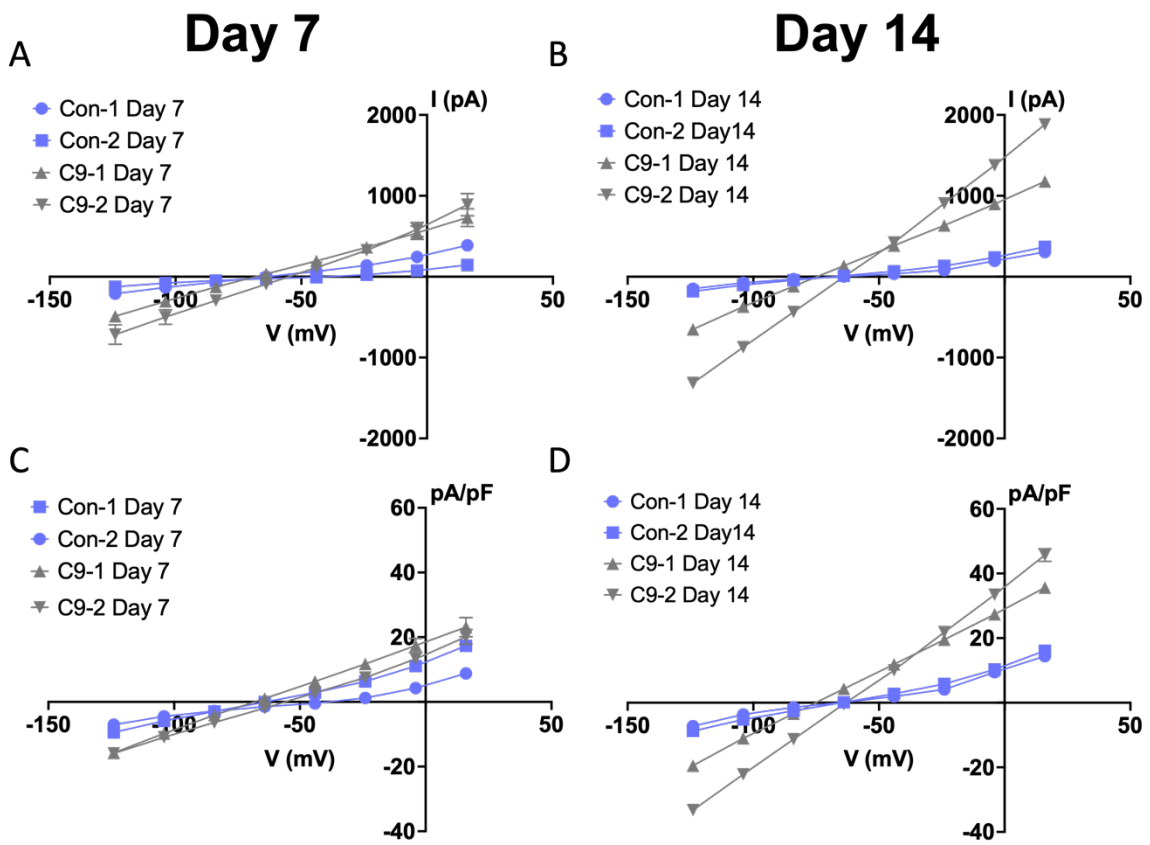

Figure 4-4. ***Membrane currents in C9ORF72^{RE} ALS iAstrocytes are enlarged****. A, B. Mean ± SEM current (I) versus voltage (V) plot of day 7 and day 14, respectively, iAstrocytes derived from Con-1 (day 7, n=9, N=3; day 14, n=20, N=4), Con-2 (day 7, n=8, N=3; day 14, n=15, N=5), C9-1 (day 7, n=9, N=3; day 14, n=32, N=7) and C9-2 (day 7, n=6, N=2; day 14, n=19, N=7). Note the increased amount of current evoked by the voltage protocol at each given potential for C9ORF72^{RE} ALS iAstrocytes. C, D. As in A, B, but for current density, which takes into account the WCC data for each individual iAstrocyte. Note that at day 14, C9ORF72^{RE} ALS iAstrocytes show an enhanced passage of current in their membranes. Note that SEM bars are hidden by the mean data points.*

C9-2 iAstrocytes and indicate that the *C9ORF72*^{RE} ALS iAstrocyte membrane currents are modestly more 'linear' at day 14 (Figure 4-5A,B). I extended this analysis to measure the rectification index (RI). The RI was measured by dividing the current amplitude evoked by the depolarising voltage step (+16 mV) by the current amplitude evoked by a voltage step (-124 mV). A statistically significant increase in RI is observed (day 14) over time compared to day 7 in all lines, except for C9-2 which has a lower RI at day 14 (Figure 4-5C). However, the rectification index data is inconclusive to the source of the membrane current dysfunction.

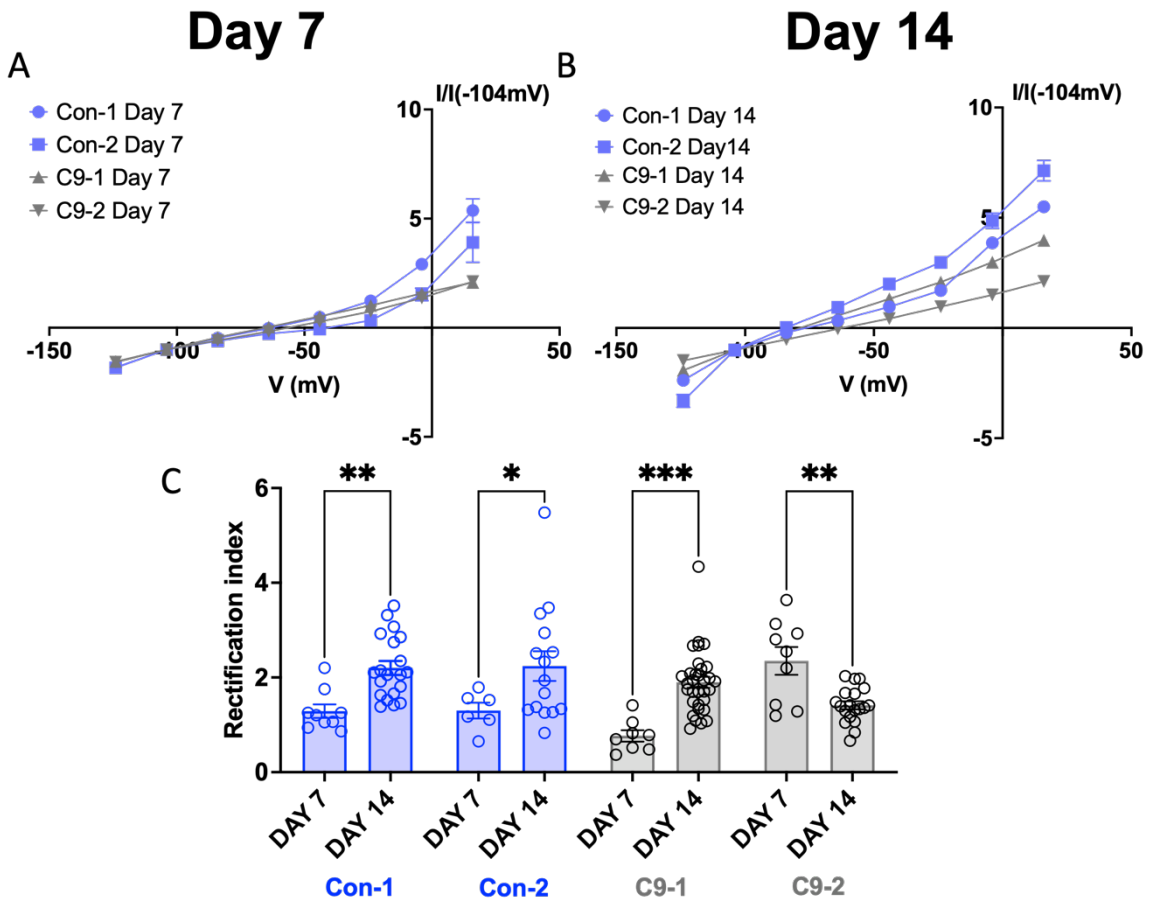

Figure 4-5. **Rectification of membrane currents are not impaired.** *A,B. Mean ± SEM normalised current [$\frac{I}{I(-104mV)}$] versus potential (V) plots of day 7 and day 14, respectively, Con-1, Con-2, C9-1 and C9-2 iAstrocytes. C, Mean ± SEM rectification index for each of the iAstrocyte lines. Rectification was determined by dividing the normalised current data obtained at 16 mV by -124 mV for each cell. Students' t-test was used to determine statistical significance between day 7 to day 14 for each line; *, p<0.05; **, p<0.01; ***, p<0.001.*

Astrocytes control ion homeostasis through multiple ion channels. Among these channels, the inwardly-rectifying K^+ channel 4.1 (Kir4.1) holds particular significance. Kir4.1 is expressed exclusively on glial cells in the CNS, the main populations being astrocytes. In homeostasis, Kir4.1 channels play a role in spatial buffering of K^+ release from neurons as well as maintaining axonal conductance (Bay and Butt 2012). Kir4.1 was found to be abnormally dysregulated in $SOD1^{G93A}$ mice and SOD1-ALS patient iPSC-derived astrocytes (Kelley et al., 2018). While Kir4.1 receives significant attention, other K^+ channels that could contribute to the observed current enhancement in *C9ORF72*^{RE} ALS iAstrocytes, like TREK-1 and TWIK-1. TREK-1 and TWIK-1, members of the two-pore domain K^+ channel family, expressed in astrocytes, are known to play a role in regulating RMP and astrocyte

excitability by mediating outward K^+ currents (Zhou et al., 2009). Interestingly, silencing of TREK-1/TWIK-1 channels in astrocytes by shRNA resulted in a phenotype similar to the control lines, suggesting potential increased expression in *C9ORF72*^{RE} ALS iAstrocytes (Mi Hwang et al., 2014). Therefore, I investigated whether the membrane current enhancement in *C9ORF72*^{RE} ALS iAstrocytes may be due to enhanced expression of Kir4.1 and TREK-1/TWIK-1 channels. Conveniently, since these are structurally related two-pore K^+ channels, these ion channel families can be blocked by extracellularly applied $BaCl_2$ (1mM). I therefore examined individual iAstrocyte currents using the same voltage-injection protocol employed as previously described and then repeated in the presence of $BaCl_2$ (1mM) for day 14 Con-1 and C9-1 iAstrocytes. Representative traces were chosen to display the effect of $BaCl_2$ (orange) on control (Con-1, blue) and C9-1 (black) iAstrocyte currents (Figure 4-6). $BaCl_2$ application on Con-1 resulted in a modest decrease in the current amplitude as observed in the current density-voltage plot (Figure 4-6B). Similarly, $BaCl_2$ did not abolish the substantial current enhancement observed in C9-1, suggesting that channels responsible for the enhancement are not inhibited by $BaCl_2$. Interestingly, $BaCl_2$ caused a shift in the reversal potential (E_{rev}). E_{rev} refers to the membrane potential at which the net current flow across the membrane is zero. The E_{rev} was quantified before and after $BaCl_2$ application for all cells investigated (Figure 4-6E), then the ΔE_{rev} (change in reversal potential) was analysed for each individual Con-1 and C9-1 iAstrocyte. Stratification of the data demonstrate that C9-1 exhibited larger ΔE_{rev} compared to Con-1, which demonstrates an increased membrane permeability to Ba^{2+}. This finding is interesting because there are only a subset of ion channels that are permeable to Ba^{2+}.

To confirm that the enhanced membrane current disturbance in *C9ORF72*^{RE} ALS iAstrocytes is not due to abnormal K^+ channel dysregulation, I repeated patch-clamp experiments using a CsCl-based intracellular patch pipette solution, where CsCl replaced K^+-gluconate as the principal constituent. Cs^+ is a potent blocker of K^+-channels and is commonly used in electrophysiological assays for this purpose (Clay and Shlesinger, 1984). CsCl caused only a modest reduction in current amplitude in both Con-2 and C9-2 iAstrocytes, as evidenced in the current density – voltage plots (Figure 4-7). However, current enhancement in C9-2

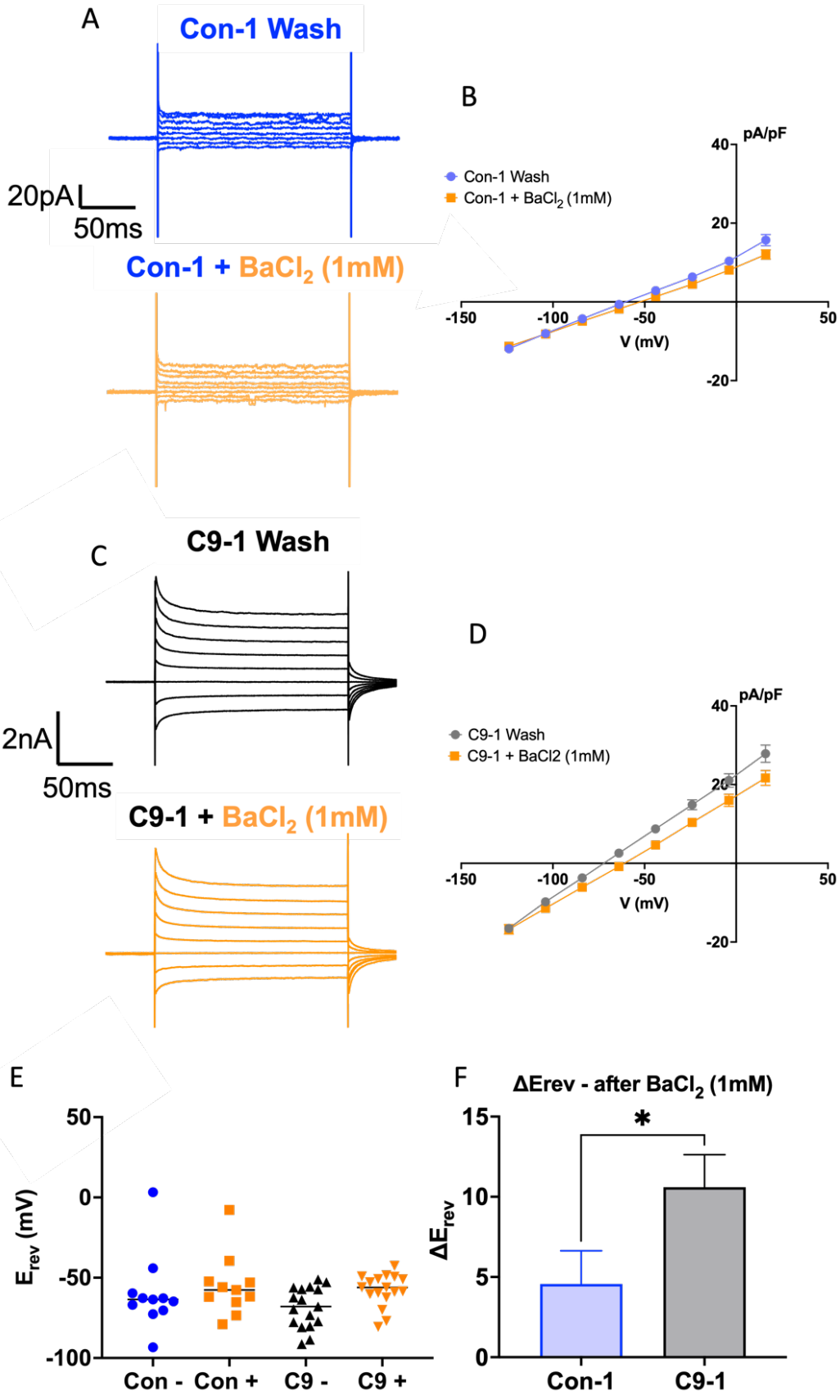

Figure 4-6. ***Membrane currents in C9ORF72^{RE} ALS iAstrocytes are not blocked by $BaCl_2$.*** *Caption on the next page.*

Figure 4-6. ***Membrane currents in C9ORF72^{RE} ALS iAstrocytes are not blocked by $BaCl_2$.*** *A. The panels show representative current traces from an individual day 14 healthy control, Con-1, iAstrocyte before and after the addition of extracellular-applied $BaCl_2$. B. Mean ± SEM current density (pA.pF) versus voltage (V) plot of day 14 Con-1 iAstrocytes in the presence and absence of $BaCl_2$ (n=11, N=4). C. The panel shows representative current traces from an individual day 14 C9-1 ALS iAstrocyte before and after the addition of $BaCl_2$. D. Mean ± SEM current density (pA.pF) versus voltage (V) plot of day 14 C9-1 iAstrocytes in the presence and absence of $BaCl_2$ (n=17, N=4). Note that $BaCl_2$ causes a more notable shift in the reversal potential (E_{rev}) of C9-1 compared to Con-1. E. Mean ± SEM E_{rev} for Con-1 and C9-1 iAstrocytes in the presence (+) and absence (-) of $BaCl_2$. F. Mean ± SEM shift in the change of reversal potential (ΔE_{rev}) for each iAstrocyte for Con-1 and C9-1 iAstrocytes induced by $BaCl_2$. Statistical significance was assessed using Student's t-test (*, p<0.05).*

iAstrocytes was crucially preserved in the CsCl intracellular solution, leading to the summation that K^+ channels are not the primarily contributors to the observed gain-of-function phenotype in *C9ORF72*^{RE} ALS iAstrocytes.

Previously, increased transient receptor potential cation channel subfamily V member 4 (TRPV4) expression in brain and spinal cord regions of SOD1^{G93A} transgenic mice has been observed in an immunohistochemical study (Lee et al., 2012). Interestingly, TRPV4 channels are expressed on astrocytes (Benfenati et al., 2011) and conduct Ba^{2+} (Bouron et al., 2015). I therefore considered TRPV4 channels as candidate contributors to the membrane current dysfunction expressed by *C9ORF72*^{RE} ALS iAstrocytes. To assess this, I performed the same voltage-injection protocol on Con-1 and C9-1 iAstrocytes and then in the presence of HC067047, a selective TRPV4 antagonist (Dias et al., 2019) to explore the contribution to the current enhancement (Figure 4-8). The application of HC067047 (green) did not alter the currents in either of the lines, Con-1 and C9-1 (Figure 4-8C), indicating that TRPV4 channels are not contributors to the observed gain-of-function current phenotype in *C9ORF72*^{RE} ALS iAstrocytes.

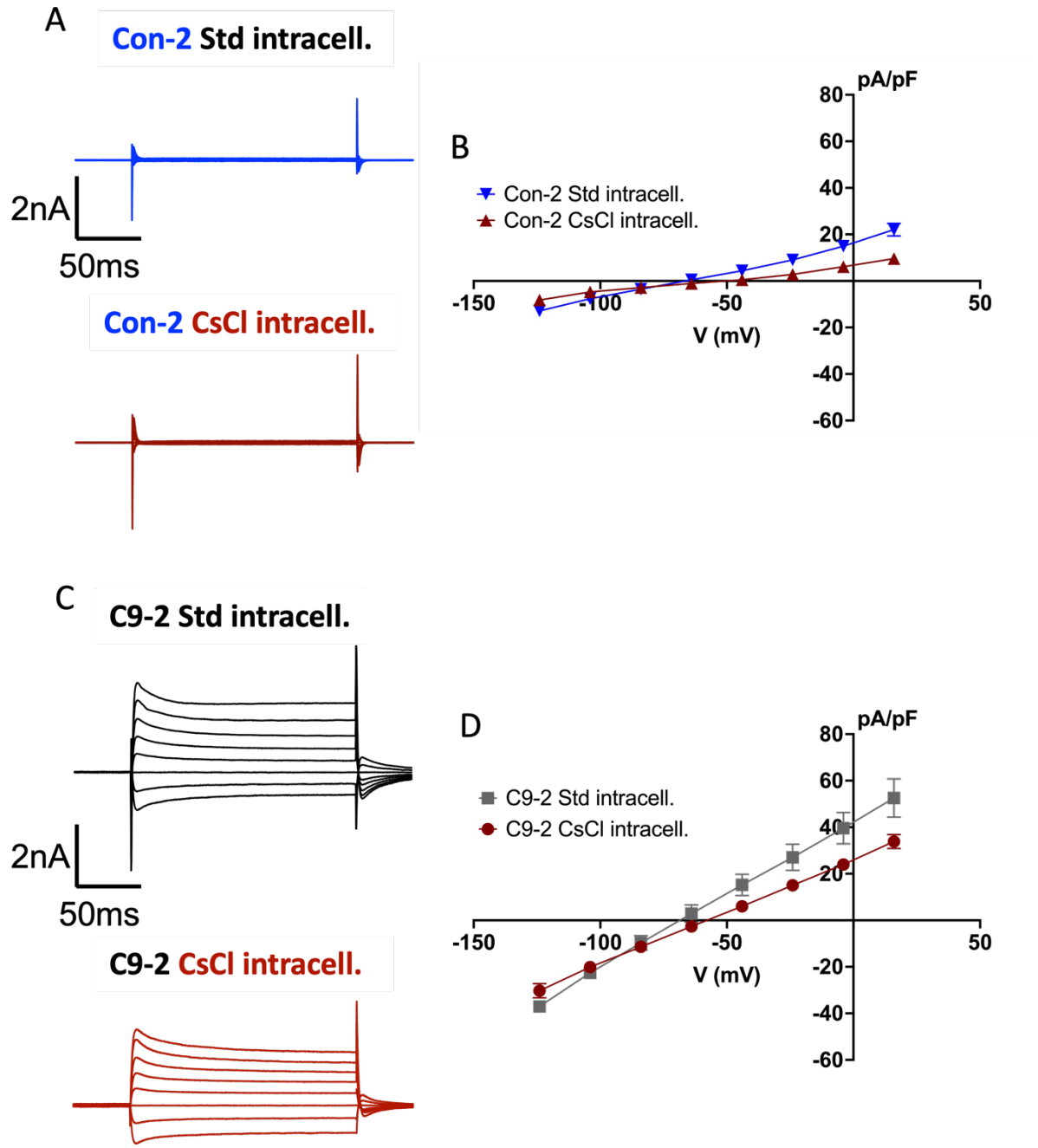

Figure 4-7. ***Membrane currents in C9ORF72^{RE} ALS iAstrocytes are not blocked by CsCl****. A. The panel shows representative voltage-step evoked current traces from individual day 14 healthy control, Con-2, iAstrocytes recorded in the presence of K-gluconate-based and a CsCl-based intracellular patch-pipette solution. B. Mean ± SEM current density (pA.pF) versus voltage (V) plot of day 14 Con-2 iAstrocytes in K^+-gluconate-based intracellular (n=6, N=2) and CsCl-based intracellular (n=6, N=2). C. The panel shows representative current traces from individual day 14 C9-2 ALS iAstrocytes in the presence of K^+-gluconate-based intracellular patch-pipette solution and CsCl-based solution. D. Mean ± SEM current density (pA.pF) versus voltage (V) plot of day 14 C9-2 iAstrocytes in K-gluconate-based intracellular (n=3, N=1) and CsCl-based intracellular (n=9, N=2).*

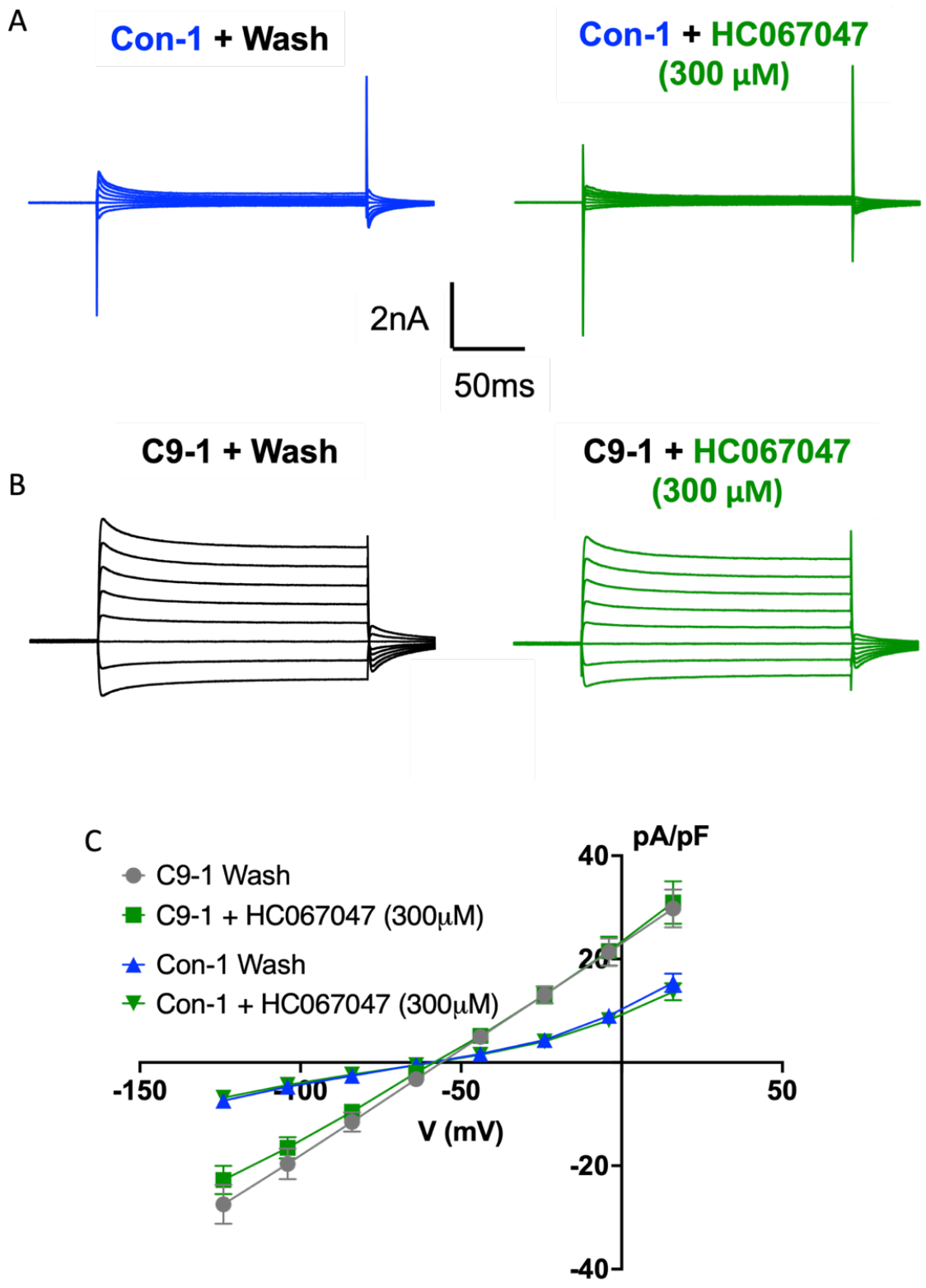

Figure 4-8. ***Membrane currents in C9ORF72^{RE} ALS iAstrocytes are not blocked by TRPV4 antagonist, HC067047****. A. The panel shows representative voltage-step evoked current traces from an individual day 14 Con-1 Astrocyte before and after the addition of extracellular-applied HC067047. B. As in A, but for C9-1 iAstrocytes. C, Mean ± SEM current density (pA.pF) versus voltage (V) plot of day 14 Con-1 and C9-1 iAstrocytes in the presence and absence of HC067047 (Con-1, n=7, N=2; C9-1, n=9, N=2).*

Glial cells express connexin channels (Giaume et al., 2021). Connexins are channel proteins that form hexameric structures called connexons. For astrocytes, the predominant connexons are composed of connexin-43 (Cx43), and to an extent, connexin-30 (Cx30) (Giaume et al., 2021). When connexons on neighbouring cells dock, they form gap junctions, enabling direct intercellular communication between glial cells. Hemichannels refer to individual connexons, functioning as channels that mediate the exchange of ions and signalling molecules between the astrocyte and its environment, including neurons (Giaume et al., 2021). Importantly, gap junctions are highly permeable to multitude of cytoplasmic molecules, including metabolites (Tabernero et al., 1996, Goldberg et al., 1999), second messengers (Lawrence et al., 1978, Sáez et al., 1989), miRNAs (Zong et al., 2016) and ionic species (Qu and Dahl, 2002, Christ et al., 1992), including Ba^{2+} (Contreras et al., 2003). Cx43 plays important roles in maintaining homeostasis, synchronizing astrocyte networks, supporting neuronal metabolism, and modulating synaptic activity and plasticity (Giaume et al., 2021). Notably, altered Cx43 expression and function have been linked to neurodegenerative diseases (Orellana et al., 2015, Xing et al., 2019, Huang et al., 2021b), including ALS (Almad et al., 2016, Keller et al., 2011, Díaz-Amarilla et al., 2011). In previous studies, upregulation of Cx43 levels in the spinal cord and motor cortex of patients with ALS and $SOD1^{G93A}$ mice was observed and the blockage of Cx43 led to neuroprotective effects (Almad et al., 2016, Díaz-Amarilla et al., 2011). Increased levels of Cx43 expression were related to increased hemichannel activity and gap junction coupling, that led to elevated concentrations of intracellular Ca^{2+} and motor neuron damage. The administration of pan-Cx43 inhibitors in $SOD1^{G93A}$ mouse model can alleviate neuronal toxicity (Takeuchi et al., 2011, Almad et al., 2016). I reasoned therefore that the increase in membrane current could be mediated by increased connexin-related dysfunction.

To assess the involvement of connexin dysfunction in the current enhancement phenotype observed in *C9ORF72*^{RE} ALS iAstrocytes, I examined the currents using the voltage-clamp protocol and then, for the same iAstrocyte, in the presence of standard extracellular solution (Figure 4-9) and once in the presence of connexin blocker, carbenoxolone (CBX, 10μM; Figure 4-9). CBX was washed onto the cells for a two minutes and recordings were taken after. Application of CBX results in a modest reduction in the current density-voltage response of the control Con-2 line (Figure 4-9D). However,

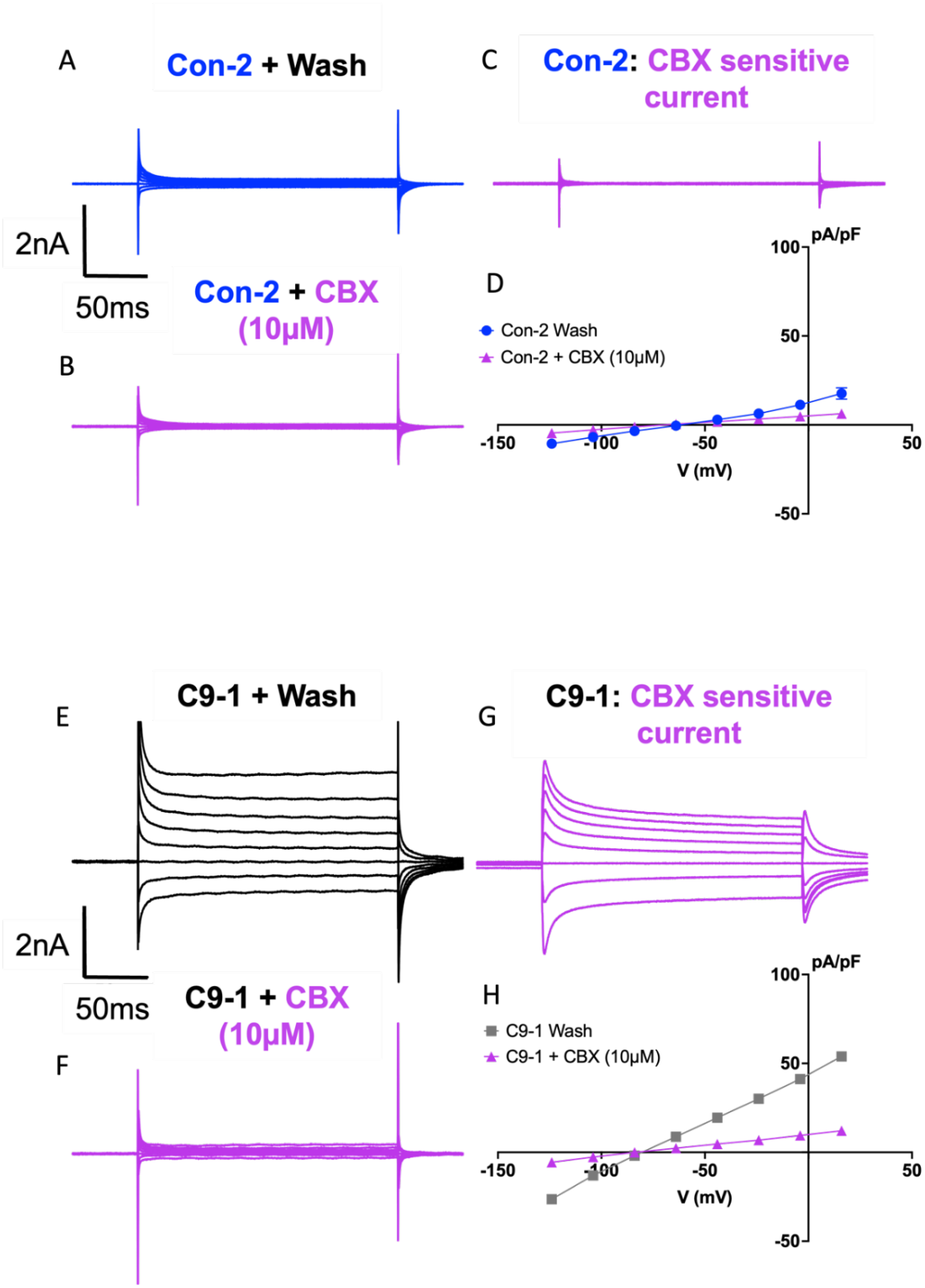

Figure 4-9. ***Connexin blocker CBX attenuates membrane current dysfunction in C9ORF72^{RE} ALS iAstrocytes****. Caption on the next page.*

Figure 4-9. ***Connexin blocker CBX attenuates membrane current dysfunction in C9ORF72^{RE} ALS iAstrocytes****. A. The panel shows representative current traces from an individual day 14 Con-2 iAstrocyte evoked by the described protocol. B. The same iAstrocyte in A in the presence of extracellularly applied CBX. C. The CBX-sensitive current for the iAstrocyte presented in A. D. Mean ± SEM current density (pA.pF) versus voltage (V) plot of day 14 Con-2 iAstrocytes in the presence and absence of CBX (n=4, N=3). E. The panel shows representative voltage-step evoked current traces from an individual day 14 C9-1 iAstrocyte. F. The same iAstrocyte in E in the presence of CBX. G. The CBX-sensitive current for the iAstrocyte presented in E. Note the high sensitivity of the current dysfunction to CBX. H, Mean ± SEM current density (pA.pF) versus voltage (V) plot of day 14 C9-1 iAstrocytes in the presence and absence of CBX (n=10, N=3).*

strikingly, CBX entirely abolished the current enhancement observed in C9-1 line (Figure 4-9F). This was quantified in a current density – voltage plot (Figure 4-9G), which demonstrates that CBX application restores the current density – voltage relationship to a control-like level. These data point towards the involvement of connexin-related dysfunction as the main contributor to the *C9ORF72*^{RE} ALS iAstrocytes current enhancement. CBX is one of the most commonly used blockers of gap junctions and hemichannels. To examine the identity of the connexin current enhancement, I examined the impact of Gap19, a Cx43 mimetic peptide that can specifically block Cx43 hemichannels without disrupting gap junction function (Abudara et al., 2014). Importantly, Gap19 remains to be fully characterised, but evidence indicates that its pharmacological mode of action is consistent with a partial allosteric modulation of Cx43-containing hemichannels via the intracellular C-terminal domain of Cx43 (Lissoni et al., 2020, Lissoni et al., 2023). Gap19 (100 μm) was supplemented to the intracellular solution and the current density examined in Con-1 and C9-1 ALS iAstrocytes in the absence and presence of Gap19 (Figure 4-10). The current density – voltage relationship was only modestly impacted in Con-1 iAstrocytes. However, consistent with a partial block of Gap19, the resultant current density – voltage relationship for C9-1 ALS astrocytes showed a partial reduction in the current density (Figure 4-10). These data are consistent with connexin Cx43 hemichannels being a major source of current dysfunction observed in *C9ORF72*^{RE} ALS iAstrocytes.

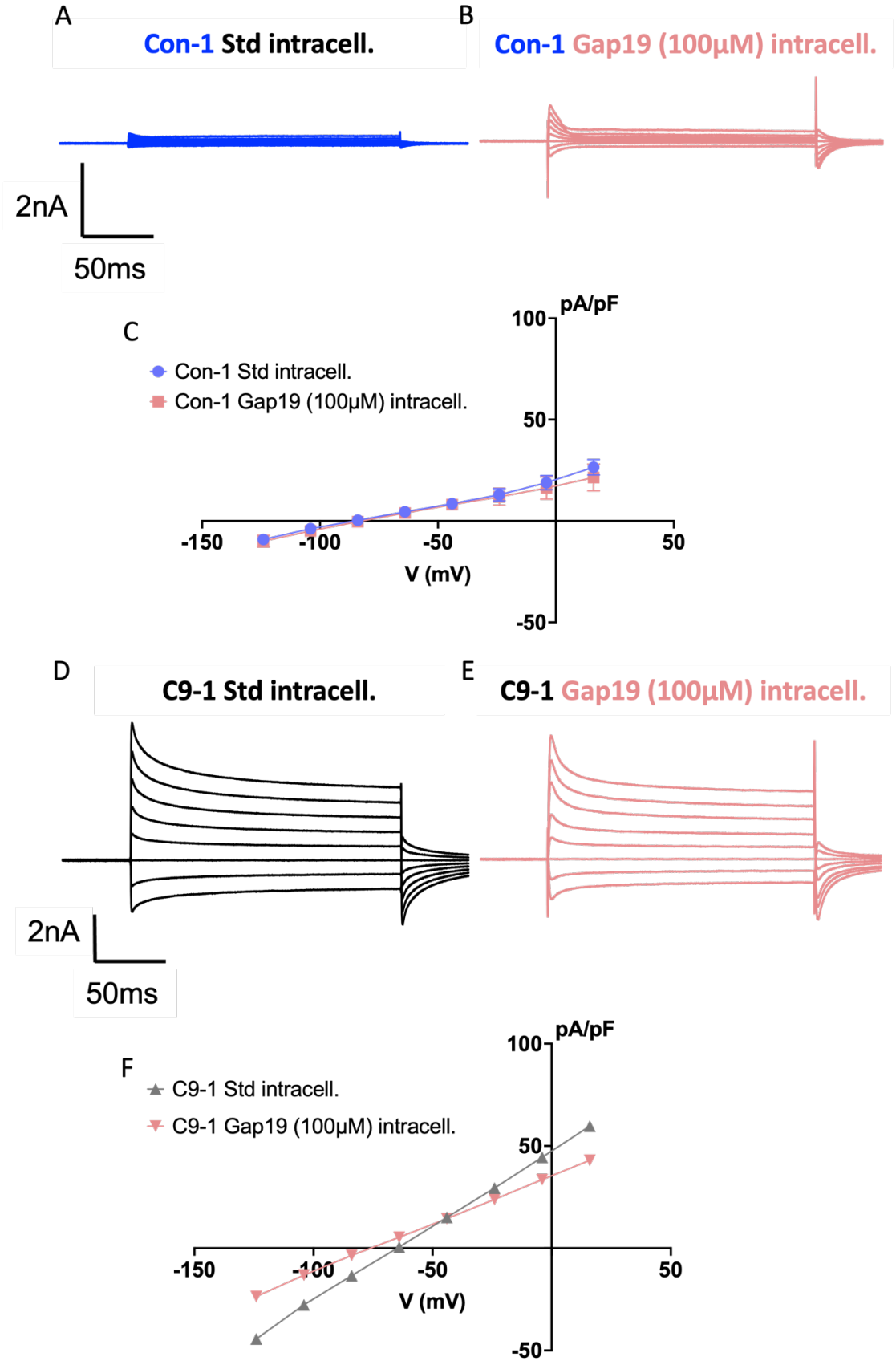

Figure 4-10. ***Hemichannel partial blocker Gap19 blocks membrane currents in C9ORF72^{RE} ALS iAstrocytes.*** *Caption on the next page.*

Figure 4-10. ***Hemichannel partial blocker Gap19 blocks membrane currents in C9ORF72^{RE} ALS iAstrocytes.*** *A,B. The panels show representative voltage-step evoked current traces from an individual day 14 Con-1 iAstrocyte in the presence of an intracellular solution supplemented without and with hemichannel blocker, Gap19, respectively. C. Mean ± SEM current density (pA.pF) versus voltage (V) plot of day 14 Con-2 iAstrocytes in the presence (n=4, N=2) and absence of Gap19 (n=4, N=2). D,E. The panels show representative voltage-step evoked current traces from individual day 14 C9-1 iAstrocytes in the presence of an intracellular solution supplemented without and with Gap19, respectively. C, D, Mean ± SEM current density (pA.pF) versus voltage (V) plot of day 14 C9-1 iAstrocytes in the presence (n=9, N=3) and absence of Gap19 (n=2, N=1).*

Next I wanted to begin to understand the underpinning mechanisms of *C9ORF72*^{RE} ALS iAstrocyte membrane dysfunction. There are three proposed mechanisms leading to neurodegeneration downstream of *C9ORF72* repeat expansion; 1) haploinsufficiency, 2) formation of RNA-foci and 3) accumulation of toxic dipeptide repeat proteins (DPRs) translated from the hexanucleotide repeat expansion (as previously described in Introduction section 1.7). While all three of these mechanisms may contribute to disease, DPRs have been identified as the prominent driver of neurodegeneration (Zu et al., 2013, Mori et al., 2013a, Mori et al., 2013c, Mizielinska et al., 2014, Ash et al., 2013). To target DPR-mediated mechanisms in iAstrocytes, I targeted Serine/arginine-rich splicing factor 1 (SRSF1). SRSF1 is a protein involved in RNA splicing and nuclear export, including mediating the nuclear export of expanded *C9ORF72* RNA transcripts for translation (Huang et al., 2003, Hautbergue et al., 2017). Building on previous work which demonstrated that depleting SRSF1 expression using a lentiviral knockdown approach in *C9ORF72*^{RE} ALS iAstrocyte can prevent motor neuron death in co-culture assays (Hautbergue et al., 2017), a lentiviral vector (LV) expressing RNAi targeting SRSF1 (SRSF-1 LV) to deplete SRSF1 in these cells was used to investigate the link between SRSF1-mediated DPR generation in *C9ORF72*^{RE} ALS iAstrocytes and the enhanced membrane current in *C9ORF72*^{RE} ALS iAstrocytes. Hautbergue et al. utilized Con-2 and C9-2 iAstrocyte lines, same as presented in this study. Here, control (Con-1) and *C9ORF72*^{RE} ALS iAstrocyte (C9-1) iAstrocytes were transduced with either SRSF1-LV or control-LV (scrambled SRSF1 RNAi; (Hautbergue et al., 2017) at two different timepoints (day 4 and day 11) and voltage-clamp recordings were performed at 72 hours after the initial LV incubation (day 7 and day 14) to assess the effect of SRSF1 depletion on

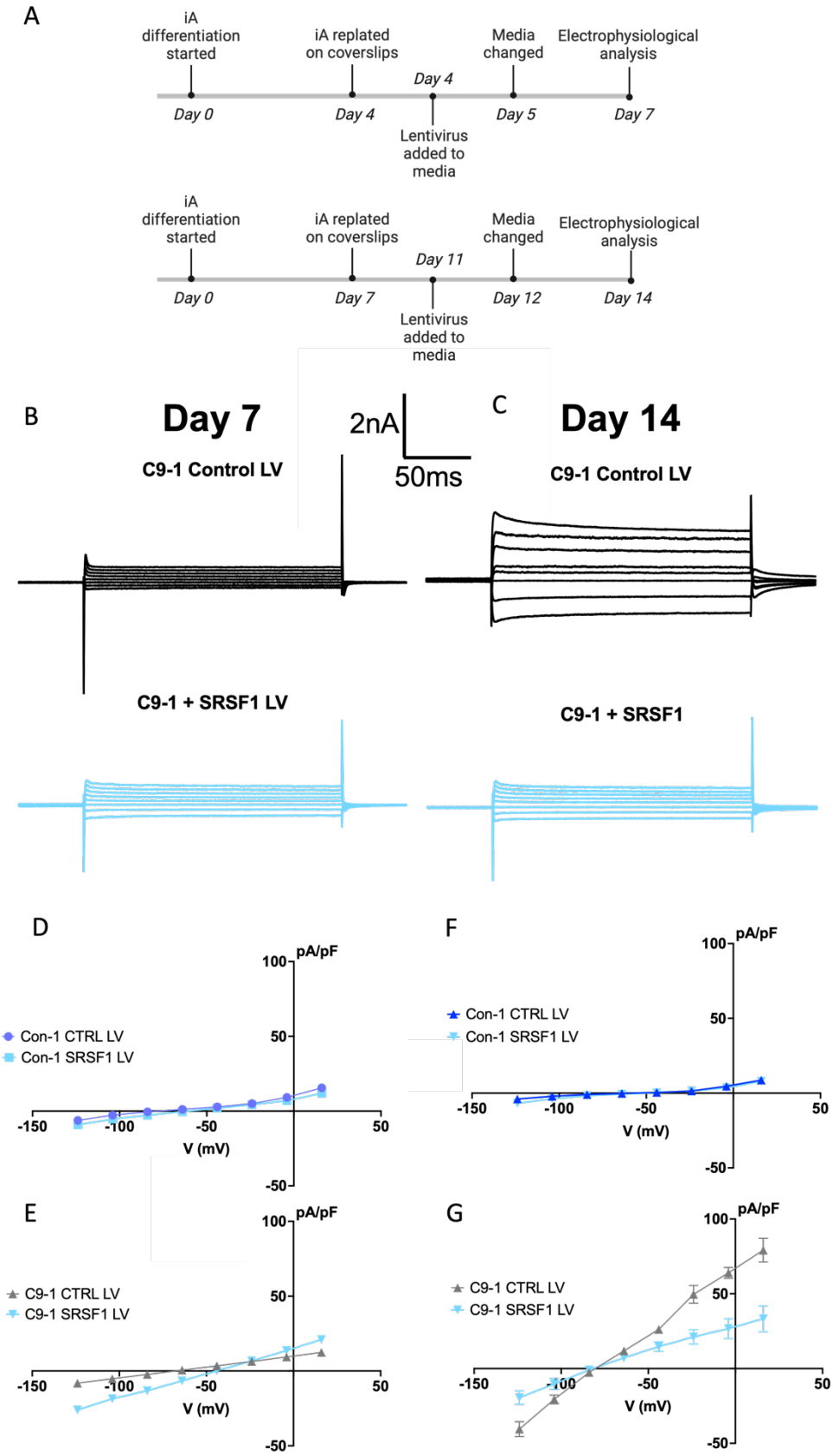

Figure 4-11. ***Membrane current dysfunction in C9ORF72^{RE} ALS iAstrocytes is sensitive to SRSF1 knock down.*** *Caption on the next page.*

Figure 4-11. ***Membrane current dysfunction in C9ORF72^{RE} ALS iAstrocytes is sensitive to SRSF1 knock down.*** *A. For electrophysiological recordings performed at day 7 or day 14, iAstrocytes were plated onto coverslips at day 4 or 7, respectively. The lentivirus was added to the cells after 6 hours of replating and left for a maximum of 24 hours. The next day, the media was changed to lentivirus-free media and electrophysiological recordings performed two days after. B,C. The panels show representative voltage-step evoked current traces from individual day 7 and day 14 C9-1 iAstrocytes, respectively, in the presence of control or SRSF1 lentivirus. Note current response reduction at day 14 in the presence of SRSF1 lentivirus. D,E. Mean ± SEM current density (pA.pF) versus voltage (V) plot of day 7 Con-1 and C9-1 iAstrocytes in the presence of control lentivirus (Con-1, n=4,N=1; C9-1, n=6, N=3) and SRSF1 lentivirus (Con-1, n=11, N=4; C9-1, n=9, N=3). F,G. Same as D,E but for day 14 in the presence of control lentivirus (Con-1, n=2,N=1; C9-1, n=3, N=2) and SRSF1 lentivirus (Con-1, n=2, N=1; C9-1, n=5, N=2). Note reduction in current density (pA.pF) in C9-1 iAstrocytes.*

membrane currents (Figure 4-11A). At day 7, no significant changes in current response were observed in either Con-1 or C9-1 ALS iAstrocytes transduced with SRSF1-LV or control-LV (Figure 4-11B,D,E). However, at day 14, C9-1 iAstrocytes treated with SRSF1-LV displayed a clear reduction in the current dysfunction observed in C9-1 iAstrocytes (Figure 4-11C,G). Notably, no changes were observed in control-LV treated C9-1 or either treatment group in Con-1 at day 14 (Figure 4-11F,G). These data demonstrate that the membrane current dysfunction in *C9ORF72*^{RE} ALS iAstrocyte is mediated, at least in part, by DPR-related mechanisms.

C9ORF72^{RE} ALS iAstrocytes are established to be toxic to MNs in ALS (Hautbergue et al., 2017). Astrocytic gap junctions play an important role in mediating injuries to the CNS. A significant increase in Cx43 was observed in models of neurotrauma (Chen et al., 2012, Sun et al., 2015) and administration of connexin blockers in these models were identified to be neuroprotective and serve as potential therapeutics (Chew et al., 2010). I therefore considered that the increased expression of connexins in *C9ORF72*^{RE} ALS iAstrocyte was a key mechanistic component in causing an increase in non-cell autonomous MN death. To explore this, I used a co-culture system. I generated control iPSC-derived MNs (Methods section 2.2.6) according to previously and widely used protocol (Du et al., 2015). At day 37 of MN culture, either control or *C9ORF72*^{RE} ALS iAstrocyte for 72 hours were cultured with the MNs (protocol described in Figure 4-12). The healthy iPSC-derived MN line was also cultured in monoculture. After 6 hours, half of the co-cultures were treated with MN day 29-

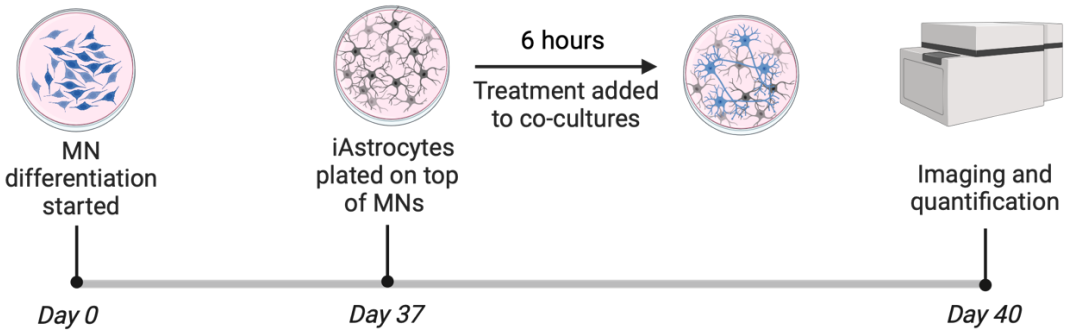

Figure 4-12. ***Schematic diagram illustrating the main steps for the co-culture experiment****. MNs were kept in culture until the end of differentiation. At day 37, iAstrocytes were plated on top of the MNs. Treatments were added 6 hours after plating. The co-cultures were fixed with 3.8% PFA after 72 hours of incubation. ICC staining was performed to demonstrate co-culture of MAP2+ motor neurons and Vimentin+ iAstrocytes. Caspase3+ MNs were quantified as a measurement of neuronal death. Imaging was performed using the wide-field In-Cell Analyzer and quantification was done using Columbus Analysis System.*

40 media (as described in Table 2-10) containing CBX (10 µM) and the other half only with MN day 29-40 media. After 72 hours, the cells were fixed and ICC experiments were performed to assess Caspase-3 expression, a marker of apoptosis, in MAP2+ MNs. Caspase-3 levels were quantified to investigate *C9ORF72*^{RE} astrocyte-mediated toxicity on healthy MNs and the potential protective effect of CBX. Our previous experiments revealed that at 10 µM, CBX eliminates the current enhancement and blocks Cx43. In the co-culture system, MN death was considerably reduced when *C9ORF72*^{RE} ALS iAstrocyte were cultured with healthy MNs and MN day 29-40 media was supplemented with CBX (10 µM) compared to when the co-culture system was fed the MN day 29-40 media in the absence of CBX. The treatments with CBX led to a 41% reduction of MN cell death in the *C9ORF72*^{RE} ALS iAstrocyte -healthy MN co-culture system. While these experiments provide valuable insights, their limitations, such as the relatively small number of replicates, necessitate careful consideration and replication. Moreover, the reprogramming process used to generate iAstrocytes and MNs may not fully recapitulate *in vivo* conditions. My co-culture approach, employing iNPCs derived from ALS patient fibroblasts and healthy donor control fibroblasts, along with iPSC-derived MNs, offers several advantages. iAstrocytes can be rapidly differentiated from iNPCs within a week, enabling a swift assessment of their impact on MN survival compared to the prolonged 12-week process of generating astrocytes from

iPSCs (Zhao et al., 2019). Survival can be evaluated by monitoring motor neuron fluorescence and counting viable cells, as detailed in this thesis and previous studies (Meyer et al., 2014; Hautbergue et al., 2017; Allen et al., 2019; Castelli et al., 2021).

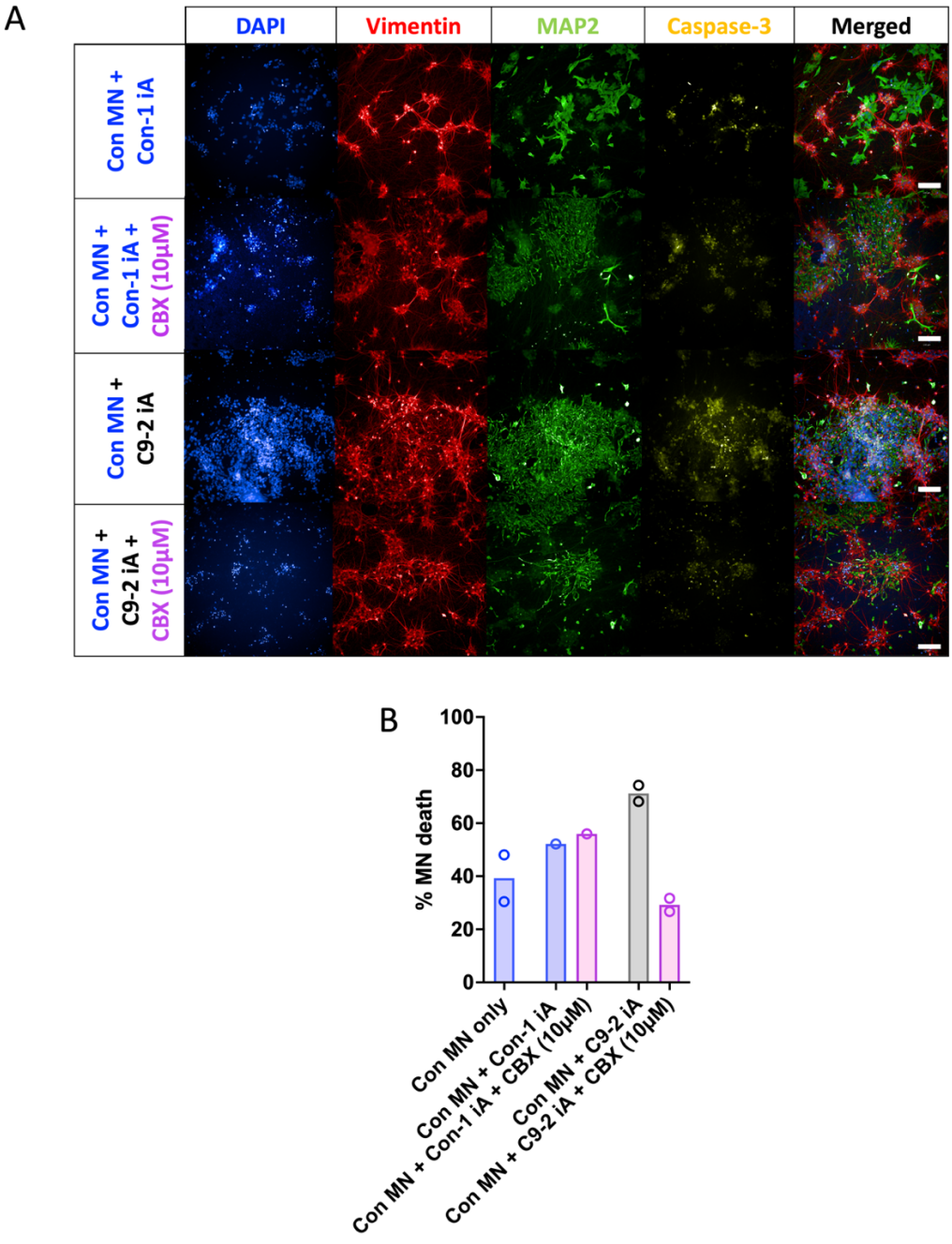

Figure 4-13. ***Preliminary data indicate that CBX causes a reduction in C9ORF72^{RE} ALS iAstrocytes-mediated motor neuron death****. A. Figure shows co-culture of MNs with iAstrocytes. ICC demonstrated cultures displayed Vimentin+ iAstrocytes and MAP2+ MNs. Caspase-3+ immunopositive MNs were quantified to determine percentage of neuronal death. B. Preliminary data depicts reduction in MN death in co-cultures in the presence of CBX. Scale bar set to 100 μm.*

4.5. Discussion

Using a combined approach utilizing human stem cell technology, patch-clamp electrophysiology, selective pharmacology and cell biology I have identified major membrane physiology disruption in *C9ORF72*^{RE} ALS iAstrocyte. I electrophysiologically demonstrated that the *C9ORF72*^{RE} ALS iAstrocytes exhibit increased membrane current passivity upon voltage stimulation as culture time progresses, suggesting that membrane current dysfunction is a progressive pathophysiology as the disease progresses. I pharmacologically determined this membrane abnormality was due to connexin dysfunction using connexin blocker CBX and the specific Cx43 hemichannel blocker Gap19. I therefore identified Cx43 hemichannel dysfunction as a main contributor to this enhanced current response. Our wider analysis did not find any deviation in functional disturbance in Ba^{2+}-sensitive two pore K^+ channels (TWIK-1/TREK-1) and Kir4.1, Cs^+-sensitive K^+ channels or TRPV4 that have previously been reported or potentially disturbed in ALS astrocytes (Kelley et al., 2018, Mi Hwang et al., 2014, Lee et al., 2012, Wang et al., 2022). To further explore the role of connexin dysregulation in *C9ORF72*^{RE} ALS iAstrocytes as a potential mechanism underlying non-cell-autonomous MN death, I employed co-cultures of *C9ORF72*^{RE} ALS iAstrocytes and healthy MNs, where I obtained preliminary data to indicate that *C9ORF72*^{RE} ALS iAstrocyte toxicity to MNs is mediated, at least in part, by connexins. I determined that connexin-mediated current dysfunction in *C9ORF72*^{RE} ALS iAstrocytes is, at least in part, due to the presence of DPRs, a hallmark pathological feature of *C9ORF72*^{RE} ALS. This novel data points towards connexin (Cx43 hemichannel) dysfunction as a pathological mechanism in *C9ORF72*^{RE} ALS iAstrocytes, contributing to non-cell-autonomous MN death.

The finding that connexins are elevated in *C9ORF72*^{RE} ALS iAstrocytes is significant. Astrocytes form a dense network via gap junctions composed primarily of the protein connexin Cx43. This network facilitates intercellular communication and supports neuronal function, through energy metabolism in neurons and impair long-term plasticity (Murphy-Royal et al., 2020). Connexin dysregulation is highly linked to pathogenesis in many neurological conditions, such as hypoxic ischemia (Tittarelli, 2021, McDouall et al., 2024) and not least, connexin dysregulation has been reported in ALS astrocytes previously. Astrocytic gap junction Cx43 was increased in the anterior horns of the spinal cords of SOD1^{G93A} mouse model during disease progression and at the end stage of ALS, suggesting

that Cx43 dysregulation can cause MN death (Cui et al., 2014). Abnormal increases in Cx43 expression both at transcription and protein level have been documented in familial ALS and sALS, as well as post-mortem sALS patient material (Almad et al., 2016, Almad et al., 2022, Gomes et al., 2022). During the work undertaken in my thesis, a significant piece of work was published confirming the notable dysregulation of connexin-mediated dysfunction in ALS astrocytes and its role in MN toxicity (Almad et al., 2022). Using human iPSC-derived astrocytes from $SOD1^{D90A}$ and $SOD1^{A4V}$ mice and sporadic ALS patients they established that Cx43 is upregulated and that Cx43-hemichannels are upregulated in ALS astrocytes. Also blockade of connexin channels prevented the ALS astrocyte toxicity to iPSC-derived MNs, very similar to our preliminary findings. Our electrophysiological data highly complements these finds, directly demonstrating the functional dysregulation of connexin channels at the astrocyte membrane, but also extending the finding to *C9ORF72*^{RE} ALS iAstrocytes. Further, using combined Cx43 knock out models with $SOD1^{G93A}$ and $SOD1^{G37R}$ mouse models, the lack of Cx43 expression slowed disease progression indicating a direct relevance of Cx43 for disease pathogenesis (Almad et al., 2022, Takeuchi et al., 2011). Collectively, our studies converge on the considerable dysregulation of connexins in ALS astrocytes which mediates toxicity to MNs.

What is it about connexins that makes them toxic to MNs? Connexin channels are permeable to numerous cytoplasmic factors in addition to simple ionic species, including metabolites, including ATP and reactive oxygen species (ROS), glutamate (Chen et al., 2012, Lanciotti et al., 2020) and inflammatory agents such cytokines (TNF-α, IL-1β, IL6; (John et al., 2003, Gadea et al., 2008, Bylicky et al., 2018). Typically, these are passed through the network of the glial syncytium to other glial cells via connexin-formed gap junctions. However, the data implicate the release of factors through Cx43 hemichannels into the media as potent mediator of toxicity. Connexin dysfunction in astrocytes leads to the excessive release of ATP and glutamate which are toxic to neighbouring neurons (Orellana et al., 2011, Takeuchi et al., 2006). Under physiological conditions, abnormally open connexin channels release glutamate into the synaptic cleft, and gap junctions decrease the expression of glutamate transporter 1 (GLT-1) (Figiel et al., 2007), responsible for the uptake of glutamate from the synaptic cleft into astrocytes (Wang et al., 2017). Accumulation of glutamate into the

synaptic cleft triggers excitotoxicity, an already established hallmark of ALS, which leads to the loss motor neuron function and cell death (Van Den Bosch et al., 2000, Van Den Bosch et al., 2006). Cx43 upregulation was observed under inflammatory conditions in transgenic $hSOD^{G93A}$ mice, leading to excessive calcium signalling, causing motor neuron excitotoxicity and death (Almad et al., 2016). While metabolic and mitochondrial dysfunction with gap stress are hallmarks of ALS and highly present in ALS iAstrocytes (Allen et al., 2019a, Vandoorne et al., 2018), the role of connexins in this pathophysiological process remains to be characterised. However, connexins have been linked to facilitating mitochondria coupling (Zhang et al., 2022a), a process generating ATP and ROS as by-products. Both ATP and ROS can be toxic at high levels, and connexin function has been associated with elevated ROS production (Zhang et al., 2022a). Moreover, connexins appear to facilitate the permeation and release of ATP and ROS, both implicated in MN toxicity (Giaume et al., 2021, Ramachandran et al., 2007, Cieślak et al., 2019, Barber and Shaw, 2010). The increase in Cx43 activity in *C9ORF72*^{RE} ALS iAstrocytes may also therefore be enhancing pathological mitochondrial coupling, leading to elevated production of toxic agents, in addition to allowing the passage of toxic agents.

What is driving connexin dysfunction? I explored the potential involvement of DPRs, a hallmark pathological feature of *C9ORF72*^{RE} ALS. Depletion of SRSF1, a protein implicated in the nuclear export of pathological C9ORF72 repeat transcripts and subsequent DPR production, significantly reduced the Cx43-mediated membrane current dysfunction in *C9ORF72*^{RE} ALS iAstrocytes. This finding indicates that DPRs are playing a role in the generation of Cx43 dysregulation. DPR pathology in astrocytes reduces their ability to uptake glutamate from their surroundings, leading to excitotoxicity in motor neurons already made vulnerable by *C9ORF72* haploinsufficiency (Shi et al., 2018). Recently, Marchi et al. demonstrated the astrocyte-to-neuron propagation of poly-GA DPRs, the most abundant form in *C9ORF72*^{RE} ALS patients (Mori et al., 2013c), although cytotoxicity was not detected in co-cultures of iAstrocytes and MNs, possibly due the requirement for additional presence of other DPR species (such as poly-GR and poly-PR) (Marchi et al., 2022) or *C9ORF72* haploinsufficiency. Interestingly, loss of functional output in MNs, without a decrease in cell viability was reported in MN co-cultured with *C9ORF72*^{RE} ALS astrocytes

harbouring RNA foci and poly-GP DPRs (Zhao et al., 2020). This study has provided direct evidence that DPRs contribute to the increase in connexin dysregulation in ALS astrocytes.

4.6. Conclusion

In conclusion, this chapter investigated the Cx43 hemichannel dysfunction as a mechanism of *C9ORF72*^{RE} ALS-mediated MN death. *C9ORF72*^{RE} ALS iAstrocytes displayed progressively enhanced membrane current passivity, indicative of impaired ion channel function. Selective blockers revealed Cx43 hemichannels as key contributors. Co-cultures with CBX, a connexin blocker, significantly reduced motor neuron death, suggesting *C9ORF72*^{RE} ALS iAstrocytes release neurotoxic agents through these channels. Furthermore, SRSF1 depletion, which reduces DPR production, diminishes Cx43 dysfunction, indicating a role of DPRs in driving connexin dysfunction. However, major questions centring on the precise timing of Cx43 dysfunction during disease progression and its generalized role to other ALS and FTD subtypes remain to be addressed.

5. Chapter 5: Connexin-mediated dysfunction is a convergent feature of ALS and is inducible

5.1. Introduction

In the previous Chapter (Chapter 4), I found how Cx43 connexin dysfunction is the main contributor to the progressive membrane current dysregulation observed in iAstrocytes generated from fibroblasts obtained from symptomatic ALS patients harbouring *C9ORF72*^{RE} mutations. Co-cultures indicated connexin dysfunction mediated motor neuron toxicity from *C9ORF72*^{RE} ALS iAstrocytes. Convergent work by Almad et al., 2022 confirms that connexin dysfunction is toxic to MNs in other ALS backgrounds. Furthermore, I determined that *C9ORF72*^{RE}-related DPRs are at least in part driving connexin dysregulation in *C9ORF72*^{RE} ALS astrocytes. However, key questions still remain regarding the mechanisms as to when and how connexins are dysregulated in ALS astrocytes, and whether connexins are functionally dysregulated in other linked and disparate neurodegenerative diseases.

Is connexin dysfunction a feature of sporadic ALS (sALS)? Connexin dysfunction appears to be conserved feature of other ALS forms. Several studies report abnormal increases in Cx43 expression at both transcriptional and protein levels in sporadic and mSOD1 ALS *in vitro* and *in vivo* models, as well as post-mortem sALS patients motor cortex, spinal cord and cerebrospinal fluid (Almad et al., 2016, Almad et al., 2022, Gomes et al., 2022). It is likely that membrane current dysfunction is a convergent feature of sporadic ALS, but remains to be determined electrophysiologically.

Hypothesis: I hypothesize that iAstrocytes derived from symptomatic sporadic ALS patients display an increase in membrane current dysfunction.

Is connexin dysfunction a feature of C9ORF72^{RE} *-mediated FTD?* The *C9ORF72*^{RE} mutation is the most common genetic cause of ALS/FTD (DeJesus-Hernandez et al., 2011). Further, ALS and FTD share convergent pathological substrates reinforcing the notion that two diseases are different manifestations of a continuum ranging from pure forms of ALS with exclusive motor involvement, to pure forms of FTD, of which the most frequent presentation is bvFTD, with exclusive cognitive and behavioural involvement, passing through hybrid form of

ALS/FTD with both cognitive and motor involvement (Burrell et al., 2016). However, the specific disease manifestations depend on the vulnerable brain regions. The first affected structures in *C9ORF72*^{RE} FTD are the cortico-striato-thalamic network (Lee et al., 2014), with the thalamus showing specific vulnerability (Bonham et al., 2023, Vatsavayai et al., 2016b), leading to progressive impairment of behaviour, language and cognitive functions in patients (Perry et al., 2017a, Vatsavayai et al., 2019). Despite the shared genetic component, significant differences in the underlying disease mechanisms for ALS and FTD need to be considered. For example, FTD cases present with distinct TDP-43 pathologies compared to ALS, indicating divergent disease pathogenesis mechanisms that involve the same TDP-43 protein (Tan et al., 2017). Genetic variants in *transmembrane protein 106 B* (*TMEM106B)* are genetic modifiers of FTD with TDP-43 pathology (FTD-TDP), influencing disease penetrance and presentation in *GRN* or *C9ORF72* expression carriers (Gallagher et al., 2014, van Blitterswijk et al., 2014). Specifically, individuals carrying the minor allele of *TREM106B* variants in the context of *C9ORF72*^{RE} mutation were found to be significantly protected from developing FTD symptoms but not ALS (van Blitterswijk et al., 2014, Deming and Cruchaga, 2014). The risk allele of *TREM106B* confers an increased susceptibility of rapid cognitive decline in FTD patients (Tropea et al., 2019), while no such association has been observed in ALS patients with or without the *C9ORF72*^{RE}, highlighting the differential impact of *TREM106B* on these neurodegenerative diseases (van Blitterswijk et al., 2014, Gallagher et al., 2014, Vass et al., 2011).

Hypothesis: Based on the distinct disease mechanisms observed in ALS and FTD, and the specific targeting of MNs by astrocyte toxicity in ALS, I hypothesize that iAstrocytes derived from *C9ORF72*^{RE} FTD patients may not exhibit the same heterogeneous connexin dysfunction observed in *C9ORF72*^{RE} ALS iAstrocytes.

Is astrocyte connexin dysfunction a feature of Alzheimer's disease (AD)? AD, the most common cause of dementia, is characterized by the presence of amyloid-β plaques and astrogliosis, both of which have been linked to astrocytic connexin function (Scheltens et al., 2016). A hallmark feature of reactive gliosis in AD is the increased formation of gap junctions and gap junction hemichannels in astrocytes (Koulakoff et al., 2012). Studies have observed increased astrocytic connexin immunoreactivity at sites of amyloid-β plaques in AD post-

mortem brain samples (Nagy et al., 1996) and AD mouse model (Mei et al., 2010). However, the mechanism regulating Cx43 expression in AD remains unclear. In older APP/PS1 mice, a murine model of familial AD, an increase in Cx43 immunoreactivity was detected in approximately 65% of amyloid-β plaques, while newly formed plaques showed minimal (less than 10%) expression. This suggests that Cx43 expression in AD may be influenced by the age of the plaque and the local inflammatory environment surrounding it (Koulakoff et al., 2012). Blockade of gap junction hemichannels in a double transgenic AD mouse model (expressing human amyloid precursor protein with K595N and M596L mutations and presenilin 1 with A264E mutation) significantly improved memory function without affecting amyloid-β deposition, suggesting a potential therapeutic target beyond plaque clearance (Takeuchi et al., 2011). The pharmaceutical testing of connexin blockers has been tested with potential therapeutics outcomes notably on neuronal degeneration, obtained with a gap junction blocker (INI-0602) or hemichannel blocker in transgenic mice expressing human amyloid-β precursor protein (Yi et al., 2016, Takeuchi et al., 2011). In addition, in APP/PS1 mice (expressing human/mouse amyloid-β precursor protein), a specific deletion of astroglial Cx43 could significantly reduce astrogliosis and increase synapse number, but have no effect on amyloid plaque formation or inflammatory response (Ren et al., 2018).

Hypothesis: I propose that electrophysiological connexin dysfunction in astrocytes is a feature of wider neurodegenerative diseases (AD), in addition to ALS.

When do connexins become dysregulated in ALS? Post-mortem sALS patient material reveals an increase in Cx43 transcript levels in the motor cortex and cervical spinal cord, with a more pronounced effect in rapidly progressing cases (deceased within 2 years after onset) compared to typical ALS disease course (deceased 2-5 years after onset) (Almad et al., 2022). This suggests that Cx43 dysfunction influences temporal course after disease onset. Importantly, reducing Cx43 expression improved disease progression in $SOD1^{G93A}$ and $SOD1^{G37R}$ mouse models (Almad et al., 2022, Takeuchi et al., 2011). It is therefore possible that astrocyte connexin dysfunction is associated with the symptomatic stage of disease.

To address this, I will take advantage of the multidisciplinary approach of using human stem cell technology, which has been reported to be able to recapitulate key clinically-determined disease stages in the form of pathological features (Ghatak et al.,

2019, Ng et al., 2022, Marei et al., 2023) and electrophysiological dysfunction linked to cognitive features of individual donors (Page et al., 2022b). These techniques may help with patient stratification and development of biomarkers and therapeutic targets in these neurodegenerative diseases (Ng et al., 2022). Importantly, directly converted cells (iAstrocytes or neurons), avoiding the iPSC stage, are reported to conserve the age-related epigenetic landscape from the cell of origin (Huh et al., 2016, Mertens et al., 2015, Gatto et al., 2021). Interestingly, Cx43 expression is known to be regulated by epigenetic modifications, such as histone acetylation (Vinken, 2016) and miRNA activity (Anderson et al., 2006). These modifications can act as a molecular switch, turning connexin gene expression on and off (Oyamada et al., 2013). This presents a unique opportunity to study the timing of connexin dysfunction in neurodegenerative diseases.

Hypothesis: Therefore, I hypothesise that examining connexin dysfunction in pre-symptomatic familial *C9ORF72*^{RE} carriers will allow to capture the relevance of connexin-mediated dysfunction as time progresses.

Why does connexin dysfunction occur in ALS? Considering that connexin dysfunction is increasingly recognised as a common feature across neurodegenerative diseases, the mechanism underlying the dysfunction may be liked to genetic and environmental factors. ALS pathogenesis is driven by various genetic and extrinsic risk factors (Grad et al., 2017). As previously demonstrated in Chapter 4, disease-associated protein repeats (DPRs) arising from the *C9ORF72*^{RE} are directly causing connexin dysfunction in *C9ORF72*^{RE} ALS iAstrocytes, establishing a link between ALS genetic mutation and connexin dysfunction. However, here I focus on the possibility that extrinsic factors can also drive connexin dysfunction in astrocytes. For example, connexins are key channels through which K^+ ions are syphoned away from the axon (Giaume et al., 2021) and it is established that elevated levels of neuronal activity and stress cause upregulation of astrocytic connexin function, especially Cx43, potentially as a mechanism to clear excess K^+ ions from the vicinity of the neuron to prevent possible excitotoxicity (Rouach et al., 2000). Further, the alteration of neuronal activity can cause considerable epigenetic changes in astrocytes leading to the dynamic regulation of membrane proteins (Hasel et al., 2017, Sardar et al., 2023). Changes in neuronal excitability in lower MNs parallel the onset of patients developing muscle

weakness, atrophy and fasciculations in ALS (Menon et al., 2015). A change from hyperexcitability leading to progressive loss of function (hypoexcitability) is a feature of lower MN in ALS disease progression (reviewed in (Pasniceanu et al., 2021)). Hyperexcitability in lower motor neurons has been established in several other ALS models and studies have used pharmacological activators of K_V7 potassium ion channels to reduce hyperexcitability in *C9ORF72*^{RE}-derived MNs with the possibility that they protect motor neurons from excitotoxicity. In the state of MN hyperexcitability, it is likely therefore that more K^+ is being released from the axon due to elevated action potential activity and astrocytes are exposed to this. Therefore, I employed an *in vitro* model where an increased extracellular K^+ was used to mirror high neuronal activity.

Hypothesis: I hypothesise that a mechanism of enhanced extracellular K^+ may be abnormally regulated in pre-symptomatic *C9ORF72*^{RE} iAstrocytes, causing a dysregulated upregulation of connexins.

5.2. Methods

The Methods employed in this Chapter are described in the following sections:

5.2.1. Direct conversion of fibroblast to iNPC (As described in Methods Section 2.2.8)

5.2.2. Differentiation of iNPCs to iNPC-astrocytes (iAstrocytes; As described in Methods Section 2.2.9)

5.2.3. ICC – iAstrocyte characterisation (As described in Methods Section 2.3)

5.2.4. Electrophysiology (As described in Methods Section 2.4)

5.3. Results

I wanted to understand if the membrane current alterations observed in *C9ORF72*^{RE} ALS iAstrocyte extend to ALS patients with different genetic back grounds to determine whether this is a convergent feature of ALS. Sporadic ALS (sALS) is the most common form of ALS, accounting for approximately 90% of cases, therefore, I have generated astrocytes from fibroblasts obtained from two sALS patients (sALS-1, 58 years old female; sALS-2, 82 years old female; full patient details available in Table 2-13). iAstrocytes were differentiated for day 7 and 14 using previously described protocol in Chapter 4 (Figure 4-1A). A healthy control iAstrocyte line (Con-2) was used for comparison (same Con-2 line as mentioned in

Chapter 4). sALS patient derived iAstrocytes efficiently differentiated and did not show any differences in cell viability (data generated by the Ferraiuolo/Shaw laboratories).

I first investigated the intrinsic membrane properties of Con-2, sALS-1 and sALS-2 iAstrocytes at day 7 and day 14. WCC measurements reveal an increase in both sALS-1 and sALS-2 compared to Con-2 at day 7 iAstrocytes (Con-2 vs sALS-1, p=0.0185; Con-2 vs sALS-2, p=0.0249; One-way ANOVA; Figure 5-1A), but not at day 14. A reducing trend in R_{in} values was observed from day 7 to day 14 for each line, as expected with maturation. Both sALS iAstrocyte lines exhibited a statistically significant decrease in R_{in} compared to Con-2 (Con-2 vs sALS-1, p=0.0076; Con-2 vs sALS-2, p=0.0304; One-way ANOVA; Figure 5-1B), but not at day 14 iAstrocytes. The RMP of sALS-1 and sALS-2 iAstrocytes appeared to be more hyperpolarized compared to Con-2 at day 7 (Con-2 vs sALS-1, p<0.0001; sALS-1 vs sALS-2, p=0.0001; One-way ANOVA; Figure 5-1C). No significant differences between Con-2 and sALS-2 were observed at day 14, but data for sALS-2 at day 14 was determined from low number of repeats. These findings demonstrate that sALS patient-derived iAstrocytes exhibit altered intrinsic membrane passive properties compared to healthy control iAstrocyte line (Con-2). Similar to *C9ORF72*^{RE} ALS iAstrocytes, sALS iAstrocytes display normal functional membrane integrity whilst presenting altered intrinsic membrane properties changes at day 7 compared to control iAstrocytes.

Next, I employed the same whole-cell voltage-step protocol, as previously described (Figure 4-3A), to characterise potential membrane current dysfunction in sALS iAstrocytes. Representative traces from Con-2, sALS-1 and sALS-2 iAstrocytes were selected to characterize each population at day 7 and day 14. sALS-1 iAstrocytes were only available at day 7. Con-2 iAstrocytes displayed current responses that were comparable at both timepoints (Figure 5-2A-top). sALS-1 and sALS-2 iAstrocytes revealed pronounced membrane currents compared to Con-2 at day 7 and a notable membrane current enhancement was observed for sALS-2 at day 14. To quantify the membrane current dysfunction, I generated mean current density - voltage plots, as previously performed. At day 7, both sALS-1 and sALS-2 iAstrocytes displayed modest increase in current responses compared to Con-2 (Figure 5-2B). However, at day 14, sALS-2 iAstrocyte line showed a clear

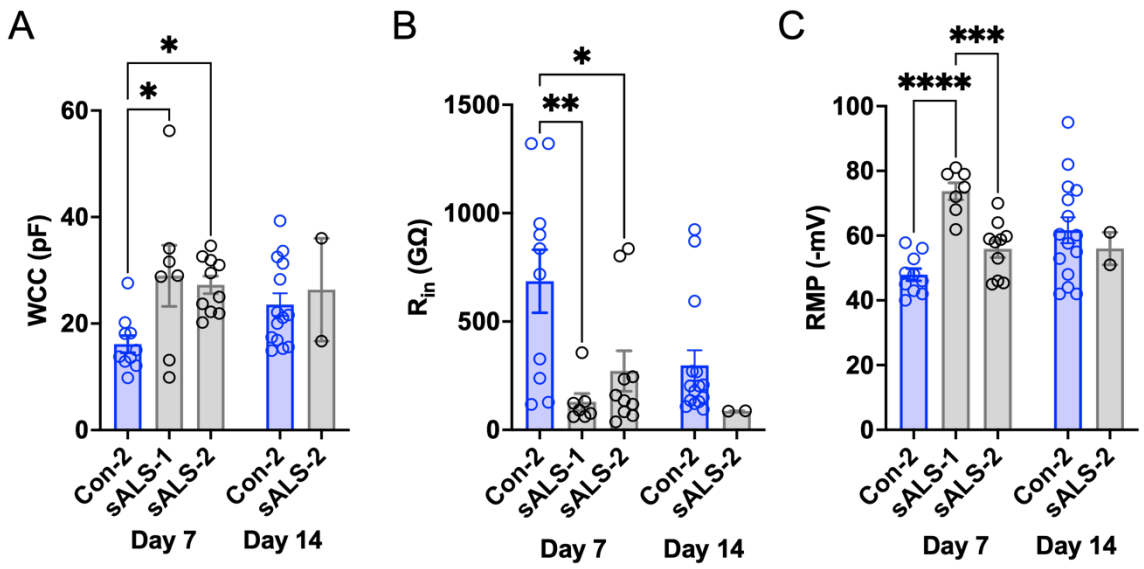

*Figure 5-1.**Passive membrane properties are impacted in sporadic ALS iAstrocytes**. A,B,C, Day 7 and day 14 mean ± SEM data of passive membrane properties, WCC, Rin and RMP, respectively, for Con-2 (day 7, n=10, N=4; day 14, n=15, N=5; Note Con-2 data includes previously presented data in Chapter 4), sALS-1 C9-1 (day 7, n=7, N=2) and sALS-2 (day 7, n=10, N=2; day 14, n=2, N=1). Statistical significance for A,B,C was assessed using One-way ANOVA (*, p<0.05; **, p<0.01; ***; P<0.001; ****, p<0.0001).*

increase in current density compared to Con-2 (Figure 5-2C), which is consistent with previously presented data from *C9ORF72*^{RE} ALS iAstrocytes. These data suggested that the membrane current dysfunction is a common feature across sALS and is not limited to *C9ORF72*^{RE} ALS iAstrocytes.

FTD clinically, pathologically and genetically overlaps with ALS (Burrell et al., 2016). I aimed to determine if the observe alterations in membrane currents of *C9ORF72*^{RE} ALS iAstrocytes extend to *C9ORF72*^{RE} FTD. Here, I generated iAstrocytes derived from fibroblasts obtained from clinically defined patients presenting FTD, but no ALS and harbouring the C9ORF72 mutation (FTD-1, 64 years old female; FTD-2, 60 years old female; FTD-3, ~72 year old male) and one healthy control (Con-2). Full patient details can be found in Table 2-13 of the Methods. Whole-cell patch-clamp recordings were performed on FTD iAstrocytes at day 14. FTD iAstrocytes displayed altered intrinsic membrane properties compared to Con-2. The WCC measurement comparison between Con-2 and all three FTD iAstrocyte lines (FTD-1, FTD-2, FTD-3) revealed 2 significant differences (Con-2 vs FTD-2, p=0.0180; Con-2 vs FTD-3,

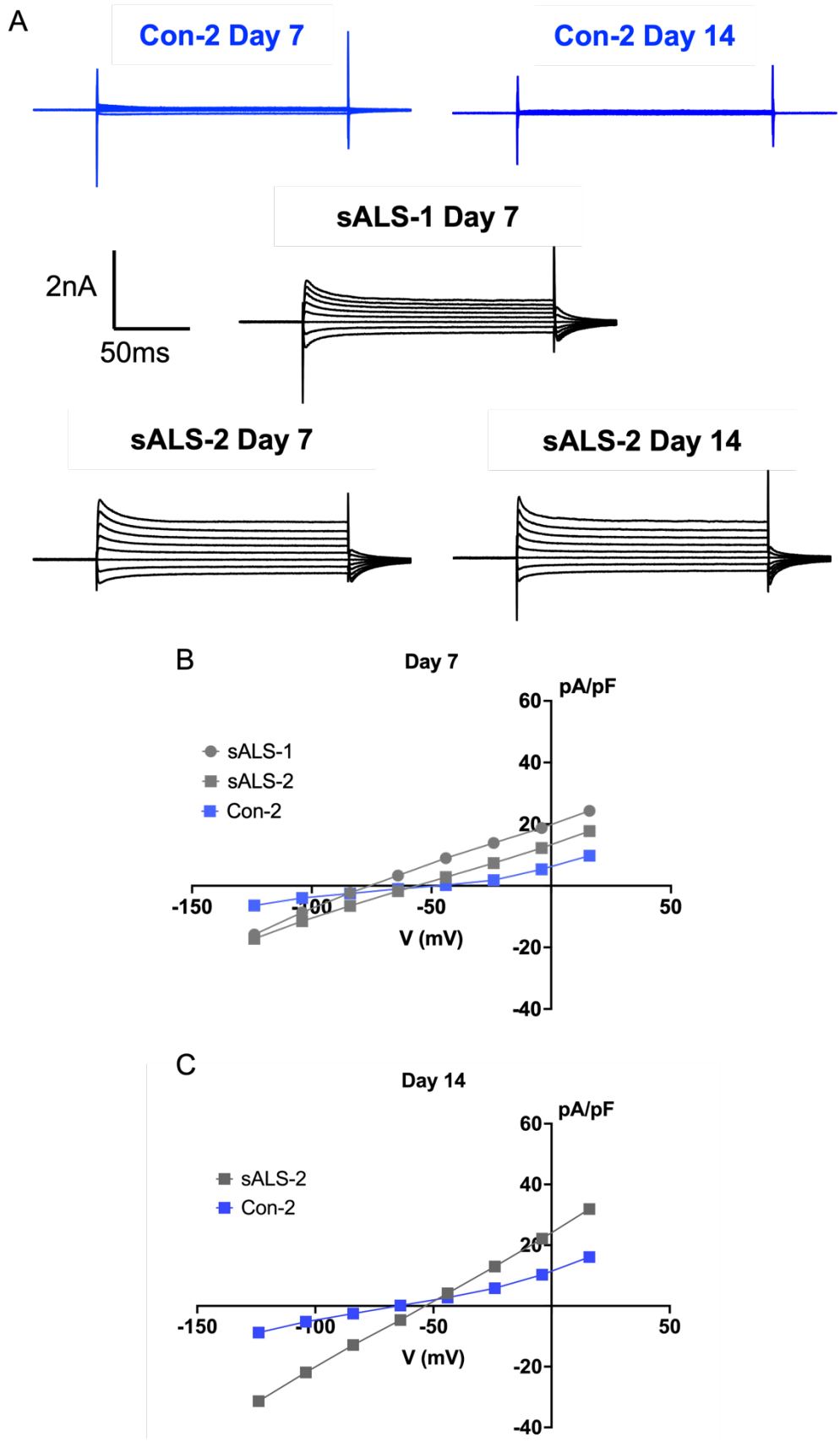

Figure 5-2. ***Membrane currents in sporadic ALS iAstrocytes are abnormally enlarged.*** *Caption on the next page.*

Figure 5-2. ***Membrane currents in sporadic ALS iAstrocytes are abnormally enlarged****. A.The panels show representative voltage-step evoked current traces from individual day 7 Con-1, sALS-1 and sALS-2 and day 14 Con-2 and sALS-2 iAstrocytes. Note the enhanced current response in the sALS iAstrocytes. B. Mean ± SEM current density (pA.pF) versus voltage (V) plot of day 7 iAstrocytes derived from Con-2 (n=10, N=4), sALS-1 (n=7, N=2) and sALS-2 (n=10, N=2). C, As in B, but for day 14. Con-2 (n=15, N=5), sALS-2 (n=2, N=1).*

p=0.0094; One-way ANOVA; Figure 5-3A) with an overall trend of higher WCC in the FTD lines compared to Con-2. A clear and highly significant reduction in R_{in} was observed in all three FTD iAstrocyte lines (FTD-1, FTD-2, FTD-3) compared to Con-2 (Con-2 vs FTD-1, p<0.0001; Con-2 vs FTD-2, p<0.0001; Con-2 vs FTD-3, p<0.0001; One-way ANOVA; Figure 5-3B). In terms of RMP, no significant changes were observed between control and FTD iAstrocyte lines (Figure 5-3C), suggesting largely unchanged RMP values. The intrinsic membrane properties of *C9ORF72*^{RE} FTD iAstrocytes are very similar to that of *C9ORF72*^{RE} ALS iAstrocytes.

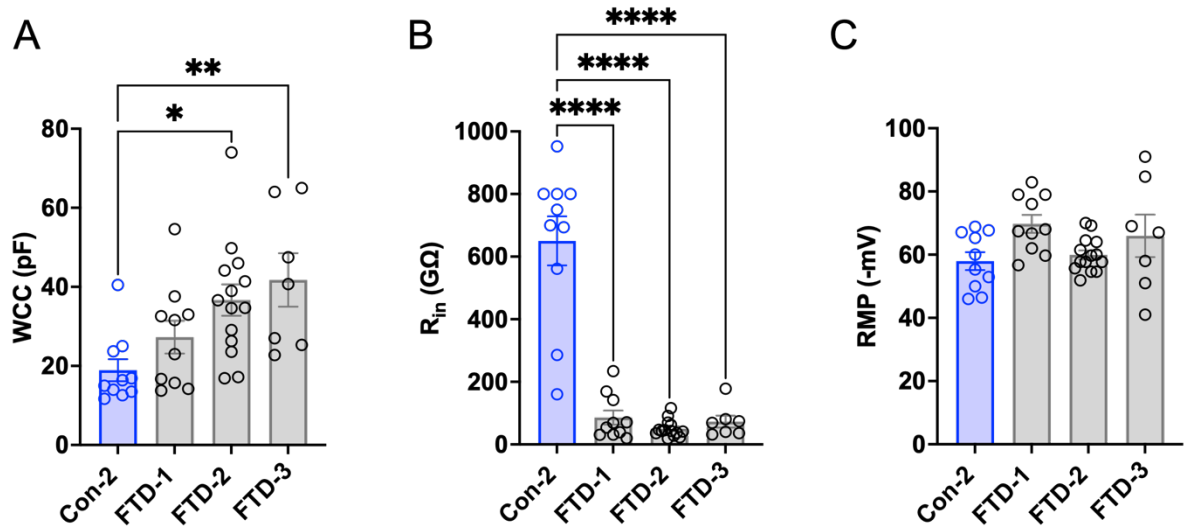

Figure 5-3. ***Passive membrane properties are impacted in C9ORF72^{RE} FTD iAstrocytes****. A,B,C. Day 14 mean ± SEM data of passive membrane properties, WCC, Rin and RMP, respectively, for Con-2 (n=10, N=2), FTD-1 (n=13, N=3), FTD-2 (n=14, N=3) and FTD-3 (n=14, N=3). Statistical significance for A,B,C was assessed using One-way ANOVA (*, p<0.05; **, p<0.01; ***; ****, p<0.0001).*

Next, I investigated the membrane currents, as previously performed (Figure 5-4). Representative traces were selected to highlight the current response to the voltage protocol across the examined conditions. At day 14, FTD-1, FTD-2, FTD-3 iAstrocytes all revealed increased membrane current response compared to Con-2 (Figure 5-4A). To normalize for the cell differences observed in the WCC data, the mean current density against potential was generated. FTD iAstrocytes demonstrate an increase in current density that correlates with a higher membrane current passivity compared to Con-2 (Figure 5-4B), thus, mirroring the abnormal membrane current properties demonstrated in *C9ORF72*^{RE} ALS and sALS iAstrocyte lines. These experiments reveal a shared mechanism across the ALS/FTD spectrum.

I determined whether astrocyte membrane current dysfunction is a wider feature of other neurodegenerative diseases. To identify if connexin-mediated current dysfunction was a characteristic feature in Alzheimer's disease, I examined membrane currents from iAstrocytes derived from Alzheimer's disease (AD) patient fibroblasts (AD, 63 years old female) and iAstrocytes derived from fibroblasts obtained from healthy individual (100 years old male patient, Con; same donor fibroblasts published in (Bell et al., 2020)).

This study generates novel insight into the electrophysiological characterisation of astrocytes from human AD patients *in vitro*. First, the intrinsic membrane properties were characterised at day 14. The WCC comparison revealed a significant increase in the AD iAstrocytes compared to Con ($p=0.0138$; Student's t-test; Figure 5-5A). The R_{in} was significantly reduced in the AD iAstrocytes compared to control ($p=0.0020$; Student's t-test; Figure 5-5B) and the RMP was more hyperpolarized in AD iAstrocytes compared to the control (Con) iAstrocytes ($p=0.0014$, Student's t-test; Figure 5-5C). These data appear to be broadly consistent with properties observed in sALS, *C9ORF72*^{RE} ALS and *C9ORF72*^{RE} FTD iAstrocytes, suggesting a common membrane dysfunction.

I looked at the current response using the voltage-clamp protocol for both Con and AD iAstrocytes. The current response in AD line is abnormally enhanced compared to Con (Figure 5-6). These finding suggest that current enhancement is also present in AD iAstrocytes. The same protocol was then repeated, for the same iAstrocyte, in the presence of CBX (10 μM) for 2 minutes (Figure 5-6B) leading to the elimination of the current

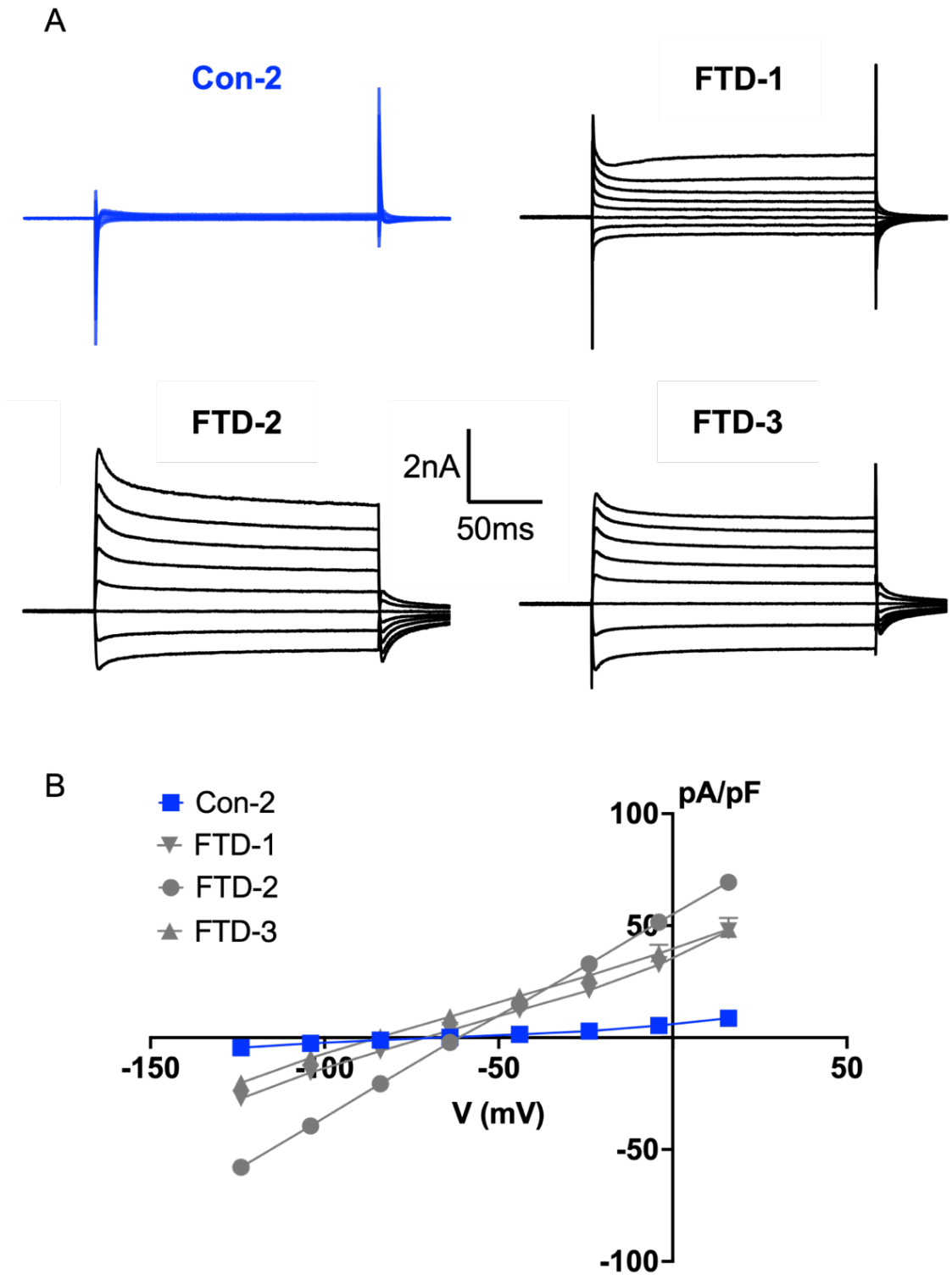

Figure 5-4. ***Membrane currents in C9ORF72^{RE} FTD iAstrocytes are abnormally enlarged****. A. The panels show representative voltage-step evoked current traces from individual day 14 Con-2, FTD-1, FTD-2 and FTD-3 iAstrocytes. Note the enhanced current response in the C9ORF72^{RE} FTD iAstrocytes. B. Mean ± SEM current density (pA.pF) versus voltage (V) plot of day 14 iAstrocytes derived from Con-2 (n=10, N=2), FTD-1 (n=13, N=3), FTD-2 (n=14, N=3) and FTD-3 (n=14, N=3).*

enhancement observed in AD iAstrocytes. The current density was measured and plotted against the voltage (Figure 5-6C), which confirms the considerable connexin-mediated membrane current dysfunction is presented and extends to AD iAstrocytes.

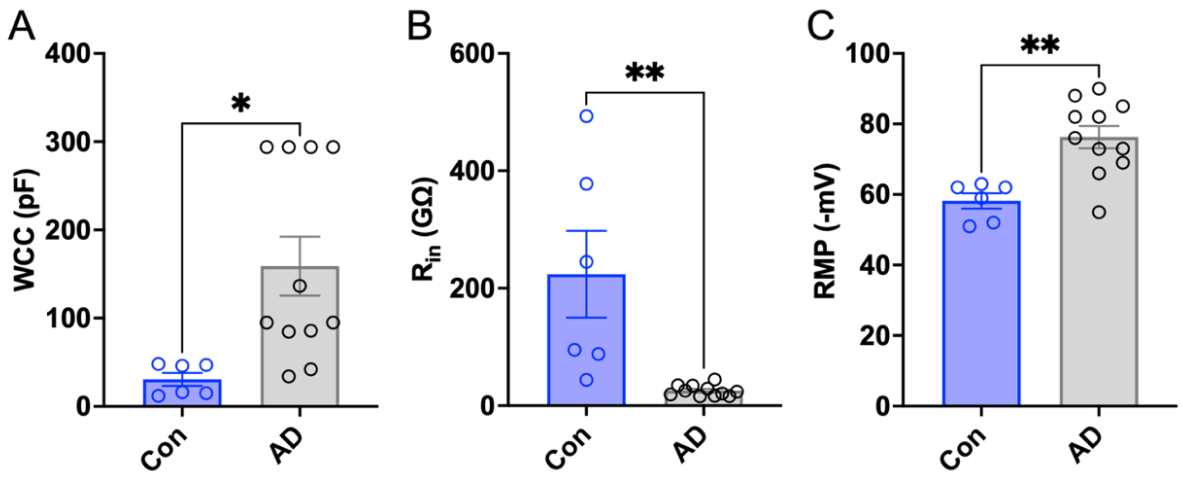

Figure 5-5. ***Passive membrane properties are impacted in Alzheimer's Disease iAstrocytes****. A,B,C. Day 14 mean ± SEM data of passive membrane properties, WCC, Rin and RMP, respectively, for Con (n=6, N=2), Alzheimer's disease (n=11, N=3). Statistical significance for A,B,C was assessed using Students' t-test (*, p<0.05; **, p<0.01).*

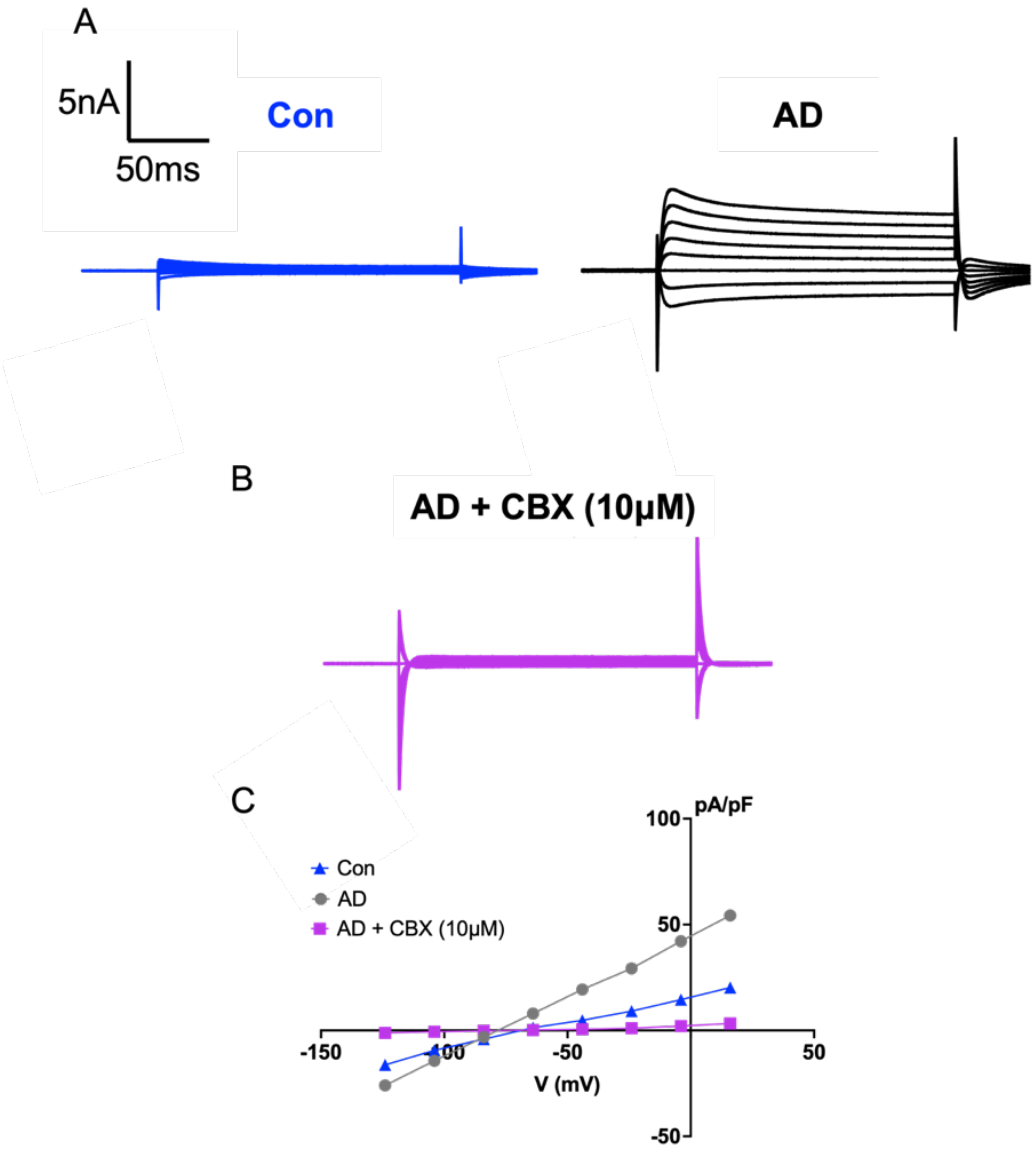

Figure 5-6. ***Membrane currents in Alzheimer's Disease iAstrocytes are abnormally enlarged.*** *A. The panels show representative voltage-step evoked current traces from individual day 14 Con and Alzheimer's disease iAstrocytes. Note the enhanced current response in the AD iAstrocytes. B,C. Representative current trace in the same Alzheimer's disease iAstrocyte in A in the presence of CBX. C. Mean ± SEM current density (pA.pF) versus voltage (V) plot of day 14 iAstrocytes derived from Con (n=6, N=2), AD (n=11, N=3) and Alzheimer's disease in the presence of CBX (n=5, N=2).*

I next wanted to investigate the properties of iAstrocytes that have been derived from pre- and post-symptomatic individuals. Patient-derived iAstrocytes offer a powerful tool for studying disease progression due to their unique advantages. Stem cell technology allows the generation of patient-derived material, which retain the individual's genetic background, which can influence disease susceptibility and progression (Ghatak et al., 2019, Ng et al., 2022, Marei et al., 2023). Also, by utilizing iAstrocytes from pre- and post-

symptomatic individuals, different stages of the disease can be assessed, which facilitates identification of early cellular and molecular changes associated with disease onset.

Importantly, iAstrocytes retain the epigenetic landscape of the original cell source (Gatto et al., 2021). Epigenetic changes can influence gene expression and potential contribute to disease development. In this regard, I investigated the electrophysiological properties of iAstrocytes derived from a family harbouring *C9ORF72*^{RE} mutations. Fibroblasts were obtained from three family members with C9ORF72 mutations: a father unaffected by ALS (Father, 69 years old male) and two genetically identical, monozygotic twins: an unaffected twin (Unaffected Twin, 37 years old male) and a symptomatic twin with *C9ORF72*^{RE} ALS. For the symptomatic twin, fibroblasts were taken at two sample points; early, 37 years old at symptom onset; and another 'late' biopsy 2 years and 4 months after symptom onset. The father has a much smaller pathogenic C9ORF72^{RE} (<100 repeats) than the twins who have similar-sized large expansions (around 800 repeats). Full patient details are available in Table 2-14 of the Methods. iAstrocytes were cultured at day 14, as previously described. iAstrocytes derived from *C9ORF72*^{RE} ALS family express specific astrocytic markers, such as CD44 and Vimentin, indicating efficient differentiation (Figure 5-7).

The intrinsic membrane properties of father, unaffected twin and the two biopsies for the affected twin iAstrocytes were recorded using whole-cell patch-clamp at day 14. No statistically significant differences in WCC values were observed between any of the iAstrocytes derived from *C9ORF72*^{RE} ALS family (Figure 5-8A). A decreased R_{in} was evident in the affected twin line at both biopsy collection timepoints compared to the unaffected father (Father vs Affected Twin Early, p=0.0323; Father vs Affected Twin Late, p=0.0048; One-way ANOVA; Figure 5-8B). The unaffected twin revealed overall lower R_{in} values compared to the father iAstrocyte line, but it did not reach statistical significance. The unaffected iAstrocytes from the Father and Unaffected Twin exhibited more depolarized RMPs compared to the Twin Affected Late iAstrocyte line (Father vs Affected Twin Late, p=0.0328; Unaffected Twin vs Affected Twin Late, p= 0.0008; One-way ANOVA; Figure 5-8C). The intrinsic membrane properties reveal that the Affected Twin iAstrocytes retain their functional membrane integrity whilst displaying significant differences in R_{in} and RMP compared to the unaffected father and Twin iAstrocytes.

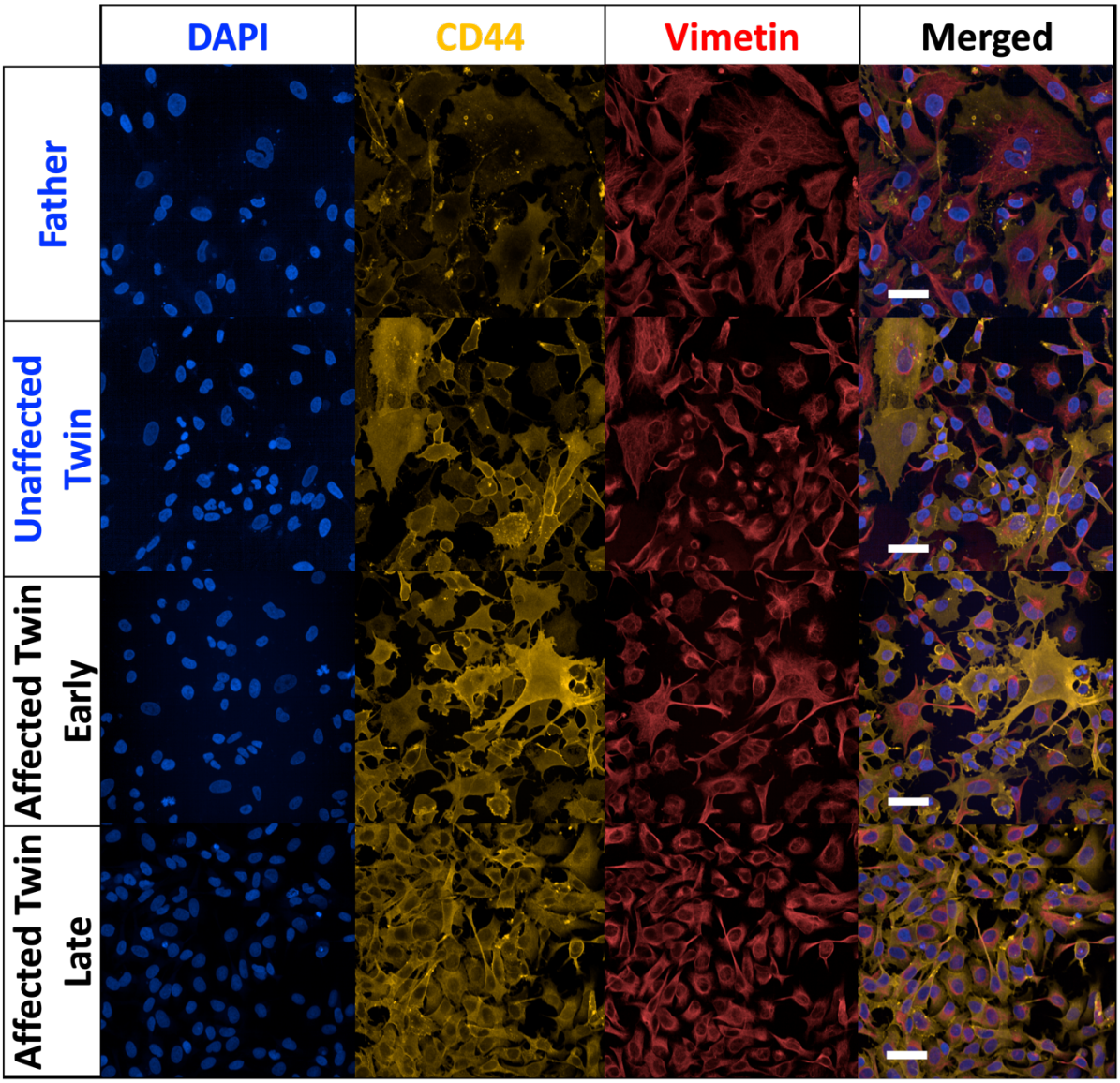

Figure 5-7. ***C9ORF72^{RE} family iAstrocytes express specific astrocytic markers at day 7****. Figure depicts iAstrocytes at day 7 in culture from a family harbouring C9ORF72^{RE} mutation. ICC staining demonstrates cultures derived from the unaffected father and twin, and the affected twin at two samples points (early and late) are highly enriched for cells harbouring key astrocyte markers CD44 (yellow) and Vimentin (red). DAPI stain is presented in blue. Scale bar set to 50μm. Stainings and images were performed/obtained by members of the Ferraiuolo/Shaw laboratories and presented with permission.*

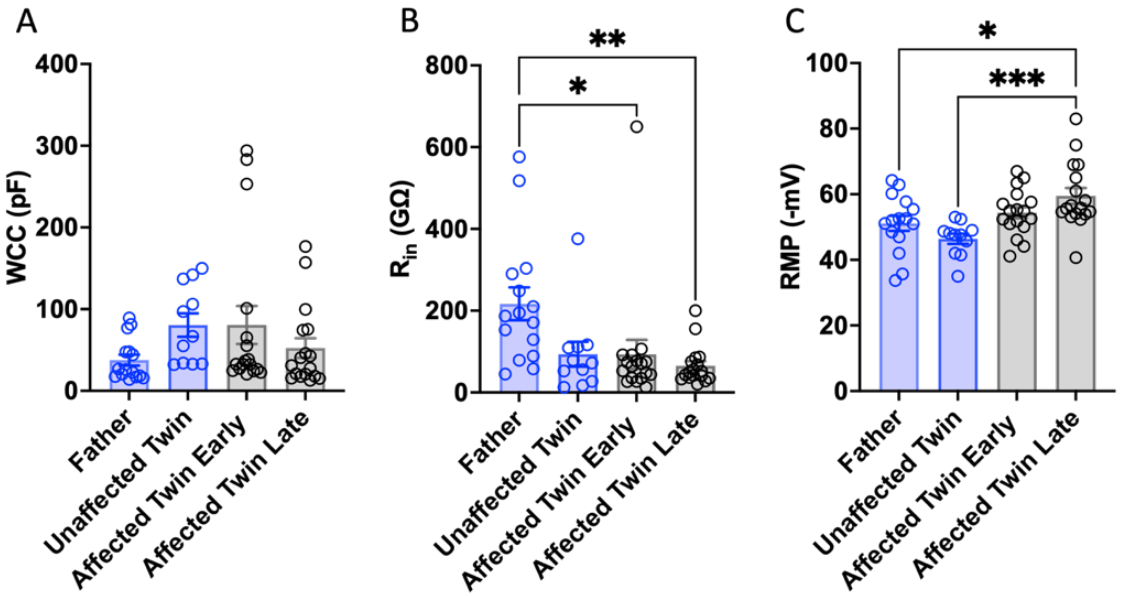

Figure 5-8. ***Passive membrane properties are impacted in C9ORF72^{RE} family iAstrocytes****. A,B,C. Day 14 mean ± SEM data of passive membrane properties, WCC, Rin and RMP, respectively, for unaffected father (n=15, N=5), unaffected twin (n=11, N=5), affected twin (early sample; n=17, N=5) and affected twin (late sample; n=17, N=5). Statistical significance for A,B,C was assessed using One-way ANOVA (*, p<0.05; **, p<0.01; ***, p<0.001).*

Membrane currents of iAstrocytes were then investigated using the voltage-clamp protocol, as previously described. Representative current traces were selected to characterize all three family members-derived iAstrocytes. The father and unaffected twin displayed comparable current responses showing small current responses, similar to healthy controls (Con-1, Con-2) iAstrocytes (Figure 5-9A, top), while the affected twin revealed distinctively larger current amplitudes which appeared to increase according to the sample point of the biopsy (Figure 5-9A, bottom). To quantify the membrane current enhancement, I constructed mean current density – voltage plots. Strikingly, unaffected lines (Father and Unaffected Twin) revealed low current density amplitudes, similar to those previously obtained for Con-1 and Con-2 iAstrocytes, while the affected twin iAstrocyte lines showed increasing current responses that are strikingly similar to those previously reported for (symptomatic) *C9ORF72*^{RE} ALS iAstrocytes (Figure 5-9B).

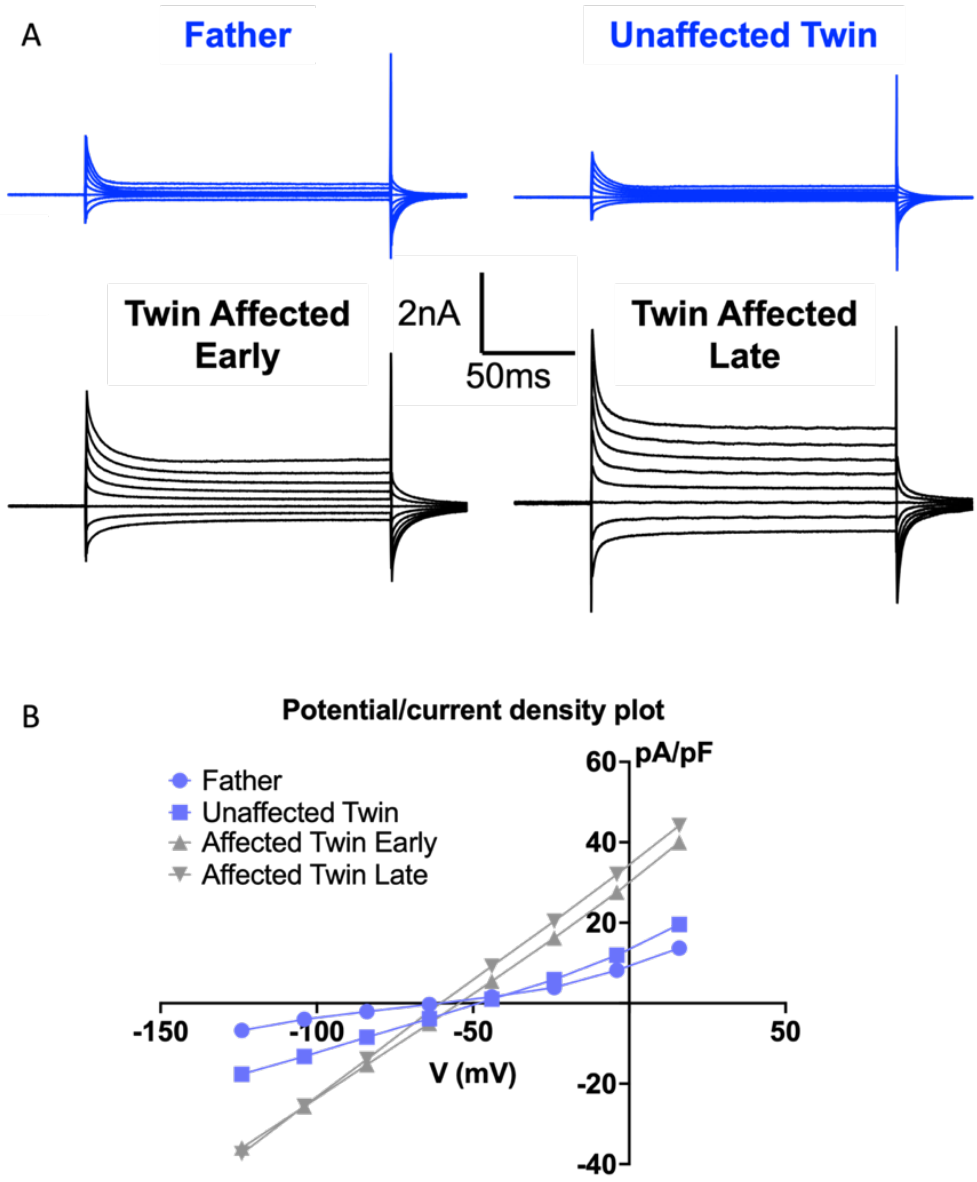

Figure 5-9. ***Membrane currents in C9ORF72^{RE} family iAstrocytes are abnormally enlarged in symptomatic patients.*** *A. The panels show representative voltage-step evoked current traces from individual day 14 unaffected father, unaffected twin, symptomatic twin (early sample) and symptomatic twin (late sample) iAstrocytes. Note the enhanced current response in the symptomatic C9ORF72^{RE} ALS iAstrocytes. B. Mean ± SEM current density (pA.pF) versus voltage (V) plot of day 14 iAstrocytes derived from the unaffected father unaffected father (n=15, N=5), unaffected twin (n=11, N=5), affected twin (early sample; n=17, N=5) and affected twin (late sample; n=17, N=5).*

To confirm that the source of increased current response in the affected twin iAstrocytes was due to connexin-mediated dysfunction, I assessed the sensitivity of currents to CBX (10 μM), as previously performed. Complete elimination of current enhancement was observed in the Affected Twin Early iAstrocytes in the presence of CBX

(Figure 5-10A,B) and was confirmed in the current density – voltage plot (Figure 5-10D), which highlighted that CBX restores the phenotype to a control-like level.

These findings suggest that Cx43-mediated current dysfunction is linked to disease progression, and the C9ORF72^{RE} alone is not sufficient for its upregulation. This is supported by evidence from monozygotic twins with *C9ORF72^{RE}*, indicating involvement of additional factors.

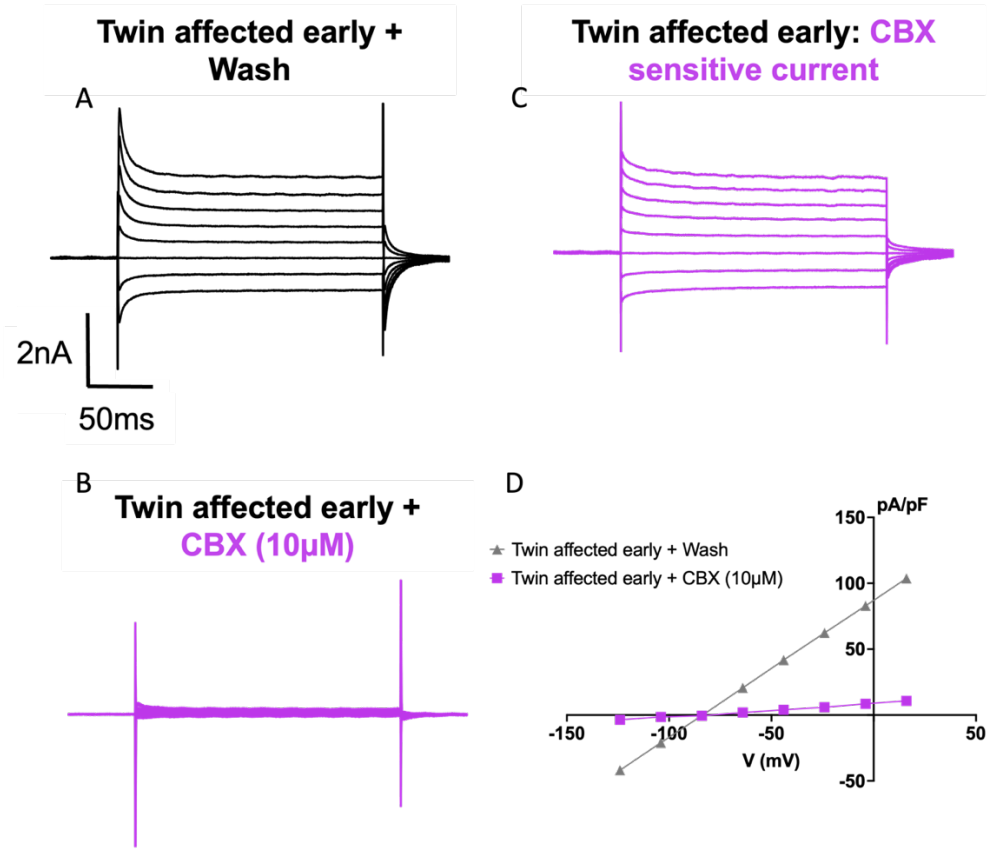

Figure 5-10. ***Membrane currents in the symptomatic C9ORF72^{RE} twin iAstrocytes are sensitive to CBX****. A. The panel shows representative voltage-step evoked current traces from individual day 14 symptomatic (late sample) C9ORF72^{RE} twin iAstrocytes. B. The same iAstrocyte in A in the presence of CBX. C. The CBX-sensitive current for the iAstrocyte presented in A. D. Mean ± SEM current density (pA.pF) versus voltage (V) plot of day 14 iAstrocytes derived from the symptomatic C9ORF72^{RE} twin in the presence and absence of CBX (n=4, N=1).*

To explore the potential that pre-symptomatic ALS iAstrocytes did not show or showed reduced connexin-mediated membrane dysfunction, I assessed the presence of connexin-mediated current enhancement in iAstrocytes derived from three pre-symptomatic *C9ORF72*^{RE} iAstrocyte patients (PreSx-1, 50 years old female; PreSx-2, 36 years old female; Prex-3, 31 years old male). The intrinsic membrane properties for pre-symptomatic were measured at day 14. PreSx-1 iAstrocyte line shown statistically higher WCC compared to Con-2 line and PreSx-2 (Con-2 vs PreSx-1, p=0.0050; PreSx-2 vs PreSx-1, p=0.0267; One-way ANOVA; Figure 5-11A), but no other differences were observed. The R_{in} was statistically decreased in all pre-symptomatic *C9ORF72*^{RE} iAstrocyte lines compared to control iAstrocyte (Con-2 vs PreSx-1, p=0.0267; Con-2 vs PreSx-2, p=0.0082; Con-2 vs PreSx-3, p=0.0372; One-way ANOVA; Figure 5-11B). For RMP, no significant differences were noticed between Con-2 and all three pre-symptomatic *C9ORF72*^{RE} iAstrocytes. Interestingly, the intrinsic membrane properties reveal a trend similar to that of (symptomatic) *C9ORF72*^{RE} ALS iAstrocytes.

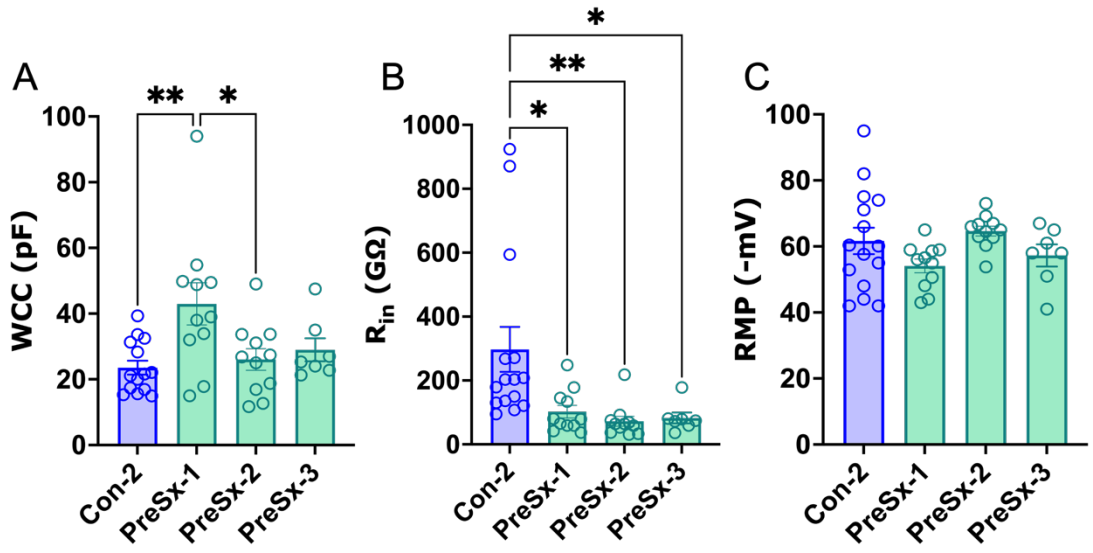

Figure 5-11. ***Passive membrane properties are impacted in pre-symptomatic C9ORF72^{RE} iAstrocytes.*** *A,B,C. Day 14 mean ± SEM data of passive membrane properties, WCC, Rin and RMP, respectively, for Con-2 (n=15, N=5; Note Con-2 as previously presented data in Chapter 4), pre-symptomatic PreSx-1 (n=11, N=3), PreSx-2 (n=11, N=3) and PreSx-3 (n=7, N=2). Statistical significance for A,B,C was assessed using One-way ANOVA (*, p<0.05; **, p<0.01).*

I then investigated membrane current dysfunction and found that the voltage-step protocol revealed variable current responses between the pre-symptomatic *C9ORF72*^{RE} iAstrocytes (Figure 5-12). The Con-2 line maintained its low current responses, PreSx-1 iAstrocytes showed only a modest increase in their current response, whilst PreSx-2 and PreSx-3 2 iAstrocyte lines revealed increasingly higher current responses (Figure 5-12A). The same trend was observed in the current density – voltage plot, where Con-2 and PreSx-1 revealed relatively low values and PreS-3 and PreSx-1 become to show more pronounced current density responses (Figure 5-12B).

Neuronal activity leads to extrusion of K^+ ions from the axon through voltage-gated K^+ channels. A fundamental homeostatic function of astrocytes is to rapidly remove the K^+ from the axon to prevent its accumulation, which can cause axonal depolarisation and pathogenic hyperexcitability (Walz, 2000). Connexins are key channels through which K^+ ions are syphoned away from the axon (Giaume et al., 2021). Increased neuronal activity has been implicated in the upregulation of astrocytic connexins, including Cx43 , as a potential homeostatic mechanism to clear elevated K^+ (Rouach et al., 2000). Increasing extracellular K^+, mirroring high neuronal activity, I hypothesise that this mechanism may be abnormally regulated in PreSx-3 *C9ORF72*^{RE} iAstrocytes, causing a dysregulated upregulation of connexins.

To address this, I incubated healthy and PreSx-3 *C9ORF72*^{RE} iAstrocytes with KCl (30 mM; and osmotic control NaCl, 30 mM) for 72 hours before examining the electrophysiological phenotype at day 14. As expected, KCl induced a modest increase in CBX-sensitive current in healthy iAstrocytes, but the CBX-sensitive current was strikingly elevated in PreSx-3 *C9ORF72*^{RE} iAstrocytes (Figure 5-13F). NaCl did not cause any upregulation in either healthy or PreSx-3 *C9ORF72*^{RE} iAstrocytes (Figure 5-13I). Interestingly, these findings demonstrate that prolonged exposure to elevated extracellular K^+ levels, as might be expected to occur during ALS disease progression (hyperexcitability), can enhance connexin-membrane dysfunction in ALS astrocytes.

The results need to be interpreted with careful consideration as limited number of samples and cell lines were used in some of the experiments presented above.

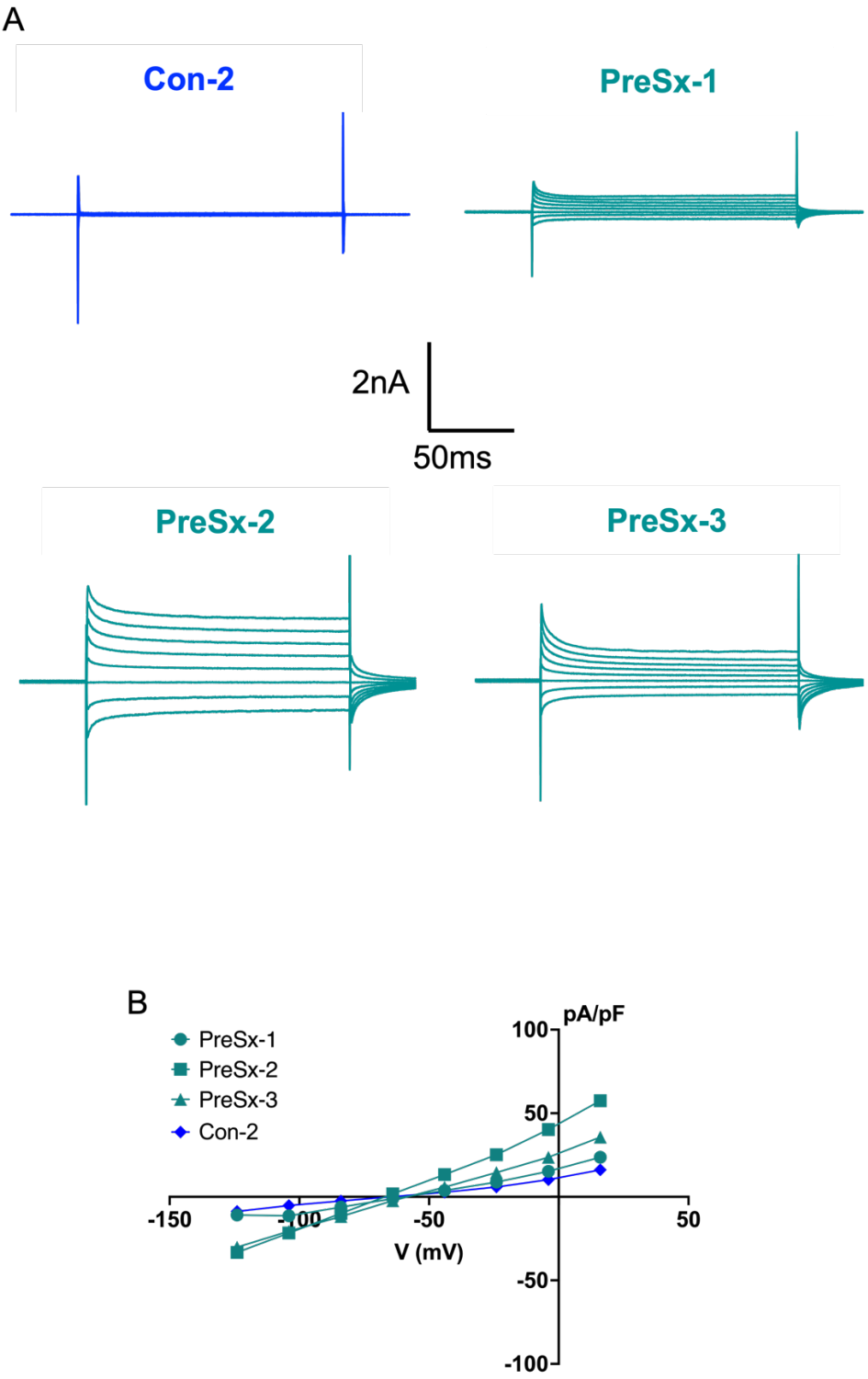

Figure 5-12. ***Membrane currents in C9ORF72^{RE} pre-symptomatic iAstrocytes are variably impacted.*** *A. The panels show representative voltage-step evoked current traces from individual day 14 Con-2, PreSx-1, PreSx-2 and PreSx-3 iAstrocytes. Note the variable current response in the pre-symptomatic C9 ALS iAstrocytes. B. Mean ± SEM current density (pA.pF) versus voltage (V) plot of day 14 iAstrocytes derived from the unaffected Con-2 (n=15, N=5; Note Con-2 data as previously presented data in Chapter 4), pre-symptomatic PreSx-1 (n=11, N=3), PreSx-2 (n=11, N=3) and PreSx-3 (n=7, N=2).*

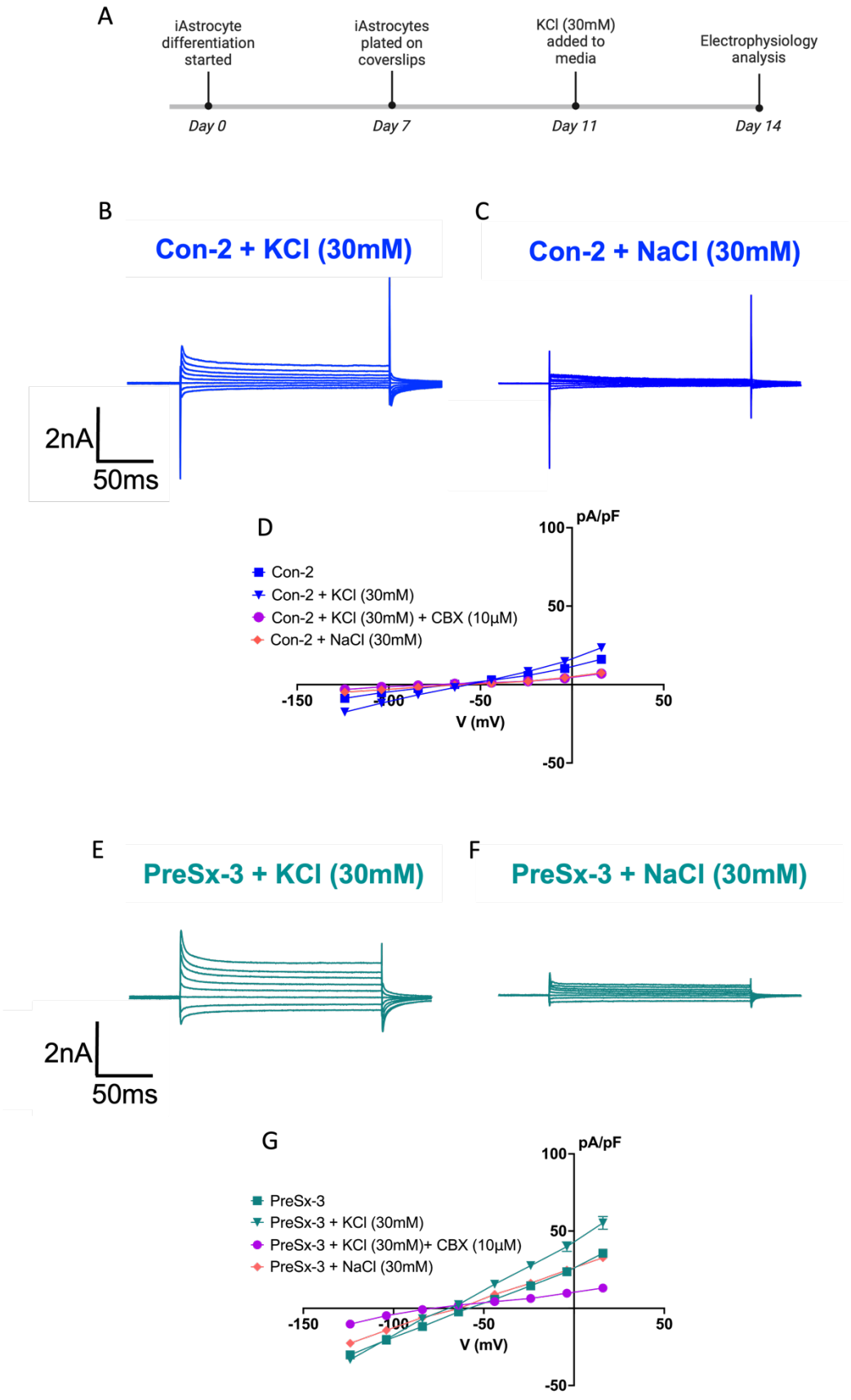

Figure 5-13. ***KCl-mediated induction of connexin dysfunction in pre-symptomatic iAstrocytes****. Caption on the next page.*

Figure 5-13. ***KCl-mediated induction of connexin dysfunction in pre-symptomatic iAstrocytes****. A. Timeline of KCl application. iAstrocytes were replated at day 7 onto coverslips and NaCl/KCl (30 mM) was added to the media at day 11 for 72 hours. Electrophysiological recordings were performed at day 14. B. The panels show representative current traces from individual Con-2 iAstrocytes preincubated with KCl. C. The panel shows representative current trace for individual Con-2 iAstrocyte in the presence of NaCl. D. Mean ± SEM current density (pA.pF) versus voltage (V) plot of day 14 Con-2 iAstrocytes pre-incubated with KCl in the absence (n=8, N=3) and presence of CBX (n=2, N=1). Con-2 in the absence of any treatment was added for reference. The incubation with NaCl did not yield any shift in the current density relationship to Con-2 (n= 6, N=3). E,F. Same as B,C for pre-symptomatic PreSx-3 iAstrocytes. G. Mean ± SEM current density (pA.pF) versus voltage (V) plot of day 14 PreSx-3 iAstrocytes pre-incubated with KCl in the absence (n=10, N=3) and presence of CBX (n=3, N=1). Note current density enhancement in PreSx-3 in the presence of KCl which is then attenuated by application of CBX. PreSx-3 data (n=7, N=2) in the absence of any treatment was displayed as reference. NaCl data (n=5, N=2) did not deviate notably from PreSx-3 alone.*

5.4. Discussion

By leveraging whole-cell patch-clamp electrophysiology, selective pharmacology, stem cell technology and cell biology techniques, I characterised novel membrane physiology defects in iAstrocytes derived from various disease backgrounds. Sporadic ALS iAstrocyte lines exhibit progressive current enhancement upon voltage stimulation. This observation indicates that the abnormal membrane current response extends to a broader spectrum of the disease. This implies that a pathway leading to connexin-mediated dysfunction is present in cells independent of the *C9ORF72*^{RE} mutation and DPR pathology.

C9ORF72^{RE} FTD iAstrocytes also displayed an increase in current density that correlates with higher membrane passivity, aligning with observations in *C9ORF72*^{RE} ALS and sALS iAstrocytes. While FTD primarily affects the pre-frontal cortex and temporal lobes, the observed membrane current enhancement reflects a broader feature of neurodegenerative diseases. Although astrocytes are toxic specifically to MNs (Di Giorgio et al., 2008, Haidet-Phillips et al., 2011, Nagai et al., 2007, Re et al., 2014), FTD pathology is known to involve astrogliosis that occurs at an early stage of disease progression and precedes neuronal loss (Su et al., 2000, Kersaitis et al., 2004). Apoptotic astrocytes in FTD have been correlated with the degree of atrophy in the frontotemporal region and significant astrogliosis has been observed to overlap with areas showing disturbed cerebral perfusion (Broe et al., 2004). Astrocytes derived from FTD patients carrying *GRN* mutation

and mice with a homozygous deletion in *GRN* display upregulation of Cx43 protein in the thalamus and frontal cortex, together with downregulation of glutamate transporter SLC1A2 that promoted profound synaptic degeneration in these areas (Marsan et al., 2023). Co-culture systems with cortical neurons and *GRN* deficient astrocytes promote synaptic and dendritic degeneration in neurons. These astrocytes fail to simulate synaptic growth and promote TDP-43 protein aggregation in cortical organoids. Immunostaining also highlighted increased expression of Cx43 in almost all FTD-GRN astrocytes compared to controls (Marsan et al., 2023). It is important to note that FTD-GRN patients have haploinsufficiency of the secreted protein prostaglandin, a mechanism that leads to neurodegeneration and the characteristic TDP-43 protein aggregation (Baker et al., 2006, Cruts et al., 2006), a common feature of ALS and ALS/FTD patients (Mackenzie and Rademakers, 2008). Therefore, the connexin phenotype in astrocytes plays a role in FTD and the increase Cx43 reported in literature in FTD models is likely to be a common feature of these neurodegenerative diseases.

Building upon the findings of abnormal membrane current response in ALS and FTD iAstrocytes, I electrophysiologically characterised iAstrocytes derived from an AD patient. The enhanced current response upon voltage injection was maintained in the AD iAstrocytes, indicating a continuation of this astrocytic membrane impairment across neurodegenerative diseases caused by connexins. These observations align with the well-established characteristic of astrocytic connexins in AD. Previous studies indicate that blocking connexin-associated channel communication can prevent memory function in AD models (Quesseveur et al., 2015, Giaume et al., 2021, Sharma et al., 2019). In AD, it is believed that pathological stimuli including β-amyloid increase expression of connexins in astrocytes which may be associated with increase activation of astrocytes in the form of astrocytosis. Studies show that overexpression of Cx43 interacts with purinergic receptors, particularly, P2Y1 receptors in transgenic model of AD and blockage of P2Y1 receptor and connexin channel inhibitor, CBX improved cognition function in APP/PS1 mice (Delekate et al., 2014). This might be due to the increase in ATP release through connexins that leads to activation of P2Y1 receptors that has a detrimental effect on neuronal viability and/or function (Kang et al., 2008, Orellana et al., 2011). The increase in glutamate release has been characterised to induce neurodegeneration and cognitive impairments in AD patients

(Hynd et al., 2004). Astrocyte connexin channels control the release of glutamate into the extracellular space (Xing et al., 2019) and the release of glutamate via Cx43 hemichannels was shown to mediate neuronal death (Orellana et al., 2011) possibly contributing to induce neurodegeneration and cognitive decline in AD patients. The data in my study extends the concept of connexin dysfunction in astrocytes to AD. The data in my study extends the concept of connexin dysfunction in astrocytes in AD. It is possible that the dysregulation of connexins mediates similar pathogenic mechanisms in ALS, FTD and AD. these diseases manifest differently. ALS primarily affects motor neurons, leading to muscle weakness and atrophy. In contrast, AD is characterised by cognitive decline, memory loss, and behavioural changes. FTD presents with progressive impairment of language, behaviour and executive function. Despite these differences, they shared underlying astrocytic dysfunction suggests a commonality in their pathophysiology. It is possible that the dysregulation of connexins mediate similar pathogenic mechanisms in ALS, FTD and AD.

To investigate if connexin upregulation was associated with symptomatic disease, I examined the electrophysiological properties of iAstrocytes derived from a family carrying *C9ORF72*^{RE} mutations with variable penetrance; a pre-symptomatic father, and two offspring who are monozygotic twins, where one is pre-symptomatic and, the other, symptomatic from which samples were taken at diagnosis and at a later disease stage. Remarkably, our data reveal that the electrophysiological phenotype is not prominent in pre-symptomatic iAstrocytes derived from the father and unaffected twin. However, for the symptomatic *C9ORF72*^{RE} iAstrocytes derived from the affected twin, the connexin phenotype is prominent and crucially, increases with disease progression. A parallel programme of work in the Shaw lab is characterising the lines and indicates both twins carry a *C9ORF72* mutation that is up to 500 repeats, as well as an identical genome, suggesting that the differences are not due to a *C9ORF72*^{RE} length effect. These data further suggest that additional factors contribute to the phenotype. Moreover, investigating pre-symptomatic iAstrocytes revealed highly variable membrane current dysfunction compared to controls. Collectively, these data suggest that connexin dysfunction in astrocytes is overall less evident in pre-symptomatic *versus* symptomatic C9ORF72^{RE} patients and that connexin dysfunction is related to the sample point of the disease course.

One possibility for this divergence is due to epigenetic dysregulation. Importantly, the direct differentiation methodology employed to generate iAstrocytes retains the epigenetic status of the cell of origin (Gatto et al., 2021). *C9ORF72*^{RE} has been shown to have increased methylation (Belzil et al., 2014, Xi et al., 2014a), and decreased transcription in ALS/FTD patients (Belzil et al., 2013, Xi et al., 2014a). Disease discordant monozygotic twins hold important potential for studies seeking to identify epigenetic and transcriptomic factors that modify the phenotype of complex diseases. Previously, identical ALS twin studies revealed no aberrant DNA methylation between siblings (Xi et al., 2014b, Young et al., 2017), but methylome-wide studies revealed an accelerated epigenetic aging in affected ALS twins (Zhang et al., 2016a, Young et al., 2017, Tarr et al., 2019), altered GABA signalling (Young et al., 2017) and immune response (Lam et al., 2016). This epigenetic age disparity may contribute to the observed astrocyte membrane dysfunction and disease progression in the affected twin compared to the unaffected sibling.

Since connexin upregulation is linked to altered neuronal activity (Rouach et al., 2000) (Charvériat et al., 2021), I explored the contribution of external factors to connexin-mediated dysfunction in control and pre-symptomatic *C9ORF72*^{RE} iAstrocytes. In control iAstrocytes, enhanced extracellular KCl mildly increased the CBX-sensitive current response, as expected in relation to their role in K^+ clearance and homeostasis (Giaume et al., 2021). However, the pre-symptomatic iAstrocytes displayed a considerably greater increase in the CBX-sensitive membrane current amplitude in response to incubation with K^+. No difference in the current dysfunction was observed in healthy or *C9ORF72*^{RE} iAstrocytes treated with osmotic control NaCl, indicating the shift is specific to increased K^+. This finding indicates that environmental factors, such as elevated extracellular K^+ concentration, mimicking increased neuronal activity, may trigger an abnormal connexin upregulation in astrocytes in individuals with the *C9ORF72*^{RE} mutation. Beyond the fact I presented preliminary data to show that the connexin phenotype in *C9ORF72*^{RE} iAstrocytes is toxic to MNs, this may link two major areas of ALS pathophysiology – hyperexcitability (and consequently increased axonal K^+ extrusion) in MNs and astrocyte-mediated MN toxicity. It is therefore possible that MN hyperexcitability, a hallmark of ALS, is likely to trigger or worsen connexin dysfunction in ALS astrocytes, potentially exacerbating the disease progress. This also potentially suggests that early hyperexcitability mediated by

MNs may drive astrocyte dysfunction, leading to further MN toxicity. Also, several lines of evidence suggest a causal link between hyperexcitability caused by intense physical activity, dysregulated energy metabolism and the risk of developing ALS (Chapman et al., 2023, Julian et al., 2021). Environmental risk factors like intense exercise influence ALS risk through epigenetic changes (Oskarsson et al., 2015). Further, intense locomotor exercise would be likely to cause high levels of axonal K^+ extrusion (Lindinger and Sjøgaard, 1991), providing a possible environmental risk factor that can drive astrocyte connexin dysregulation and subsequent astrocyte-mediated MN toxicity. During high-intensity physical activity, leads to increased extracellular K^+ accumulation and subsequent upregulation of astrocytic connexins, including Cx43 , potentially as a compensatory mechanism to clear excess K^+ (Rouach et al., 2000). My results reveal that iAstrocytes derived from pre-symptomatic individuals with an ALS risk genotype display a significant increase in membrane current response upon voltage stimulation compared to healthy controls probably due to accelerated epigenetic aging (Young et al., 2017). This finding aligns with the concept that vigorous exercise in genetically predisposed individual might lead to cellular stress and connexin upregulation. iAstrocytes derived from pre-symptomatic patients containing ALS mutations may also retain epigenetic signals that make them vulnerable to developing this dysfunctional connexin phenotype upon stress exposure.

5.5. Conclusion

In conclusion, I identified a unifying feature of enhanced membrane current response in iAstrocytes derived from ALS, FTD and AD patients. This finding indicates connexin dysfunction as a common pathological mechanism across neurodegenerative diseases. This connexin-mediated dysfunction appears in pre-symptomatic individuals and can be exacerbated by toxic environmental factors. Increased extracellular K^+ mimicking enhanced neuronal activity leads to connexin dysfunction in presymptomatic *C9ORF72*^{RE} individuals, likely influenced by epigenetic signatures. These findings suggest connexin dysfunction as an important modulator of toxicity over a broad range of neurodegenerative diseases. Exploring the potential for modulating connexin function through therapeutic strategies could improve interventions in neurodegenerative diseases, which will be further described in Chapter 6.

6. Chapter 6: Discussion and Future Research

6.1. Introduction

The overarching aims of this research were to:

i. Investigate the functional electrophysiological properties of human *in vitro*-derived medium spiny neurons (MSNs) generated from *C9ORF72*^{RE} patients.

ii. Investigate the functional electrophysiological properties of human *in vitro*-derived astrocytes derived from *C9ORF72*^{RE} patients.

I have discussed the immediate results of these investigations in relation to core hypotheses and objectives in each of the individual Results chapters. Here, I summarise these core findings and conclusions, discuss further questions and areas for further investigation.

6.2. In vitro-derived *C9ORF72*^{RE} MSNs are hypoexcitable.

In Chapter 3, I performed the first electrophysiological investigation of MSNs in the context of FTD/ALS and determined that they are dysfunctional. This provides the first electrophysiological evidence that other neuronal types in ALS/FTD other than cortical and motor neurons are dysfunctional (reviewed in (Pasniceanu et al., 2021)) are disturbed. My main findings from this work are summarised as:

- *In vitro* iPSC-derived *C9ORF72*^{RE} MSNs display intrinsic hypoexcitability, but are not compromised in terms of their viability or other aspects of electrophysiological maturation;
- *C9ORF72*^{RE} MSNs are hypoexcitable because they notably display slowed altered AP waveforms, which show impaired depolarisation and repolarisation phases.
- Consistent with hypoexcitability, I also demonstrate that the AP waveform of *C9ORF72*^{RE} MSNs appears to display modest changes to the amplitude and AHP.
- The AP waveform appears to be fundamentally impacted by a reduced expression of I_K channels, but not Na_V or I_A. This scenario is most plausibly explainable by potential differences in AIS location, including a potentially altered site of functional I_K expression away from the cell body.

6.3. Future work

Establishing whether MSN hypoexcitability is a convergent feature of FTD/ALS. The data I have obtained is exclusive to the *C9ORF72*^{RE} mutation. However, neuroimaging data highlight frontostriatal impairments in ALS patients with *C9ORF72*^{RE}, as well as in presymptomatic *C9ORF72*^{RE} carriers (Bede et al., 2013b, Walhout et al., 2015, Machts et al., 2015a, Lee and Huang, 2017, De Vocht et al., 2020). It will therefore be important to determine whether MSNs derived from sporadic ALS and other patients containing mutations are hypoexcitable to establish whether this is a converging phenotype.

Establishing the identity of I_K channel dysfunction and potential AIS dysfunction in FTD/ALS. An outcome of the study shows that I_K channels are reduced in functional expression and *C9ORF72*^{RE} MSNs are hypoexcitable. As discussed, this is apparent disagreement with data from ALS MNs that show reduced I_K is associated with hyperexcitability in which reduced I_K channels and K_V7.2-containing channels are potentially implicated (Wainger et al., 2014). However, the data obtained in this study are highly consistent with another scenario where I_K channels can be positioned in a different position in the axon, specifically aligned to an altered position of the axon initial segment further away from the cell body, to cause hypoexcitability (Lezmy et al., 2017). Similarly, K_V7.2-containing channels are implicated in generating this excitability property. It is therefore critical to establish both the identity of the specific I_K channel implicated in the dysregulation and any shifts in AIS. Identification of I_K channel subunits would be best undertaken using a multimodal approach, including western blot (ideally membrane fraction) and the use of selective pharmacology. For example, to test the hypothesis of (M-channel) K_V7.2 dysregulation and dysfunction in *C9ORF72*^{RE} MSNs it will be important to test the acute effect of M-channel blockers, linopirdine or XE-991 (Fontán-Lozano et al., 2011, Dirkx et al., 2020), using whole-cell current-clamp electrophysiology experiments, as highlighted in my study. I hypothesize that such compounds would not impact on *C9ORF72*^{RE} MSNs as much as on controls, but if my hypothesis is correct, this would cause hyperexcitability in controls and further hypoexcitability in *C9ORF72*^{RE} MSNs, because the I_K channels would be located at different positions. Moreover, enhancing K_V7.2 function through activators like ezogabine may reinforce this. The positioning and morphology of the AIS in *C9ORF72*^{RE} MSNs compared to

controls can be determined using specific markers of the AIS, such as Ankyrin-G. It will be important to align these data with specific markers of the I_K channel identified to determine a possible distal shift of such I_K channels along the axon due to altered AIS positioning. My data is also consistent with a scenario where Na_V functional expression is not altered, but the depolarisation phase of the AP is altered, suggesting also a more distal shift of the AIS. It will be important to use this aligned data to confirm using immunocytochemistry that Na_V channels are also distally shifted. Such data also permit the ability to similarly examine the striatum in FTD/ALS post-mortem material for similar changes to examine whether such defects are evident at the end-stage of disease.

Does hypoexcitability lead to a loss of GABA-ergic function? Although enriched populations of electrophysiologically mature GABA-ergic MSNs were generated and cultured *in vitro*, these models lack the complex cellular interactions present in the striatum and the cortico-striato-nigral networks to investigate the hypothesis that hypoexcitability in MSNs can lead to disinhibition of MSN targets. The interaction between MSNs, dopaminergic neurons from the substantia nigra pars compacta, neurons of the globus pallidus interna and subthalamic nucleus and, furthermore, glutamatergic cortical inputs are fundamental for regulating reward processing, cognition and other functions (Gerfen and Bolam, 2016). Also, glutamatergic projection neurons from the cerebral cortex into the striatum are thought to play a key role in the development of MSNs (Steiner and Tseng, 2016), highlighting that dopamine appears to increase the excitability of MSNs (Nagai et al., 2016). To address these limitations, it is therefore important to investigate MSNs in a more relevant environment that include their innervating and target contacts. Typically, this would be achieved by two approaches involving transgenic rodent models of FTD/ALS and more elaborate human stem cell technology based models. Transgenic FTD/ALS rodent models have been developed to study the pathophysiology of disease progression, however many of these models harbour caveats, including the fact that some do not faithfully recapitulate disease (Balendra and Isaacs, 2018, Philips and Rothstein, 2015, Zhu et al., 2023). However, SOD1 mouse models have been shown to display MSN abnormalities (Geracitano et al., 2003, Joyce et al., 2015). Striatal MSNs in $SOD1^{G93A}$ mice show a loss of spine density from P65-75 onward (Fogarty et al., 2016a), suggesting that synaptic inputs

into MSNs maybe a site of excitotoxicity. Interestingly, one study from $SOD1^{G93A}$ mouse model demonstrated that degeneration of the dopaminergic neurons affects striatal-related synaptic plasticity and behaviour, providing cellular evidence of striatal involvement and cognitive defects observed in FTD/ALS animal model (Geracitano et al., 2003). Furthermore, transgenic mice expressing human tau protein (MAPT) suggest that synaptic defects within the striatum may be a viable therapeutic target for cognitive dysfunction in FTD/ALS (Lui et al., 2016, Petkau et al., 2012). Further, TDP-43ΔNLS transgenic mouse models exhibit FTD/ALS-like phenotypes or cognitive deficits and present with neuronal loss and hallmark cytoplasmic TDP-43 inclusions in the striatum, but not striatal atrophy (Walker et al., 2015). These emerging data suggest that transgenic models, with careful appreciation of their limitations, may be useful for further investigation of striatal dysfunction in FTD/ALS.

Human co-culture or multi-culture systems that incorporate MSN with their targets may offer an alternative controllable environment to study MSN dysfunction in relation to their inputs and targets in FTD/ALS. For example, Iannielli et al. implemented a microfluidic system for long-term and stable culture of iPSC-derived MSNs and dopaminergic neurons with functional synapses (Iannielli et al., 2019), allowing for pharmacological testing to identify potential defects at the synapse, and identify compounds that protect synapse function in the context of disease. Microfluidic devices can be further integrated with microelectrode arrays (MEA) (Bruno et al., 2020) and patch-clamp recordings (Yan and Wu, 2013) therefore permitting investigation into the functional connectivity of these neurons. Also, advances in stem cell technology led to the development of human striatal organoids and cortico-striatal assembloids from human iPSCs, which appear to recapitulate aspects of intrinsic electrophysiological properties of rodent MSNs (Miura et al., 2020). These 3D cultures offer a more faithful circuit representation of striatal cellular architecture compared to 2D cultures therefore permitting study of MSNs connectivity in a human context.

Interestingly, MSN cultures contain very little astrocytes. My data therefore suggest that the intrinsic excitability phenotype I observe is likely to be cell autonomous. Noting that astrocytes are reported to have impact on lower motor neuron excitability, in addition to viability, to cause hypoexcitability (Zhao et al., 2020). This appears to suggest that MSNs

are intrinsically more vulnerable to changes in excitability. Noting that MSN excitability is known to be modulated by astrocytes (Nagai et al., 2019, Khakh, 2019), it would be therefore important to assess MSN excitability in the presence of healthy and *C9ORF72*^{RE} astrocytes.

What type of MSNs are iPSC-derived MSNs? Striatal MSNs are divided into D1-type dopamine receptor and D2-type dopamine receptor output neurons to form the 'direct' and 'indirect' pathway, respectively (Gerfen et al., 1990b, Albin et al., 1995). The direct pathway MSNs directly transmit information to output nuclei (globus pallidus pars interna and substantia nigra pars reticulata). This inhibition caused by GABAergic MSNs of the substantia nigra pars reticulata leads to disinhibition of the thalamic glutamatergic neurons which receive substantia nigra pars reticulata input and project to the cortex. Conversely, the indirect pathway MSNs project to the same substantia nigra pars reticulata through globus pallidus pars externa and the subthalamic nucleus. The indirect and direct pathways of the striatum are established to be aligned to specific behaviours and cognitive functions (Nonomura et al., 2018). MSNs can exhibit characteristics of both pathways as a number of studies have shown that D1 and D2 receptors co-exist within the same MSN (Perreault et al., 2011). Interestingly, iPSC-derived striatal protocols appear to report a mixture of D1 *versus* D2 MSNs (Fjodorova et al., 2015, Conforti et al., 2022). Notably, the *C9ORF72*^{RE} MSNs used in this study likely represent a heterogeneous population of D1- and D2-type neurons. Further studies should aim to selectively isolate D1 and D2 subtypes to gain more precise understanding of their role in *C9ORF72*^{RE} FTD/ALS. It would be important to know if these neurons are reflective of such MSN types to align any potential electrophysiological properties to MSN type, and by inference the direct and indirect pathways. Furthermore, MSNs feature in different parts of the striatum, which is differentially impacted in FTD/ALS (ventral) *versus* Huntington's disease (dorsal). New knowledge of developmental regional markers of MSNs is emerging (He et al., 2021) and will be important to determine in these cultures to align our cultures with such striatal markers. However, no iPSC protocol has yet determined whether iPSC-MSNs are of specific striatal identity. Interestingly, recently cortical neurons in SOD1^{G93A} mice were shown to exhibit a distinct subtype of Gprin3-expressing neurons which were specifically vulnerable to degeneration, which is highly

expressed within the striatum (Moya et al., 2022). It is known that Gprin3-expressing neurons in the striatum are part of the indirect pathway and is linked to MSN neuronal excitability (Moya et al., 2022). My study provides the impetus to begin further detailed studies as to which MSNs are vulnerable in FTD/ALS.

6.4. What is the translational relevance of this study?

When does MSN hypoexcitability initiate in disease? My *in vitro* data indicates that *C9ORF72*^{RE} MSNs become in dysfunctional with culture time, suggesting that hypoexcitability of MSNs progressively become more intense with time. This is in line with the idea that axonal and neuronal dysfunction precedes neuronal death in patients (Iwai et al., 2016). However, it is important to reflect that this is an *in vitro* model, where timelines of phenotypic development may be skewed compared to native FTD/ALS patients (Zhang et al., 2013). In this regard, longitudinal, multimodal neuroimaging offers a complementary approach for investigating MSN dysfunction in *C9ORF72*^{RE} FTD/ALS patients. Neuronal loss within the striatum of FTD/ALS patients, striatal atrophy and altered diffusivity in patients are documented alterations in FTD/ALS patients (Riku et al., 2016, Kato et al., 1994). MRI and vertex analysis have demonstrated a robust correlation between striatal dysfunction and disrupted frontostriatal networks in ALS patients with in *C9ORF72*^{RE}, as well as in presymptomatic in *C9ORF72*^{RE} carriers when compared to non-carriers (Bede et al., 2013b, Lee and Huang, 2017, Walhout et al., 2015, De Vocht et al., 2020), suggesting a loss-of-function within these networks. Striatal grey matter deficits have been observed in asymptomatic *C9ORF72*^{RE} carriers (Lee et al., 2017b). Further, the presence of striatal atrophy in ALS patients with no cognitive impairments (Bede et al., 2013a, Tae et al., 2020) might suggest that subtle cognitive/behavioural deficits, which do not satisfy current criteria, may be present early during disease course (Tae et al., 2020), but also striatal alterations might be present before the overt TDP-43 pathological burden (during stage 1 of disease) (Brettschneider et al., 2013). Most of these studies compare ALS with controls, but not FTD, and only few studies address the importance of the striatum by stratifying the samples according to cognitive/behavioural status (Bede et al., 2013a, Lee et al., 2017b, Tae et al., 2020). The MRI-based evidence appears a reliable indicator of disease severity and

progression from an early and even presymptomatic stage. Such studies are important to conduct to determine the pathophysiology within the striatum (and MSNs) in FTD/ALS patients over time. Furthermore, the observed hypoexcitability in MSNs described in my thesis aligns with the notion that neuronal dysfunction can precede neuronal death in neurodegenerative. This suggests that early intervention strategies aimed at preserving neuronal function may be beneficial in slowing disease progression and improving patient outcome.

Is MSN hypoexcitability targetable for therapeutic benefit? MSNs are a considered target for numerous neurological diseases (Rikani et al., 2014, Witzig et al., 2020) and brain conditions (Zhao et al., 2022b, Durieux et al., 2009, Tsutsui-Kimura et al., 2017). Interestingly, other GABA-ergic neurons, including cortical and spinal interneurons, in FTD/ALS appear to be vulnerable and exhibit excitability issues, including hypoexcitability (Estebanez et al., 2017, Lin et al., 2021, Tsuiji et al., 2017, Khademullah et al., 2020). This potentially enhancing GABA-ergic function, as suggested by hypoexcitable MSNs, could assist in regaining MSN function, but also may have systemic benefit in other brain regions affected in disease.

The promotion of increased excitability through the inhibition of small conductance Ca^{2+}-activated K_V (SK) channels showed appears to be a promising therapeutic target in ALS MNs (Catanese et al., 2021, Castelli et al., 2021). SK channels are responsible for the AHP phase of the AP and their blockade with apamin leads to increased firing (Brownstone, 2006, Catanese et al., 2021). However, this is directly contrasted with the work of Wainger et al., who promote the reduction of hyperexcitability in MNs as therapeutic (Wainger et al., 2014). The AP waveform shows impairments in the repolarisation phase and depolarisation phase. Targeting these specifically are the most intuitive therapeutic targets emerging from this work. K_V channels are modulators that have been evaluated or are currently investigated for their potential role in management of ALS. Specifically, $K_V7.2$ (I_K type) channels emerge as a promising therapeutic target in ALS. Ezogabine, an antiepileptic drug activating these channels, counteracts the reduced expression of $K_V7.2$ observed in ALS lower MNs (Jiang et al., 2005). High-throughput screening supports this strategy, identifying K_V7 channels are key in reducing excitotoxicity in human iPSC-derived MNs (Huang et al., 2021a). Ezogabine effectively reduced hyperexcitability and extended survival in ALS

models, highlighting its potential benefit (Wainger et al., 2014, Wainger et al., 2021). However, limited patient number, short treatment duration, and lack of selectivity led to frequent adverse effects (Wainger et al., 2021). More specific K_V7 channel openers, QRL-101 (QurAlis) are being developed and currently undergoing clinical trials, offering possible improvement in the treatment of MN hyperexcitability-induced disease progression of ALS (QurAlis, 2024). However, our study indicates that Kv7.2 maybe alternately dysregulated in MSNs compared to MNs and could be unsuitable for MSN hypoexcitability. Studies also explored 4-aminopyridine (4-AP), an I_A channel antagonist, to address neuronal hypoexcitability on *FUS* and *SOD1* iPSC-derived MNs (Naujock et al., 2016). 4-AP restored spontaneous activity patterns and synaptic input by inhibiting I_A K^+ currents (Naujock et al., 2016). Whilst likely to increase excitability of MSNs, I_A regulation may not be the most appropriate long term pharmacological solution. Future work isolating the key underpinning I_K channel causing dysfunction will allow more specific pharmacological targeting of the repolarisation phase. However, the data also suggest a shift in AIS location in *C9ORF72*^{RE} MSNs, but interestingly, the AIS structure may be a valid target. Recently, restoring axonal organelle motility through magnetic field stimulation was proposed as an alternative therapeutic approach in *FUS* MNs (Kandhavivorn et al., 2023). It is therefore possible that this non-invasive approach, which can be targeted to specific brain regions, could yield a future corrective AIS therapy.

Importantly, Riluzole is the only approved drug for ALS in Europe (Lacomblez et al., 1996, Bensimon et al., 1994). Riluzole reduces neuronal excitability and it is believed Riluzole inhibits persistent Na^+ currents on glutamatergic nerve terminals and/or activation of a G-protein-dependent signalling cascade, and potentially by non-competitive blockage of NMDA receptors (Geevasinga et al., 2016a, Doble, 1996). My finding that *C9ORF72*^{RE} MSNs are hypoexcitable means that riluzole is likely to potentially worsen this hypoexcitability and its downstream effects.

6.5. Summary

In this work I have begun to elucidate the electrophysiological abnormalities in *C9ORF72*^{RE} MSNs, marking a significant stride in understanding the broader neuronal dysfunction associated with FTD/ALS. The data unveiled intrinsic hypoexcitability in these neurons, attributed to altered action potential waveforms and impaired ion channel functionality, particularly I_K channels. These findings provide direct evidence that dysregulation in non-cortical and non-motor neurons could also be pivotal in the pathogenesis of FTD/ALS. As such, this study sets the stage for future research aimed at corroborating the hypoexcitability as a convergent feature across various genetic mutations implicated in FTD/ALS, which is suggested by patient neuroimaging data. The exploration into the specific I_K channel dysfunction and potential alterations in AIS positioning may provide promising avenues for targeted pharmacological interventions. The potential implications of MSN dysfunction may reverberate through broader cortico-striato-nigral networks, via impaired GABA-ergic MSN signalling, thus influencing cognitive and behavioural aspects of the disease. Further work will require to confirm this using experimental models where striatal circuitry is modelled appropriately.

In summary, this research illuminates the electrophysiological dysfunction of *C9ORF72*^{RE} MSNs, thereby deepening our understanding of FTD/ALS pathogenesis and offering critical insights for new therapeutic advancements.

6.6. In vitro-derived astrocytes obtained from symptomatic ALS patients display connexin dysfunction.

In Chapters 4 and 5, I performed the first electrophysiological investigation of astrocytes in the context of ALS and determined that they display exhibit considerable dysfunction associated with their membranes due to connexin dysregulation. My main findings from this work are summarised as;

- *In vitro*, directly differentiated astrocytes derived from symptomatic *C9ORF72*^{RE} and sporadic ALS patients display a membrane dysfunction caused by connexin dysfunction. These iAstrocytes are not compromised in terms of their viability, as determined by the fact that they displayed healthy resting membrane potentials.
- The connexin dysfunction was due to an increase in functional expression of Cx43 hemichannels.
- Preliminary data indicated that astrocyte-mediated MN toxicity is mediated by astrocyte connexin dysfunction.
- Astrocyte connexin dysfunction also appears to be a convergent feature in astrocytes obtained from symptomatic Alzheimer's Disease, and furthermore, *C9ORF72*^{RE}-mediated FTD. In the latter, it appears that there is potential for heterogeneity between patients.
- *C9ORF72*^{RE} astrocyte membrane dysfunction is driven, at least in part, via the production of dipeptide repeat proteins.
- Astrocyte connexin dysfunction is prominent in astrocytes derived from symptomatic *C9ORF72*^{RE} ALS patients, but is less prominent in astrocytes derived from pre-symptomatic *C9ORF72*^{RE} patients, suggesting that additional factors besides the *C9ORF72*^{RE} mutation are determinants of connexin dysfunction.
- *C9ORF72*^{RE} astrocyte connexin dysfunction can be enhanced by extracellular K^+, suggesting that extrusion of K^+ via neuronal activity can drive astrocyte dysfunction.

6.7. Future work

Does Cx43 dysfunction solely mediate connexin-dependent effects on ALS astrocytes? My findings using a combined electrophysiological and selective pharmacological approach to determine the involvement of connexin, specifically Cx43 hemichannel-mediated dysfunction in the astrocyte membrane. These data directly correspond to the findings of Almad et al. that implicate Cx43 as the main contributor to the astrocyte-mediated toxicity in ALS (Almad et al., 2022). Importantly, Cx30 subunits are the other prominent Cx subunit expressed by astrocytes (Nagy et al., 1999, Ghézali et al., 2020). Whilst Cx30 was not implicated by Almad et al., 2022, there remains no specific Cx30 pharmacological blocker to test whether Cx30 is functional upregulated or not. This is confounded by the fact that Cx43 blocker Gap19 is a negative allosteric modulator, which remains to be fully characterised. Interestingly, Cx30 subunits displayed high expression in pre-symptomatic $SOD1^{G93A}$ mice (Hashimoto et al., 2022) contradicting Almad et al., 2022. Cx30 knockout $SOD1^{G93A}$ mice delayed disease onset, preventing anterior horn cells degeneration compared to wild-type $SOD1^{G93A}$ mice. Also, the knockout Cx30 model exhibited reduced astrocyte activation. These findings suggest Cx30 upregulation in the prodromal disease stage might offer neuroprotection by mitigating astrocytic inflammation, while Cx43 is linked to disease onset and potentially contributes to disease progression (Hashimoto et al., 2022). In this regard, it would be important to employ a knockdown strategy, for example siRNA technology, to selectively dissect the contribution of Cx30 and Cx43 to the enhanced current dysfunction in the ALS iAstrocytes. Further, extending this dissection to the pre-symptomatic versus symptomatic *C9ORF72*^{RE} astrocytes would reveal whether Cx30 and Cx43 dysregulation is potentially linked to specific disease phases.

Does connexin dysfunction drive astrocyte pathogenesis in addition to mediating MN toxicity? The preliminary data obtained in this study and other studies (Almad et al., 2022) position astrocyte connexin membrane channels as a key mediator of MN toxicity. It has been discussed that connexins are key mediators of numerous potential toxic agents, including ATP, reactive oxygen species, inflammatory mediators and glutamate. Whilst it is important which of these toxic agents are key mediators of MN toxicity, it is important to establish whether connexin dysregulation can also drive astrocyte pathogenesis.

Metabolic and mitochondrial dysfunction leading to oxidative stress are hallmarks of ALS and is highly evident in ALS iAstrocytes (Allen et al., 2019a, Vandoorne et al., 2018). Interestingly, connexins facilitate mitochondrial coupling, a process by which the electron transport chain uses redox energy to produce ATP via ATP synthase and ROS as a by-product, and have been shown to drive ROS production (Zhang et al., 2022a). Further, reduced astrocyte connexin function has been found to be neuroprotective under ischemia, supporting the notion that connexin upregulation has considerable potential to be pathogenic in conditions of oxidative stress (Schulz et al., 2015, Ma et al., 2018). It will therefore be important to test the hypothesis that increased connexin activity in ALS iAstrocytes is enhancing mitochondrial coupling, causing increased production of toxic agents, which can permeate connexins to reach MNs. This can be examined a XF metabolic bioanalyzer, which allows a detailed dissection of mitochondrial processes including coupling and uncoupling processes. Related to this, there is a potential localization of Cx43 hemichannels to the mitochondrial outer membrane (Zhang et al., 2022a). While the precise functions of mitochondrial connexins remain to be discovered, their interaction with mitochondrial ATP synthase suggests a role in promoting mitochondrial coupling (Zhang et al., 2022a). It will therefore be important to determine whether Cx43 expression is also increased in mitochondria using western blot of mitochondria isolated from iAstrocytes using an ultracentrifugation method. This rationale leads to the proposal that increased connexin activity in iAstrocytes is also pathogenically enhancing mitochondrial coupling, causing increased production of toxic agents, which can permeate connexins to reach MNs. Interestingly, a controlled elevation of uncoupling processes, including in astrocytes, is supported by numerous studies as neuroprotective and stands as a route for therapeutic advancements in neurodegenerative diseases, including Alzheimer's Disease (Andrews et al., 2005, Geisler et al., 2017, Perreten Lambert et al., 2014). Investigation of pre-symptomatic *C9ORF72*^{RE} astrocytes, in this regard, would be highly interesting, where they would be expected not to deliver the same level of toxicity to MNs, and potentially less mitochondrial dysfunction, due to less prominent connexin dysfunction.

What are the pathological drivers of connexin dysfunction in astrocytes? My data indicate that *C9ORF72*^{RE} astrocyte dysfunction is mediated, at least in part, by dipeptide repeat proteins,

which are generated by non-AUG RAN translation of transcribed elements of the hexanucleotide repeat expansion. Given that there are 5 independent species of DPRs (Donnelly et al., 2013, Mori et al., 2013b, Gendron et al., 2013), it will be important to determine which of these DPRs are responsible for toxicity. To investigate this, it would be possible to introduce individual poly-DPR constructs to astrocytes using an established lentiviral transduction method (for example, (Vanneste et al., 2019)). Critically, other mechanisms are potentially at play in *C9ORF72*^{RE} backgrounds, including haploinsufficiency of the C9ORF72 protein and also RNA foci (Gendron et al., 2014, Mizielinska and Isaacs, 2014). Similarly, it will be important to determine the level of connexin dysfunction using selective knock down tools (Hautbergue et al., 2017, Bauer et al., 2022b).

The above scenarios are selective to *C9ORF72*^{RE} backgrounds only. The hallmark pathology for FTD/ALS is TDP-43 pathology, including sporadic ALS. It will therefore be important to explore whether TDP-43 pathology-related dysfunction is associated with astrocyte dysfunction. This can be explored using mutant TDP-43 mouse models and also the potential of obtaining fibroblasts from mTDP-43 FTD/ALS patients. However, patients harbouring TDP-43 mutation are extremely rare. Probing astrocytes using novel tools that allow the detection of early TDP-43 condensation stages in the form of RNA aptamers (Zacco et al., 2022) may reveal an association with connexin dysfunction.

All the above scenarios deal with drivers related to genetic and pathological impairments in FTD/ALS. However, my data has demonstrated that extrinsic influences, i.e., elevated extracellular K^+, can drive connexin dysfunction in astrocytes with the *C9ORF72*^{RE} mutation. I propose that this mechanism links potential MN hyperexcitability, a hallmark feature of ALS, with the initiation of connexin dysfunction. Importantly, numerous reports link elevated neuronal activity with the formation of pathological species such as TDP-43 and DPRs (Weskamp et al., 2020). It will therefore be important to determine whether such processes are play in ALS astrocytes. This can be explored in co-cultures with MNs where it is possible to induce MN firing activity, and thus K^+ extrusion, using selective Na_v opener, veratridine. For control, would perform assays with veratridine and Na_v blocker tetrodotoxin. I know that such compounds will not impact astrocytes since our patch-clamp recordings show no Na_v in iAstrocytes. I will measure the electrophysiological currents from iAstrocytes to determine whether connexin upregulation has been induced.

However, my new data from monozygotic pre-symptomatic *C9ORF72*^{RE} iAstrocytes and symptomatic *C9ORF72*^{RE} iAstrocyte twins show prominent connexin dysfunction in symptomatic *C9ORF72*^{RE} iAstrocytes. However, these cultures are enriched for astrocytes, containing no neurons (Meyer et al., 2014). There are therefore intrinsic drivers of connexin dysfunction that we do not yet fully understand. Epigenetic disturbances are detected and emerging as key disease regulators in ALS, including modifiers of disease onset (Zhang et al., 2021, Yazar et al., 2023, Young et al., 2017). Since connexins are regulated by epigenetic mechanisms (Oyamada et al., 2013) and because the lines are genetically identical with an equivalent *C9ORF72*^{RE} mutation, I propose that the phenotypic change from pre-symptomatic *C9ORF72*^{RE} iAstrocytes to symptomatic *C9ORF72*^{RE} iAstrocytes is epigenetically controlled. In this regard, neuronal activity is a key driver of epigenetic activity to regulate astrocyte membrane function (Rouach et al., 2000, Sardar et al., 2023) and thus effects of K^+ can be equally driven by epigenetic mechanisms. To understand the intrinsic dysregulation in symptomatic *C9ORF72*^{RE} iAstrocytes I propose to conduct both RNA-sequencing and ATAC-(assay for transposase-accessible chromatin)-sequencing to establish the major gene expression and epigenetic differences between pre-symptomatic *C9ORF72*^{RE} iAstrocytes, symptomatic *C9ORF72*^{RE} iAstrocytes and healthy iAstrocytes. These data will enable the pinpointing of key epigenetic changes associated with astrocyte phenoconversion and connexin dysfunction, and to identify potential therapeutic targets. Importantly, my data showed that astrocyte derived from *C9ORF72*^{RE} FTD patients showed that the astrocyte membrane dysfunction was highly variable between individuals. It is also possible that epigenetic, in addition to genetic, modulators are at play to cause different levels of astrocyte dysfunction between FTD and ALS patients. To advance our understanding of epigenetic changes and other extrinsic risks, large scale long-running longitudinal studies are required including asymptomatic mutation carriers, such as the AMBRoSIA (A Multi-centre Biomarker Research Strategy in ALS) study (Shepheard et al., 2021), which my study has initially taken advantage of. My data and others, therefore, propose a scenario linking neuronal hyperexcitability with molecular and genetic perturbations that drive abnormal connexin upregulation in ALS astrocytes to cause MN toxicity.

6.8. Is astrocyte connexin dysfunction a therapeutic target?

The study of Almad et al. (2022) demonstrating that selective knock down of CX43 in SOD1^{G93A} mouse models delays disease onset presents important preclinical evidence that Cx43 dysfunction is a potential therapeutic target. Several drugs with potent actions on connexin-mediated communication have been used as tools for studying connexin-containing channels. Carbenoxolone (CBX), used in this work, causes a potent but nonspecific inhibition of gap junction coupling and hemichannels (Roux et al., 2015, Davidson et al., 1986). CBX is clinically utilised as a peptic ulcer treatment (Pinder et al., 1976), but is unable to cross the blood-brain barrier (Leshchenko et al., 2006), making its use in ALS challenging. Similarly, synthetic peptides such as Cx43 hemichannel blocker that mimic a short stretch of amino acids on the extracellular loops to inhibit Cx43 subunit function, are not fully characterised and only partially modulate connexin function (Lissoni et al., 2020, Lissoni et al., 2023) and they do not have the capacity to cross the blood brain barrier, limiting their clinical abilities.

Tonabersat, a reported Cx43 hemichannel blocker at low concentrations has been shown to reduce age-related macular degeneration and improve retinal function in rat models through the block of Cx43 hemichannels (Kim et al., 2017b). However, its full pharmacological action remains to be elucidated (Lyon et al., 2020). Tonabersat reduced neurogenic inflammation and antagonized hyperexcitability in models of migraine, condition linked to upregulation of Cx43 (Durham and Garrett, 2009, Sarrouilhe et al., 2014). Almad tested the effect of tonabersat in human iPSC-derived models (co-cultures of iPSC-derived astrocytes and motor neurons) and SOD1 ^{G93A} mice (Almad et al., 2022). Tonabersat did not affect Cx43 protein level, suggesting a neuroprotective role came from blocking Cx43 hemichannels. The neuroprotective effect was seen in later stages of disease only, preventing astrocyte-mediated MN death and hyperexcitability. Interestingly, this drug reduced markers of astrocyte and microglial activation (GFAP and Iba1), suggesting its potential to modulate neuroinflammation alongside MN protection (Almad et al., 2022). Further research on Cx43 hemichannel blockers holds potential for the development of novel therapeutic strategies to slow ALS progression and improve patient outcomes.

Considering the increase Cx43 protein level in CSF samples, motor cortex and spinal cord tissue obtained from ALS patients (Almad et al., 2022), the parameters can be used as

biomarkers of disease. Interestingly, such samples are taken by the AMBRoSIA study and permit future correlative research linking the amount of Cx43 protein level with electrophysiological investigation of iAstrocytes obtained from the same patients, including both pre-symptomatic and symptomatic individuals. The data established in this study indicate that the Cx43 level in patient CSF may present a valuable measure of astrocyte dysfunction in ALS patients in the future.

6.9. Summary

In conclusion, this research has provided pivotal insights into the role of astrocyte connexin dysfunction in the pathogenesis of ALS. Our findings demonstrate that iAstrocytes from symptomatic *C9ORF72*^{RE} and sporadic ALS patients exhibit membrane dysfunction due to connexin dysregulation, specifically an increase in Cx43 hemichannel expression. This dysfunction contributes to astrocyte-mediated motor neuron toxicity and is exacerbated by extracellular K^+ levels. Moreover, connexin dysregulation is a shared feature in other neurodegenerative diseases like AD and FTD. Future studies should focus on dissecting the roles of Cx30 and Cx43 in disease progression, exploring the potential therapeutic targeting of connexin dysfunction, and understanding the underlying pathological drivers, including the role of dipeptide repeat proteins and epigenetic modifications. Our work underscores the significance of astrocyte connexin dysfunction as a potential therapeutic target and biomarker for ALS, offering promising avenues for developing novel treatments and diagnostic approaches to improve patient outcomes.

7. References

ABUDARA, V., BECHBERGER, J., FREITAS-ANDRADE, M., DE BOCK, M., WANG, N., BULTYNCK, G., NAUS, C. C., LEYBAERT, L. & GIAUME, C. 2014. The connexin43 mimetic peptide Gap19 inhibits hemichannels without altering gap junctional communication in astrocytes. *Frontiers in cellular neuroscience,* 8**,** 306.

ADENZATO, M., CAVALLO, M. & ENRICI, I. 2010. Theory of mind ability in the behavioural variant of frontotemporal dementia: an analysis of the neural, cognitive, and social levels. *Neuropsychologia,* 48**,** 2-12.

AGARWAL, S., HIGHTON-WILLIAMSON, E., CAGA, J., HOWELLS, J., DHARMADASA, T., MATAMALA, J. M., MA, Y., SHIBUYA, K., HODGES, J. R., AHMED, R. M., VUCIC, S. & KIERNAN, M. C. 2021. Motor cortical excitability predicts cognitive phenotypes in amyotrophic lateral sclerosis. *Sci Rep,* 11**,** 2172.

AGOSTA, F., FERRARO, P. M., RIVA, N., SPINELLI, E. G., CHIO, A., CANU, E., VALSASINA, P., LUNETTA, C., IANNACCONE, S. & COPETTI, M. 2016. Structural brain correlates of cognitive and behavioral impairment in MND. *Human brain mapping,* 37**,** 1614-1626.

AHMED, R. M., BOCCHETTA, M., TODD, E. G., TSE, N. Y., DEVENNEY, E. M., TU, S., CAGA, J., HODGES, J. R., HALLIDAY, G. M., IRISH, M., KIERNAN, M. C., PIGUET, O. & ROHRER, J. D. 2021. Tackling clinical heterogeneity across the amyotrophic lateral sclerosis–frontotemporal dementia spectrum using a transdiagnostic approach. *Brain Communications,* 3.

AL-CHALABI, A., FANG, F., HANBY, M. F., LEIGH, P. N., SHAW, C. E., YE, W. & RIJSDIJK, F. 2010. An estimate of amyotrophic lateral sclerosis heritability using twin data. *J Neurol Neurosurg Psychiatry,* 81**,** 1324-6.

AL-CHALABI, A., JONES, A., TROAKES, C., KING, A., AL-SARRAJ, S. & VAN DEN BERG, L. H. 2012. The genetics and neuropathology of amyotrophic lateral sclerosis. *Acta Neuropathol,* 124**,** 339-52.

AL-SARRAJ, S., KING, A., TROAKES, C., SMITH, B., MAEKAWA, S., BODI, I., ROGELJ, B., AL-CHALABI, A., HORTOBÁGYI, T. & SHAW, C. E. 2011. p62 positive, TDP-43 negative, neuronal cytoplasmic and intranuclear inclusions in the cerebellum and hippocampus define the pathology of C9orf72-linked FTLD and MND/ALS. *Acta Neuropathol,* 122**,** 691-702.

ALBIN, R. L., YOUNG, A. B. & PENNEY, J. B. 1995. The functional anatomy of disorders of the basal ganglia. *Trends in neurosciences,* 18**,** 63-64.

ALEXANDER, G. E., DELONG, M. R. & STRICK, P. L. 1986. Parallel organization of functionally segregated circuits linking basal ganglia and cortex. *Annual review of neuroscience,* 9**,** 357-381.

ALLEN, N. J. & BARRES, B. A. 2009. Glia—more than just brain glue. *Nature,* 457**,** 675-677.

ALLEN, N. J. & EROGLU, C. 2017. Cell biology of astrocyte-synapse interactions. *Neuron,* 96**,** 697-708.

ALLEN, N. J. & LYONS, D. A. 2018. Glia as architects of central nervous system formation and function. *Science,* 362**,** 181-185.

ALLEN, S. P., HALL, B., CASTELLI, L. M., FRANCIS, L., WOOF, R., SISKOS, A. P., KOULOURA, E., GRAY, E., THOMPSON, A. G., TALBOT, K., HIGGINBOTTOM, A., MYSZCZYNSKA, M., ALLEN, C. F., STOPFORD, M. J., HEMINGWAY, J., BAUER, C. S., WEBSTER, C. P., DE VOS,

K. J., TURNER, M. R., KEUN, H. C., HAUTBERGUE, G. M., FERRAIUOLO, L. & SHAW, P. J. 2019a. Astrocyte adenosine deaminase loss increases motor neuron toxicity in amyotrophic lateral sclerosis. *Brain,* 142**,** 586-605.

ALLEN, S. P., HALL, B., WOOF, R., FRANCIS, L., GATTO, N., SHAW, A. C., MYSZCZYNSKA, M., HEMINGWAY, J., COLDICOTT, I., WILLCOCK, A., JOB, L., HUGHES, R. M., BOSCHIAN, C., BAYATTI, N., HEATH, P. R., BANDMANN, O., MORTIBOYS, H., FERRAIUOLO, L. & SHAW, P. J. 2019b. C9orf72 expansion within astrocytes reduces metabolic flexibility in amyotrophic lateral sclerosis. *Brain,* 142**,** 3771-3790.

ALLODI, I., MONTAÑANA-ROSELL, R., SELVAN, R., LÖW, P. & KIEHN, O. 2021. Locomotor deficits in a mouse model of ALS are paralleled by loss of V1-interneuron connections onto fast motor neurons. *Nature Communications,* 12**,** 3251.

ALMAD, A. A., DORESWAMY, A., GROSS, S. K., RICHARD, J. P., HUO, Y., HAUGHEY, N. & MARAGAKIS, N. J. 2016. Connexin 43 in astrocytes contributes to motor neuron toxicity in amyotrophic lateral sclerosis. *Glia,* 64**,** 1154-1169.

ALMAD, A. A., TAGA, A., JOSEPH, J., GROSS, S. K., WELSH, C., PATANKAR, A., RICHARD, J.-P., RUST, K., POKHAREL, A., PLOTT, C., LILLO, M., DASTGHEYB, R., EGGAN, K., HAUGHEY, N., CONTRERAS, J. E. & MARAGAKIS, N. J. 2022. Cx43 hemichannels contribute to astrocyte-mediated toxicity in sporadic and familial ALS. *Proceedings of the National Academy of Sciences of the United States of America,* 119**,** e2107391119.

ANDERSON, C., CATOE, H. & WERNER, R. 2006. MIR-206 regulates connexin43 expression during skeletal muscle development. *Nucleic acids research,* 34**,** 5863-5871.

ANDREWS, Z. B., DIANO, S. & HORVATH, T. L. 2005. Mitochondrial uncoupling proteins in the CNS: in support of function and survival. *Nat Rev Neurosci,* 6**,** 829-40.

AOKI, Y., MANZANO, R., LEE, Y., DAFINCA, R., AOKI, M., DOUGLAS, A. G. L., VARELA, M. A., SATHYAPRAKASH, C., SCABER, J., BARBAGALLO, P., VADER, P., MÄGER, I., EZZAT, K., TURNER, M. R., ITO, N., GASCO, S., OHBAYASHI, N., EL ANDALOUSSI, S., TAKEDA, S., FUKUDA, M., TALBOT, K. & WOOD, M. J. A. 2017. C9orf72 and RAB7L1 regulate vesicle trafficking in amyotrophic lateral sclerosis and frontotemporal dementia. *Brain,* 140**,** 887-897.

ARAI, T., HASEGAWA, M., AKIYAMA, H., IKEDA, K., NONAKA, T., MORI, H., MANN, D., TSUCHIYA, K., YOSHIDA, M. & HASHIZUME, Y. 2006. TDP-43 is a component of ubiquitin-positive tau-negative inclusions in frontotemporal lobar degeneration and amyotrophic lateral sclerosis. *Biochemical and biophysical research communications,* 351**,** 602-611.

ARAKI, R., HOKI, Y., SUGA, T., OBARA, C., SUNAYAMA, M., IMADOME, K., FUJITA, M., KAMIMURA, S., NAKAMURA, M., WAKAYAMA, S., NAGY, A., WAKAYAMA, T. & ABE, M. 2020. Genetic aberrations in iPSCs are introduced by a transient G1/S cell cycle checkpoint deficiency. *Nat Commun,* 11**,** 197.

ARAQUE, A., CARMIGNOTO, G., HAYDON, P. G., OLIET, S. H., ROBITAILLE, R. & VOLTERRA, A. 2014. Gliotransmitters travel in time and space. *Neuron,* 81**,** 728-39.

ARREDONDO, C., CEFALIELLO, C., DYRDA, A., JURY, N., MARTINEZ, P., DÍAZ, I., AMARO, A., TRAN, H., MORALES, D., PERTUSA, M., STOICA, L., FRITZ, E., CORVALÁN, D., ABARZÚA, S., MÉNDEZ-RUETTE, M., FERNÁNDEZ, P., ROJAS, F., KUMAR, M. S., AGUILAR, R., ALMEIDA, S., WEISS, A., BUSTOS, F. J., GONZÁLEZ-NILO, F., OTERO, C., TEVY, M. F., BOSCO, D. A., SÁEZ, J. C., KÄHNE, T., GAO, F.-B., BERRY, J. D., NICHOLSON, K., SENA-ESTEVES, M., MADRID, R., VARELA, D., MONTECINO, M., BROWN, R. H. & VAN

ZUNDERT, B. 2022. Excessive release of inorganic polyphosphate by ALS/FTD astrocytes causes non-cell-autonomous toxicity to motoneurons. *Neuron,* 110**,** 1656-1670.e12.

ASH, P. E., BIENIEK, K. F., GENDRON, T. F., CAULFIELD, T., LIN, W. L., DEJESUS-HERNANDEZ, M., VAN BLITTERSWIJK, M. M., JANSEN-WEST, K., PAUL, J. W., 3RD, RADEMAKERS, R., BOYLAN, K. B., DICKSON, D. W. & PETRUCELLI, L. 2013. Unconventional translation of C9ORF72 GGGGCC expansion generates insoluble polypeptides specific to c9FTD/ALS. *Neuron,* 77**,** 639-46.

AVERSANO, S., CAIAZZA, C. & CAIAZZO, M. 2022. Induced pluripotent stem cell-derived and directly reprogrammed neurons to study neurodegenerative diseases: The impact of aging signatures. *Front Aging Neurosci,* 14**,** 1069482.

BABORIE, A., GRIFFITHS, T. D., JAROS, E., PERRY, R., MCKEITH, I. G., BURN, D. J., MASUDA-SUZUKAKE, M., HASEGAWA, M., ROLLINSON, S., PICKERING-BROWN, S., ROBINSON, A. C., DAVIDSON, Y. S. & MANN, D. M. 2015. Accumulation of dipeptide repeat proteins predates that of TDP-43 in frontotemporal lobar degeneration associated with hexanucleotide repeat expansions in C9ORF72 gene. *Neuropathol Appl Neurobiol,* 41**,** 601-12.

BÁEZ-MENDOZA, R. & SCHULTZ, W. 2013. The role of the striatum in social behavior. *Front Neurosci,* 7**,** 233.

BAKER, M., MACKENZIE, I. R., PICKERING-BROWN, S. M., GASS, J., RADEMAKERS, R., LINDHOLM, C., SNOWDEN, J., ADAMSON, J., SADOVNICK, A. D. & ROLLINSON, S. 2006. Mutations in progranulin cause tau-negative frontotemporal dementia linked to chromosome 17. *Nature,* 442**,** 916-919.

BALDWIN, K. R., GODENA, V. K., HEWITT, V. L. & WHITWORTH, A. J. 2016. Axonal transport defects are a common phenotype in Drosophila models of ALS. *Hum Mol Genet,* 25**,** 2378-2392.

BALENDRA, R. & ISAACS, A. M. 2018. C9orf72-mediated ALS and FTD: multiple pathways to disease. *Nat Rev Neurol,* 14**,** 544-558.

BALLEINE, B. W., DELGADO, M. R. & HIKOSAKA, O. 2007. The role of the dorsal striatum in reward and decision-making. *J Neurosci,* 27**,** 8161-5.

BARBEITO, L. 2018. Astrocyte-based cell therapy: new hope for amyotrophic lateral sclerosis patients? *Stem Cell Research & Therapy,* 9**,** 241.

BARBER, S. C. & SHAW, P. J. 2010. Oxidative stress in ALS: key role in motor neuron injury and therapeutic target. *Free Radic Biol Med,* 48**,** 629-41.

BARBIER, M., CAMUZAT, A., EL HACHIMI, K., GUEGAN, J., RINALDI, D., LATTANTE, S., HOUOT, M., SÁNCHEZ-VALLE, R., SABATELLI, M. & ANTONELL, A. 2021a. SLITRK2, an X-linked modifier of the age at onset in C9orf72 frontotemporal lobar degeneration. *Brain,* 144**,** 2798-2811.

BARBIER, M., CAMUZAT, A., HACHIMI, K. E., GUEGAN, J., RINALDI, D., LATTANTE, S., HOUOT, M., SÁNCHEZ-VALLE, R., SABATELLI, M., ANTONELL, A., MOLINA-PORCEL, L., CLOT, F., COURATIER, P., VAN DER ENDE, E., VAN DER ZEE, J., MANZONI, C., CAMU, W., CAZENEUVE, C., SELLAL, F., DIDIC, M., GOLFIER, V., PASQUIER, F., DUYCKAERTS, C., ROSSI, G., BRUNI, A. C., ALVAREZ, V., GÓMEZ-TORTOSA, E., DE MENDONÇA, A., GRAFF, C., MASELLIS, M., NACMIAS, B., OUMOUSSA, B. M., JORNEA, L., FORLANI, S., VAN DEERLIN, V., ROHRER, J. D., GELPI, E., RADEMAKERS, R., VAN SWIETEN, J., LE GUERN, E., VAN BROECKHOVEN, C., FERRARI, R., GÉNIN, E., BRICE, A. & LE BER, I. 2021b.

SLITRK2, an X-linked modifier of the age at onset in C9orf72 frontotemporal lobar degeneration. *Brain,* 144**,** 2798-2811.

BAUER, C. S., COHEN, R. N., SIRONI, F., LIVESEY, M. R., GILLINGWATER, T. H., HIGHLEY, J. R., FILLINGHAM, D. J., COLDICOTT, I., SMITH, E. F., GIBSON, Y. B., WEBSTER, C. P., GRIERSON, A. J., BENDOTTI, C. & DE VOS, K. J. 2022a. An interaction between synapsin and C9orf72 regulates excitatory synapses and is impaired in ALS/FTD. *Acta Neuropathol,* 144**,** 437-464.

BAUER, C. S., WEBSTER, C. P., SHAW, A. C., KOK, J. R., CASTELLI, L. M., LIN, Y. H., SMITH, E. F., ILLANES-ÁLVAREZ, F., HIGGINBOTTOM, A., SHAW, P. J., AZZOUZ, M., FERRAIUOLO, L., HAUTBERGUE, G. M., GRIERSON, A. J. & DE VOS, K. J. 2022b. Loss of TMEM106B exacerbates C9ALS/FTD DPR pathology by disrupting autophagosome maturation. *Front Cell Neurosci,* 16**,** 1061559.

BECK, J., POULTER, M., HENSMAN, D., ROHRER, J. D., MAHONEY, C. J., ADAMSON, G., CAMPBELL, T., UPHILL, J., BORG, A. & FRATTA, P. 2013. Large C9orf72 hexanucleotide repeat expansions are seen in multiple neurodegenerative syndromes and are more frequent than expected in the UK population. *The American Journal of Human Genetics,* 92**,** 345-353.

BECKER, A. J., MCCULLOCH, E. A. & TILL, J. E. 1963. Cytological Demonstration of the Clonal Nature of Spleen Colonies Derived from Transplanted Mouse Marrow Cells. *Nature,* 197**,** 452-454.

BEDE, P., BOKDE, A. L., BYRNE, S., ELAMIN, M., MCLAUGHLIN, R. L., KENNA, K., FAGAN, A. J., PENDER, N., BRADLEY, D. G. & HARDIMAN, O. 2013a. Multiparametric MRI study of ALS stratified for the C9orf72 genotype. *Neurology,* 81**,** 361-9.

BEDE, P., ELAMIN, M., BYRNE, S., MCLAUGHLIN, R. L., KENNA, K., VAJDA, A., PENDER, N., BRADLEY, D. G. & HARDIMAN, O. 2013b. Basal ganglia involvement in amyotrophic lateral sclerosis. *Neurology,* 81**,** 2107-15.

BELL, S. M., DE MARCO, M., BARNES, K., SHAW, P. J., FERRAIUOLO, L., BLACKBURN, D. J., MORTIBOYS, H. & VENNERI, A. 2020. Deficits in Mitochondrial Spare Respiratory Capacity Contribute to the Neuropsychological Changes of Alzheimer's Disease. *Journal of Personalized Medicine,* 10**,** 32.

BELZIL, V. V., BAUER, P. O., GENDRON, T. F., MURRAY, M. E., DICKSON, D. & PETRUCELLI, L. 2014. Characterization of DNA hypermethylation in the cerebellum of c9FTD/ALS patients. *Brain research,* 1584**,** 15-21.

BELZIL, V. V., BAUER, P. O., PRUDENCIO, M., GENDRON, T. F., STETLER, C. T., YAN, I. K., PREGENT, L., DAUGHRITY, L., BAKER, M. C. & RADEMAKERS, R. 2013. Reduced C9orf72 gene expression in c9FTD/ALS is caused by histone trimethylation, an epigenetic event detectable in blood. *Acta neuropathologica,* 126**,** 895-905.

BENDOTTI, C., TORTAROLO, M., SUCHAK, S. K., CALVARESI, N., CARVELLI, L., BASTONE, A., RIZZI, M., RATTRAY, M. & MENNINI, T. 2001. Transgenic SOD1 G93A mice develop reduced GLT-1 in spinal cord without alterations in cerebrospinal fluid glutamate levels. *Journal of neurochemistry,* 79**,** 737-746.

BENFENATI, V., CAPRINI, M., DOVIZIO, M., MYLONAKOU, M. N., FERRONI, S., OTTERSEN, O. P. & AMIRY-MOGHADDAM, M. 2011. An aquaporin-4/transient receptor potential vanilloid 4 (AQP4/TRPV4) complex is essential for cell-volume control in astrocytes. *Proc Natl Acad Sci U S A,* 108**,** 2563-8.

BENNINGER, F., GLAT, M. J., OFFEN, D. & STEINER, I. 2016. Glial fibrillary acidic protein as a marker of astrocytic activation in the cerebrospinal fluid of patients with amyotrophic lateral sclerosis. *J Clin Neurosci,* 26**,** 75-8.

BENNION CALLISTER, J., RYAN, S., SIM, J., ROLLINSON, S. & PICKERING-BROWN, S. M. 2016. Modelling C9orf72 dipeptide repeat proteins of a physiologically relevant size. *Hum Mol Genet,* 25**,** 5069-5082.

BENSIMON, G., LACOMBLEZ, L. & MEININGER, V. 1994. A controlled trial of riluzole in amyotrophic lateral sclerosis. ALS/Riluzole Study Group. *N Engl J Med,* 330**,** 585-91.

BENUSSI, A., COSSEDDU, M., FILARETO, I., DELL'ERA, V., ARCHETTI, S., SOFIA COTELLI, M., MICHELI, A., PADOVANI, A. & BORRONI, B. 2016. Impaired long-term potentiation-like cortical plasticity in presymptomatic genetic frontotemporal dementia. *Ann Neurol,* 80**,** 472-6.

BERTOUX, M., FLANAGAN, E. C., HOBBS, M., RUIZ-TAGLE, A., DELGADO, C., MIRANDA, M., IBÁÑEZ, A., SLACHEVSKY, A. & HORNBERGER, M. 2018. Structural anatomical investigation of long-term memory deficit in behavioral frontotemporal dementia. *Journal of Alzheimer's Disease,* 62**,** 1887-1900.

BERTOUX, M., O'CALLAGHAN, C., FLANAGAN, E., HODGES, J. R. & HORNBERGER, M. 2015. Fronto-Striatal Atrophy in Behavioral Variant Frontotemporal Dementia and Alzheimer's Disease. *Front Neurol,* 6**,** 147.

BHANDARI, R., KUHAD, A. & KUHAD, A. 2018. Edaravone: a new hope for deadly amyotrophic lateral sclerosis. *Drugs Today (Barc),* 54**,** 349-360.

BILSLAND, L. G., NIRMALANANTHAN, N., YIP, J., GREENSMITH, L. & DUCHEN, M. R. 2008. Expression of mutant SOD1 in astrocytes induces functional deficits in motoneuron mitochondria. *J Neurochem,* 107**,** 1271-83.

BILSLAND, L. G., SAHAI, E., KELLY, G., GOLDING, M., GREENSMITH, L. & SCHIAVO, G. 2010. Deficits in axonal transport precede ALS symptoms in vivo. *Proceedings of the National Academy of Sciences,* 107**,** 20523-20528.

BIRGER, A., BEN-DOR, I., OTTOLENGHI, M., TURETSKY, T., GIL, Y., SWEETAT, S., PEREZ, L., BELZER, V., CASDEN, N. & STEINER, D. 2019. Human iPSC-derived astrocytes from ALS patients with mutated C9ORF72 show increased oxidative stress and neurotoxicity. EBioMedicine 50: 274–289.

BIUNDO, F., DEL PRETE, D., ZHANG, H., ARANCIO, O. & D'ADAMIO, L. 2018. A role for tau in learning, memory and synaptic plasticity. *Sci Rep,* 8**,** 3184.

BLAIR, H. A. 2023. Tofersen: First Approval. *Drugs,* 83**,** 1039-1043.

BOCCHETTA, M., MALPETTI, M., TODD, E. G., ROWE, J. B. & ROHRER, J. D. 2021a. Looking beneath the surface: the importance of subcortical structures in frontotemporal dementia. *Brain Commun,* 3**,** fcab158.

BOCCHETTA, M., TODD, E. G., PEAKMAN, G., CASH, D. M., CONVERY, R. S., RUSSELL, L. L., THOMAS, D. L., IGLESIAS, J. E., VAN SWIETEN, J. C. & JISKOOT, L. C. 2021b. Differential early subcortical involvement in genetic FTD within the GENFI cohort. *NeuroImage: Clinical,* 30**,** 102646.

BOEYNAEMS, S., BOGAERT, E., KOVACS, D., KONIJNENBERG, A., TIMMERMAN, E., VOLKOV, A., GUHAROY, M., DE DECKER, M., JASPERS, T., RYAN, V. H., JANKE, A. M., BAATSEN, P., VERCRUYSSE, T., KOLAITIS, R. M., DAELEMANS, D., TAYLOR, J. P., KEDERSHA, N., ANDERSON, P., IMPENS, F., SOBOTT, F., SCHYMKOWITZ, J., ROUSSEAU, F., FAWZI, N. L., ROBBERECHT, W., VAN DAMME, P., TOMPA, P. & VAN DEN BOSCH, L. 2017. Phase

Separation of C9orf72 Dipeptide Repeats Perturbs Stress Granule Dynamics. *Mol Cell,* 65**,** 1044-1055.e5.

BONHAM, L. W., GEIER, E. G., SIRKIS, D. W., LEONG, J. K., RAMOS, E. M., WANG, Q., KARYDAS, A., LEE, S. E., STURM, V. E. & SAWYER, R. P. 2023. Radiogenomics of C9orf72 expansion carriers reveals global transposable element derepression and enables prediction of thalamic atrophy and clinical impairment. *Journal of Neuroscience,* 43**,** 333-345.

BONNEVIE, V., DIMINTIYANOVA, K., HEDEGAARD, A., LEHNHOFF, J., GRØNDAHL, L., MOLDOVAN, M. & MEEHAN, C. 2020. Shorter axon initial segments do not cause repetitive firing impairments in the adult presymptomatic G127X SOD-1 Amyotrophic Lateral Sclerosis mouse. *Scientific reports,* 10**,** 1280.

BOOKER, S. A., DE OLIVEIRA, L. S., ANSTEY, N. J., KOZIC, Z., DANDO, O. R., JACKSON, A. D., BAXTER, P. S., ISOM, L. L., SHERMAN, D. L. & HARDINGHAM, G. E. 2020. Input-output relationship of CA1 pyramidal neurons reveals intact homeostatic mechanisms in a mouse model of fragile X syndrome. *Cell Reports,* 32.

BOURON, A., KISELYOV, K. & OBERWINKLER, J. 2015. Permeation, regulation and control of expression of TRP channels by trace metal ions. *Pflugers Arch,* 467**,** 1143-64.

BOYLAN, K. 2015. Familial Amyotrophic Lateral Sclerosis. *Neurol Clin,* 33**,** 807-30.

BREEVOORT, S., GIBSON, S., FIGUEROA, K., BROMBERG, M. & PULST, S. 2022. Expanding Clinical Spectrum of C9ORF72-Related Disorders and Promising Therapeutic Strategies: A Review. *Neurol Genet,* 8**,** e670.

BRETTSCHNEIDER, J., DEL TREDICI, K., TOLEDO, J. B., ROBINSON, J. L., IRWIN, D. J., GROSSMAN, M., SUH, E., VAN DEERLIN, V. M., WOOD, E. M., BAEK, Y., KWONG, L., LEE, E. B., ELMAN, L., MCCLUSKEY, L., FANG, L., FELDENGUT, S., LUDOLPH, A. C., LEE, V. M., BRAAK, H. & TROJANOWSKI, J. Q. 2013. Stages of pTDP-43 pathology in amyotrophic lateral sclerosis. *Ann Neurol,* 74**,** 20-38.

BRETTSCHNEIDER, J., VAN DEERLIN, V. M., ROBINSON, J. L., KWONG, L., LEE, E. B., ALI, Y. O., SAFREN, N., MONTEIRO, M. J., TOLEDO, J. B., ELMAN, L., MCCLUSKEY, L., IRWIN, D. J., GROSSMAN, M., MOLINA-PORCEL, L., LEE, V. M. & TROJANOWSKI, J. Q. 2012. Pattern of ubiquilin pathology in ALS and FTLD indicates presence of C9ORF72 hexanucleotide expansion. *Acta Neuropathol,* 123**,** 825-39.

BROE, M., KRIL, J. & HALLIDAY, G. M. 2004. Astrocytic degeneration relates to the severity of disease in frontotemporal dementia. *Brain,* 127**,** 2214-2220.

BROOKS, B. R., MILLER, R. G., SWASH, M. & MUNSAT, T. L. 2000. El Escorial revisited: revised criteria for the diagnosis of amyotrophic lateral sclerosis. *Amyotroph Lateral Scler Other Motor Neuron Disord,* 1**,** 293-9.

BROWNSTONE, R. M. 2006. Beginning at the end: repetitive firing properties in the final common pathway. *Prog Neurobiol,* 78**,** 156-72.

BRUIJN, L., BECHER, M., LEE, M., ANDERSON, K., JENKINS, N. A., COPELAND, N. G., SISODIA, S., ROTHSTEIN, J., BORCHELT, D. & PRICE, D. 1997. ALS-linked SOD1 mutant G85R mediates damage to astrocytes and promotes rapidly progressive disease with SOD1-containing inclusions. *Neuron,* 18**,** 327-338.

BRUNO, G., COLISTRA, N., MELLE, G., CEREA, A., HUBAREVICH, A., DELEYE, L., DE ANGELIS, F. & DIPALO, M. 2020. Microfluidic Multielectrode Arrays for Spatially Localized Drug Delivery and Electrical Recordings of Primary Neuronal Cultures. *Front Bioeng Biotechnol,* 8**,** 626.

BURATTI, E. & BARALLE, F. E. 2012. TDP-43: gumming up neurons through protein-protein and protein-RNA interactions. *Trends Biochem Sci,* 37**,** 237-47.

BURATTI, E., BRINDISI, A., GIOMBI, M., TISMINETZKY, S., AYALA, Y. M. & BARALLE, F. E. 2005. TDP-43 binds heterogeneous nuclear ribonucleoprotein A/B through its C-terminal tail: an important region for the inhibition of cystic fibrosis transmembrane conductance regulator exon 9 splicing. *J Biol Chem,* 280**,** 37572-84.

BURBERRY, A., SUZUKI, N., WANG, J. Y., MOCCIA, R., MORDES, D. A., STEWART, M. H., SUZUKI-UEMATSU, S., GHOSH, S., SINGH, A., MERKLE, F. T., KOSZKA, K., LI, Q. Z., ZON, L., ROSSI, D. J., TROWBRIDGE, J. J., NOTARANGELO, L. D. & EGGAN, K. 2016. Loss-of-function mutations in the C9ORF72 mouse ortholog cause fatal autoimmune disease. *Sci Transl Med,* 8**,** 347ra93.

BURLEY, S., BECCANO-KELLY, D. A., TALBOT, K., LLANA, O. C. & WADE-MARTINS, R. 2022. Hyperexcitability in young iPSC-derived C9ORF72 mutant motor neurons is associated with increased intracellular calcium release. *Sci Rep,* 12**,** 7378.

BURRELL, J. R., HALLIDAY, G. M., KRIL, J. J., ITTNER, L. M., GÖTZ, J., KIERNAN, M. C. & HODGES, J. R. 2016. The frontotemporal dementia-motor neuron disease continuum. *Lancet,* 388**,** 919-31.

BURSCH, F., KALMBACH, N., NAUJOCK, M., STAEGE, S., EGGENSCHWILER, R., ABO-RADY, M., JAPTOK, J., GUO, W., HENSEL, N., REINHARDT, P., BOECKERS, T. M., CANTZ, T., STERNECKERT, J., VAN DEN BOSCH, L., HERMANN, A., PETRI, S. & WEGNER, F. 2019. Altered calcium dynamics and glutamate receptor properties in iPSC-derived motor neurons from ALS patients with C9orf72, FUS, SOD1 or TDP43 mutations. *Human Molecular Genetics,* 28**,** 2835-2850.

BUTTI, Z., PAN, Y. E., GIACOMOTTO, J. & PATTEN, S. A. 2021. Reduced C9orf72 function leads to defective synaptic vesicle release and neuromuscular dysfunction in zebrafish. *Communications Biology,* 4**,** 792.

BUTTI, Z. & PATTEN, S. A. 2019. RNA dysregulation in amyotrophic lateral sclerosis. *Frontiers in genetics,* 9**,** 419229.

BYLICKY, M. A., MUELLER, G. P. & DAY, R. M. 2018. Mechanisms of endogenous neuroprotective effects of astrocytes in brain injury. *Oxidative medicine and cellular longevity,* 2018.

CAPPELLO, V. & FRANCOLINI, M. 2017. Neuromuscular Junction Dismantling in Amyotrophic Lateral Sclerosis. *Int J Mol Sci,* 18.

CASSINA, P., CASSINA, A., PEHAR, M., CASTELLANOS, R., GANDELMAN, M., DE LEÓN, A., ROBINSON, K. M., MASON, R. P., BECKMAN, J. S., BARBEITO, L. & RADI, R. 2008. Mitochondrial dysfunction in SOD1G93A-bearing astrocytes promotes motor neuron degeneration: prevention by mitochondrial-targeted antioxidants. *J Neurosci,* 28**,** 4115-22.

CASTELLI, L. M., CUTILLO, L., SOUZA, C. D. S., SANCHEZ-MARTINEZ, A., GRANATA, I., LIN, Y.-H., MYSZCZYNSKA, M. A., HEATH, P. R., LIVESEY, M. R., NING, K., AZZOUZ, M., SHAW, P. J., GUARRACINO, M. R., WHITWORTH, A. J., FERRAIUOLO, L., MILO, M. & HAUTBERGUE, G. M. 2021. SRSF1-dependent inhibition of C9ORF72-repeat RNA nuclear export: genome-wide mechanisms for neuroprotection in amyotrophic lateral sclerosis. *Molecular Neurodegeneration,* 16**,** 53.

CATANESE, A., RAJKUMAR, S., SOMMER, D., FREISEM, D., WIRTH, A., ALY, A., MASSA-LÓPEZ, D., OLIVIERI, A., TORELLI, F., IOANNIDIS, V., LIPECKA, J., GUERRERA, I. C., ZYTNICKI,

D., LUDOLPH, A., KABASHI, E., MULAW, M. A., ROSELLI, F. & BÖCKERS, T. M. 2021. Synaptic disruption and CREB-regulated transcription are restored by K(+) channel blockers in ALS. *EMBO Mol Med,* 13**,** e13131.

CAVARSAN, C. F., STEELE, P. R., GENRY, L. T., REEDICH, E. J., MCCANE, L. M., LAPRE, K. J., PURITZ, A. C., MANUEL, M., KATENKA, N. & QUINLAN, K. A. 2023. Inhibitory interneurons show early dysfunction in a SOD1 mouse model of amyotrophic lateral sclerosis. *The Journal of Physiology,* 601**,** 647-667.

CHANG, Q. & MARTIN, L. J. 2009. Glycinergic innervation of motoneurons is deficient in amyotrophic lateral sclerosis mice: a quantitative confocal analysis. *Am J Pathol,* 174**,** 574-85.

CHAPMAN, L., COOPER-KNOCK, J. & SHAW, P. 2023. Physical activity as an exogenous risk factor for amyotrophic lateral sclerosis: a review of the evidence. *Brain : a journal of neurology,* 146.

CHARVÉRIAT, M., MOUTHON, F., REIN, W. & VERKHRATSKY, A. 2021. Connexins as therapeutic targets in neurological and neuropsychiatric disorders. *Biochimica et Biophysica Acta (BBA) - Molecular Basis of Disease,* 1867**,** 166098.

CHEN, M. J., KRESS, B., HAN, X., MOLL, K., PENG, W., JI, R. R. & NEDERGAARD, M. 2012. Astrocytic CX43 hemichannels and gap junctions play a crucial role in development of chronic neuropathic pain following spinal cord injury. *Glia,* 60**,** 1660-70.

CHEN, Y., LIN, Z., CHEN, X., CAO, B., WEI, Q., OU, R., ZHAO, B., SONG, W., WU, Y. & SHANG, H.-F. 2016. Large C9orf72 repeat expansions are seen in Chinese patients with sporadic amyotrophic lateral sclerosis. *Neurobiology of aging,* 38**,** 217. e15-217. e22.

CHEW, S. S., JOHNSON, C. S., GREEN, C. R. & DANESH-MEYER, H. V. 2010. Role of connexin43 in central nervous system injury. *Exp Neurol,* 225**,** 250-61.

CHIÒ, A., LOGROSCINO, G., HARDIMAN, O., SWINGLER, R., MITCHELL, D., BEGHI, E. & TRAYNOR, B. G. 2009. Prognostic factors in ALS: A critical review. *Amyotroph Lateral Scler,* 10**,** 310-23.

CHIÒ, A., RESTAGNO, G., BRUNETTI, M., OSSOLA, I., CALVO, A., CANOSA, A., MOGLIA, C., FLORIS, G., TACCONI, P. & MARROSU, F. 2012. ALS/FTD phenotype in two Sardinian families carrying both C9ORF72 and TARDBP mutations. *Journal of Neurology, Neurosurgery & Psychiatry,* 83**,** 730-733.

CHOI, S. Y., LOPEZ-GONZALEZ, R., KRISHNAN, G., PHILLIPS, H. L., LI, A. N., SEELEY, W. W., YAO, W.-D., ALMEIDA, S. & GAO, F.-B. 2019. C9ORF72-ALS/FTD-associated poly (GR) binds Atp5a1 and compromises mitochondrial function in vivo. *Nature neuroscience,* 22**,** 851-862.

CHRIST, G. J., MORENO, A. P., MELMAN, A. & SPRAY, D. C. 1992. Gap junction-mediated intercellular diffusion of Ca2+ in cultured human corporal smooth muscle cells. *American Journal of Physiology-Cell Physiology,* 263**,** C373-C383.

CHRISTIDI, F., KARAVASILIS, E., RENTZOS, M., KELEKIS, N., EVDOKIMIDIS, I. & BEDE, P. 2018. Clinical and radiological markers of extra-motor deficits in amyotrophic lateral sclerosis. *Frontiers in neurology,* 9**,** 1005.

CIEŚLAK, M., ROSZEK, K. & WUJAK, M. 2019. Purinergic implication in amyotrophic lateral sclerosis-from pathological mechanisms to therapeutic perspectives. *Purinergic Signal,* 15**,** 1-15.

CIURA, S., LATTANTE, S., LE BER, I., LATOUCHE, M., TOSTIVINT, H., BRICE, A. & KABASHI, E. 2013. Loss of function of C9orf72 causes motor deficits in a zebrafish model of amyotrophic lateral sclerosis. *Ann Neurol,* 74**,** 180-7.

CLARK, R. M., CLARK, C. M., LEWIS, K. E. A., DYER, M. S., CHUCKOWREE, J. A., HOYLE, J. A., BLIZZARD, C. A. & DICKSON, T. C. 2023. Intranasal neuropeptide Y1 receptor antagonism improves motor deficits in symptomatic SOD1 ALS mice. *Ann Clin Transl Neurol,* 10**,** 1985-1999.

CLAY, J. R. & SHLESINGER, M. F. 1984. Analysis of the effects of cesium ions on potassium channel currents in biological membranes. *J Theor Biol,* 107**,** 189-201.

CLEMENT, A. M., NGUYEN, M. D., ROBERTS, E. A., GARCIA, M. L., BOILLÉE, S., RULE, M., MCMAHON, A. P., DOUCETTE, W., SIWEK, D., FERRANTE, R. J., BROWN, R. H., JULIEN, J.-P., GOLDSTEIN, L. S. B. & CLEVELAND, D. W. 2003. Wild-Type Nonneuronal Cells Extend Survival of SOD1 Mutant Motor Neurons in ALS Mice. *Science,* 302**,** 113-117.

CLEVELAND, D. W. & ROTHSTEIN, J. D. 2001. From Charcot to Lou Gehrig: deciphering selective motor neuron death in ALS. *Nat Rev Neurosci,* 2**,** 806-19.

COLEMAN, M. P. 2022. Axon Biology in ALS: Mechanisms of Axon Degeneration and Prospects for Therapy. *Neurotherapeutics,* 19**,** 1133-1144.

CONFORTI, P., BOCCHI, V. D., CAMPUS, I., SCARAMUZZA, L., GALIMBERTI, M., LISCHETTI, T., TALPO, F., PEDRAZZOLI, M., MURGIA, A., FERRARI, I., CORDIGLIERI, C., FASCIANI, A., ARENAS, E., FELSENFELD, D., BIELLA, G., BESUSSO, D. & CATTANEO, E. 2022. In vitro-derived medium spiny neurons recapitulate human striatal development and complexity at single-cell resolution. *Cell Rep Methods,* 2**,** 100367.

CONSONNI, M., CONTARINO, V. E., CATRICALÀ, E., DALLA BELLA, E., PENSATO, V., GELLERA, C., LAURIA, G. & CAPPA, S. F. 2018. Cortical markers of cognitive syndromes in amyotrophic lateral sclerosis. *Neuroimage Clin,* 19**,** 675-682.

CONTRERAS, J. E., SÁEZ, J. C., BUKAUSKAS, F. F. & BENNETT, M. V. 2003. Gating and regulation of connexin 43 (Cx43) hemichannels. *Proc Natl Acad Sci U S A,* 100**,** 11388-93.

COOPER-KNOCK, J., HEWITT, C., HIGHLEY, J. R., BROCKINGTON, A., MILANO, A., MAN, S., MARTINDALE, J., HARTLEY, J., WALSH, T. & GELSTHORPE, C. 2012. Clinico-pathological features in amyotrophic lateral sclerosis with expansions in C9ORF72. *Brain,* 135**,** 751-764.

COOPER-KNOCK, J., HIGGINBOTTOM, A., STOPFORD, M. J., HIGHLEY, J. R., INCE, P. G., WHARTON, S. B., PICKERING-BROWN, S., KIRBY, J., HAUTBERGUE, G. M. & SHAW, P. J. 2015. Antisense RNA foci in the motor neurons of C9ORF72-ALS patients are associated with TDP-43 proteinopathy. *Acta Neuropathol,* 130**,** 63-75.

COZZOLINO, M. & CARRÌ, M. T. 2012. Mitochondrial dysfunction in ALS. *Prog Neurobiol,* 97**,** 54-66.

CRINION, J., TURNER, R., GROGAN, A., HANAKAWA, T., NOPPENEY, U., DEVLIN, J. T., ASO, T., URAYAMA, S., FUKUYAMA, H., STOCKTON, K., USUI, K., GREEN, D. W. & PRICE, C. J. 2006. Language control in the bilingual brain. *Science,* 312**,** 1537-40.

CRITTENDEN, J. R. & GRAYBIEL, A. M. 2011. Basal Ganglia disorders associated with imbalances in the striatal striosome and matrix compartments. *Frontiers in neuroanatomy,* 5**,** 59.

CROWN, A. M., ROBERTS, B. L., CROSBY, K., BROWN, H., AYERS, J. I., HART, P. J. & BORCHELT, D. R. 2019. Experimental Mutations in Superoxide Dismutase 1 Provide Insight into

Potential Mechanisms Involved in Aberrant Aggregation in Familial Amyotrophic Lateral Sclerosis. *G3 (Bethesda),* 9**,** 719-728.

CRUTS, M., GIJSELINCK, I., VAN DER ZEE, J., ENGELBORGHS, S., WILS, H., PIRICI, D., RADEMAKERS, R., VANDENBERGHE, R., DERMAUT, B. & MARTIN, J.-J. 2006. Null mutations in progranulin cause ubiquitin-positive frontotemporal dementia linked to chromosome 17q21. *Nature,* 442**,** 920-924.

CUI, Y., MASAKI, K., YAMASAKI, R., IMAMURA, S., SUZUKI, S. O., HAYASHI, S., SATO, S., NAGARA, Y., KAWAMURA, M. F. & KIRA, J.-I. 2014. Extensive dysregulations of oligodendrocytic and astrocytic connexins are associated with disease progression in an amyotrophic lateral sclerosis mouse model. *Journal of neuroinflammation,* 11**,** 1-16.

CYKOWSKI, M. D., DICKSON, D. W., POWELL, S. Z., ARUMANAYAGAM, A. S., RIVERA, A. L. & APPEL, S. H. 2019. Dipeptide repeat (DPR) pathology in the skeletal muscle of ALS patients with C9ORF72 repeat expansion. *Acta Neuropathol,* 138**,** 667-670.

DAFINCA, R., BARBAGALLO, P., FARRIMOND, L., CANDALIJA, A., SCABER, J., ABABNEH, N. A., SATHYAPRAKASH, C., VOWLES, J., COWLEY, S. A. & TALBOT, K. 2020. Impairment of Mitochondrial Calcium Buffering Links Mutations in C9ORF72 and TARDBP in iPS-Derived Motor Neurons from Patients with ALS/FTD. *Stem Cell Reports,* 14**,** 892-908.

DAFINCA, R., SCABER, J., ABABNEH, N., LALIC, T., WEIR, G., CHRISTIAN, H., VOWLES, J., DOUGLAS, A. G., FLETCHER-JONES, A., BROWNE, C., NAKANISHI, M., TURNER, M. R., WADE-MARTINS, R., COWLEY, S. A. & TALBOT, K. 2016. C9orf72 Hexanucleotide Expansions Are Associated with Altered Endoplasmic Reticulum Calcium Homeostasis and Stress Granule Formation in Induced Pluripotent Stem Cell-Derived Neurons from Patients with Amyotrophic Lateral Sclerosis and Frontotemporal Dementia. *Stem Cells,* 34**,** 2063-78.

DAVIDSON, J. S., BAUMGARTEN, I. M. & HARLEY, E. H. 1986. Reversible inhibition of intercellular junctional communication by glycyrrhetinic acid. *Biochemical and Biophysical Research Communications,* 134**,** 29-36.

DAVIDSON, Y., ROBINSON, A. C., LIU, X., WU, D., TROAKES, C., ROLLINSON, S., MASUDA-SUZUKAKE, M., SUZUKI, G., NONAKA, T., SHI, J., TIAN, J., HAMDALLA, H., EALING, J., RICHARDSON, A., JONES, M., PICKERING-BROWN, S., SNOWDEN, J. S., HASEGAWA, M. & MANN, D. M. 2016. Neurodegeneration in frontotemporal lobar degeneration and motor neurone disease associated with expansions in C9orf72 is linked to TDP-43 pathology and not associated with aggregated forms of dipeptide repeat proteins. *Neuropathol Appl Neurobiol,* 42**,** 242-54.

DE CONTI, L., AKINYI, M. V., MENDOZA-MALDONADO, R., ROMANO, M., BARALLE, M. & BURATTI, E. 2015. TDP-43 affects splicing profiles and isoform production of genes involved in the apoptotic and mitotic cellular pathways. *Nucleic Acids Res,* 43**,** 8990-9005.

DE VOCHT, J., BLOMMAERT, J., DEVROME, M., RADWAN, A., VAN WEEHAEGHE, D., DE SCHAEPDRYVER, M., CECCARINI, J., REZAEI, A., SCHRAMM, G., VAN AALST, J., CHIÒ, A., PAGANI, M., STAM, D., VAN ESCH, H., LAMAIRE, N., VERHAEGEN, M., MERTENS, N., POESEN, K., VAN DEN BERG, L. H., VAN ES, M. A., VANDENBERGHE, R., VANDENBULCKE, M., VAN DEN STOCK, J., KOOLE, M., DUPONT, P., VAN LAERE, K. & VAN DAMME, P. 2020. Use of Multimodal Imaging and Clinical Biomarkers in Presymptomatic Carriers of C9orf72 Repeat Expansion. *JAMA Neurol,* 77**,** 1008-1017.

DE VOS, K. J., CHAPMAN, A. L., TENNANT, M. E., MANSER, C., TUDOR, E. L., LAU, K.-F., BROWNLEES, J., ACKERLEY, S., SHAW, P. J. & MCLOUGHLIN, D. M. 2007. Familial amyotrophic lateral sclerosis-linked SOD1 mutants perturb fast axonal transport to reduce axonal mitochondria content. *Human molecular genetics,* 16**,** 2720-2728.

DEJESUS-HERNANDEZ, M., FINCH, N. A., WANG, X., GENDRON, T. F., BIENIEK, K. F., HECKMAN, M. G., VASILEVICH, A., MURRAY, M. E., ROUSSEAU, L., WEESNER, R., LUCIDO, A., PARSONS, M., CHEW, J., JOSEPHS, K. A., PARISI, J. E., KNOPMAN, D. S., PETERSEN, R. C., BOEVE, B. F., GRAFF-RADFORD, N. R., DE BOER, J., ASMANN, Y. W., PETRUCELLI, L., BOYLAN, K. B., DICKSON, D. W., VAN BLITTERSWIJK, M. & RADEMAKERS, R. 2017. In-depth clinico-pathological examination of RNA foci in a large cohort of C9ORF72 expansion carriers. *Acta Neuropathol,* 134**,** 255-269.

DEJESUS-HERNANDEZ, M., MACKENZIE, I. R., BOEVE, B. F., BOXER, A. L., BAKER, M., RUTHERFORD, N. J., NICHOLSON, A. M., FINCH, N. A., FLYNN, H., ADAMSON, J., KOURI, N., WOJTAS, A., SENGDY, P., HSIUNG, G. Y., KARYDAS, A., SEELEY, W. W., JOSEPHS, K. A., COPPOLA, G., GESCHWIND, D. H., WSZOLEK, Z. K., FELDMAN, H., KNOPMAN, D. S., PETERSEN, R. C., MILLER, B. L., DICKSON, D. W., BOYLAN, K. B., GRAFF-RADFORD, N. R. & RADEMAKERS, R. 2011. Expanded GGGGCC hexanucleotide repeat in noncoding region of C9ORF72 causes chromosome 9p-linked FTD and ALS. *Neuron,* 72**,** 245-56.

DELEKATE, A., FÜCHTEMEIER, M., SCHUMACHER, T., ULBRICH, C., FODDIS, M. & PETZOLD, G. C. 2014. Metabotropic P2Y1 receptor signalling mediates astrocytic hyperactivity in vivo in an Alzheimer's disease mouse model. *Nature Communications,* 5**,** 5422.

DELGADO, M. R. 2007. Reward-related responses in the human striatum. *Annals of the New York Academy of Sciences,* 1104**,** 70-88.

DEMING, Y. & CRUCHAGA, C. 2014. TMEM106B: a strong FTLD disease modifier. *Acta neuropathologica,* 127**,** 419-422.

DEVENNEY, E., HORNBERGER, M., IRISH, M., MIOSHI, E., BURRELL, J., TAN, R., KIERNAN, M. C. & HODGES, J. R. 2014. Frontotemporal dementia associated with the C9ORF72 mutation: a unique clinical profile. *JAMA Neurol,* 71**,** 331-9.

DEVLIN, A.-C., BURR, K., BOROOAH, S., FOSTER, J. D., CLEARY, E. M., GETI, I., VALLIER, L., SHAW, C. E., CHANDRAN, S. & MILES, G. B. 2015. Human iPSC-derived motoneurons harbouring TARDBP or C9ORF72 ALS mutations are dysfunctional despite maintaining viability. *Nature Communications,* 6**,** 5999.

DEVOS, D., MOREAU, C., KYHENG, M., GARÇON, G., ROLLAND, A. S., BLASCO, H., GELÉ, P., TIMOTHÉE LENGLET, T., VEYRAT-DUREBEX, C. & CORCIA, P. 2019. A ferroptosis–based panel of prognostic biomarkers for Amyotrophic Lateral Sclerosis. *Scientific reports,* 9**,** 2918.

DHARMADASA, T., SCABER, J., EDMOND, E., MARSDEN, R., THOMPSON, A., TALBOT, K. & TURNER, M. R. 2022. Genetic testing in motor neurone disease. *Pract Neurol,* 22**,** 107-116.

DI GIORGIO, F. P., BOULTING, G. L., BOBROWICZ, S. & EGGAN, K. C. 2008. Human embryonic stem cell-derived motor neurons are sensitive to the toxic effect of glial cells carrying an ALS-causing mutation. *Cell Stem Cell,* 3**,** 637-48.

DI GIORGIO, F. P., CARRASCO, M. A., SIAO, M. C., MANIATIS, T. & EGGAN, K. 2007. Non-cell autonomous effect of glia on motor neurons in an embryonic stem cell-based ALS model. *Nat Neurosci,* 10**,** 608-14.

DIAB, R., PILOTTO, F. & SAXENA, S. 2023. Autophagy and neurodegeneration: Unraveling the role of C9ORF72 in the regulation of autophagy and its relationship to ALS-FTD pathology. *Front Cell Neurosci,* 17**,** 1086895.

DIAS, F. C., ALVES, V. S., MATIAS, D. O., FIGUEIREDO, C. P., MIRANDA, A. L. P., PASSOS, G. F. & COSTA, R. 2019. The selective TRPV4 channel antagonist HC-067047 attenuates mechanical allodynia in diabetic mice. *European Journal of Pharmacology,* 856**,** 172408.

DÍAZ-AMARILLA, P., OLIVERA-BRAVO, S., TRIAS, E., CRAGNOLINI, A., MARTÍNEZ-PALMA, L., CASSINA, P., BECKMAN, J. & BARBEITO, L. 2011. Phenotypically aberrant astrocytes that promote motoneuron damage in a model of inherited amyotrophic lateral sclerosis. *Proceedings of the National Academy of Sciences,* 108**,** 18126-18131.

DIRKX, N., MICELI, F., TAGLIALATELA, M. & WECKHUYSEN, S. 2020. The Role of Kv7.2 in Neurodevelopment: Insights and Gaps in Our Understanding. *Front Physiol,* 11**,** 570588.

DOBLE, A. 1996. The pharmacology and mechanism of action of riluzole. *Neurology,* 47**,** 233S-241S.

DOLS-ICARDO, O., GARCÍA-REDONDO, A., ROJAS-GARCÍA, R., SÁNCHEZ-VALLE, R., NOGUERA, A., GÓMEZ-TORTOSA, E., PASTOR, P., HERNÁNDEZ, I., ESTEBAN-PÉREZ, J. & SUÁREZ-CALVET, M. 2014. Characterization of the repeat expansion size in C9orf72 in amyotrophic lateral sclerosis and frontotemporal dementia. *Human molecular genetics,* 23**,** 749-754.

DONNELLY, C. J., ZHANG, P.-W., PHAM, J. T., HAEUSLER, A. R., MISTRY, N. A., VIDENSKY, S., DALEY, E. L., POTH, E. M., HOOVER, B. & FINES, D. M. 2013. RNA toxicity from the ALS/FTD C9ORF72 expansion is mitigated by antisense intervention. *Neuron,* 80**,** 415-428.

DU, Z.-W., CHEN, H., LIU, H., LU, J., QIAN, K., HUANG, C.-L., ZHONG, X., FAN, F. & ZHANG, S.-C. 2015. Generation and expansion of highly pure motor neuron progenitors from human pluripotent stem cells. *Nature Communications,* 6**,** 6626.

DUPUIS, L., GONZALEZ DE AGUILAR, J.-L., ECHANIZ-LAGUNA, A., ESCHBACH, J., RENE, F., OUDART, H., HALTER, B., HUZE, C., SCHAEFFER, L. & BOUILLAUD, F. 2009. Muscle mitochondrial uncoupling dismantles neuromuscular junction and triggers distal degeneration of motor neurons. *PloS one,* 4**,** e5390.

DURHAM, P. L. & GARRETT, F. G. 2009. Neurological mechanisms of migraine: potential of the gap-junction modulator tonabersat in prevention of migraine. *Cephalalgia,* 29 Suppl 2**,** 1-6.

DURIEUX, P. F., BEARZATTO, B., GUIDUCCI, S., BUCH, T., WAISMAN, A., ZOLI, M., SCHIFFMANN, S. N. & DE KERCHOVE D'EXAERDE, A. 2009. D2R striatopallidal neurons inhibit both locomotor and drug reward processes. *Nature neuroscience,* 12**,** 393-395.

DYER, M. S., REALE, L. A., LEWIS, K. E., WALKER, A. K., DICKSON, T. C., WOODHOUSE, A. & BLIZZARD, C. A. 2021. Mislocalisation of TDP-43 to the cytoplasm causes cortical hyperexcitability and reduced excitatory neurotransmission in the motor cortex. *J Neurochem,* 157**,** 1300-1315.

EISEN, A., BRAAK, H., DEL TREDICI, K., LEMON, R., LUDOLPH, A. C. & KIERNAN, M. C. 2017. Cortical influences drive amyotrophic lateral sclerosis. *J Neurol Neurosurg Psychiatry,* 88**,** 917-924.

ENGLUND, B., BRUN, A., GUSTAFSON, L., PASSANT, U., MANN, D., NEARY, D. & SNOWDEN, J. 1994. Clinical and neuropathological criteria for frontotemporal dementia. *J Neurol Neurosurg Psychiatry,* 57**,** 416-8.

ESCARTIN, C., GALEA, E., LAKATOS, A., O'CALLAGHAN, J. P., PETZOLD, G. C., SERRANO-POZO, A., STEINHÄUSER, C., VOLTERRA, A., CARMIGNOTO, G., AGARWAL, A., ALLEN, N. J., ARAQUE, A., BARBEITO, L., BARZILAI, A., BERGLES, D. E., BONVENTO, G., BUTT, A. M., CHEN, W.-T., COHEN-SALMON, M., CUNNINGHAM, C., DENEEN, B., DE STROOPER, B., DÍAZ-CASTRO, B., FARINA, C., FREEMAN, M., GALLO, V., GOLDMAN, J. E., GOLDMAN, S. A., GÖTZ, M., GUTIÉRREZ, A., HAYDON, P. G., HEILAND, D. H., HOL, E. M., HOLT, M. G., IINO, M., KASTANENKA, K. V., KETTENMANN, H., KHAKH, B. S., KOIZUMI, S., LEE, C. J., LIDDELOW, S. A., MACVICAR, B. A., MAGISTRETTI, P., MESSING, A., MISHRA, A., MOLOFSKY, A. V., MURAI, K. K., NORRIS, C. M., OKADA, S., OLIET, S. H. R., OLIVEIRA, J. F., PANATIER, A., PARPURA, V., PEKNA, M., PEKNY, M., PELLERIN, L., PEREA, G., PÉREZ-NIEVAS, B. G., PFRIEGER, F. W., POSKANZER, K. E., QUINTANA, F. J., RANSOHOFF, R. M., RIQUELME-PEREZ, M., ROBEL, S., ROSE, C. R., ROTHSTEIN, J. D., ROUACH, N., ROWITCH, D. H., SEMYANOV, A., SIRKO, S., SONTHEIMER, H., SWANSON, R. A., VITORICA, J., WANNER, I.-B., WOOD, L. B., WU, J., ZHENG, B., ZIMMER, E. R., ZOREC, R., SOFRONIEW, M. V. & VERKHRATSKY, A. 2021. Reactive astrocyte nomenclature, definitions, and future directions. *Nature Neuroscience,* 24**,** 312-325.

ESTEBANEZ, L., HOFFMANN, D., VOIGT, B. C. & POULET, J. F. 2017. Parvalbumin-expressing GABAergic neurons in primary motor cortex signal reaching. *Cell reports,* 20**,** 308-318.

EVANS, M. D., DUMITRESCU, A. S., KRUIJSSEN, D. L., TAYLOR, S. E. & GRUBB, M. S. 2015. Rapid modulation of axon initial segment length influences repetitive spike firing. *Cell reports,* 13**,** 1233-1245.

EVANS, M. J. & KAUFMAN, M. H. 1981. Establishment in culture of pluripotential cells from mouse embryos. *Nature,* 292**,** 154-6.

FARG, M. A., SUNDARAMOORTHY, V., SULTANA, J. M., YANG, S., ATKINSON, R. A., LEVINA, V., HALLORAN, M. A., GLEESON, P. A., BLAIR, I. P., SOO, K. Y., KING, A. E. & ATKIN, J. D. 2014. C9ORF72, implicated in amytrophic lateral sclerosis and frontotemporal dementia, regulates endosomal trafficking. *Hum Mol Genet,* 23**,** 3579-95.

FERRAIUOLO, L., HIGGINBOTTOM, A., HEATH, P. R., BARBER, S., GREENALD, D., KIRBY, J. & SHAW, P. J. 2011. Dysregulation of astrocyte-motoneuron cross-talk in mutant superoxide dismutase 1-related amyotrophic lateral sclerosis. *Brain,* 134**,** 2627-41.

FERRANTE, R. J., BROWNE, S. E., SHINOBU, L. A., BOWLING, A. C., BAIK, M. J., MACGARVEY, U., KOWALL, N. W., BROWN JR, R. H. & BEAL, M. F. 1997a. Evidence of increased oxidative damage in both sporadic and familial amyotrophic lateral sclerosis. *Journal of neurochemistry,* 69**,** 2064-2074.

FERRANTE, R. J., SHINOBU, L. A., SCHULZ, J. B., MATTHEWS, R. T., THOMAS, C. E., KOWALL, N. W., GURNEY, M. E. & BEAL, M. F. 1997b. Increased 3-nitrotyrosine and oxidative damage in mice with a human copper/zinc superoxide dismutase mutation. *Annals of Neurology: Official Journal of the American Neurological Association and the Child Neurology Society,* 42**,** 326-334.

FIGIEL, M., ALLRITZ, C., LEHMANN, C. & ENGELE, J. 2007. Gap junctional control of glial glutamate transporter expression. *Molecular and Cellular Neuroscience,* 35**,** 130-137.

FJODOROVA, M., NOAKES, Z. & LI, M. 2015. How to make striatal projection neurons. *Neurogenesis (Austin),* 2**,** e1100227.

FOGARTY, M. J., KLENOWSKI, P. M., LEE, J. D., DRIEBERG-THOMPSON, J. R., BARTLETT, S. E., NGO, S. T., HILLIARD, M. A., BELLINGHAM, M. C. & NOAKES, P. G. 2016a. Cortical synaptic and dendritic spine abnormalities in a presymptomatic TDP-43 model of amyotrophic lateral sclerosis. *Sci Rep,* 6**,** 37968.

FOGARTY, M. J., MU, E. W., NOAKES, P. G., LAVIDIS, N. A. & BELLINGHAM, M. C. 2016b. Marked changes in dendritic structure and spine density precede significant neuronal death in vulnerable cortical pyramidal neuron populations in the SOD1 G93A mouse model of amyotrophic lateral sclerosis. *Acta neuropathologica communications,* 4**,** 1-21.

FOGARTY, M. J., MU, E. W. H., LAVIDIS, N. A., NOAKES, P. G. & BELLINGHAM, M. C. 2017. Motor Areas Show Altered Dendritic Structure in an Amyotrophic Lateral Sclerosis Mouse Model. *Front Neurosci,* 11**,** 609.

FONTÁN-LOZANO, A., SUÁREZ-PEREIRA, I., DELGADO-GARCÍA, J. M. & CARRIÓN, A. M. 2011. The M-current inhibitor XE991 decreases the stimulation threshold for long-term synaptic plasticity in healthy mice and in models of cognitive disease. *Hippocampus,* 21**,** 22-32.

FORAN, E. & TROTTI, D. 2009. Glutamate transporters and the excitotoxic path to motor neuron degeneration in amyotrophic lateral sclerosis. *Antioxid Redox Signal,* 11**,** 1587-602.

FRATTA, P., MIZIELINSKA, S., NICOLL, A. J., ZLOH, M., FISHER, E. M., PARKINSON, G. & ISAACS, A. M. 2012. C9orf72 hexanucleotide repeat associated with amyotrophic lateral sclerosis and frontotemporal dementia forms RNA G-quadruplexes. *Sci Rep,* 2**,** 1016.

FREIBAUM, B. D., LU, Y., LOPEZ-GONZALEZ, R., KIM, N. C., ALMEIDA, S., LEE, K.-H., BADDERS, N., VALENTINE, M., MILLER, B. L., WONG, P. C., PETRUCELLI, L., KIM, H. J., GAO, F.-B. & TAYLOR, J. P. 2015a. GGGGCC repeat expansion in C9orf72 compromises nucleocytoplasmic transport. *Nature,* 525**,** 129-133.

FREIBAUM, B. D., LU, Y., LOPEZ-GONZALEZ, R., KIM, N. C., ALMEIDA, S., LEE, K. H., BADDERS, N., VALENTINE, M., MILLER, B. L., WONG, P. C., PETRUCELLI, L., KIM, H. J., GAO, F. B. & TAYLOR, J. P. 2015b. GGGGCC repeat expansion in C9orf72 compromises nucleocytoplasmic transport. *Nature,* 525**,** 129-33.

FREIBAUM, B. D. & TAYLOR, J. P. 2017. The Role of Dipeptide Repeats in C9ORF72-Related ALS-FTD. *Front Mol Neurosci,* 10**,** 35.

FRERE, S. & SLUTSKY, I. 2018. Alzheimer's disease: from firing instability to homeostasis network collapse. *Neuron,* 97**,** 32-58.

FRICK, P., SELLIER, C., MACKENZIE, I. R. A., CHENG, C. Y., TAHRAOUI-BORIES, J., MARTINAT, C., PASTERKAMP, R. J., PRUDLO, J., EDBAUER, D., OULAD-ABDELGHANI, M., FEEDERLE, R., CHARLET-BERGUERAND, N. & NEUMANN, M. 2018. Novel antibodies reveal presynaptic localization of C9orf72 protein and reduced protein levels in C9orf72 mutation carriers. *Acta Neuropathol Commun,* 6**,** 72.

FUMAGALLI, L., YOUNG, F. L., BOEYNAEMS, S., DE DECKER, M., MEHTA, A. R., SWIJSEN, A., FAZAL, R., GUO, W., MOISSE, M., BECKERS, J., DEDEENE, L., SELVARAJ, B. T., VANDOORNE, T., MADAN, V., VAN BLITTERSWIJK, M., RAITCHEVA, D., MCCAMPBELL, A., POESEN, K., GITLER, A. D., KOCH, P., VANDEN BERGHE, P., THAL, D. R., VERFAILLIE, C., CHANDRAN, S., VAN DEN BOSCH, L., BULLOCK, S. L. & VAN DAMME, P. 2021. C9orf72-derived arginine-containing dipeptide repeats associate with axonal transport machinery and impede microtubule-based motility. *Sci Adv,* 7.

GADEA, A., SCHINELLI, S. & GALLO, V. 2008. Endothelin-1 regulates astrocyte proliferation and reactive gliosis via a JNK/c-Jun signaling pathway. *Journal of Neuroscience,* 28**,** 2394-2408.

GAGE, FRED H. & TEMPLE, S. 2013. Neural Stem Cells: Generating and Regenerating the Brain. *Neuron,* 80**,** 588-601.

GALLAGHER, M. D., SUH, E., GROSSMAN, M., ELMAN, L., MCCLUSKEY, L., VAN SWIETEN, J. C., AL-SARRAJ, S., NEUMANN, M., GELPI, E. & GHETTI, B. 2014. TMEM106B is a genetic modifier of frontotemporal lobar degeneration with C9orf72 hexanucleotide repeat expansions. *Acta neuropathologica,* 127**,** 407-418.

GALLIANO, E., HAHN, C., BROWNE, L. P., VILLAMAYOR, P. R., TUFO, C., CRESPO, A. & GRUBB, M. S. 2021. Brief sensory deprivation triggers cell type-specific structural and functional plasticity in olfactory bulb neurons. *Journal of Neuroscience,* 41**,** 2135-2151.

GAO, K., LIN, Z., WEN, S. & JIANG, Y. 2022. Potassium channels and epilepsy. *Acta Neurol Scand,* 146**,** 699-707.

GARIBOTTO, V., BORRONI, B., AGOSTI, C., PREMI, E., ALBERICI, A., EICKHOFF, S. B., BRAMBATI, S. M., BELLELLI, G., GASPAROTTI, R. & PERANI, D. 2011. Subcortical and deep cortical atrophy in frontotemporal lobar degeneration. *Neurobiology of aging,* 32**,** 875-884.

GATTO, N., DOS SANTOS SOUZA, C., SHAW, A. C., BELL, S. M., MYSZCZYNSKA, M. A., POWERS, S., MEYER, K., CASTELLI, L. M., KARYKA, E., MORTIBOYS, H., AZZOUZ, M., HAUTBERGUE, G. M., MÁRKUS, N. M., SHAW, P. J. & FERRAIUOLO, L. 2021. Directly converted astrocytes retain the ageing features of the donor fibroblasts and elucidate the astrocytic contribution to human CNS health and disease. *Aging Cell,* 20**,** e13281.

GEEVASINGA, N., MENON, P., HOWELLS, J., NICHOLSON, G. A., KIERNAN, M. C. & VUCIC, S. 2015. Axonal ion channel dysfunction in c9orf72 familial amyotrophic lateral sclerosis. *JAMA Neurol,* 72**,** 49-57.

GEEVASINGA, N., MENON, P., NG, K., VAN DEN BOS, M., BYTH, K., KIERNAN, M. C. & VUCIC, S. 2016a. Riluzole exerts transient modulating effects on cortical and axonal hyperexcitability in ALS. *Amyotrophic Lateral Sclerosis and Frontotemporal Degeneration,* 17**,** 580-588.

GEEVASINGA, N., MENON, P., ÖZDINLER, P. H., KIERNAN, M. C. & VUCIC, S. 2016b. Pathophysiological and diagnostic implications of cortical dysfunction in ALS. *Nat Rev Neurol,* 12**,** 651-661.

GEISLER, J. G., MAROSI, K., HALPERN, J. & MATTSON, M. P. 2017. DNP, mitochondrial uncoupling, and neuroprotection: A little dab'll do ya. *Alzheimers Dement,* 13**,** 582-591.

GENÇ, B., JARA, J. H., LAGRIMAS, A. K., PYTEL, P., ROOS, R. P., MESULAM, M. M., GEULA, C., BIGIO, E. H. & ÖZDINLER, P. H. 2017. Apical dendrite degeneration, a novel cellular pathology for Betz cells in ALS. *Scientific reports,* 7**,** 41765.

GENDRON, T. F., BELZIL, V. V., ZHANG, Y.-J. & PETRUCELLI, L. 2014. Mechanisms of toxicity in C9FTLD/ALS. *Acta neuropathologica,* 127**,** 359-376.

GENDRON, T. F., BIENIEK, K. F., ZHANG, Y.-J., JANSEN-WEST, K., ASH, P. E., CAULFIELD, T., DAUGHRITY, L., DUNMORE, J. H., CASTANEDES-CASEY, M. & CHEW, J. 2013. Antisense transcripts of the expanded C9ORF72 hexanucleotide repeat form nuclear RNA foci

and undergo repeat-associated non-ATG translation in c9FTD/ALS. *Acta neuropathologica,* 126**,** 829-844.

GENG, Y. & CAI, Q. 2024. Role of C9orf72 hexanucleotide repeat expansions in ALS/FTD pathogenesis. *Front Mol Neurosci,* 17**,** 1322720.

GERACITANO, R., PAOLUCCI, E., PRISCO, S., GUATTEO, E., ZONA, C., LONGONE, P., AMMASSARI-TEULE, M., BERNARDI, G., BERRETTA, N. & MERCURI, N. 2003. Altered long-term corticostriatal synaptic plasticity in transgenic mice overexpressing human CU/ZN superoxide dismutase (GLY93→ ALA) mutation. *Neuroscience,* 118**,** 399-408.

GERFEN, C. R. & BOLAM, J. P. 2016. Chapter 1 - The Neuroanatomical Organization of the Basal Ganglia. *In:* STEINER, H. & TSENG, K. Y. (eds.) *Handbook of Behavioral Neuroscience.* Elsevier.

GERFEN, C. R., ENGBER, T. M., MAHAN, L. C., SUSEL, Z., CHASE, T. N., MONSMA, F. J., JR. & SIBLEY, D. R. 1990a. D1 and D2 dopamine receptor-regulated gene expression of striatonigral and striatopallidal neurons. *Science,* 250**,** 1429-32.

GERFEN, C. R., ENGBER, T. M., MAHAN, L. C., SUSEL, Z., CHASE, T. N., MONSMA JR, F. J. & SIBLEY, D. R. 1990b. D1 and D2 dopamine receptor-regulated gene expression of striatonigral and striatopallidal neurons. *Science,* 250**,** 1429-1432.

GERFEN, C. R. & SURMEIER, D. J. 2011. Modulation of Striatal Projection Systems by Dopamine. *Annual Review of Neuroscience,* 34**,** 441-466.

GERTLER, T. S., CHAN, C. S. & SURMEIER, D. J. 2008. Dichotomous anatomical properties of adult striatal medium spiny neurons. *J Neurosci,* 28**,** 10814-24.

GHASEMI, M., KEYHANIAN, K. & DOUTHWRIGHT, C. 2021. Glial Cell Dysfunction in C9orf72-Related Amyotrophic Lateral Sclerosis and Frontotemporal Dementia. *Cells,* 10.

GHATAK, S., DOLATABADI, N., TRUDLER, D., ZHANG, X., WU, Y., MOHATA, M., AMBASUDHAN, R., TALANTOVA, M. & LIPTON, S. A. 2019. Mechanisms of hyperexcitability in Alzheimer's disease hiPSC-derived neurons and cerebral organoids vs isogenic controls. *Elife,* 8.

GHÉZALI, G., VASILE, F., CURRY, N., FANTHAM, M., CHEUNG, G., EZAN, P., COHEN-SALMON, M., KAMINSKI, C. & ROUACH, N. 2020. Neuronal activity drives astroglial connexin 30 in perisynaptic processes and shapes its functions. *Cerebral Cortex,* 30**,** 753-766.

GIAUME, C., NAUS, C. C., SÁEZ, J. C. & LEYBAERT, L. 2021. Glial Connexins and Pannexins in the Healthy and Diseased Brain. *Physiol Rev,* 101**,** 93-145.

GIJSELINCK, I., VAN MOSSEVELDE, S., VAN DER ZEE, J., SIEBEN, A., ENGELBORGHS, S., DE BLEECKER, J., IVANOIU, A., DERYCK, O., EDBAUER, D. & ZHANG, M. 2016. The C9orf72 repeat size correlates with onset age of disease, DNA methylation and transcriptional downregulation of the promoter. *Molecular psychiatry,* 21**,** 1112-1124.

GJORGJIEVA, J., MEASE, R. A., MOODY, W. J. & FAIRHALL, A. L. 2014. Intrinsic neuronal properties switch the mode of information transmission in networks. *PLoS Comput Biol,* 10**,** e1003962.

GOETHALS, S. & BRETTE, R. 2020. Theoretical relation between axon initial segment geometry and excitability. *eLife,* 9**,** e53432.

GOLDBERG, G. S., LAMPE, P. D. & NICHOLSON, B. J. 1999. Selective transfer of endogenous metabolites through gap junctions composed of different connexins. *Nat Cell Biol,* 1**,** 457-9.

GOLDSTEIN, L. H. & ABRAHAMS, S. 2013. Changes in cognition and behaviour in amyotrophic lateral sclerosis: nature of impairment and implications for assessment. *Lancet Neurol,* 12**,** 368-80.

GOMES, C., CUNHA, C., NASCIMENTO, F., RIBEIRO, J. A., VAZ, A. R. & BRITES, D. 2019. Cortical Neurotoxic Astrocytes with Early ALS Pathology and miR-146a Deficit Replicate Gliosis Markers of Symptomatic SOD1G93A Mouse Model. *Mol Neurobiol,* 56**,** 2137-2158.

GOMES, C., SEQUEIRA, C., BARBOSA, M., CUNHA, C., VAZ, A. R. & BRITES, D. 2020. Astrocyte regional diversity in ALS includes distinct aberrant phenotypes with common and causal pathological processes. *Experimental Cell Research,* 395**,** 112209.

GOMES, C., SEQUEIRA, C., LIKHITE, S., DENNYS, C. N., KOLB, S. J., SHAW, P. J., VAZ, A. R., KASPAR, B. K., MEYER, K. & BRITES, D. 2022. Neurotoxic Astrocytes Directly Converted from Sporadic and Familial ALS Patient Fibroblasts Reveal Signature Diversities and miR-146a Theragnostic Potential in Specific Subtypes. *Cells,* 11.

GOVAARTS, R., BEELDMAN, E., FRASCHINI, M., GRIFFA, A., ENGELS, M. M. A., VAN ES, M. A., VELDINK, J. H., VAN DEN BERG, L. H., VAN DER KOOI, A. J., PIJNENBURG, Y. A. L., DE VISSER, M., STAM, C. J., RAAPHORST, J. & HILLEBRAND, A. 2022. Cortical and subcortical changes in resting-state neuronal activity and connectivity in early symptomatic ALS and advanced frontotemporal dementia. *NeuroImage: Clinical,* 34**,** 102965.

GRAD, L. I., ROULEAU, G. A., RAVITS, J. & CASHMAN, N. R. 2017. Clinical spectrum of amyotrophic lateral sclerosis (ALS). *Cold Spring Harbor perspectives in medicine,* 7**,** a024117.

GRAVELAND, G. A. & DIFIGLIA, M. 1985. The frequency and distribution of medium-sized neurons with indented nuclei in the primate and rodent neostriatum. *Brain Res,* 327**,** 307-11.

GREEN, J., PICKLES, A., PASCO, G., BEDFORD, R., WAN, M. W., ELSABBAGH, M., SLONIMS, V., GLIGA, T., JONES, E., CHEUNG, C., CHARMAN, T. & JOHNSON, M. 2017. Randomised trial of a parent-mediated intervention for infants at high risk for autism: longitudinal outcomes to age 3 years. *J Child Psychol Psychiatry,* 58**,** 1330-1340.

GREENE, D. L. & HOSHI, N. 2017. Modulation of Kv7 channels and excitability in the brain. *Cell Mol Life Sci,* 74**,** 495-508.

GREGORY, J. M., LIVESEY, M. R., MCDADE, K., SELVARAJ, B. T., BARTON, S. K., CHANDRAN, S. & SMITH, C. 2020. Dysregulation of AMPA receptor subunit expression in sporadic ALS post-mortem brain. *J Pathol,* 250**,** 67-78.

GULLEDGE, A. T. & BRAVO, J. J. 2016. Neuron Morphology Influences Axon Initial Segment Plasticity. *eneuro,* 3**,** ENEURO.0085-15.2016.

GUNES, Z. I., KAN, V. W. Y., YE, X. & LIEBSCHER, S. 2020. Exciting Complexity: The Role of Motor Circuit Elements in ALS Pathophysiology. *Front Neurosci,* 14**,** 573.

GUO, W., NAUJOCK, M., FUMAGALLI, L., VANDOORNE, T., BAATSEN, P., BOON, R., ORDOVÁS, L., PATEL, A., WELTERS, M., VANWELDEN, T., GEENS, N., TRICOT, T., BENOY, V., STEYAERT, J., LEFEBVRE-OMAR, C., BOESMANS, W., JARPE, M., STERNECKERT, J., WEGNER, F., PETRI, S., BOHL, D., VANDEN BERGHE, P., ROBBERECHT, W., VAN DAMME, P., VERFAILLIE, C. & VAN DEN BOSCH, L. 2017. HDAC6 inhibition reverses axonal transport defects in motor neurons derived from FUS-ALS patients. *Nat Commun,* 8**,** 861.

GURDON, J. B. 1962. The developmental capacity of nuclei taken from intestinal epithelium cells of feeding tadpoles. *J Embryol Exp Morphol,* 10**,** 622-40.

GURNEY, M. E., PU, H., CHIU, A. Y., DAL CANTO, M. C., POLCHOW, C. Y., ALEXANDER, D. D., CALIENDO, J., HENTATI, A., KWON, Y. W. & DENG, H.-X. 1994. Motor neuron degeneration in mice that express a human Cu, Zn superoxide dismutase mutation. *Science,* 264**,** 1772-1775.

GUTTENPLAN, K. A., WEIGEL, M. K., ADLER, D. I., COUTHOUIS, J., LIDDELOW, S. A., GITLER, A. D. & BARRES, B. A. 2020. Knockout of reactive astrocyte activating factors slows disease progression in an ALS mouse model. *Nat Commun,* 11**,** 3753.

HADANO, S., OTOMO, A., KUNITA, R., SUZUKI-UTSUNOMIYA, K., AKATSUKA, A., KOIKE, M., AOKI, M., UCHIYAMA, Y., ITOYAMA, Y. & IKEDA, J. E. 2010. Loss of ALS2/Alsin exacerbates motor dysfunction in a SOD1-expressing mouse ALS model by disturbing endolysosomal trafficking. *PLoS One,* 5**,** e9805.

HAIDAR, M., VIDEN, A., CUIC, B., WANG, T., ROSIER, M., TOMAS, D., MILLS, S. A., GOVIER-COLE, A., DJOUMA, E., LUIKINGA, S., RYTOVA, V., BARTON, S. K., GONSALVEZ, D. G., PALMER, L. M., MCLEAN, C., KIERNAN, M. C., VUCIC, S. & TURNER, B. J. 2021. Cortical hyperexcitability drives dying forward ALS symptoms and pathology in mice. *bioRxiv***,** 2021.08.13.456320.

HAIDET-PHILLIPS, A. M., HESTER, M. E., MIRANDA, C. J., MEYER, K., BRAUN, L., FRAKES, A., SONG, S., LIKHITE, S., MURTHA, M. J., FOUST, K. D., RAO, M., EAGLE, A., KAMMESHEIDT, A., CHRISTENSEN, A., MENDELL, J. R., BURGHES, A. H. & KASPAR, B. K. 2011. Astrocytes from familial and sporadic ALS patients are toxic to motor neurons. *Nat Biotechnol,* 29**,** 824-8.

HALABI, C., HALABI, A., DEAN, D. L., WANG, P.-N., BOXER, A. L., TROJANOWSKI, J. Q., DEARMOND, S. J., MILLER, B. L., KRAMER, J. H. & SEELEY, W. W. 2013. Patterns of striatal degeneration in frontotemporal dementia. *Alzheimer disease and associated disorders,* 27**,** 74.

HALL, E. D., ANDRUS, P. K., OOSTVEEN, J. A., FLECK, T. J. & GURNEY, M. E. 1998. Relationship of oxygen radical-induced lipid peroxidative damage to disease onset and progression in a transgenic model of familial ALS. *Journal of neuroscience research,* 53**,** 66-77.

HAMILL, O. P., MARTY, A., NEHER, E., SAKMANN, B. & SIGWORTH, F. J. 1981. Improved patch-clamp techniques for high-resolution current recording from cells and cell-free membrane patches. *Pflügers Archiv,* 391**,** 85-100.

HAN, X., JING, M. Y., ZHAO, T. Y., WU, N., SONG, R. & LI, J. 2017. Role of dopamine projections from ventral tegmental area to nucleus accumbens and medial prefrontal cortex in reinforcement behaviors assessed using optogenetic manipulation. *Metab Brain Dis,* 32**,** 1491-1502.

HANDLEY, E. E., PITMAN, K. A., DAWKINS, E., YOUNG, K. M., CLARK, R. M., JIANG, T. C., TURNER, B. J., DICKSON, T. C. & BLIZZARD, C. A. 2017. Synapse Dysfunction of Layer V Pyramidal Neurons Precedes Neurodegeneration in a Mouse Model of TDP-43 Proteinopathies. *Cereb Cortex,* 27**,** 3630-3647.

HANDLEY, E. E., REALE, L. A., CHUCKOWREE, J. A., DYER, M. S., BARNETT, G. L., CLARK, C. M., BENNETT, W., DICKSON, T. C. & BLIZZARD, C. A. 2022. Estrogen Enhances Dendrite Spine Function and Recovers Deficits in Neuroplasticity in the prp TDP-43A315T

Mouse Model of Amyotrophic Lateral Sclerosis. *Molecular Neurobiology,* 59**,** 2962-2976.

HARDIMAN, O., AL-CHALABI, A., CHIO, A., CORR, E. M., LOGROSCINO, G., ROBBERECHT, W., SHAW, P. J., SIMMONS, Z. & VAN DEN BERG, L. H. 2017. Amyotrophic lateral sclerosis. *Nat Rev Dis Primers,* 3**,** 17071.

HARLEY, P., KERINS, C., GATT, A., NEVES, G., RICCIO, F., MACHADO, C. B., CHEESBROUGH, A., R'BIBO, L., BURRONE, J. & LIEBERAM, I. 2023. Aberrant axon initial segment plasticity and intrinsic excitability of ALS hiPSC motor neurons. *Cell Reports,* 42**,** 113509.

HARMS, M. B., CADY, J., ZAIDMAN, C., COOPER, P., BALI, T., ALLRED, P., CRUCHAGA, C., BAUGHN, M., LIBBY, R. T. & PESTRONK, A. 2013. Lack of C9ORF72 coding mutations supports a gain of function for repeat expansions in amyotrophic lateral sclerosis. *Neurobiology of aging,* 34**,** 2234. e13-2234. e19.

HASEL, P., DANDO, O., JIWAJI, Z., BAXTER, P., TODD, A. C., HERON, S., MÁRKUS, N. M., MCQUEEN, J., HAMPTON, D. W., TORVELL, M., TIWARI, S. S., MCKAY, S., ERASO-PICHOT, A., ZORZANO, A., MASGRAU, R., GALEA, E., CHANDRAN, S., WYLLIE, D. J. A., SIMPSON, T. I. & HARDINGHAM, G. E. 2017. Neurons and neuronal activity control gene expression in astrocytes to regulate their development and metabolism. *Nature Communications,* 8**,** 15132.

HASHIMOTO, Y., YAMASAKI, R., KO, S., MATSUO, E., KOBAYAKAWA, Y., MASAKI, K., MATSUSE, D. & ISOBE, N. 2022. Connexin 30 Deficiency Ameliorates Disease Progression at the Early Phase in a Mouse Model of Amyotrophic Lateral Sclerosis by Suppressing Glial Inflammation. *International Journal of Molecular Sciences,* 23**,** 16046.

HAUTBERGUE, G. M., CASTELLI, L. M., FERRAIUOLO, L., SANCHEZ-MARTINEZ, A., COOPER-KNOCK, J., HIGGINBOTTOM, A., LIN, Y.-H., BAUER, C. S., DODD, J. E., MYSZCZYNSKA, M. A., ALAM, S. M., GARNERET, P., CHANDRAN, J. S., KARYKA, E., STOPFORD, M. J., SMITH, E. F., KIRBY, J., MEYER, K., KASPAR, B. K., ISAACS, A. M., EL-KHAMISY, S. F., DE VOS, K. J., NING, K., AZZOUZ, M., WHITWORTH, A. J. & SHAW, P. J. 2017. SRSF1-dependent nuclear export inhibition of C9ORF72 repeat transcripts prevents neurodegeneration and associated motor deficits. *Nature Communications,* 8**,** 16063.

HE, J., KLEYMAN, M., CHEN, J., ALIKAYA, A., ROTHENHOEFER, K. M., OZTURK, B. E., WIRTHLIN, M., BOSTAN, A. C., FISH, K., BYRNE, L. C., PFENNING, A. R. & STAUFFER, W. R. 2021. Transcriptional and anatomical diversity of medium spiny neurons in the primate striatum. *Current Biology,* 31**,** 5473-5486.e6.

HENKEL, L. M., KANKOWSKI, S., MOELLENKAMP, T. M., SMANDZICH, N. J., SCHWARZ, S., DI FONZO, A., GÖHRING, G., HÖGLINGER, G. & WEGNER, F. 2023. iPSC-Derived Striatal Medium Spiny Neurons from Patients with Multiple System Atrophy Show Hypoexcitability and Elevated α-Synuclein Release. *Cells,* 12.

HENSTRIDGE, C. M., SIDERIS, D. I., CARROLL, E., ROTARIU, S., SALOMONSSON, S., TZIORAS, M., MCKENZIE, C.-A., SMITH, C., VON ARNIM, C. A. & LUDOLPH, A. C. 2018. Synapse loss in the prefrontal cortex is associated with cognitive decline in amyotrophic lateral sclerosis. *Acta neuropathologica,* 135**,** 213-226.

HIEBERT, N. M., VO, A., HAMPSHIRE, A., OWEN, A. M., SEERGOBIN, K. N. & MACDONALD, P. A. 2014. Striatum in stimulus-response learning via feedback and in decision making. *Neuroimage,* 101**,** 448-57.

HIGASHIHARA, M., PAVEY, N., VAN DEN BOS, M., MENON, P., KIERNAN, M. C. & VUCIC, S. 2021. Association of Cortical Hyperexcitability and Cognitive Impairment in Patients With Amyotrophic Lateral Sclerosis. *Neurology,* 96**,** e2090-e2097.

HIGHLEY, J. R., KIRBY, J., JANSWEIJER, J. A., WEBB, P. S., HEWAMADDUMA, C. A., HEATH, P. R., HIGGINBOTTOM, A., RAMAN, R., FERRAIUOLO, L., COOPER-KNOCK, J., MCDERMOTT, C. J., WHARTON, S. B., SHAW, P. J. & INCE, P. G. 2014. Loss of nuclear TDP-43 in amyotrophic lateral sclerosis (ALS) causes altered expression of splicing machinery and widespread dysregulation of RNA splicing in motor neurones. *Neuropathol Appl Neurobiol,* 40**,** 670-85.

HILLE, B. 1978. Ionic channels in excitable membranes. Current problems and biophysical approaches. *Biophys J,* 22**,** 283-94.

HO, W. Y., AGRAWAL, I., TYAN, S. H., SANFORD, E., CHANG, W. T., LIM, K., ONG, J., TAN, B. S. Y., MOE, A. A. K., YU, R., WONG, P., TUCKER-KELLOGG, G., KOO, E., CHUANG, K. H. & LING, S. C. 2021. Dysfunction in nonsense-mediated decay, protein homeostasis, mitochondrial function, and brain connectivity in ALS-FUS mice with cognitive deficits. *Acta Neuropathol Commun,* 9**,** 9.

HO, W. Y., NAVAKKODE, S., LIU, F., SOONG, T. W. & LING, S. C. 2020. Deregulated expression of a longevity gene, Klotho, in the C9orf72 deletion mice with impaired synaptic plasticity and adult hippocampal neurogenesis. *Acta Neuropathol Commun,* 8**,** 155.

HOWLAND, D. S., LIU, J., SHE, Y., GOAD, B., MARAGAKIS, N. J., KIM, B., ERICKSON, J., KULIK, J., DEVITO, L. & PSALTIS, G. 2002. Focal loss of the glutamate transporter EAAT2 in a transgenic rat model of SOD1 mutant-mediated amyotrophic lateral sclerosis (ALS). *Proceedings of the National Academy of Sciences,* 99**,** 1604-1609.

HOYE, M.L., REGAN, M.R., JENSEN, L.A., LAKE, A.M., REDDY, L.V., VIDENSKY, S., RICHARD, J.P., MARAGAKIS, N.J., ROTHSTEIN, J.D., DOUGHERTY, J.D. AND MILLER, T.M., 2018. Motor neuron-derived microRNAs cause astrocyte dysfunction in amyotrophic lateral sclerosis. *Brain*, *141*(9), pp.2561-2575.

HSIUNG, G. Y., DEJESUS-HERNANDEZ, M., FELDMAN, H. H., SENGDY, P., BOUCHARD-KERR, P., DWOSH, E., BUTLER, R., LEUNG, B., FOK, A., RUTHERFORD, N. J., BAKER, M., RADEMAKERS, R. & MACKENZIE, I. R. 2012. Clinical and pathological features of familial frontotemporal dementia caused by C9ORF72 mutation on chromosome 9p. *Brain,* 135**,** 709-22.

HU, W. T., SEELAAR, H., JOSEPHS, K. A., KNOPMAN, D. S., BOEVE, B. F., SORENSON, E. J., MCCLUSKEY, L., ELMAN, L., SCHELHAAS, H. J., PARISI, J. E., KUESTERS, B., LEE, V. M.-Y., TROJANOWSKI, J. Q., PETERSEN, R. C., VAN SWIETEN, J. C. & GROSSMAN, M. 2009. Survival Profiles of Patients With Frontotemporal Dementia and Motor Neuron Disease. *Archives of Neurology,* 66**,** 1359-1364.

HUANG, X., ROET, K. C. D., ZHANG, L., BRAULT, A., BERG, A. P., JEFFERSON, A. B., KLUG-MCLEOD, J., LEACH, K. L., VINCENT, F., YANG, H., COYLE, A. J., JONES, L. H., FROST, D., WISKOW, O., CHEN, K., MAEDA, R., GRANTHAM, A., DORNON, M. K., KLIM, J. R., SIEKMANN, M. T., ZHAO, D., LEE, S., EGGAN, K. & WOOLF, C. J. 2021a. Human amyotrophic lateral sclerosis excitability phenotype screen: Target discovery and validation. *Cell Rep,* 35**,** 109224.

HUANG, X., SU, Y., WANG, N., LI, H., LI, Z., YIN, G., CHEN, H., NIU, J. & YI, C. 2021b. Astroglial Connexins in Neurodegenerative Diseases. *Front Mol Neurosci,* 14**,** 657514.

HUANG, Y., GATTONI, R., STÉVENIN, J. & STEITZ, J. A. 2003. SR Splicing Factors Serve as Adapter Proteins for TAP-Dependent mRNA Export. *Molecular Cell,* 11**,** 837-843.

HUBER, N., HOFFMANN, D., GINIATULLINA, R., ROSTALSKI, H., LESKELÄ, S., TAKALO, M., NATUNEN, T., SOLJE, E., REMES, A. M., GINIATULLIN, R., HILTUNEN, M. & HAAPASALO, A. 2022. C9orf72 hexanucleotide repeat expansion leads to altered neuronal and dendritic spine morphology and synaptic dysfunction. *Neurobiology of Disease,* 162**,** 105584.

HUH, C. J., ZHANG, B., VICTOR, M. B., DAHIYA, S., BATISTA, L. F., HORVATH, S. & YOO, A. S. 2016. Maintenance of age in human neurons generated by microRNA-based neuronal conversion of fibroblasts. *Elife,* 5.

HYND, M. R., SCOTT, H. L. & DODD, P. R. 2004. Glutamate-mediated excitotoxicity and neurodegeneration in Alzheimer's disease. *Neurochem Int,* 45**,** 583-95.

IACOANGELI, A., AL KHLEIFAT, A., JONES, A. R., SPROVIERO, W., SHATUNOV, A., OPIE-MARTIN, S., MORRISON, K. E., SHAW, P. J., SHAW, C. E., FOGH, I., DOBSON, R. J., NEWHOUSE, S. J., AL-CHALABI, A. & ALZHEIMER'S DISEASE NEUROIMAGING, I. 2019. C9orf72 intermediate expansions of 24–30 repeats are associated with ALS. *Acta Neuropathologica Communications,* 7**,** 115.

IANNIELLI, A., UGOLINI, G. S., CORDIGLIERI, C., BIDO, S., RUBIO, A., COLASANTE, G., VALTORTA, M., CABASSI, T., RASPONI, M. & BROCCOLI, V. 2019. Reconstitution of the Human Nigro-striatal Pathway on-a-Chip Reveals OPA1-Dependent Mitochondrial Defects and Loss of Dopaminergic Synapses. *Cell Rep,* 29**,** 4646-4656.e4.

IHARA, Y., NOBUKUNI, K., TAKATA, H. & HAYABARA, T. 2005. Oxidative stress and metal content in blood and cerebrospinal fluid of amyotrophic lateral sclerosis patients with and without a Cu, Zn-superoxide dismutase mutation. *Neurological research,* 27**,** 105-108.

IRWIN, D. J., MCMILLAN, C. T., BRETTSCHNEIDER, J., LIBON, D. J., POWERS, J., RASCOVSKY, K., TOLEDO, J. B., BOLLER, A., BEKISZ, J., CHANDRASEKARAN, K., WOOD, E. M., SHAW, L. M., WOO, J. H., COOK, P. A., WOLK, D. A., ARNOLD, S. E., VAN DEERLIN, V. M., MCCLUSKEY, L. F., ELMAN, L., LEE, V. M., TROJANOWSKI, J. Q. & GROSSMAN, M. 2013. Cognitive decline and reduced survival in C9orf72 expansion frontotemporal degeneration and amyotrophic lateral sclerosis. *J Neurol Neurosurg Psychiatry,* 84**,** 163-9.

IVKOVIC, S. & EHRLICH, M. E. 1999. Expression of the striatal DARPP-32/ARPP-21 phenotype in GABAergic neurons requires neurotrophins in vivo and in vitro. *J Neurosci,* 19**,** 5409-19.

IWAI, Y., SHIBUYA, K., MISAWA, S., SEKIGUCHI, Y., WATANABE, K., AMINO, H. & KUWABARA, S. 2016. Axonal Dysfunction Precedes Motor Neuronal Death in Amyotrophic Lateral Sclerosis. *PLoS One,* 11**,** e0158596.

JAMANN, N., DANNEHL, D., LEHMANN, N., WAGENER, R., THIELEMANN, C., SCHULTZ, C., STAIGER, J., KOLE, M. H. & ENGELHARDT, M. 2021. Sensory input drives rapid homeostatic scaling of the axon initial segment in mouse barrel cortex. *Nature Communications,* 12**,** 23.

JELÍNEK, M., BALUŠÍKOVÁ, K., SCHMIEDLOVÁ, M., NĚMCOVÁ-FÜRSTOVÁ, V., ŠRÁMEK, J., STANČÍKOVÁ, J., ZANARDI, I., OJIMA, I. & KOVÁŘ, J. 2015. The role of individual caspases in cell death induction by taxanes in breast cancer cells. *Cancer Cell Int,* 15**,** 8.

JENSEN, B. K., SCHULDI, M. H., MCAVOY, K., RUSSELL, K. A., BOEHRINGER, A., CURRAN, B. M., KRISHNAMURTHY, K., WEN, X., WESTERGARD, T., MA, L., HAEUSLER, A. R., EDBAUER, D., PASINELLI, P. & TROTTI, D. 2020. Synaptic dysfunction induced by glycine-alanine dipeptides in C9orf72-ALS/FTD is rescued by SV2 replenishment. *EMBO Mol Med,* 12**,** e10722.

JIANG, J., ZHU, Q., GENDRON, T. F., SABERI, S., MCALONIS-DOWNES, M., SEELMAN, A., STAUFFER, J. E., JAFAR-NEJAD, P., DRENNER, K., SCHULTE, D., CHUN, S., SUN, S., LING, S. C., MYERS, B., ENGELHARDT, J., KATZ, M., BAUGHN, M., PLATOSHYN, O., MARSALA, M., WATT, A., HEYSER, C. J., ARD, M. C., DE MUYNCK, L., DAUGHRITY, L. M., SWING, D. A., TESSAROLLO, L., JUNG, C. J., DELPOUX, A., UTZSCHNEIDER, D. T., HEDRICK, S. M., DE JONG, P. J., EDBAUER, D., VAN DAMME, P., PETRUCELLI, L., SHAW, C. E., BENNETT, C. F., DA CRUZ, S., RAVITS, J., RIGO, F., CLEVELAND, D. W. & LAGIER-TOURENNE, C. 2016. Gain of Toxicity from ALS/FTD-Linked Repeat Expansions in C9ORF72 Is Alleviated by Antisense Oligonucleotides Targeting GGGGCC-Containing RNAs. *Neuron,* 90**,** 535-50.

JIANG, Y. M., YAMAMOTO, M., KOBAYASHI, Y., YOSHIHARA, T., LIANG, Y., TERAO, S., TAKEUCHI, H., ISHIGAKI, S., KATSUNO, M. & ADACHI, H. 2005. Gene expression profile of spinal motor neurons in sporadic amyotrophic lateral sclerosis. *Annals of neurology,* 57**,** 236-251.

JIMÉNEZ-BALADO, J. & EICH, T. S. 2021. GABAergic dysfunction, neural network hyperactivity and memory impairments in human aging and Alzheimer's disease. *Seminars in Cell & Developmental Biology,* 116**,** 146-159.

JIN, H. A., MCMILLAN, C. T., YANNATOS, I., FISHER, L., RHODES, E., JACOBY, S. F., IRWIN, D. J. & MASSIMO, L. 2023. Racial Differences in Clinical Presentation in Individuals Diagnosed With Frontotemporal Dementia. *JAMA Neurology,* 80**,** 1191-1198.

JOHN, G. R., LEE, S. C. & BROSNAN, C. F. 2003. Cytokines: powerful regulators of glial cell activation. *The Neuroscientist,* 9**,** 10-22.

JOYCE, N. C. & CARTER, G. T. 2013. Electrodiagnosis in persons with amyotrophic lateral sclerosis. *Pm r,* 5**,** S89-95.

JOYCE, P. I., MCGOLDRICK, P., SACCON, R. A., WEBER, W., FRATTA, P., WEST, S. J., ZHU, N., CARTER, S., PHATAK, V., STEWART, M., SIMON, M., KUMAR, S., HEISE, I., BROS-FACER, V., DICK, J., CORROCHANO, S., STANFORD, M. J., LUONG, T. V., NOLAN, P. M., MEYER, T., BRANDNER, S., BENNETT, D. L., OZDINLER, P. H., GREENSMITH, L., FISHER, E. M. & ACEVEDO-AROZENA, A. 2015. A novel SOD1-ALS mutation separates central and peripheral effects of mutant SOD1 toxicity. *Hum Mol Genet,* 24**,** 1883-97.

JULIAN, T. H., GLASCOW, N., BARRY, A. D. F., MOLL, T., HARVEY, C., KLIMENTIDIS, Y. C., NEWELL, M., ZHANG, S., SNYDER, M. P., COOPER-KNOCK, J. & SHAW, P. J. 2021. Physical exercise is a risk factor for amyotrophic lateral sclerosis: Convergent evidence from Mendelian randomisation, transcriptomics and risk genotypes. *EBioMedicine,* 68**,** 103397.

KABASHI, E., VALDMANIS, P. N., DION, P., SPIEGELMAN, D., MCCONKEY, B. J., VANDE VELDE, C., BOUCHARD, J. P., LACOMBLEZ, L., POCHIGAEVA, K., SALACHAS, F., PRADAT, P. F., CAMU, W., MEININGER, V., DUPRE, N. & ROULEAU, G. A. 2008. TARDBP mutations in individuals with sporadic and familial amyotrophic lateral sclerosis. *Nat Genet,* 40**,** 572-4.

KANDHAVIVORN, W., GLAS, H., HERRMANNSDÖRFER, T., BÖCKERS, T. M., UHLARZ, M., GRONEMANN, J., FUNK, R. H. W., PIETZSCH, J., PAL, A. & HERMANN, A. 2023. Restoring Axonal Organelle Motility and Regeneration in Cultured FUS-ALS Motoneurons through Magnetic Field Stimulation Suggests an Alternative Therapeutic Approach. *Cells,* 12.

KANG, J., KANG, N., LOVATT, D., TORRES, A., ZHAO, Z., LIN, J. & NEDERGAARD, M. 2008. Connexin 43 hemichannels are permeable to ATP. *J Neurosci,* 28**,** 4702-11.

KAPHZAN, H., BUFFINGTON, S. A., JUNG, J. I., RASBAND, M. N. & KLANN, E. 2011. Alterations in intrinsic membrane properties and the axon initial segment in a mouse model of Angelman syndrome. *Journal of Neuroscience,* 31**,** 17637-17648.

KATO, S., HAYASHI, H. & YAGISHITA, A. 1993. Involvement of the frontotemporal lobe and limbic system in amyotrophic lateral sclerosis: as assessed by serial computed tomography and magnetic resonance imaging. *Journal of the neurological sciences,* 116**,** 52-58.

KATO, S., ODA, M., HAYASHI, H., KAWATA, A. & SHIMIZU, T. 1994. Participation of the limbic system and its associated areas in the dementia of amyotrophic lateral sclerosis. *J Neurol Sci,* 126**,** 62-9.

KELLER, A. F., GRAVEL, M. & KRIZ, J. 2011. Treatment with minocycline after disease onset alters astrocyte reactivity and increases microgliosis in SOD1 mutant mice. *Exp Neurol,* 228**,** 69-79.

KELLEY, K. W., BEN HAIM, L., SCHIRMER, L., TYZACK, G. E., TOLMAN, M., MILLER, J. G., TSAI, H.-H., CHANG, S. M., MOLOFSKY, A. V., YANG, Y., PATANI, R., LAKATOS, A., ULLIAN, E. M. & ROWITCH, D. H. 2018. Kir4.1-Dependent Astrocyte-Fast Motor Neuron Interactions Are Required for Peak Strength. *Neuron,* 98**,** 306-319.e7.

KERSAITIS, C., HALLIDAY, G. M. & KRIL, J. J. 2004. Regional and cellular pathology in frontotemporal dementia: relationship to stage of disease in cases with and without Pick bodies. *Acta neuropathologica,* 108**,** 515-523.

KHADEMULLAH, C. S., AQRABAWI, A. J., PLACE, K. M., DARGAEI, Z., LIANG, X., PRESSEY, J. C., BEDARD, S., YANG, J. W., GARAND, D. & KERAMIDIS, I. 2020. Cortical interneuron-mediated inhibition delays the onset of amyotrophic lateral sclerosis. *Brain,* 143**,** 800-810.

KHAKH, B. S. 2019. Astrocyte–Neuron Interactions in the Striatum: Insights on Identity, Form, and Function. *Trends in Neurosciences,* 42**,** 617-630.

KIA, A., MCAVOY, K., KRISHNAMURTHY, K., TROTTI, D. & PASINELLI, P. 2018. Astrocytes expressing ALS-linked mutant FUS induce motor neuron death through release of tumor necrosis factor-alpha. *Glia,* 66**,** 1016-1033.

KIERNAN, M. C., VUCIC, S., CHEAH, B. C., TURNER, M. R., EISEN, A., HARDIMAN, O., BURRELL, J. R. & ZOING, M. C. 2011. Amyotrophic lateral sclerosis. *The Lancet,* 377**,** 942-955.

KIM, H.-J., RAPHAEL, A. R., LADOW, E. S., MCGURK, L., WEBER, R. A., TROJANOWSKI, J. Q., LEE, V. M., FINKBEINER, S., GITLER, A. D. & BONINI, N. M. 2014. Therapeutic modulation of eIF2α phosphorylation rescues TDP-43 toxicity in amyotrophic lateral sclerosis disease models. *Nature genetics,* 46**,** 152-160.

KIM, J., HUGHES, E. G., SHETTY, A. S., ARLOTTA, P., GOFF, L. A., BERGLES, D. E. & BROWN, S. P. 2017a. Changes in the Excitability of Neocortical Neurons in a Mouse Model of Amyotrophic Lateral Sclerosis Are Not Specific to Corticospinal Neurons and Are Modulated by Advancing Disease. *J Neurosci,* 37**,** 9037-9053.

KIM, Y., GRIFFIN, J. M., NOR, M. N. M., ZHANG, J., FREESTONE, P. S., DANESH-MEYER, H. V., RUPENTHAL, I. D., ACOSTA, M., NICHOLSON, L. F. B., O'CARROLL, S. J. & GREEN, C. R. 2017b. Tonabersat Prevents Inflammatory Damage in the Central Nervous System by Blocking Connexin43 Hemichannels. *Neurotherapeutics,* 14**,** 1148-1165.

KOLE, M. H., ILSCHNER, S. U., KAMPA, B. M., WILLIAMS, S. R., RUBEN, P. C. & STUART, G. J. 2008. Action potential generation requires a high sodium channel density in the axon initial segment. *Nature neuroscience,* 11**,** 178-186.

KONG, J. & XU, Z. 1998. Massive mitochondrial degeneration in motor neurons triggers the onset of amyotrophic lateral sclerosis in mice expressing a mutant SOD1. *Journal of Neuroscience,* 18**,** 3241-3250.

KONOPKA, A., WHELAN, D. R., JAMALI, M. S., PERRI, E., SHAHHEYDARI, H., TOTH, R. P., PARAKH, S., ROBINSON, T., CHEONG, A. & MEHTA, P. 2020. Impaired NHEJ repair in amyotrophic lateral sclerosis is associated with TDP-43 mutations. *Molecular neurodegeneration,* 15**,** 1-28.

KOPPERS, M., BLOKHUIS, A. M., WESTENENG, H. J., TERPSTRA, M. L., ZUNDEL, C. A., VIEIRA DE SÁ, R., SCHELLEVIS, R. D., WAITE, A. J., BLAKE, D. J., VELDINK, J. H., VAN DEN BERG, L. H. & PASTERKAMP, R. J. 2015. C9orf72 ablation in mice does not cause motor neuron degeneration or motor deficits. *Ann Neurol,* 78**,** 426-38.

KOULAKOFF, A., MEI, X., ORELLANA, J. A., SÁEZ, J. C. & GIAUME, C. 2012. Glial connexin expression and function in the context of Alzheimer's disease. *Biochimica et Biophysica Acta (BBA)-Biomembranes,* 1818**,** 2048-2057.

KOVANDA, A., ZALAR, M., ŠKET, P., PLAVEC, J. & ROGELJ, B. 2015. Anti-sense DNA d(GGCCCC)n expansions in C9ORF72 form i-motifs and protonated hairpins. *Scientific Reports,* 5**,** 17944.

KOZA, P., BEROUN, A., KONOPKA, A., GÓRKIEWICZ, T., BIJOCH, L., TORRES, J. C., BULSKA, E., KNAPSKA, E., KACZMAREK, L. & KONOPKA, W. 2019. Neuronal TDP-43 depletion affects activity-dependent plasticity. *Neurobiology of Disease,* 130**,** 104499.

KUBA, H., OICHI, Y. & OHMORI, H. 2010. Presynaptic activity regulates Na+ channel distribution at the axon initial segment. *Nature,* 465**,** 1075-1078.

KUMFOR, F. & PIGUET, O. 2012. Disturbance of emotion processing in frontotemporal dementia: a synthesis of cognitive and neuroimaging findings. *Neuropsychology review,* 22**,** 280-297.

KWON, I., XIANG, S., KATO, M., WU, L., THEODOROPOULOS, P., WANG, T., KIM, J., YUN, J., XIE, Y. & MCKNIGHT, S. L. 2014. Poly-dipeptides encoded by the C9orf72 repeats bind nucleoli, impede RNA biogenesis, and kill cells. *Science,* 345**,** 1139-45.

LACOMBLEZ, L., BENSIMON, G., LEIGH, P. N., GUILLET, P. & MEININGER, V. 1996. Dose-ranging study of riluzole in amyotrophic lateral sclerosis. Amyotrophic Lateral Sclerosis/Riluzole Study Group II. *Lancet (London, England),* 347**,** 1425-1431.

LAGIER-TOURENNE, C., BAUGHN, M., RIGO, F., SUN, S., LIU, P., LI, H. R., JIANG, J., WATT, A. T., CHUN, S., KATZ, M., QIU, J., SUN, Y., LING, S. C., ZHU, Q., POLYMENIDOU, M., DRENNER, K., ARTATES, J. W., MCALONIS-DOWNES, M., MARKMILLER, S., HUTT, K. R., PIZZO, D. P., CADY, J., HARMS, M. B., BALOH, R. H., VANDENBERG, S. R., YEO, G. W., FU, X. D., BENNETT, C. F., CLEVELAND, D. W. & RAVITS, J. 2013. Targeted degradation of sense and antisense C9orf72 RNA foci as therapy for ALS and frontotemporal degeneration. *Proc Natl Acad Sci U S A,* 110**,** E4530-9.

LALL, D., LORENZINI, I., MOTA, T. A., BELL, S., MAHAN, T. E., ULRICH, J. D., DAVTYAN, H., REXACH, J. E., MUHAMMAD, A. G. & SHELEST, O. 2021. C9orf72 deficiency promotes microglial-mediated synaptic loss in aging and amyloid accumulation. *Neuron,* 109**,** 2275-2291. e8.

LAM, L., CHIN, L., HALDER, R. C., SAGONG, B., FAMENINI, S., SAYRE, J., MONTOYA, D., RUBBI, L., PELLEGRINI, M. & FIALA, M. 2016. Epigenetic changes in T-cell and monocyte signatures and production of neurotoxic cytokines in ALS patients. *The FASEB Journal,* 30**,** 3461.

LAM, R. S., TÖPFER, F. M., WOOD, P. G., BUSSKAMP, V. & BAMBERG, E. 2017. Functional maturation of human stem cell-derived neurons in long-term cultures. *PloS one,* 12**,** e0169506.

LANCIEGO, J. L., LUQUIN, N. & OBESO, J. A. 2012. Functional neuroanatomy of the basal ganglia. *Cold Spring Harb Perspect Med,* 2**,** a009621.

LANCIOTTI, A., BRIGNONE, M. S., BELFIORE, M., COLUMBA-CABEZAS, S., MALLOZZI, C., VINCENTINI, O., MOLINARI, P., PETRUCCI, T. C., VISENTIN, S. & AMBROSINI, E. 2020. Megalencephalic leukoencephalopathy with subcortical cysts disease-linked MLC1 protein favors gap-junction intercellular communication by regulating connexin 43 trafficking in astrocytes. *Cells,* 9**,** 1425.

LANDIN-ROMERO, R., KUMFOR, F., LEYTON, C. E., IRISH, M., HODGES, J. R. & PIGUET, O. 2017. Disease-specific patterns of cortical and subcortical degeneration in a longitudinal study of Alzheimer's disease and behavioural-variant frontotemporal dementia. *Neuroimage,* 151**,** 72-80.

LARSSON, H. P. 2013. What determines the kinetics of the slow afterhyperpolarization (sAHP) in neurons? *Biophys J,* 104**,** 281-3.

LASHLEY, T., ROHRER, J. D., MEAD, S. & REVESZ, T. 2015. Review: an update on clinical, genetic and pathological aspects of frontotemporal lobar degenerations. *Neuropathol Appl Neurobiol,* 41**,** 858-81.

LAWRENCE, T. S., BEERS, W. H. & GILULA, N. B. 1978. Transmission of hormonal stimulation by cell-to-cell communication. *Nature,* 272**,** 501-6.

LE CANN, K., FOERSTER, A., RÖSSELER, C., ERICKSON, A., HAUTVAST, P., GIESSELMANN, S., PENSOLD, D., KURTH, I., ROTHERMEL, M., MATTIS, V. B., ZIMMER-BENSCH, G., VON HÖRSTEN, S., DENECKE, B., CLARNER, T., MEENTS, J. & LAMPERT, A. 2021. The difficulty to model Huntington's disease in vitro using striatal medium spiny neurons differentiated from human induced pluripotent stem cells. *Sci Rep,* 11**,** 6934.

LEE, E. B., PORTA, S., MICHAEL BAER, G., XU, Y., SUH, E., KWONG, L. K., ELMAN, L., GROSSMAN, M., LEE, V. M.-Y. & IRWIN, D. J. 2017a. Expansion of the classification of FTLD-TDP: distinct pathology associated with rapidly progressive frontotemporal degeneration. *Acta neuropathologica,* 134**,** 65-78.

LEE, J. C., JOO, K. M., CHOE, S. Y. & CHA, C. I. 2012. Region-specific changes in the immunoreactivity of TRPV4 expression in the central nervous system of SOD1(G93A) transgenic mice as an in vivo model of amyotrophic lateral sclerosis. *J Mol Histol,* 43**,** 625-31.

LEE, K. H., ZHANG, P., KIM, H. J., MITREA, D. M., SARKAR, M., FREIBAUM, B. D., CIKA, J., COUGHLIN, M., MESSING, J., MOLLIEX, A., MAXWELL, B. A., KIM, N. C., TEMIROV, J., MOORE, J., KOLAITIS, R. M., SHAW, T. I., BAI, B., PENG, J., KRIWACKI, R. W. & TAYLOR,

J. P. 2016. C9orf72 Dipeptide Repeats Impair the Assembly, Dynamics, and Function of Membrane-Less Organelles. *Cell,* 167**,** 774-788.e17.

LEE, S. & HUANG, E. J. 2017. Modeling ALS and FTD with iPSC-derived neurons. *Brain Research,* 1656**,** 88-97.

LEE, S. E., KHAZENZON, A. M., TRUJILLO, A. J., GUO, C. C., YOKOYAMA, J. S., SHA, S. J., TAKADA, L. T., KARYDAS, A. M., BLOCK, N. R. & COPPOLA, G. 2014. Altered network connectivity in frontotemporal dementia with C9orf72 hexanucleotide repeat expansion. *Brain,* 137**,** 3047-3060.

LEE, S. E., SIAS, A. C., MANDELLI, M. L., BROWN, J. A., BROWN, A. B., KHAZENZON, A. M., VIDOVSZKY, A. A., ZANTO, T. P., KARYDAS, A. M., PRIBADI, M., DOKURU, D., COPPOLA, G., GESCHWIND, D. H., RADEMAKERS, R., GORNO-TEMPINI, M. L., ROSEN, H. J., MILLER, B. L. & SEELEY, W. W. 2017b. Network degeneration and dysfunction in presymptomatic C9ORF72 expansion carriers. *Neuroimage Clin,* 14**,** 286-297.

LEE, Y. B., CHEN, H. J., PERES, J. N., GOMEZ-DEZA, J., ATTIG, J., STALEKAR, M., TROAKES, C., NISHIMURA, A. L., SCOTTER, E. L., VANCE, C., ADACHI, Y., SARDONE, V., MILLER, J. W., SMITH, B. N., GALLO, J. M., ULE, J., HIRTH, F., ROGELJ, B., HOUART, C. & SHAW, C. E. 2013. Hexanucleotide repeats in ALS/FTD form length-dependent RNA foci, sequester RNA binding proteins, and are neurotoxic. *Cell Rep,* 5**,** 1178-86.

LEMON, R. N. 2008. Descending pathways in motor control. *Annu. Rev. Neurosci.,* 31**,** 195-218.

LEROY, F. & ZYTNICKI, D. 2015. Is hyperexcitability really guilty in amyotrophic lateral sclerosis? *Neural Regen Res,* 10**,** 1413-5.

LESHCHENKO, Y., LIKHODII, S., YUE, W., BURNHAM, W. M. & PEREZ VELAZQUEZ, J. L. 2006. Carbenoxolone does not cross the blood brain barrier: an HPLC study. *BMC Neurosci,* 7**,** 3.

LEZMY, J., LIPINSKY, M., KHRAPUNSKY, Y., PATRICH, E., SHALOM, L., PERETZ, A., FLEIDERVISH, I. A. & ATTALI, B. 2017. M-current inhibition rapidly induces a unique CK2-dependent plasticity of the axon initial segment. *Proc Natl Acad Sci U S A,* 114**,** E10234-e10243.

LI, J., PARK, E., ZHONG, L. R. & CHEN, L. 2019. Homeostatic synaptic plasticity as a metaplasticity mechanism - a molecular and cellular perspective. *Curr Opin Neurobiol,* 54**,** 44-53.

LIN, L., YUAN, J., SANDER, B. & GOLAS, M. M. 2015. In Vitro Differentiation of Human Neural Progenitor Cells Into Striatal GABAergic Neurons. *Stem Cells Transl Med,* 4**,** 775-88.

LIN, Y., MORI, E., KATO, M., XIANG, S., WU, L., KWON, I. & MCKNIGHT, S. L. 2016. Toxic PR Poly-Dipeptides Encoded by the C9orf72 Repeat Expansion Target LC Domain Polymers. *Cell,* 167**,** 789-802.e12.

LIN, Z., KIM, E., AHMED, M., HAN, G., SIMMONS, C., REDHEAD, Y., BARTLETT, J., PENA ALTAMIRA, L. E., CALLAGHAN, I. & WHITE, M. A. 2021. MRI-guided histology of TDP-43 knock-in mice implicates parvalbumin interneuron loss, impaired neurogenesis and aberrant neurodevelopment in amyotrophic lateral sclerosis-frontotemporal dementia. *Brain Communications,* 3**,** fcab114.

LINDAU, M., JELIC, V., JOHANSSON, S. E., ANDERSEN, C., WAHLUND, L. O. & ALMKVIST, O. 2003. Quantitative EEG abnormalities and cognitive dysfunctions in frontotemporal dementia and Alzheimer's disease. *Dement Geriatr Cogn Disord,* 15**,** 106-14.

LINDINGER, M. I. & SJØGAARD, G. 1991. Potassium Regulation during Exercise and Recovery. *Sports Medicine,* 11**,** 382-401.

LINO, M. M., SCHNEIDER, C. & CARONI, P. 2002. Accumulation of SOD1 mutants in postnatal motoneurons does not cause motoneuron pathology or motoneuron disease. *Journal of Neuroscience,* 22**,** 4825-4832.

LISSONI, A., TAO, S., ALLEWAERT, R., WITSCHAS, K. & LEYBAERT, L. 2023. Cx43 Hemichannel and Panx1 Channel Modulation by Gap19 and (10)Panx1 Peptides. *Int J Mol Sci,* 24.

LISSONI, A., WANG, N., NEZLOBINSKII, T., DE SMET, M., PANFILOV, A. V., VANDERSICKEL, N., LEYBAERT, L. & WITSCHAS, K. 2020. Gap19, a Cx43 Hemichannel Inhibitor, Acts as a Gating Modifier That Decreases Main State Opening While Increasing Substate Gating. *International Journal of Molecular Sciences,* 21**,** 7340.

LIU, J. & WANG, F. 2017. Role of neuroinflammation in amyotrophic lateral sclerosis: cellular mechanisms and therapeutic implications. *Frontiers in immunology,* 8**,** 291752.

LIU, T., WOO, J. A., BUKHARI, M. Z., WANG, X., YAN, Y., BUOSI, S. C., ERMEKBAEVA, A., SISTA, A., KOTSIVIRAS, P., LEPOCHAT, P., CHACKO, A., ZHAO, X. & KANG, D. E. 2022. Modulation of synaptic plasticity, motor unit physiology, and TDP-43 pathology by CHCHD10. *Acta Neuropathol Commun,* 10**,** 95.

LIU, Y., PATTAMATTA, A., ZU, T., REID, T., BARDHI, O., BORCHELT, D. R., YACHNIS, A. T. & RANUM, L. P. 2016. C9orf72 BAC Mouse Model with Motor Deficits and Neurodegenerative Features of ALS/FTD. *Neuron,* 90**,** 521-34.

LIVESEY, M. R., MAGNANI, D., CLEARY, E. M., VASISTHA, N. A., JAMES, O. T., SELVARAJ, B. T., BURR, K., STORY, D., SHAW, C. E., KIND, P. C., HARDINGHAM, G. E., WYLLIE, D. J. & CHANDRAN, S. 2016. Maturation and electrophysiological properties of human pluripotent stem cell-derived oligodendrocytes. *Stem Cells,* 34**,** 1040-53.

LOGROSCINO, G. & CHIÒ, A. 2020. Amyotrophic lateral sclerosis (ALS) and fronto-temporal dementia (FTD). *In:* BRAYNE, C., FEIGIN, V. L., LAUNER, L. J., LOGROSCINO, G., BRAYNE, C., FEIGIN, V. L., LAUNER, L. J. & LOGROSCINO, G. (eds.) *Oxford Textbook of Neurologic and Neuropsychiatric Epidemiology.* Oxford University Press.

LOGROSCINO, G., PICCININNI, M., GRAFF, C., HARDIMAN, O., LUDOLPH, A. C., MORENO, F., OTTO, M., REMES, A. M., ROWE, J. B., SEELAAR, H., SOLJE, E., STEFANOVA, E., TRAYKOV, L., JELIC, V., RYDELL, M. T., PENDER, N., ANDERL-STRAUB, S., BARANDIARAN, M., GABILONDO, A., KRÜGER, J., MURLEY, A. G., RITTMAN, T., VAN DER ENDE, E. L., VAN SWIETEN, J. C., HARTIKAINEN, P., STOJMENOVIĆ, G. M., MEHRABIAN, S., BENUSSI, L., ALBERICI, A., DELL'ABATE, M. T., ZECCA, C., BORRONI, B. & GROUP, F. 2023. Incidence of Syndromes Associated With Frontotemporal Lobar Degeneration in 9 European Countries. *JAMA Neurology,* 80**,** 279-286.

LOMEN-HOERTH, C., ANDERSON, T. & MILLER, B. 2002. The overlap of amyotrophic lateral sclerosis and frontotemporal dementia. *Neurology,* 59**,** 1077-1079.

LOOI, J. & WALTERFANG, M. 2013. Striatal morphology as a biomarker in neurodegenerative disease. *Molecular Psychiatry,* 18**,** 417-424.

LOPEZ-GONZALEZ, R., LU, Y., GENDRON, T. F., KARYDAS, A., TRAN, H., YANG, D., PETRUCELLI, L., MILLER, B. L., ALMEIDA, S. & GAO, F. B. 2016. Poly(GR) in C9ORF72-Related ALS/FTD Compromises Mitochondrial Function and Increases Oxidative Stress and DNA Damage in iPSC-Derived Motor Neurons. *Neuron,* 92**,** 383-391.

LUI, H., ZHANG, J., MAKINSON, S. R., CAHILL, M. K., KELLEY, K. W., HUANG, H. Y., SHANG, Y., OLDHAM, M. C., MARTENS, L. H., GAO, F., COPPOLA, G., SLOAN, S. A., HSIEH, C. L., KIM, C. C., BIGIO, E. H., WEINTRAUB, S., MESULAM, M. M., RADEMAKERS, R., MACKENZIE, I. R., SEELEY, W. W., KARYDAS, A., MILLER, B. L., BORRONI, B., GHIDONI, R., FARESE, R.

V., JR., PAZ, J. T., BARRES, B. A. & HUANG, E. J. 2016. Progranulin Deficiency Promotes Circuit-Specific Synaptic Pruning by Microglia via Complement Activation. *Cell,* 165**,** 921-35.

LYON, H., SHOME, A., RUPENTHAL, I. D., GREEN, C. R. & MUGISHO, O. O. 2020. Tonabersat Inhibits Connexin43 Hemichannel Opening and Inflammasome Activation in an In Vitro Retinal Epithelial Cell Model of Diabetic Retinopathy. *Int J Mol Sci,* 22.

MA, D., FENG, L., CHENG, Y., XIN, M., YOU, J., YIN, X., HAO, Y., CUI, L. & FENG, J. 2018. Astrocytic gap junction inhibition by carbenoxolone enhances the protective effects of ischemic preconditioning following cerebral ischemia. *Journal of Neuroinflammation,* 15**,** 198.

MA, X. R., PRUDENCIO, M., KOIKE, Y., VATSAVAYAI, S. C., KIM, G., HARBINSKI, F., BRINER, A., RODRIGUEZ, C. M., GUO, C., AKIYAMA, T., SCHMIDT, H. B., CUMMINGS, B. B., WYATT, D. W., KURYLO, K., MILLER, G., MEKHOUBAD, S., SALLEE, N., MEKONNEN, G., GANSER, L., RUBIEN, J. D., JANSEN-WEST, K., COOK, C. N., PICKLES, S., OSKARSSON, B., GRAFF-RADFORD, N. R., BOEVE, B. F., KNOPMAN, D. S., PETERSEN, R. C., DICKSON, D. W., SHORTER, J., MYONG, S., GREEN, E. M., SEELEY, W. W., PETRUCELLI, L. & GITLER, A. D. 2022. TDP-43 represses cryptic exon inclusion in the FTD–ALS gene UNC13A. *Nature,* 603**,** 124-130.

MACHTS, J., LOEWE, K., KAUFMANN, J., JAKUBICZKA, S., ABDULLA, S., PETRI, S., DENGLER, R., HEINZE, H.-J., VIELHABER, S. & SCHOENFELD, M. A. 2015a. Basal ganglia pathology in ALS is associated with neuropsychological deficits. *Neurology,* 85**,** 1301-1309.

MACHTS, J., LOEWE, K., KAUFMANN, J., JAKUBICZKA, S., ABDULLA, S., PETRI, S., DENGLER, R., HEINZE, H.-J., VIELHABER, S., SCHOENFELD, M. A. & BEDE, P. 2015b. Basal ganglia pathology in ALS is associated with neuropsychological deficits. *Neurology,* 85**,** 1301-1309.

MACKENZIE, I. R., FRICK, P. & NEUMANN, M. 2014. The neuropathology associated with repeat expansions in the C9ORF72 gene. *Acta Neuropathol,* 127**,** 347-57.

MACKENZIE, I. R., NEUMANN, M., BABORIE, A., SAMPATHU, D. M., DU PLESSIS, D., JAROS, E., PERRY, R. H., TROJANOWSKI, J. Q., MANN, D. M. & LEE, V. M. 2011. A harmonized classification system for FTLD-TDP pathology. *Acta Neuropathol,* 122**,** 111-3.

MACKENZIE, I. R., NEUMANN, M., BIGIO, E. H., CAIRNS, N. J., ALAFUZOFF, I., KRIL, J., KOVACS, G. G., GHETTI, B., HALLIDAY, G., HOLM, I. E., INCE, P. G., KAMPHORST, W., REVESZ, T., ROZEMULLER, A. J., KUMAR-SINGH, S., AKIYAMA, H., BABORIE, A., SPINA, S., DICKSON, D. W., TROJANOWSKI, J. Q. & MANN, D. M. 2010. Nomenclature and nosology for neuropathologic subtypes of frontotemporal lobar degeneration: an update. *Acta Neuropathol,* 119**,** 1-4.

MACKENZIE, I. R. A. & RADEMAKERS, R. 2008. The role of transactive response DNA-binding protein-43 in amyotrophic lateral sclerosis and frontotemporal dementia. *Current Opinion in Neurology,* 21.

MADILL, M., MCDONAGH, K., MA, J., VAJDA, A., MCLOUGHLIN, P., O'BRIEN, T., HARDIMAN, O. & SHEN, S. 2017. Amyotrophic lateral sclerosis patient iPSC-derived astrocytes impair autophagy via non-cell autonomous mechanisms. *Mol Brain,* 10**,** 22.

MADJI HOUNOUM, B., MAVEL, S., COQUE, E., PATIN, F., VOURC'H, P., MAROUILLAT, S., NADAL-DESBARATS, L., EMOND, P., CORCIA, P., ANDRES, C. R., RAOUL, C. & BLASCO, H. 2017.

Wildtype motoneurons, ALS-Linked SOD1 mutation and glutamate profoundly modify astrocyte metabolism and lactate shuttling. *Glia,* 65**,** 592-605.

MAHONEY, C. J., DOWNEY, L. E., RIDGWAY, G. R., BECK, J., CLEGG, S., BLAIR, M., FINNEGAN, S., LEUNG, K. K., YEATMAN, T., GOLDEN, H., MEAD, S., ROHRER, J. D., FOX, N. C. & WARREN, J. D. 2012. Longitudinal neuroimaging and neuropsychological profiles of frontotemporal dementia with C9ORF72 expansions. *Alzheimers Res Ther,* 4**,** 41.

MAHONEY, D. J., KACZOR, J. J., BOURGEOIS, J., YASUDA, N. & TARNOPOLSKY, M. A. 2006. Oxidative stress and antioxidant enzyme upregulation in SOD1-G93A mouse skeletal muscle. *Muscle Nerve,* 33**,** 809-16.

MAJOUNIE, E., RENTON, A. E., MOK, K., DOPPER, E. G., WAITE, A., ROLLINSON, S., CHIÒ, A., RESTAGNO, G., NICOLAOU, N., SIMON-SANCHEZ, J., VAN SWIETEN, J. C., ABRAMZON, Y., JOHNSON, J. O., SENDTNER, M., PAMPHLETT, R., ORRELL, R. W., MEAD, S., SIDLE, K. C., HOULDEN, H., ROHRER, J. D., MORRISON, K. E., PALL, H., TALBOT, K., ANSORGE, O., HERNANDEZ, D. G., AREPALLI, S., SABATELLI, M., MORA, G., CORBO, M., GIANNINI, F., CALVO, A., ENGLUND, E., BORGHERO, G., FLORIS, G. L., REMES, A. M., LAAKSOVIRTA, H., MCCLUSKEY, L., TROJANOWSKI, J. Q., VAN DEERLIN, V. M., SCHELLENBERG, G. D., NALLS, M. A., DRORY, V. E., LU, C. S., YEH, T. H., ISHIURA, H., TAKAHASHI, Y., TSUJI, S., LE BER, I., BRICE, A., DREPPER, C., WILLIAMS, N., KIRBY, J., SHAW, P., HARDY, J., TIENARI, P. J., HEUTINK, P., MORRIS, H. R., PICKERING-BROWN, S. & TRAYNOR, B. J. 2012. Frequency of the C9orf72 hexanucleotide repeat expansion in patients with amyotrophic lateral sclerosis and frontotemporal dementia: a cross-sectional study. *Lancet Neurol,* 11**,** 323-30.

MARCHI, P. M., MARRONE, L., BRASSEUR, L., COENS, A., WEBSTER, C. P., BOUSSET, L., DESTRO, M., SMITH, E. F., WALTHER, C. G., ALFRED, V., MARROCCELLA, R., GRAVES, E. J., ROBINSON, D., SHAW, A. C., WAN, L. M., GRIERSON, A. J., EBBENS, S. J., DE VOS, K. J., HAUTBERGUE, G. M., FERRAIUOLO, L., MELKI, R. & AZZOUZ, M. 2022. C9ORF72-derived poly-GA DPRs undergo endocytic uptake in iAstrocytes and spread to motor neurons. *Life Sci Alliance,* 5.

MAREI, H. E., KHAN, M. U. A. & HASAN, A. 2023. Potential use of iPSCs for disease modeling, drug screening, and cell-based therapy for Alzheimer's disease. *Cellular & Molecular Biology Letters,* 28**,** 98.

MARIANI, M., KARKI, R., SPENNATO, M., PANDYA, D., HE, S., ANDREOLI, M., FIEDLER, P. & FERLINI, C. 2015. Class III β-tubulin in normal and cancer tissues. *Gene,* 563**,** 109-114.

MARSAN, E., VELMESHEV, D., RAMSEY, A., PATEL, R. K., ZHANG, J., KOONTZ, M., ANDREWS, M. G., DE MAJO, M., MORA, C., BLUMENFELD, J., LI, A. N., SPINA, S., GRINBERG, L. T., SEELEY, W. W., MILLER, B. L., ULLIAN, E. M., KRUMMEL, M. F., KRIEGSTEIN, A. R. & HUANG, E. J. 2023. Astroglial toxicity promotes synaptic degeneration in the thalamocortical circuit in frontotemporal dementia with GRN mutations. *J Clin Invest,* 133.

MARTÍNEZ-SILVA, M. L., IMHOFF-MANUEL, R. D., SHARMA, A., HECKMAN, C. J., SHNEIDER, N. A., ROSELLI, F., ZYTNICKI, D. & MANUEL, M. 2018. Hypoexcitability precedes denervation in the large fast-contracting motor units in two unrelated mouse models of ALS. *Elife,* 7.

MASELLI, R. A., WOLLMAN, R. L., LEUNG, C., DISTAD, B., PALOMBI, S., RICHMAN, D. P., SALAZAR-GRUESO, E. F. & ROOS, R. P. 1993. Neuromuscular transmission in amyotrophic lateral sclerosis. *Muscle Nerve,* 16**,** 1193-203.

MAVRIDIS, I. N. & PYRGELIS, E.-S. 2022. Nucleus accumbens atrophy in Parkinson's disease (Mavridis' atrophy): 10 years later. *American Journal of Neurodegenerative Disease,* 11**,** 17.

MCDOUALL, A., WASSINK, G., RANASINGHE, S., ZHOU, K. Q., KARUNASINGHE, R. N., DEAN, J. M. & DAVIDSON, J. O. 2024. Blockade of connexin hemichannels with tonabersat protects against mild hypoxic ischemic brain injury in neonatal rats. *Experimental Neurology,* 371**,** 114611.

MCGINTY, V. B., LARDEUX, S., TAHA, S. A., KIM, J. J. & NICOLA, S. M. 2013. Invigoration of reward seeking by cue and proximity encoding in the nucleus accumbens. *Neuron,* 78**,** 910-922.

MCKHANN, G. M., 2ND, D'AMBROSIO, R. & JANIGRO, D. 1997. Heterogeneity of astrocyte resting membrane potentials and intercellular coupling revealed by whole-cell and gramicidin-perforated patch recordings from cultured neocortical and hippocampal slice astrocytes. *J Neurosci,* 17**,** 6850-63.

MEHTA, A. R., GREGORY, J. M., DANDO, O., CARTER, R. N., BURR, K., NANDA, J., STORY, D., MCDADE, K., SMITH, C., MORTON, N. M., MAHAD, D. J., HARDINGHAM, G. E., CHANDRAN, S. & SELVARAJ, B. T. 2021. Mitochondrial bioenergetic deficits in C9orf72 amyotrophic lateral sclerosis motor neurons cause dysfunctional axonal homeostasis. *Acta Neuropathol,* 141**,** 257-279.

MEI, X., EZAN, P., GIAUME, C. & KOULAKOFF, A. 2010. Astroglial connexin immunoreactivity is specifically altered at β-amyloid plaques in β-amyloid precursor protein/presenilin1 mice. *Neuroscience,* 171**,** 92-105.

MÉNDEZ-LÓPEZ, I., SANCHO-BIELSA, F. J., ENGEL, T., GARCÍA, A. G. & PADÍN, J. F. 2021. Progressive Mitochondrial SOD1(G93A) Accumulation Causes Severe Structural, Metabolic and Functional Aberrations through OPA1 Down-Regulation in a Mouse Model of Amyotrophic Lateral Sclerosis. *Int J Mol Sci,* 22.

MENON, P., HIGASHIHARA, M., VAN DEN BOS, M., GEEVASINGA, N., KIERNAN, M. C. & VUCIC, S. 2020. Cortical hyperexcitability evolves with disease progression in ALS. *Annals of Clinical and Translational Neurology,* 7**,** 733-741.

MENON, P., KIERNAN, M. C. & VUCIC, S. 2015. Cortical hyperexcitability precedes lower motor neuron dysfunction in ALS. *Clin Neurophysiol,* 126**,** 803-9.

MERTENS, J., PAQUOLA, A. C. M., KU, M., HATCH, E., BÖHNKE, L., LADJEVARDI, S., MCGRATH, S., CAMPBELL, B., LEE, H., HERDY, J. R., GONÇALVES, J. T., TODA, T., KIM, Y., WINKLER, J., YAO, J., HETZER, M. W. & GAGE, F. H. 2015. Directly Reprogrammed Human Neurons Retain Aging-Associated Transcriptomic Signatures and Reveal Age-Related Nucleocytoplasmic Defects. *Cell Stem Cell,* 17**,** 705-718.

MEYER, K., FERRAIUOLO, L., MIRANDA, C. J., LIKHITE, S., MCELROY, S., RENUSCH, S., DITSWORTH, D., LAGIER-TOURENNE, C., SMITH, R. A., RAVITS, J., BURGHES, A. H., SHAW, P. J., CLEVELAND, D. W., KOLB, S. J. & KASPAR, B. K. 2014. Direct conversion of patient fibroblasts demonstrates non-cell autonomous toxicity of astrocytes to motor neurons in familial and sporadic ALS. *Proc Natl Acad Sci U S A,* 111**,** 829-32.

MI HWANG, E., KIM, E., YARISHKIN, O., HO WOO, D., HAN, K.-S., PARK, N., BAE, Y., WOO, J., KIM, D., PARK, M., LEE, C. J. & PARK, J.-Y. 2014. A disulphide-linked heterodimer of TWIK-1 and TREK-1 mediates passive conductance in astrocytes. *Nature Communications,* 5**,** 3227.

MIGNOGNA, M. L., MUSARDO, S., RANIERI, G., GELMINI, S., ESPINOSA, P., MARRA, P., BELLOLI, S., MURTAJ, V., MORESCO, R. M., BELLONE, C. & D'ADAMO, P. 2021. RAB39B-mediated trafficking of the GluA2-AMPAR subunit controls dendritic spine maturation and intellectual disability-related behaviour. *Mol Psychiatry,* 26**,** 6531-6549.

MILIOTO, C., CARCOLÉ, M., GIBLIN, A., CONEYS, R., ATTREBI, O., AHMED, M., HARRIS, S. S., LEE, B. I., YANG, M., ELLINGFORD, R. A., NIRUJOGI, R. S., BIGGS, D., SALOMONSSON, S., ZANOVELLO, M., DE OLIVEIRA, P., KATONA, E., GLARIA, I., MIKHEENKO, A., GEARY, B., UDINE, E., VAIZOGLU, D., ANOAR, S., JOTANGIYA, K., CROWLEY, G., SMEETH, D. M., ADAMS, M. L., NICCOLI, T., RADEMAKERS, R., VAN BLITTERSWIJK, M., DEVOY, A., HONG, S., PARTRIDGE, L., COYNE, A. N., FRATTA, P., ALESSI, D. R., DAVIES, B., BUSCHE, M. A., GREENSMITH, L., FISHER, E. M. C. & ISAACS, A. M. 2024. PolyGR and polyPR knock-in mice reveal a conserved neuroprotective extracellular matrix signature in C9orf72 ALS/FTD neurons. *Nature Neuroscience,* 27**,** 643-655.

MILLER, B. L., IKONTE, C., PONTON, M., LEVY, M., BOONE, K., DARBY, A., BERMAN, N., MENA, I. & CUMMINGS, J. L. 1997. A study of the Lund-Manchester research criteria for frontotemporal dementia. *Neurology,* 48**,** 937-941.

MITCHELL, J. M., O'NEIL, J. P., JANABI, M., MARKS, S. M., JAGUST, W. J. & FIELDS, H. L. 2012. Alcohol consumption induces endogenous opioid release in the human orbitofrontal cortex and nucleus accumbens. *Sci Transl Med,* 4**,** 116ra6.

MIURA, Y., LI, M.-Y., BIREY, F., IKEDA, K., REVAH, O., THETE, M. V., PARK, J.-Y., PUNO, A., LEE, S. H., PORTEUS, M. H. & PAŞCA, S. P. 2020. Generation of human striatal organoids and cortico-striatal assembloids from human pluripotent stem cells. *Nature Biotechnology,* 38**,** 1421-1430.

MIZIELINSKA, S., GRÖNKE, S., NICCOLI, T., RIDLER, C. E., CLAYTON, E. L., DEVOY, A., MOENS, T., NORONA, F. E., WOOLLACOTT, I. O. C., PIETRZYK, J., CLEVERLEY, K., NICOLL, A. J., PICKERING-BROWN, S., DOLS, J., CABECINHA, M., HENDRICH, O., FRATTA, P., FISHER, E. M. C., PARTRIDGE, L. & ISAACS, A. M. 2014. C9orf72 repeat expansions cause neurodegeneration in Drosophila through arginine-rich proteins. *Science,* 345**,** 1192-1194.

MIZIELINSKA, S. & ISAACS, A. M. 2014. C9orf72 amyotrophic lateral sclerosis and frontotemporal dementia: gain or loss of function? *Current opinion in neurology,* 27**,** 515-523.

MIZIELINSKA, S., LASHLEY, T., NORONA, F. E., CLAYTON, E. L., RIDLER, C. E., FRATTA, P. & ISAACS, A. M. 2013. C9orf72 frontotemporal lobar degeneration is characterised by frequent neuronal sense and antisense RNA foci. *Acta Neuropathol,* 126**,** 845-57.

MIZIELINSKA, S., RIDLER, C. E., BALENDRA, R., THOENG, A., WOODLING, N. S., GRÄSSER, F. A., PLAGNOL, V., LASHLEY, T., PARTRIDGE, L. & ISAACS, A. M. 2017. Bidirectional nucleolar dysfunction in C9orf72 frontotemporal lobar degeneration. *Acta Neuropathologica Communications,* 5**,** 29.

MOENS, T. G., NICCOLI, T., WILSON, K. M., ATILANO, M. L., BIRSA, N., GITTINGS, L. M., HOLBLING, B. V., DYSON, M. C., THOENG, A., NEEVES, J., GLARIA, I., YU, L., BUSSMANN, J., STORKEBAUM, E., PARDO, M., CHOUDHARY, J. S., FRATTA, P., PARTRIDGE, L. & ISAACS, A. M. 2019. C9orf72 arginine-rich dipeptide proteins interact with ribosomal proteins in vivo to induce a toxic translational arrest that is rescued by eIF1A. *Acta Neuropathol,* 137**,** 487-500.

MÖLLER, C., DIELEMAN, N., VAN DER FLIER, W. M., VERSTEEG, A., PIJNENBURG, Y., SCHELTENS, P., BARKHOF, F. & VRENKEN, H. 2015a. More atrophy of deep gray matter structures in frontotemporal dementia compared to Alzheimer's disease. *Journal of Alzheimer's Disease,* 44**,** 635-647.

MÖLLER, C., HAFKEMEIJER, A., PIJNENBURG, Y. A., ROMBOUTS, S. A., VAN DER GROND, J., DOPPER, E., VAN SWIETEN, J., VERSTEEG, A., POUWELS, P. J. & BARKHOF, F. 2015b. Joint assessment of white matter integrity, cortical and subcortical atrophy to distinguish AD from behavioral variant FTD: A two-center study. *NeuroImage: Clinical,* 9**,** 418-429.

MONGIAT, L. A., ESPÓSITO, M. S., LOMBARDI, G. & SCHINDER, A. F. 2009. Reliable activation of immature neurons in the adult hippocampus. *PLoS One,* 4**,** e5320.

MONTIBELLER, L., TAN, L. Y., KIM, J. K., PAUL, P. & DE BELLEROCHE, J. 2020. Tissue-selective regulation of protein homeostasis and unfolded protein response signalling in sporadic ALS. *Journal of Cellular and Molecular Medicine,* 24**,** 6055-6069.

MORI, K., ARZBERGER, T., GRÄSSER, F. A., GIJSELINCK, I., MAY, S., RENTZSCH, K., WENG, S. M., SCHLUDI, M. H., VAN DER ZEE, J., CRUTS, M., VAN BROECKHOVEN, C., KREMMER, E., KRETZSCHMAR, H. A., HAASS, C. & EDBAUER, D. 2013a. Bidirectional transcripts of the expanded C9orf72 hexanucleotide repeat are translated into aggregating dipeptide repeat proteins. *Acta Neuropathol,* 126**,** 881-93.

MORI, K., WENG, S.-M., ARZBERGER, T., MAY, S., RENTZSCH, K., KREMMER, E., SCHMID, B., KRETZSCHMAR, H. A., CRUTS, M. & VAN BROECKHOVEN, C. 2013b. The C9orf72 GGGGCC repeat is translated into aggregating dipeptide-repeat proteins in FTLD/ALS. *Science,* 339**,** 1335-1338.

MORI, K., WENG, S. M., ARZBERGER, T., MAY, S., RENTZSCH, K., KREMMER, E., SCHMID, B., KRETZSCHMAR, H. A., CRUTS, M., VAN BROECKHOVEN, C., HAASS, C. & EDBAUER, D. 2013c. The C9orf72 GGGGCC repeat is translated into aggregating dipeptide-repeat proteins in FTLD/ALS. *Science,* 339**,** 1335-8.

MORIGAKI, R. & GOTO, S. 2017. Striatal Vulnerability in Huntington's Disease: Neuroprotection Versus Neurotoxicity. *Brain Sci,* 7.

MORRISON, B. M., GORDON, J. W., RIPPS, M. E. & MORRISON, J. H. 1996. Quantitative immunocytochemical analysis of the spinal cord in G86R superoxide dismutase transgenic mice: neurochemical correlates of selective vulnerability. *Journal of Comparative Neurology,* 373**,** 619-631.

MOYA, M. V., KIM, R. D., RAO, M. N., COTTO, B. A., PICKETT, S. B., SFERRAZZA, C. E., HEINTZ, N. & SCHMIDT, E. F. 2022. Unique molecular features and cellular responses differentiate two populations of motor cortical layer 5b neurons in a preclinical model of ALS. *Cell Rep,* 38**,** 110556.

MURPHY, N. A., ARTHUR, K. C., TIENARI, P. J., HOULDEN, H., CHIÒ, A. & TRAYNOR, B. J. 2017. Age-related penetrance of the C9orf72 repeat expansion. *Scientific reports,* 7**,** 2116.

MURPHY-ROYAL, C., JOHNSTON, A. D., BOYCE, A. K. J., DIAZ-CASTRO, B., INSTITORIS, A., PERINGOD, G., ZHANG, O., STOUT, R. F., SPRAY, D. C., THOMPSON, R. J., KHAKH, B. S., BAINS, J. S. & GORDON, G. R. 2020. Stress gates an astrocytic energy reservoir to impair synaptic plasticity. *Nat Commun,* 11**,** 2014.

NAGAI, J., RAJBHANDARI, A. K., GANGWANI, M. R., HACHISUKA, A., COPPOLA, G., MASMANIDIS, S. C., FANSELOW, M. S. & KHAKH, B. S. 2019. Hyperactivity with

Disrupted Attention by Activation of an Astrocyte Synaptogenic Cue. *Cell,* 177**,** 1280-1292.e20.

NAGAI, M., RE, D. B., NAGATA, T., CHALAZONITIS, A., JESSELL, T. M., WICHTERLE, H. & PRZEDBORSKI, S. 2007. Astrocytes expressing ALS-linked mutated SOD1 release factors selectively toxic to motor neurons. *Nat Neurosci,* 10**,** 615-22.

NAGAI, T., NAKAMUTA, S., KURODA, K., NAKAUCHI, S., NISHIOKA, T., TAKANO, T., ZHANG, X., TSUBOI, D., FUNAHASHI, Y., NAKANO, T., YOSHIMOTO, J., KOBAYASHI, K., UCHIGASHIMA, M., WATANABE, M., MIURA, M., NISHI, A., KOBAYASHI, K., YAMADA, K., AMANO, M. & KAIBUCHI, K. 2016. Phosphoproteomics of the Dopamine Pathway Enables Discovery of Rap1 Activation as a Reward Signal In Vivo. *Neuron,* 89**,** 550-565.

NAGY, J., LI, W., HERTZBERG, E. & MAROTTA, C. 1996. Elevated connexin43 immunoreactivity at sites of amyloid plaques in Alzheimer's disease. *Brain research,* 717**,** 173-178.

NAGY, J., PATEL, D., OCHALSKI, P. & STELMACK, G. 1999. Connexin30 in rodent, cat and human brain: selective expression in gray matter astrocytes, co-localization with connexin43 at gap junctions and late developmental appearance. *Neuroscience,* 88**,** 447-468.

NASCIMENTO, A. I., DA SILVA, T. F., FERNANDES, E. C., LUZ, L. L., MAR, F. M., SAFRONOV, B. V. & SOUSA, M. M. 2022. Sensory neurons have an axon initial segment that initiates spontaneous activity in neuropathic pain. *Brain,* 145**,** 1632-1640.

NASSEROLESLAMI, B., DUKIC, S., BRODERICK, M., MOHR, K., SCHUSTER, C., GAVIN, B., MCLAUGHLIN, R., HEVERIN, M., VAJDA, A., IYER, P. M., PENDER, N., BEDE, P., LALOR, E. C. & HARDIMAN, O. 2019. Characteristic Increases in EEG Connectivity Correlate With Changes of Structural MRI in Amyotrophic Lateral Sclerosis. *Cereb Cortex,* 29**,** 27-41.

NAUJOCK, M., STANSLOWSKY, N., BUFLER, S., NAUMANN, M., REINHARDT, P., STERNECKERT, J., KEFALAKES, E., KASSEBAUM, C., BURSCH, F., LOJEWSKI, X., STORCH, A., FRICKENHAUS, M., BOECKERS, T. M., PUTZ, S., DEMESTRE, M., LIEBAU, S., KLINGENSTEIN, M., LUDOLPH, A. C., DENGLER, R., KIM, K. S., HERMANN, A., WEGNER, F. & PETRI, S. 2016. 4-Aminopyridine Induced Activity Rescues Hypoexcitable Motor Neurons from Amyotrophic Lateral Sclerosis Patient-Derived Induced Pluripotent Stem Cells. *Stem Cells,* 34**,** 1563-75.

NAUMENKO, N., POLLARI, E., KURRONEN, A., GINIATULLINA, R., SHAKIRZYANOVA, A., MAGGA, J., KOISTINAHO, J. & GINIATULLIN, R. 2011. Gender-Specific Mechanism of Synaptic Impairment and Its Prevention by GCSF in a Mouse Model of ALS. *Front Cell Neurosci,* 5**,** 26.

NEARY, D., SNOWDEN, J. S., GUSTAFSON, L., PASSANT, U., STUSS, D., BLACK, S., FREEDMAN, M., KERTESZ, A., ROBERT, P. & ALBERT, M. 1998. Frontotemporal lobar degeneration: a consensus on clinical diagnostic criteria. *Neurology,* 51**,** 1546-1554.

NEUMANN, M., SAMPATHU, D. M., KWONG, L. K., TRUAX, A. C., MICSENYI, M. C., CHOU, T. T., BRUCE, J., SCHUCK, T., GROSSMAN, M. & CLARK, C. M. 2006a. Ubiquitinated TDP-43 in frontotemporal lobar degeneration and amyotrophic lateral sclerosis. *Science,* 314**,** 130-133.

NEUMANN, M., SAMPATHU, D. M., KWONG, L. K., TRUAX, A. C., MICSENYI, M. C., CHOU, T. T., BRUCE, J., SCHUCK, T., GROSSMAN, M., CLARK, C. M., MCCLUSKEY, L. F., MILLER, B. L., MASLIAH, E., MACKENZIE, I. R., FELDMAN, H., FEIDEN, W., KRETZSCHMAR, H. A., TROJANOWSKI, J. Q. & LEE, V. M. 2006b. Ubiquitinated TDP-43 in frontotemporal lobar degeneration and amyotrophic lateral sclerosis. *Science,* 314**,** 130-3.

NG, B., ROWLAND, H. A., WEI, T., ARUNASALAM, K., HAYES, E. M., KOYCHEV, I., HEDEGAARD, A., RIBE, E. M., CHAN, D., CHESSELL, T., FFYTCHE, D., GUNN, R. N., KOCAGONCU, E., LAWSON, J., MALHOTRA, P. A., RIDHA, B. H., ROWE, J. B., THOMAS, A. J., ZAMBONI, G., BUCKLEY, N. J., CADER, Z. M., LOVESTONE, S. & WADE-MARTINS, R. 2022. Neurons derived from individual early Alzheimer's disease patients reflect their clinical vulnerability. *Brain Commun,* 4**,** fcac267.

NISHIDA, K., YOSHIMURA, M., ISOTANI, T., YOSHIDA, T., KITAURA, Y., SAITO, A., MII, H., KATO, M., TAKEKITA, Y., SUWA, A., MORITA, S. & KINOSHITA, T. 2011. Differences in quantitative EEG between frontotemporal dementia and Alzheimer's disease as revealed by LORETA. *Clin Neurophysiol,* 122**,** 1718-25.

NISHIHIRA, Y., TAN, C. F., ONODERA, O., TOYOSHIMA, Y., YAMADA, M., MORITA, T., NISHIZAWA, M., KAKITA, A. & TAKAHASHI, H. 2008. Sporadic amyotrophic lateral sclerosis: two pathological patterns shown by analysis of distribution of TDP-43-immunoreactive neuronal and glial cytoplasmic inclusions. *Acta Neuropathol,* 116**,** 169-82.

NONOMURA, S., NISHIZAWA, K., SAKAI, Y., KAWAGUCHI, Y., KATO, S., UCHIGASHIMA, M., WATANABE, M., YAMANAKA, K., ENOMOTO, K., CHIKEN, S., SANO, H., SOMA, S., YOSHIDA, J., SAMEJIMA, K., OGAWA, M., KOBAYASHI, K., NAMBU, A., ISOMURA, Y. & KIMURA, M. 2018. Monitoring and Updating of Action Selection for Goal-Directed Behavior through the Striatal Direct and Indirect Pathways. *Neuron,* 99**,** 1302-1314.e5.

NORDIN, A., AKIMOTO, C., WUOLIKAINEN, A., ALSTERMARK, H., JONSSON, P., BIRVE, A., MARKLUND, S. L., GRAFFMO, K. S., FORSBERG, K. & BRÄNNSTRÖM, T. 2015. Extensive size variability of the GGGGCC expansion in C9orf72 in both neuronal and non-neuronal tissues in 18 patients with ALS or FTD. *Human molecular genetics,* 24**,** 3133-3142.

ONESTO, E., COLOMBRITA, C., GUMINA, V., BORGHI, M. O., DUSI, S., DORETTI, A., FAGIOLARI, G., INVERNIZZI, F., MOGGIO, M. & TIRANTI, V. 2016. Gene-specific mitochondria dysfunctions in human TARDBP and C9ORF72 fibroblasts. *Acta neuropathologica communications,* 4**,** 1-14.

ORELLANA, J. A., FROGER, N., EZAN, P., JIANG, J. X., BENNETT, M. V., NAUS, C. C., GIAUME, C. & SÁEZ, J. C. 2011. ATP and glutamate released via astroglial connexin 43 hemichannels mediate neuronal death through activation of pannexin 1 hemichannels. *J Neurochem,* 118**,** 826-40.

ORELLANA, J. A., MORAGA-AMARO, R., DÍAZ-GALARCE, R., ROJAS, S., MATURANA, C. J., STEHBERG, J. & SÁEZ, J. C. 2015. Restraint stress increases hemichannel activity in hippocampal glial cells and neurons. *Front Cell Neurosci,* 9**,** 102.

ORTIZ-RODRIGUEZ, A. & AREVALO, M. A. 2020. The Contribution of Astrocyte Autophagy to Systemic Metabolism. *Int J Mol Sci,* 21.

OSKARSSON, B., HORTON, D. K. & MITSUMOTO, H. 2015. Potential Environmental Factors in Amyotrophic Lateral Sclerosis. *Neurol Clin,* 33**,** 877-88.

OYAMADA, M., TAKEBE, K. & OYAMADA, Y. 2013. Regulation of connexin expression by transcription factors and epigenetic mechanisms. *Biochimica et Biophysica Acta (BBA) - Biomembranes,* 1828**,** 118-133.

PAGE, S. C., SRIPATHY, S. R., FARINELLI, F., YE, Z., WANG, Y., HILER, D. J., PATTIE, E. A., NGUYEN, C. V., TIPPANI, M. & MOSES, R. L. 2022a. Electrophysiological measures from human iPSC-derived neurons are associated with schizophrenia clinical status and

predict individual cognitive performance. *Proceedings of the National Academy of Sciences,* 119**,** e2109395119.

PAGE, S. C., SRIPATHY, S. R., FARINELLI, F., YE, Z., WANG, Y., HILER, D. J., PATTIE, E. A., NGUYEN, C. V., TIPPANI, M., MOSES, R. L., CHEN, H. Y., TRAN, M. N., EAGLES, N. J., STOLZ, J. M., CATALLINI, J. L., 2ND, SOUDRY, O. R., DICKINSON, D., BERMAN, K. F., APUD, J. A., WEINBERGER, D. R., MARTINOWICH, K., JAFFE, A. E., STRAUB, R. E. & MAHER, B. J. 2022b. Electrophysiological measures from human iPSC-derived neurons are associated with schizophrenia clinical status and predict individual cognitive performance. *Proc Natl Acad Sci U S A,* 119.

PALMINHA, N. M., DOS SANTOS SOUZA, C., GRIFFIN, J., LIAO, C., FERRAIUOLO, L. & EL-KHAMISY, S. F. 2022. Defective repair of topoisomerase I induced chromosomal damage in Huntington's disease. *Cellular and Molecular Life Sciences,* 79**,** 160.

PARAKH, S. & ATKIN, J. D. 2016. Protein folding alterations in amyotrophic lateral sclerosis. *Brain Research,* 1648**,** 633-649.

PARAMESWARAN, J., ZHANG, N., BRAEMS, E., TILAHUN, K., PANT, D. C., YIN, K., ASRESS, S., HEEREN, K., BANERJEE, A., DAVIS, E., SCHWARTZ, S. L., CONN, G. L., BASSELL, G. J., VAN DEN BOSCH, L. & JIANG, J. 2023. Antisense, but not sense, repeat expanded RNAs activate PKR/eIF2α-dependent ISR in C9ORF72 FTD/ALS. *Elife,* 12.

PASNICEANU, I. S., ATWAL, M. S., SOUZA, C. D. S., FERRAIUOLO, L. & LIVESEY, M. R. 2021. Emerging Mechanisms Underpinning Neurophysiological Impairments in C9ORF72 Repeat Expansion-Mediated Amyotrophic Lateral Sclerosis/Frontotemporal Dementia. *Front Cell Neurosci,* 15**,** 784833.

PATTON, M. H., BIZUP, B. T. & GRACE, A. A. 2013. The infralimbic cortex bidirectionally modulates mesolimbic dopamine neuron activity via distinct neural pathways. *J Neurosci,* 33**,** 16865-73.

PAULI, W. M., O'REILLY, R. C., YARKONI, T. & WAGER, T. D. 2016. Regional specialization within the human striatum for diverse psychological functions. *Proceedings of the National Academy of Sciences,* 113**,** 1907-1912.

PEHAR, M., HARLAN, B. A., KILLOY, K. M. & VARGAS, M. R. 2017. Role and Therapeutic Potential of Astrocytes in Amyotrophic Lateral Sclerosis. *Curr Pharm Des,* 23**,** 5010-5021.

PENG, A. Y. T., AGRAWAL, I., HO, W. Y., YEN, Y.-C., PINTER, A. J., LIU, J., PHUA, Q. X. C., KOH, K. B., CHANG, J.-C. & SANFORD, E. 2020. Loss of TDP-43 in astrocytes leads to motor deficits by triggering A1-like reactive phenotype and triglial dysfunction. *Proceedings of the National Academy of Sciences,* 117**,** 29101-29112.

PENGO, M., ALBERICI, A., LIBRI, I., BENUSSI, A., GADOLA, Y., ASHTON, N. J., ZETTERBERG, H., BLENNOW, K. & BORRONI, B. 2022. Sex influences clinical phenotype in frontotemporal dementia. *Neurol Sci,* 43**,** 5281-5287.

PERKINS, E. M., BURR, K., BANERJEE, P., MEHTA, A. R., DANDO, O., SELVARAJ, B. T., SUMINAITE, D., NANDA, J., HENSTRIDGE, C. M., GILLINGWATER, T. H., HARDINGHAM, G. E., WYLLIE, D. J. A., CHANDRAN, S. & LIVESEY, M. R. 2021. Altered network properties in C9ORF72 repeat expansion cortical neurons are due to synaptic dysfunction. *Mol Neurodegener,* 16**,** 13.

PERREAULT, M. L., HASBI, A., O'DOWD, B. F. & GEORGE, S. R. 2011. The Dopamine D1–D2 Receptor Heteromer in Striatal Medium Spiny Neurons: Evidence for a Third Distinct Neuronal Pathway in Basal Ganglia. *Frontiers in Neuroanatomy,* 5.

PERRETEN LAMBERT, H., ZENGER, M., AZARIAS, G., CHATTON, J. Y., MAGISTRETTI, P. J. & LENGACHER, S. 2014. Control of mitochondrial pH by uncoupling protein 4 in astrocytes promotes neuronal survival. *J Biol Chem,* 289**,** 31014-28.

PERRY, D. C., BROWN, J. A., POSSIN, K. L., DATTA, S., TRUJILLO, A., RADKE, A., KARYDAS, A., KORNAK, J., SIAS, A. C. & RABINOVICI, G. D. 2017a. Clinicopathological correlations in behavioural variant frontotemporal dementia. *Brain,* 140**,** 3329-3345.

PERRY, D. C., STURM, V. E., SEELEY, W. W., MILLER, B. L., KRAMER, J. H. & ROSEN, H. J. 2014. Anatomical correlates of reward-seeking behaviours in behavioural variant frontotemporal dementia. *Brain,* 137**,** 1621-1626.

PERRY, S., HAN, Y., DAS, A. & DICKMAN, D. 2017b. Homeostatic plasticity can be induced and expressed to restore synaptic strength at neuromuscular junctions undergoing ALS-related degeneration. *Hum Mol Genet,* 26**,** 4153-4167.

PETERS, O. M., CABRERA, G. T., TRAN, H., GENDRON, T. F., MCKEON, J. E., METTERVILLE, J., WEISS, A., WIGHTMAN, N., SALAMEH, J., KIM, J., SUN, H., BOYLAN, K. B., DICKSON, D., KENNEDY, Z., LIN, Z., ZHANG, Y. J., DAUGHRITY, L., JUNG, C., GAO, F. B., SAPP, P. C., HORVITZ, H. R., BOSCO, D. A., BROWN, S. P., DE JONG, P., PETRUCELLI, L., MUELLER, C. & BROWN, R. H., JR. 2015. Human C9ORF72 Hexanucleotide Expansion Reproduces RNA Foci and Dipeptide Repeat Proteins but Not Neurodegeneration in BAC Transgenic Mice. *Neuron,* 88**,** 902-909.

PETKAU, T. L., NEAL, S. J., MILNERWOOD, A., MEW, A., HILL, A. M., ORBAN, P., GREGG, J., LU, G., FELDMAN, H. H., MACKENZIE, I. R., RAYMOND, L. A. & LEAVITT, B. R. 2012. Synaptic dysfunction in progranulin-deficient mice. *Neurobiol Dis,* 45**,** 711-22.

PHATNANI, H. P., GUARNIERI, P., FRIEDMAN, B. A., CARRASCO, M. A., MURATET, M., O'KEEFFE, S., NWAKEZE, C., PAULI-BEHN, F., NEWBERRY, K. M., MEADOWS, S. K., TAPIA, J. C., MYERS, R. M. & MANIATIS, T. 2013. Intricate interplay between astrocytes and motor neurons in ALS. *Proc Natl Acad Sci U S A,* 110**,** E756-65.

PHELPS, E. A. & LEDOUX, J. E. 2005. Contributions of the amygdala to emotion processing: from animal models to human behavior. *Neuron,* 48**,** 175-187.

PHILIPS, T. & ROTHSTEIN, J. D. 2015. Rodent Models of Amyotrophic Lateral Sclerosis. *Curr Protoc Pharmacol,* 69**,** 5.67.1-5.67.21.

PINDER, R. M., BROGDEN, R. N., SAWYER, P. R., SPEIGHT, T. M., SPENCER, R. & AVERY, G. S. 1976. Carbenoxolone: a review of its pharmacological properties and therapeutic efficacy in peptic ulcer disease. *Drugs,* 11**,** 245-307.

PROUDFOOT, M., GUTOWSKI, N. J., EDBAUER, D., HILTON, D. A., STEPHENS, M., RANKIN, J. & MACKENZIE, I. R. 2014. Early dipeptide repeat pathology in a frontotemporal dementia kindred with C9ORF72 mutation and intellectual disability. *Acta neuropathologica,* 127**,** 451-458.

PROUDFOOT, M., ROHENKOHL, G., QUINN, A., COLCLOUGH, G. L., WUU, J., TALBOT, K., WOOLRICH, M. W., BENATAR, M., NOBRE, A. C. & TURNER, M. R. 2017. Altered cortical beta-band oscillations reflect motor system degeneration in amyotrophic lateral sclerosis. *Hum Brain Mapp,* 38**,** 237-254.

PROVENZANO, F., NYBERG, S., GIUNTI, D., TORAZZA, C., PARODI, B., BONIFACINO, T., USAI, C., KERLERO DE ROSBO, N., MILANESE, M., UCCELLI, A., SHAW, P. J., FERRAIUOLO, L. & BONANNO, G. 2022. Micro-RNAs Shuttled by Extracellular Vesicles Secreted from Mesenchymal Stem Cells Dampen Astrocyte Pathological Activation and Support Neuroprotection in In-Vitro Models of ALS. *Cells,* 11.

PRUDENCIO, M., BELZIL, V. V., BATRA, R., ROSS, C. A., GENDRON, T. F., PREGENT, L. J., MURRAY, M. E., OVERSTREET, K. K., PIAZZA-JOHNSTON, A. E. & DESARO, P. 2015. Distinct brain transcriptome profiles in C9orf72-associated and sporadic ALS. *Nature neuroscience,* 18**,** 1175-1182.

QIAN, K., HUANG, H., PETERSON, A., HU, B., MARAGAKIS, N. J., MING, G.-L., CHEN, H. & ZHANG, S.-C. 2017. Sporadic ALS astrocytes induce neuronal degeneration in vivo. *Stem cell reports,* 8**,** 843-855.

QU, Y. & DAHL, G. 2002. Function of the voltage gate of gap junction channels: Selective exclusion of molecules. *Proceedings of the National Academy of Sciences,* 99**,** 697-702.

QUAEGEBEUR, A., GLARIA, I., LASHLEY, T. & ISAACS, A. M. 2020. Soluble and insoluble dipeptide repeat protein measurements in C9orf72-frontotemporal dementia brains show regional differential solubility and correlation of poly-GR with clinical severity. *Acta Neuropathol Commun,* 8**,** 184.

QUESSEVEUR, G., PORTAL, B., BASILE, J.-A., EZAN, P., MATHOU, A., HALLEY, H., LELOUP, C., FIORAMONTI, X., DÉGLON, N. & GIAUME, C. 2015. Attenuated levels of hippocampal connexin 43 and its phosphorylation correlate with antidepressant-and anxiolytic-like activities in mice. *Frontiers in cellular neuroscience,* 9**,** 490.

RAMACHANDRAN, S., XIE, L. H., JOHN, S. A., SUBRAMANIAM, S. & LAL, R. 2007. A novel role for connexin hemichannel in oxidative stress and smoking-induced cell injury. *PLoS One,* 2**,** e712.

RAMESH, N. & PANDEY, U. B. 2017. Autophagy dysregulation in ALS: when protein aggregates get out of hand. *Frontiers in molecular neuroscience,* 10**,** 263.

RANUM, L. P. & DAY, J. W. 2004. Myotonic dystrophy: RNA pathogenesis comes into focus. *Am J Hum Genet,* 74**,** 793-804.

RASCOVSKY, K., HODGES, J. R., KNOPMAN, D., MENDEZ, M. F., KRAMER, J. H., NEUHAUS, J., VAN SWIETEN, J. C., SEELAAR, H., DOPPER, E. G. & ONYIKE, C. U. 2011. Sensitivity of revised diagnostic criteria for the behavioural variant of frontotemporal dementia. *Brain,* 134**,** 2456-2477.

RE, D. B., LE VERCHE, V., YU, C., AMOROSO, M. W., POLITI, K. A., PHANI, S., IKIZ, B., HOFFMANN, L., KOOLEN, M., NAGATA, T., PAPADIMITRIOU, D., NAGY, P., MITSUMOTO, H., KARIYA, S., WICHTERLE, H., HENDERSON, C. E. & PRZEDBORSKI, S. 2014. Necroptosis drives motor neuron death in models of both sporadic and familial ALS. *Neuron,* 81**,** 1001-1008.

REDGRAVE, P., RODRIGUEZ, M., SMITH, Y., RODRIGUEZ-OROZ, M. C., LEHERICY, S., BERGMAN, H., AGID, Y., DELONG, M. R. & OBESO, J. A. 2010. Goal-directed and habitual control in the basal ganglia: implications for Parkinson's disease. *Nat Rev Neurosci,* 11**,** 760-72.

REI, N., ROMBO, D. M., FERREIRA, M. F., BAQI, Y., MÜLLER, C. E., RIBEIRO, J. A., SEBASTIÃO, A. M. & VAZ, S. H. 2020. Hippocampal synaptic dysfunction in the SOD1G93A mouse model of Amyotrophic Lateral Sclerosis: Reversal by adenosine A2AR blockade. *Neuropharmacology,* 171**,** 108106.

REN, R., ZHANG, L. & WANG, M. 2018. Specific deletion connexin43 in astrocyte ameliorates cognitive dysfunction in APP/PS1 mice. *Life sciences,* 208**,** 175-191.

RENTON, A. E., CHIÒ, A. & TRAYNOR, B. J. 2014. State of play in amyotrophic lateral sclerosis genetics. *Nature Neuroscience,* 17**,** 17-23.

RENTON, A. E., MAJOUNIE, E., WAITE, A., SIMÓN-SÁNCHEZ, J., ROLLINSON, S., GIBBS, J. R., SCHYMICK, J. C., LAAKSOVIRTA, H., VAN SWIETEN, J. C., MYLLYKANGAS, L., KALIMO, H., PAETAU, A., ABRAMZON, Y., REMES, A. M., KAGANOVICH, A., SCHOLZ, S. W., DUCKWORTH, J., DING, J., HARMER, D. W., HERNANDEZ, D. G., JOHNSON, J. O., MOK, K., RYTEN, M., TRABZUNI, D., GUERREIRO, R. J., ORRELL, R. W., NEAL, J., MURRAY, A., PEARSON, J., JANSEN, I. E., SONDERVAN, D., SEELAAR, H., BLAKE, D., YOUNG, K., HALLIWELL, N., CALLISTER, J. B., TOULSON, G., RICHARDSON, A., GERHARD, A., SNOWDEN, J., MANN, D., NEARY, D., NALLS, M. A., PEURALINNA, T., JANSSON, L., ISOVIITA, V. M., KAIVORINNE, A. L., HÖLTTÄ-VUORI, M., IKONEN, E., SULKAVA, R., BENATAR, M., WUU, J., CHIÒ, A., RESTAGNO, G., BORGHERO, G., SABATELLI, M., HECKERMAN, D., ROGAEVA, E., ZINMAN, L., ROTHSTEIN, J. D., SENDTNER, M., DREPPER, C., EICHLER, E. E., ALKAN, C., ABDULLAEV, Z., PACK, S. D., DUTRA, A., PAK, E., HARDY, J., SINGLETON, A., WILLIAMS, N. M., HEUTINK, P., PICKERING-BROWN, S., MORRIS, H. R., TIENARI, P. J. & TRAYNOR, B. J. 2011. A hexanucleotide repeat expansion in C9ORF72 is the cause of chromosome 9p21-linked ALS-FTD. *Neuron,* 72**,** 257-68.

RIKANI, A. A., CHOUDHRY, Z., CHOUDHRY, A. M., RIZVI, N., IKRAM, H., MOBASSARAH, N. J. & TULI, S. 2014. The mechanism of degeneration of striatal neuronal subtypes in Huntington disease. *Annals of neurosciences,* 21**,** 112.

RIKU, Y., WATANABE, H., YOSHIDA, M., MIMURO, M., IWASAKI, Y., MASUDA, M., ISHIGAKI, S., KATSUNO, M. & SOBUE, G. 2016. Marked Involvement of the Striatal Efferent System in TAR DNA-Binding Protein 43 kDa-Related Frontotemporal Lobar Degeneration and Amyotrophic Lateral Sclerosis. *Journal of Neuropathology & Experimental Neurology,* 75**,** 801-811.

ROBERTSON, J., SANELLI, T., XIAO, S., YANG, W., HORNE, P., HAMMOND, R., PIORO, E. P. & STRONG, M. J. 2007. Lack of TDP-43 abnormalities in mutant SOD1 transgenic mice shows disparity with ALS. *Neurosci Lett,* 420**,** 128-32.

ROHRER, J. D., GUERREIRO, R., VANDROVCOVA, J., UPHILL, J., REIMAN, D., BECK, J., ISAACS, A. M., AUTHIER, A., FERRARI, R., FOX, N. C., MACKENZIE, I. R., WARREN, J. D., DE SILVA, R., HOLTON, J., REVESZ, T., HARDY, J., MEAD, S. & ROSSOR, M. N. 2009. The heritability and genetics of frontotemporal lobar degeneration. *Neurology,* 73**,** 1451-6.

ROSEN, D. R., SIDDIQUE, T., PATTERSON, D., FIGLEWICZ, D. A., SAPP, P., HENTATI, A., DONALDSON, D., GOTO, J., O'REGAN, J. P. & DENG, H.-X. 1993. Mutations in Cu/Zn superoxide dismutase gene are associated with familial amyotrophic lateral sclerosis. *Nature,* 362**,** 59-62.

ROSEN, H. J., ALLISON, S. C., SCHAUER, G. F., GORNO-TEMPINI, M. L., WEINER, M. W. & MILLER, B. L. 2005. Neuroanatomical correlates of behavioural disorders in dementia. *Brain,* 128**,** 2612-2625.

ROSENBLUM, L. T. & TROTTI, D. 2017. EAAT2 and the Molecular Signature of Amyotrophic Lateral Sclerosis. *Adv Neurobiol,* 16**,** 117-136.

ROSSI, D., BRAMBILLA, L., VALORI, C. F., RONCORONI, C., CRUGNOLA, A., YOKOTA, T., BREDESEN, D. E. & VOLTERRA, A. 2008. Focal degeneration of astrocytes in amyotrophic lateral sclerosis. *Cell Death Differ,* 15**,** 1691-700.

ROTHSTEIN, J. D., DYKES-HOBERG, M., PARDO, C. A., BRISTOL, L. A., JIN, L., KUNCL, R. W., KANAI, Y., HEDIGER, M. A., WANG, Y., SCHIELKE, J. P. & WELTY, D. F. 1996. Knockout of

glutamate transporters reveals a major role for astroglial transport in excitotoxicity and clearance of glutamate. *Neuron,* 16**,** 675-86.

ROTHSTEIN, J. D., MARTIN, L. J. & KUNCL, R. W. 1992. Decreased glutamate transport by the brain and spinal cord in amyotrophic lateral sclerosis. *N Engl J Med,* 326**,** 1464-8.

ROTHSTEIN, J. D., VAN KAMMEN, M., LEVEY, A. I., MARTIN, L. J. & KUNCL, R. W. 1995. Selective loss of glial glutamate transporter GLT-1 in amyotrophic lateral sclerosis. *Ann Neurol,* 38**,** 73-84.

ROUACH, N., GLOWINSKI, J. & GIAUME, C. 2000. Activity-dependent neuronal control of gap-junctional communication in astrocytes. *J Cell Biol,* 149**,** 1513-26.

ROUX, L., MADAR, A., LACROIX, M. M., YI, C., BENCHENANE, K. & GIAUME, C. 2015. Astroglial Connexin 43 Hemichannels Modulate Olfactory Bulb Slow Oscillations. *J Neurosci,* 35**,** 15339-52.

RÜB, U., VONSATTEL, J. P., HEINSEN, H. & KORF, H. W. 2015. The Neuropathology of Huntington´s disease: classical findings, recent developments and correlation to functional neuroanatomy. *Adv Anat Embryol Cell Biol,* 217**,** 1-146.

RUSINA, R., VANDENBERGHE, R. & BRUFFAERTS, R. 2021. Cognitive and Behavioral Manifestations in ALS: Beyond Motor System Involvement. *Diagnostics (Basel),* 11.

SABA, L., VISCOMI, M. T., CAIOLI, S., PIGNATARO, A., BISICCHIA, E., PIERI, M., MOLINARI, M., AMMASSARI-TEULE, M. & ZONA, C. 2016. Altered Functionality, Morphology, and Vesicular Glutamate Transporter Expression of Cortical Motor Neurons from a Presymptomatic Mouse Model of Amyotrophic Lateral Sclerosis. *Cereb Cortex,* 26**,** 1512-28.

SABERI, S., STAUFFER, J. E., JIANG, J., GARCIA, S. D., TAYLOR, A. E., SCHULTE, D., OHKUBO, T., SCHLOFFMAN, C. L., MALDONADO, M. & BAUGHN, M. 2018. Sense-encoded poly-GR dipeptide repeat proteins correlate to neurodegeneration and uniquely co-localize with TDP-43 in dendrites of repeat-expanded C9orf72 amyotrophic lateral sclerosis. *Acta neuropathologica,* 135**,** 459-474.

SACCON, R. A., BUNTON-STASYSHYN, R. K., FISHER, E. M. & FRATTA, P. 2013. Is SOD1 loss of function involved in amyotrophic lateral sclerosis? *Brain,* 136**,** 2342-58.

SÁEZ, J. C., CONNOR, J. A., SPRAY, D. C. & BENNETT, M. V. 1989. Hepatocyte gap junctions are permeable to the second messenger, inositol 1,4,5-trisphosphate, and to calcium ions. *Proc Natl Acad Sci U S A,* 86**,** 2708-12.

SAHADEVAN, S., HEMBACH, K. M., TANTARDINI, E., PÉREZ-BERLANGA, M., HRUSKA-PLOCHAN, M., MEGAT, S., WEBER, J., SCHWARZ, P., DUPUIS, L., ROBINSON, M. D., DE ROSSI, P. & POLYMENIDOU, M. 2021. Synaptic FUS accumulation triggers early misregulation of synaptic RNAs in a mouse model of ALS. *Nat Commun,* 12**,** 3027.

SAKAE, N., BIENIEK, K. F., ZHANG, Y.-J., ROSS, K., GENDRON, T. F., MURRAY, M. E., RADEMAKERS, R., PETRUCELLI, L. & DICKSON, D. W. 2018. Poly-GR dipeptide repeat polymers correlate with neurodegeneration and Clinicopathological subtypes in C9ORF72-related brain disease. *Acta neuropathologica communications,* 6**,** 1-13.

SARDAR, D., CHENG, Y. T., WOO, J., CHOI, D. J., LEE, Z. F., KWON, W., CHEN, H. C., LOZZI, B., CERVANTES, A., RAJENDRAN, K., HUANG, T. W., JAIN, A., ARENKIEL, B. R., MAZE, I. & DENEEN, B. 2023. Induction of astrocytic Slc22a3 regulates sensory processing through histone serotonylation. *Science,* 380**,** eade0027.

SAREEN, D., O'ROURKE, J. G., MEERA, P., MUHAMMAD, A. K., GRANT, S., SIMPKINSON, M., BELL, S., CARMONA, S., ORNELAS, L., SAHABIAN, A., GENDRON, T., PETRUCELLI, L.,

BAUGHN, M., RAVITS, J., HARMS, M. B., RIGO, F., BENNETT, C. F., OTIS, T. S., SVENDSEN, C. N. & BALOH, R. H. 2013. Targeting RNA foci in iPSC-derived motor neurons from ALS patients with a C9ORF72 repeat expansion. *Sci Transl Med,* 5**,** 208ra149.

SARROUILHE, D., DEJEAN, C. & MESNIL, M. 2014. Involvement of gap junction channels in the pathophysiology of migraine with aura. *Frontiers in physiology,* 5**,** 78.

SASAKI, S. & MARUYAMA, S. 1992. Increase in diameter of the axonal initial segment is an early change in amyotrophic lateral sclerosis. *Journal of the neurological sciences,* 110**,** 114-120.

SCEKIC-ZAHIROVIC, J., SANJUAN-RUIZ, I., KAN, V., MEGAT, S., DE ROSSI, P., DIETERLÉ, S., CASSEL, R., JAMET, M., KESSLER, P. & WIESNER, D. 2021. Cytoplasmic FUS triggers early behavioral alterations linked to cortical neuronal hyperactivity and inhibitory synaptic defects. *Nature Communications,* 12**,** 3028.

SCHANZ, O., BAGEAC, D., BRAUN, L., TRAYNOR, B. J., LEHKY, T. J. & FLOETER, M. K. 2016. Cortical hyperexcitability in patients with C9ORF72 mutations: Relationship to phenotype. *Muscle & Nerve,* 54**,** 264-269.

SCHELTENS, P., BLENNOW, K., BRETELER, M. M. B., DE STROOPER, B., FRISONI, G. B., SALLOWAY, S. & VAN DER FLIER, W. M. 2016. Alzheimer's disease. *The Lancet,* 388**,** 505-517.

SCHLUDI, M. H., MAY, S., GRÄSSER, F. A., RENTZSCH, K., KREMMER, E., KÜPPER, C., KLOPSTOCK, T., ARZBERGER, T., EDBAUER, D., GERMAN CONSORTIUM FOR FRONTOTEMPORAL LOBAR, D. & BAVARIAN BRAIN BANKING, A. 2015. Distribution of dipeptide repeat proteins in cellular models and C9orf72 mutation cases suggests link to transcriptional silencing. *Acta Neuropathologica,* 130**,** 537-555.

SCHULZ, R., GÖRGE, P. M., GÖRBE, A., FERDINANDY, P., LAMPE, P. D. & LEYBAERT, L. 2015. Connexin 43 is an emerging therapeutic target in ischemia/reperfusion injury, cardioprotection and neuroprotection. *Pharmacol Ther,* 153**,** 90-106.

SEELAAR, H., ROHRER, J. D., PIJNENBURG, Y. A., FOX, N. C. & VAN SWIETEN, J. C. 2011. Clinical, genetic and pathological heterogeneity of frontotemporal dementia: a review. *J Neurol Neurosurg Psychiatry,* 82**,** 476-86.

SELVARAJ, B. T., LIVESEY, M. R., ZHAO, C., GREGORY, J. M., JAMES, O. T., CLEARY, E. M., CHOUHAN, A. K., GANE, A. B., PERKINS, E. M., DANDO, O., LILLICO, S. G., LEE, Y.-B., NISHIMURA, A. L., PORECI, U., THANKAMONY, S., PRAY, M., VASISTHA, N. A., MAGNANI, D., BOROOAH, S., BURR, K., STORY, D., MCCAMPBELL, A., SHAW, C. E., KIND, P. C., AITMAN, T. J., WHITELAW, C. B. A., WILMUT, I., SMITH, C., MILES, G. B., HARDINGHAM, G. E., WYLLIE, D. J. A. & CHANDRAN, S. 2018. C9ORF72 repeat expansion causes vulnerability of motor neurons to Ca2+-permeable AMPA receptor-mediated excitotoxicity. *Nature Communications,* 9**,** 347.

SEPHTON, C. F., TANG, A. A., KULKARNI, A., WEST, J., BROOKS, M., STUBBLEFIELD, J. J., LIU, Y., ZHANG, M. Q., GREEN, C. B. & HUBER, K. M. 2014. Activity-dependent FUS dysregulation disrupts synaptic homeostasis. *Proceedings of the National Academy of Sciences,* 111**,** E4769-E4778.

SHARMA, S., SHARMA, N., SAINI, A. & NEHRU, B. 2019. Carbenoxolone Reverses the Amyloid Beta 1-42 Oligomer-Induced Oxidative Damage and Anxiety-Related Behavior in Rats. *Neurotox Res,* 35**,** 654-667.

SHAROT, T., DE MARTINO, B. & DOLAN, R. J. 2009. How choice reveals and shapes expected hedonic outcome. *J Neurosci,* 29**,** 3760-5.

SHAW, P. J., INCE, P. G., FALKOUS, G. & MANTLE, D. 1995. Oxidative damage to protein in sporadic motor neuron disease spinal cord. *Annals of Neurology: Official Journal of the American Neurological Association and the Child Neurology Society,* 38**,** 691-695.

SHELLIKERI, S., KARTHIKEYAN, V., MARTINO, R., BLACK, S. E., ZINMAN, L., KEITH, J. & YUNUSOVA, Y. 2017. The neuropathological signature of bulbar-onset ALS: A systematic review. *Neurosci Biobehav Rev,* 75**,** 378-392.

SHEPHEARD, S. R., PARKER, M. D., COOPER-KNOCK, J., VERBER, N. S., TUDDENHAM, L., HEATH, P., BEAUCHAMP, N., PLACE, E., SOLLARS, E. S. A., TURNER, M. R., MALASPINA, A., FRATTA, P., HEWAMADDUMA, C., JENKINS, T. M., MCDERMOTT, C. J., WANG, D., KIRBY, J. & SHAW, P. J. 2021. Value of systematic genetic screening of patients with amyotrophic lateral sclerosis. *Journal of Neurology, Neurosurgery & Psychiatry,* 92**,** 510-518.

SHI, Y., LIN, S., STAATS, K. A., LI, Y., CHANG, W.-H., HUNG, S.-T., HENDRICKS, E., LINARES, G. R., WANG, Y. & SON, E. Y. 2018. Haploinsufficiency leads to neurodegeneration in C9ORF72 ALS/FTD human induced motor neurons. *Nature medicine,* 24**,** 313-325.

SHIBUYA, K., PARK, S. B., GEEVASINGA, N., MENON, P., HOWELLS, J., SIMON, N. G., HUYNH, W., NOTO, Y., GÖTZ, J., KRIL, J. J., ITTNER, L. M., HODGES, J., HALLIDAY, G., VUCIC, S. & KIERNAN, M. C. 2016. Motor cortical function determines prognosis in sporadic ALS. *Neurology,* 87**,** 513-20.

SHIMOJO, M., TAKUWA, H., TAKADO, Y., TOKUNAGA, M., TSUKAMOTO, S., MINATOHARA, K., ONO, M., SEKI, C., MAEDA, J., URUSHIHATA, T., MINAMIHISAMATSU, T., AOKI, I., KAWAMURA, K., ZHANG, M.-R., SUHARA, T., SAHARA, N. & HIGUCHI, M. 2020. Selective Disruption of Inhibitory Synapses Leading to Neuronal Hyperexcitability at an Early Stage of Tau Pathogenesis in a Mouse Model. *The Journal of Neuroscience,* 40**,** 3491-3501.

SIES, H. 2015. Oxidative stress: a concept in redox biology and medicine. *Redox biology,* 4**,** 180-183.

SIMINOVITCH, L., MCCULLOCH, E. A. & TILL, J. E. 1963. THE DISTRIBUTION OF COLONY-FORMING CELLS AMONG SPLEEN COLONIES. *J Cell Comp Physiol,* 62**,** 327-36.

SIMPSON, E., HENRY, Y., HENKEL, J., SMITH, R. & APPEL, S. H. 2004. Increased lipid peroxidation in sera of ALS patients: a potential biomarker of disease burden. *Neurology,* 62**,** 1758-1765.

SIRKIS, D. W., GEIER, E. G., BONHAM, L. W., KARCH, C. M. & YOKOYAMA, J. S. 2019. Recent advances in the genetics of frontotemporal dementia. *Curr Genet Med Rep,* 7**,** 41-52.

SLEIGH, J. N., ROSSOR, A. M., FELLOWS, A. D., TOSOLINI, A. P. & SCHIAVO, G. 2019. Axonal transport and neurological disease. *Nature Reviews Neurology,* 15**,** 691-703.

SLEIGH, J. N., TOSOLINI, A. P., GORDON, D., DEVOY, A., FRATTA, P., FISHER, E. M., TALBOT, K. & SCHIAVO, G. 2020. Mice carrying ALS mutant TDP-43, but not mutant FUS, display in vivo defects in axonal transport of signaling endosomes. *Cell Reports,* 30**,** 3655-3662. e2.

SMOLIN, B., KARRY, R., GAL-BEN-ARI, S. & BEN-SHACHAR, D. 2012. Differential expression of genes encoding neuronal ion-channel subunits in major depression, bipolar disorder and schizophrenia: implications for pathophysiology. *International Journal of Neuropsychopharmacology,* 15**,** 869-882.

SNOWDEN, J. S., NEARY, D. & MANN, D. M. 2002. Frontotemporal dementia. *Br J Psychiatry,* 180**,** 140-3.

SNOWDEN, J. S., ROLLINSON, S., THOMPSON, J. C., HARRIS, J. M., STOPFORD, C. L., RICHARDSON, A. M., JONES, M., GERHARD, A., DAVIDSON, Y. S., ROBINSON, A., GIBBONS, L., HU, Q., DUPLESSIS, D., NEARY, D., MANN, D. M. & PICKERING-BROWN, S. M. 2012. Distinct clinical and pathological characteristics of frontotemporal dementia associated with C9ORF72 mutations. *Brain,* 135**,** 693-708.

SOHN, P. D., HUANG, C. T.-L., YAN, R., FAN, L., TRACY, T. E., CAMARGO, C. M., MONTGOMERY, K. M., ARHAR, T., MOK, S.-A. & FREILICH, R. 2019. Pathogenic tau impairs axon initial segment plasticity and excitability homeostasis. *Neuron,* 104**,** 458-470. e5.

SOLOMON, D. A., STEPTO, A., AU, W. H., ADACHI, Y., DIAPER, D. C., HALL, R., REKHI, A., BOUDI, A., TZIORTZOUDA, P., LEE, Y. B., SMITH, B., BRIDI, J. C., SPINELLI, G., DEARLOVE, J., HUMPHREY, D. M., GALLO, J. M., TROAKES, C., FANTO, M., SOLLER, M., ROGELJ, B., PARSONS, R. B., SHAW, C. E., HORTOBÁGYI, T. & HIRTH, F. 2018. A feedback loop between dipeptide-repeat protein, TDP-43 and karyopherin-α mediates C9orf72-related neurodegeneration. *Brain,* 141**,** 2908-2924.

SOLTANI, M. H., PICHARDO, R., SONG, Z., SANGHA, N., CAMACHO, F., SATYAMOORTHY, K., SANGUEZA, O. P. & SETALURI, V. 2005. Microtubule-Associated Protein 2, a Marker of Neuronal Differentiation, Induces Mitotic Defects, Inhibits Growth of Melanoma Cells, and Predicts Metastatic Potential of Cutaneous Melanoma. *The American Journal of Pathology,* 166**,** 1841-1850.

SPALLONI, A., ORIGLIA, N., SGOBIO, C., TRABALZA, A., NUTINI, M., BERRETTA, N., BERNARDI, G., DOMENICI, L., AMMASSARI-TEULE, M. & LONGONE, P. 2011. Postsynaptic alteration of NR2A subunit and defective autophosphorylation of alphaCaMKII at threonine-286 contribute to abnormal plasticity and morphology of upper motor neurons in presymptomatic SOD1G93A mice, a murine model for amyotrophic lateral sclerosis. *Cerebral cortex,* 21**,** 796-805.

SREEDHARAN, J., BLAIR, I. P., TRIPATHI, V. B., HU, X., VANCE, C., ROGELJ, B., ACKERLEY, S., DURNALL, J. C., WILLIAMS, K. L., BURATTI, E., BARALLE, F., DE BELLEROCHE, J., MITCHELL, J. D., LEIGH, P. N., AL-CHALABI, A., MILLER, C. C., NICHOLSON, G. & SHAW, C. E. 2008. TDP-43 mutations in familial and sporadic amyotrophic lateral sclerosis. *Science,* 319**,** 1668-72.

STARR, A. & SATTLER, R. 2018. Synaptic dysfunction and altered excitability in C9ORF72 ALS/FTD. *Brain Res,* 1693**,** 98-108.

STEINER, H. & TSENG, K. Y. 2016. *Handbook of Basal Ganglia Structure and Function, Second Edition*.

STRONG, M. J., ABRAHAMS, S., GOLDSTEIN, L. H., WOOLLEY, S., MCLAUGHLIN, P., SNOWDEN, J., MIOSHI, E., ROBERTS-SOUTH, A., BENATAR, M., HORTOBÁGYI, T., ROSENFELD, J., SILANI, V., INCE, P. G. & TURNER, M. R. 2017. Amyotrophic lateral sclerosis - frontotemporal spectrum disorder (ALS-FTSD): Revised diagnostic criteria. *Amyotrophic Lateral Sclerosis and Frontotemporal Degeneration,* 18**,** 153-174.

STYR, B. & SLUTSKY, I. 2018. Imbalance between firing homeostasis and synaptic plasticity drives early-phase Alzheimer's disease. *Nat Neurosci,* 21**,** 463-473.

SU, J. H., NICHOL, K. E., SITCH, T., SHEU, P., CHUBB, C., MILLER, B. L., TOMASELLI, K. J., KIM, R. C. & COTMAN, C. W. 2000. DNA damage and activated caspase-3 expression in

neurons and astrocytes: evidence for apoptosis in frontotemporal dementia. *Exp Neurol,* 163**,** 9-19.

SUN, L., GAO, J., ZHAO, M., CUI, J., LI, Y., YANG, X., JING, X. & WU, Z. 2015. A novel cognitive impairment mechanism that astrocytic p-connexin 43 promotes neuronic autophagy via activation of P2X7R and down-regulation of GLT-1 expression in the hippocampus following traumatic brain injury in rats. *Behav Brain Res,* 291**,** 315-324.

SUNICO, C. R., DOMÍNGUEZ, G., GARCÍA-VERDUGO, J. M., OSTA, R., MONTERO, F. & MORENO-LÓPEZ, B. 2011. Reduction in the motoneuron inhibitory/excitatory synaptic ratio in an early-symptomatic mouse model of amyotrophic lateral sclerosis. *Brain Pathol,* 21**,** 1-15.

SYNOFZIK, M., FERNÁNDEZ-SANTIAGO, R., MAETZLER, W., SCHÖLS, L. & ANDERSEN, P. M. 2010. The human G93A SOD1 phenotype closely resembles sporadic amyotrophic lateral sclerosis. *J Neurol Neurosurg Psychiatry,* 81**,** 764-7.

TABERNERO, A., GIAUME, C. & MEDINA, J. M. 1996. Endothelin-1 regulates glucose utilization in cultured astrocytes by controlling intercellular communication through gap junctions. *Glia,* 16**,** 187-95.

TAE, W. S., SUNG, J. H., BAEK, S. H., LEE, C. N. & KIM, B. J. 2020. Shape Analysis of the Subcortical Nuclei in Amyotrophic Lateral Sclerosis without Cognitive Impairment. *J Clin Neurol,* 16**,** 592-598.

TAHA, D. M., CLARKE, B. E., HALL, C. E., TYZACK, G. E., ZIFF, O. J., GREENSMITH, L., KALMAR, B., AHMED, M., ALAM, A. & THELIN, E. P. 2022. Astrocytes display cell autonomous and diverse early reactive states in familial amyotrophic lateral sclerosis. *Brain,* 145**,** 481-489.

TAKAHASHI, K., TANABE, K., OHNUKI, M., NARITA, M., ICHISAKA, T., TOMODA, K. & YAMANAKA, S. 2007. Induction of pluripotent stem cells from adult human fibroblasts by defined factors. *Cell,* 131**,** 861-72.

TAKAHASHI, K. & YAMANAKA, S. 2006. Induction of Pluripotent Stem Cells from Mouse Embryonic and Adult Fibroblast Cultures by Defined Factors. *Cell,* 126**,** 663-676.

TAKEUCHI, H., JIN, S., WANG, J., ZHANG, G., KAWANOKUCHI, J., KUNO, R., SONOBE, Y., MIZUNO, T. & SUZUMURA, A. 2006. Tumor necrosis factor-α induces neurotoxicity via glutamate release from hemichannels of activated microglia in an autocrine manner. *Journal of Biological Chemistry,* 281**,** 21362-21368.

TAKEUCHI, H., MIZOGUCHI, H., DOI, Y., JIN, S., NODA, M., LIANG, J., LI, H., ZHOU, Y., MORI, R. & YASUOKA, S. 2011. Blockade of gap junction hemichannel suppresses disease progression in mouse models of amyotrophic lateral sclerosis and Alzheimer's disease. *PloS one,* 6**,** e21108.

TALBOT, P. R., GOULDING, P. J., LLOYD, J. J., SNOWDEN, J. S., NEARY, D. & TESTA, H. J. 1995. Inter-relation between" classic" motor neuron disease and frontotemporal dementia: neuropsychological and single photon emission computed tomography study. *Journal of Neurology, Neurosurgery & Psychiatry,* 58**,** 541-547.

TAN, R. H., YANG, Y., KIM, W. S., DOBSON-STONE, C., KWOK, J. B., KIERNAN, M. C. & HALLIDAY, G. M. 2017. Distinct TDP-43 inclusion morphologies in frontotemporal lobar degeneration with and without amyotrophic lateral sclerosis. *Acta Neuropathologica Communications,* 5**,** 76.

TAO, Z., WANG, H., XIA, Q., LI, K., LI, K., JIANG, X., XU, G., WANG, G. & YING, Z. 2015. Nucleolar stress and impaired stress granule formation contribute to C9orf72 RAN translation-induced cytotoxicity. *Human molecular genetics,* 24**,** 2426-2441.

TARR, I. S., MCCANN, E. P., BENYAMIN, B., PETERS, T. J., TWINE, N. A., ZHANG, K. Y., ZHAO, Q., ZHANG, Z.-H., ROWE, D. B., NICHOLSON, G. A., BAUER, D., CLARK, S. J., BLAIR, I. P. & WILLIAMS, K. L. 2019. Monozygotic twins and triplets discordant for amyotrophic lateral sclerosis display differential methylation and gene expression. *Scientific Reports,* 9**,** 8254.

TASAKI, I. & HAGIWAR, A. S. 1957. Demonstration of two stable potential states in the squid giant axon under tetraethylammonium chloride. *J Gen Physiol,* 40**,** 859-85.

TEPPER, J. M. & BOLAM, J. P. 2004. Functional diversity and specificity of neostriatal interneurons. *Curr Opin Neurobiol,* 14**,** 685-92.

THOMSON, J. A., ITSKOVITZ-ELDOR, J., SHAPIRO, S. S., WAKNITZ, M. A., SWIERGIEL, J. J., MARSHALL, V. S. & JONES, J. M. 1998. Embryonic stem cell lines derived from human blastocysts. *Science,* 282**,** 1145-7.

TIMMINS, H. C., VUCIC, S. & KIERNAN, M. C. 2023. Cortical hyperexcitability in amyotrophic lateral sclerosis: from pathogenesis to diagnosis. *Curr Opin Neurol,* 36**,** 353-359.

TITTARELLI, A. 2021. Connexin channels modulation in pathophysiology and treatment of immune and inflammatory disorders. *Biochimica et Biophysica Acta (BBA) - Molecular Basis of Disease,* 1867**,** 166258.

TOSOLINI, A. P., SLEIGH, J. N., SURANA, S., RHYMES, E. R., CAHALAN, S. D. & SCHIAVO, G. 2022. BDNF-dependent modulation of axonal transport is selectively impaired in ALS. *Acta Neuropathologica Communications,* 10**,** 121.

TRAN, H., ALMEIDA, S., MOORE, J., GENDRON, T. F., CHALASANI, U., LU, Y., DU, X., NICKERSON, J. A., PETRUCELLI, L., WENG, Z. & GAO, F. B. 2015. Differential Toxicity of Nuclear RNA Foci versus Dipeptide Repeat Proteins in a Drosophila Model of C9ORF72 FTD/ALS. *Neuron,* 87**,** 1207-1214.

TRITSCH, N. X. & SABATINI, B. L. 2012. Dopaminergic modulation of synaptic transmission in cortex and striatum. *Neuron,* 76**,** 33-50.

TROAKES, C., MAEKAWA, S., WIJESEKERA, L., ROGELJ, B., SIKLÓS, L., BELL, C., SMITH, B., NEWHOUSE, S., VANCE, C., JOHNSON, L., HORTOBÁGYI, T., SHATUNOV, A., AL-CHALABI, A., LEIGH, N., SHAW, C. E., KING, A. & AL-SARRAJ, S. 2012. An MND/ALS phenotype associated with C9orf72 repeat expansion: abundant p62-positive, TDP-43-negative inclusions in cerebral cortex, hippocampus and cerebellum but without associated cognitive decline. *Neuropathology,* 32**,** 505-14.

TROPEA, T. F., MAK, J., GUO, M. H., XIE, S. X., SUH, E., RICK, J., SIDEROWF, A., WEINTRAUB, D., GROSSMAN, M., IRWIN, D., WOLK, D. A., TROJANOWSKI, J. Q., VAN DEERLIN, V. & CHEN-PLOTKIN, A. S. 2019. TMEM106B Effect on cognition in Parkinson disease and frontotemporal dementia. *Ann Neurol,* 85**,** 801-811.

TSAI, R. M. & BOXER, A. L. 2014. Treatment of frontotemporal dementia. *Curr Treat Options Neurol,* 16**,** 319.

TSUIJI, H., INOUE, I., TAKEUCHI, M., FURUYA, A., YAMAKAGE, Y., WATANABE, S., KOIKE, M., HATTORI, M. & YAMANAKA, K. 2017. TDP-43 accelerates age-dependent degeneration of interneurons. *Scientific reports,* 7**,** 14972.

TSUTSUI-KIMURA, I., TAKIUE, H., YOSHIDA, K., XU, M., YANO, R., OHTA, H., NISHIDA, H., BOUCHEKIOUA, Y., OKANO, H., UCHIGASHIMA, M., WATANABE, M., TAKATA, N., DREW,

M. R., SANO, H., MIMURA, M. & TANAKA, K. F. 2017. Dysfunction of ventrolateral striatal dopamine receptor type 2-expressing medium spiny neurons impairs instrumental motivation. *Nature Communications,* 8**,** 14304.

TU, P.-H., RAJU, P., ROBINSON, K. A., GURNEY, M. E., TROJANOWSKI, J. Q. & LEE, V. 1996. Transgenic mice carrying a human mutant superoxide dismutase transgene develop neuronal cytoskeletal pathology resembling human amyotrophic lateral sclerosis lesions. *Proceedings of the National Academy of Sciences,* 93**,** 3155-3160.

TU, W. Y., XU, W., ZHANG, J., QI, S., BAI, L., SHEN, C. & ZHANG, K. 2023. C9orf72 poly-GA proteins impair neuromuscular transmission. *Zool Res,* 44**,** 331-340.

TURNER, M. R. & VERSTRAETE, E. 2015. What does imaging reveal about the pathology of amyotrophic lateral sclerosis? *Curr Neurol Neurosci Rep,* 15**,** 45.

UDAGAWA, T., FUJIOKA, Y., TANAKA, M., HONDA, D., YOKOI, S., RIKU, Y., IBI, D., NAGAI, T., YAMADA, K., WATANABE, H., KATSUNO, M., INADA, T., OHNO, K., SOKABE, M., OKADO, H., ISHIGAKI, S. & SOBUE, G. 2015. FUS regulates AMPA receptor function and FTLD/ALS-associated behaviour via GluA1 mRNA stabilization. *Nat Commun,* 6**,** 7098.

UPADHYA, R., ZINGG, W., SHETTY, S. & SHETTY, A. K. 2020. Astrocyte-derived extracellular vesicles: Neuroreparative properties and role in the pathogenesis of neurodegenerative disorders. *Journal of controlled release,* 323**,** 225-239.

URWIN, H., JOSEPHS, K. A., ROHRER, J. D., MACKENZIE, I. R., NEUMANN, M., AUTHIER, A., SEELAAR, H., VAN SWIETEN, J. C., BROWN, J. M., JOHANNSEN, P., NIELSEN, J. E., HOLM, I. E., DICKSON, D. W., RADEMAKERS, R., GRAFF-RADFORD, N. R., PARISI, J. E., PETERSEN, R. C., HATANPAA, K. J., WHITE, C. L., 3RD, WEINER, M. F., GESER, F., VAN DEERLIN, V. M., TROJANOWSKI, J. Q., MILLER, B. L., SEELEY, W. W., VAN DER ZEE, J., KUMAR-SINGH, S., ENGELBORGHS, S., DE DEYN, P. P., VAN BROECKHOVEN, C., BIGIO, E. H., DENG, H. X., HALLIDAY, G. M., KRIL, J. J., MUNOZ, D. G., MANN, D. M., PICKERING-BROWN, S. M., DOODEMAN, V., ADAMSON, G., GHAZI-NOORI, S., FISHER, E. M., HOLTON, J. L., REVESZ, T., ROSSOR, M. N., COLLINGE, J., MEAD, S. & ISAACS, A. M. 2010. FUS pathology defines the majority of tau- and TDP-43-negative frontotemporal lobar degeneration. *Acta Neuropathol,* 120**,** 33-41.

VAHSEN, B. F., GRAY, E., THOMPSON, A. G., ANSORGE, O., ANTHONY, D. C., COWLEY, S. A., TALBOT, K. & TURNER, M. R. 2021. Non-neuronal cells in amyotrophic lateral sclerosis — from pathogenesis to biomarkers. *Nature Reviews Neurology,* 17**,** 333-348.

VAN BLITTERSWIJK, M., MULLEN, B., NICHOLSON, A. M., BIENIEK, K. F., HECKMAN, M. G., BAKER, M. C., DEJESUS-HERNANDEZ, M., FINCH, N. A., BROWN, P. H., MURRAY, M. E., HSIUNG, G.-Y. R., STEWART, H., KARYDAS, A. M., FINGER, E., KERTESZ, A., BIGIO, E. H., WEINTRAUB, S., MESULAM, M., HATANPAA, K. J., WHITE III, C. L., STRONG, M. J., BEACH, T. G., WSZOLEK, Z. K., LIPPA, C., CASELLI, R., PETRUCELLI, L., JOSEPHS, K. A., PARISI, J. E., KNOPMAN, D. S., PETERSEN, R. C., MACKENZIE, I. R., SEELEY, W. W., GRINBERG, L. T., MILLER, B. L., BOYLAN, K. B., GRAFF-RADFORD, N. R., BOEVE, B. F., DICKSON, D. W. & RADEMAKERS, R. 2014. TMEM106B protects C9ORF72 expansion carriers against frontotemporal dementia. *Acta Neuropathologica,* 127**,** 397-406.

VAN DEERLIN, V. M., LEVERENZ, J. B., BEKRIS, L. M., BIRD, T. D., YUAN, W., ELMAN, L. B., CLAY, D., WOOD, E. M., CHEN-PLOTKIN, A. S., MARTINEZ-LAGE, M., STEINBART, E., MCCLUSKEY, L., GROSSMAN, M., NEUMANN, M., WU, I. L., YANG, W. S., KALB, R., GALASKO, D. R., MONTINE, T. J., TROJANOWSKI, J. Q., LEE, V. M., SCHELLENBERG, G.

D. & YU, C. E. 2008. TARDBP mutations in amyotrophic lateral sclerosis with TDP-43 neuropathology: a genetic and histopathological analysis. *Lancet Neurol,* 7**,** 409-16.

VAN DEN BOSCH, L., VAN DAMME, P., BOGAERT, E. & ROBBERECHT, W. 2006. The role of excitotoxicity in the pathogenesis of amyotrophic lateral sclerosis. *Biochim Biophys Acta,* 1762**,** 1068-82.

VAN DEN BOSCH, L., VANDENBERGHE, W., KLAASSEN, H., VAN HOUTTE, E. & ROBBERECHT, W. 2000. Ca(2+)-permeable AMPA receptors and selective vulnerability of motor neurons. *J Neurol Sci,* 180**,** 29-34.

VAN HARTEN, A. C., PHATNANI, H. & PRZEDBORSKI, S. 2021. Non-cell-autonomous pathogenic mechanisms in amyotrophic lateral sclerosis. *Trends in neurosciences,* 44**,** 658-668.

VAN SWIETEN, J. & SPILLANTINI, M. G. 2007. Hereditary frontotemporal dementia caused by Tau gene mutations. *Brain Pathol,* 17**,** 63-73.

VAN ZUNDERT, B., PEUSCHER, M. H., HYNYNEN, M., CHEN, A., NEVE, R. L., BROWN, R. H., JR., CONSTANTINE-PATON, M. & BELLINGHAM, M. C. 2008. Neonatal neuronal circuitry shows hyperexcitable disturbance in a mouse model of the adult-onset neurodegenerative disease amyotrophic lateral sclerosis. *J Neurosci,* 28**,** 10864-74.

VANDOORNE, T., DE BOCK, K. & VAN DEN BOSCH, L. 2018. Energy metabolism in ALS: an underappreciated opportunity? *Acta Neuropathol,* 135**,** 489-509.

VANNESTE, J., VERCRUYSSE, T., BOEYNAEMS, S., SICART, A., VAN DAMME, P., DAELEMANS, D. & VAN DEN BOSCH, L. 2019. C9orf72-generated poly-GR and poly-PR do not directly interfere with nucleocytoplasmic transport. *Sci Rep,* 9**,** 15728.

VARCIANNA, A., MYSZCZYNSKA, M. A., CASTELLI, L. M., O'NEILL, B., KIM, Y., TALBOT, J., NYBERG, S., NYAMALI, I., HEATH, P. R., STOPFORD, M. J., HAUTBERGUE, G. M. & FERRAIUOLO, L. 2019. Micro-RNAs secreted through astrocyte-derived extracellular vesicles cause neuronal network degeneration in C9orf72 ALS. *EBioMedicine,* 40**,** 626-635.

VARGAS, J. N. S., SLEIGH, J. N. & SCHIAVO, G. 2022. Coupling axonal mRNA transport and local translation to organelle maintenance and function. *Current Opinion in Cell Biology,* 74**,** 97-103.

VASS, R., ASHBRIDGE, E., GESER, F., HU, W. T., GROSSMAN, M., CLAY-FALCONE, D., ELMAN, L., MCCLUSKEY, L., LEE, V. M., VAN DEERLIN, V. M., TROJANOWSKI, J. Q. & CHEN-PLOTKIN, A. S. 2011. Risk genotypes at TMEM106B are associated with cognitive impairment in amyotrophic lateral sclerosis. *Acta Neuropathol,* 121**,** 373-80.

VATSAVAYAI, S. C., NANA, A. L., YOKOYAMA, J. S. & SEELEY, W. W. 2019. C9orf72-FTD/ALS pathogenesis: evidence from human neuropathological studies. *Acta neuropathologica,* 137**,** 1-26.

VATSAVAYAI, S. C., YOON, S. J., GARDNER, R. C., GENDRON, T. F., VARGAS, J. N., TRUJILLO, A., PRIBADI, M., PHILLIPS, J. J., GAUS, S. E., HIXSON, J. D., GARCIA, P. A., RABINOVICI, G. D., COPPOLA, G., GESCHWIND, D. H., PETRUCELLI, L., MILLER, B. L. & SEELEY, W. W. 2016a. Timing and significance of pathological features in C9orf72 expansion-associated frontotemporal dementia. *Brain,* 139**,** 3202-3216.

VATSAVAYAI, S. C., YOON, S. J., GARDNER, R. C., GENDRON, T. F., VARGAS, J. N. S., TRUJILLO, A., PRIBADI, M., PHILLIPS, J. J., GAUS, S. E. & HIXSON, J. D. 2016b. Timing and significance of pathological features in C9orf72 expansion-associated frontotemporal dementia. *Brain,* 139**,** 3202-3216.

VELEBIT, J., HORVAT, A., SMOLIČ, T., PRPAR MIHEVC, S., ROGELJ, B., ZOREC, R. & VARDJAN, N. 2020. Astrocytes with TDP-43 inclusions exhibit reduced noradrenergic cAMP and Ca2+ signaling and dysregulated cell metabolism. *Scientific reports,* 10**,** 6003.

VERKHRATSKY, A. & NEDERGAARD, M. 2018. Physiology of Astroglia. *Physiol Rev,* 98**,** 239-389.

VERKHRATSKY, A., PARPURA, V., VARDJAN, N. & ZOREC, R. 2019. Physiology of Astroglia. *Adv Exp Med Biol,* 1175**,** 45-91.

VINKEN, M. 2016. Regulation of connexin signaling by the epigenetic machinery. *Biochim Biophys Acta,* 1859**,** 262-8.

VOLKOW, N. D., WANG, G. J., TELANG, F., FOWLER, J. S., LOGAN, J., JAYNE, M., MA, Y., PRADHAN, K. & WONG, C. 2007. Profound decreases in dopamine release in striatum in detoxified alcoholics: possible orbitofrontal involvement. *J Neurosci,* 27**,** 12700-6.

VOORN, P., VANDERSCHUREN, L. J., GROENEWEGEN, H. J., ROBBINS, T. W. & PENNARTZ, C. M. 2004. Putting a spin on the dorsal-ventral divide of the striatum. *Trends Neurosci,* 27**,** 468-74.

VUCIC, S., NICHOLSON, G. A. & KIERNAN, M. C. 2008. Cortical hyperexcitability may precede the onset of familial amyotrophic lateral sclerosis. *Brain,* 131**,** 1540-50.

VUCIC, S., ZIEMANN, U., EISEN, A., HALLETT, M. & KIERNAN, M. C. 2013. Transcranial magnetic stimulation and amyotrophic lateral sclerosis: pathophysiological insights. *J Neurol Neurosurg Psychiatry,* 84**,** 1161-70.

WAINGER, B. J. & CUDKOWICZ, M. E. 2015. Cortical Hyperexcitability in Amyotrophic Lateral Sclerosis: C9orf72 Repeats. *JAMA Neurol,* 72**,** 1235-6.

WAINGER, B. J., KISKINIS, E., MELLIN, C., WISKOW, O., HAN, S. S., SANDOE, J., PEREZ, N. P., WILLIAMS, L. A., LEE, S., BOULTING, G., BERRY, J. D., BROWN, R. H., JR., CUDKOWICZ, M. E., BEAN, B. P., EGGAN, K. & WOOLF, C. J. 2014. Intrinsic membrane hyperexcitability of amyotrophic lateral sclerosis patient-derived motor neurons. *Cell Rep,* 7**,** 1-11.

WAINGER, B. J., MACKLIN, E. A., VUCIC, S., MCILDUFF, C. E., PAGANONI, S., MARAGAKIS, N. J., BEDLACK, R., GOYAL, N. A., RUTKOVE, S. B., LANGE, D. J., RIVNER, M. H., GOUTMAN, S. A., LADHA, S. S., MAURICIO, E. A., BALOH, R. H., SIMMONS, Z., POTHIER, L., KASSIS, S. B., LA, T., HALL, M., EVORA, A., KLEMENTS, D., HURTADO, A., PEREIRA, J. D., KOH, J., CELNIK, P. A., CHAUDHRY, V., GABLE, K., JUEL, V. C., PHIELIPP, N., MAREI, A., ROSENQUIST, P., MEEHAN, S., OSKARSSON, B., LEWIS, R. A., KAUR, D., KISKINIS, E., WOOLF, C. J., EGGAN, K., WEISS, M. D., BERRY, J. D., DAVID, W. S., DAVILA-PEREZ, P., CAMPRODON, J. A., PASCUAL-LEONE, A., KIERNAN, M. C., SHEFNER, J. M., ATASSI, N. & CUDKOWICZ, M. E. 2021. Effect of Ezogabine on Cortical and Spinal Motor Neuron Excitability in Amyotrophic Lateral Sclerosis: A Randomized Clinical Trial. *JAMA Neurol,* 78**,** 186-196.

WAITE, A. J., BÄUMER, D., EAST, S., NEAL, J., MORRIS, H. R., ANSORGE, O. & BLAKE, D. J. 2014. Reduced C9orf72 protein levels in frontal cortex of amyotrophic lateral sclerosis and frontotemporal degeneration brain with the C9ORF72 hexanucleotide repeat expansion. *Neurobiol Aging,* 35**,** 1779.e5-1779.e13.

WALDVOGEL, H. J., KIM, E. H., TIPPETT, L. J., VONSATTEL, J. P. & FAULL, R. L. 2015. The Neuropathology of Huntington's Disease. *Curr Top Behav Neurosci,* 22**,** 33-80.

WALHOUT, R., SCHMIDT, R., WESTENENG, H.-J., VERSTRAETE, E., SEELEN, M., VAN RHEENEN, W., DE REUS, M. A., VAN ES, M. A., HENDRIKSE, J., VELDINK, J. H., VAN DEN HEUVEL,

M. P. & VAN DEN BERG, L. H. 2015. Brain morphologic changes in asymptomatic C9orf72 repeat expansion carriers. *Neurology,* 85**,** 1780-1788.

WALKER, A. K., SPILLER, K. J., GE, G., ZHENG, A., XU, Y., ZHOU, M., TRIPATHY, K., KWONG, L. K., TROJANOWSKI, J. Q. & LEE, V. M. 2015. Functional recovery in new mouse models of ALS/FTLD after clearance of pathological cytoplasmic TDP-43. *Acta Neuropathol,* 130**,** 643-60.

WALZ, W. 2000. Role of astrocytes in the clearance of excess extracellular potassium. *Neurochemistry international,* 36**,** 291-300.

WANG, L., GUTMANN, D. H. & ROOS, R. P. 2011. Astrocyte loss of mutant SOD1 delays ALS disease onset and progression in G85R transgenic mice. *Human molecular genetics,* 20**,** 286-293.

WANG, P., ZHANG, H., HAN, L. & ZHOU, Y. 2016. Cortical function in Alzheimer's disease and frontotemporal dementia. *Transl Neurosci,* 7**,** 116-125.

WANG, Q., JIE, W., LIU, J. H., YANG, J. M. & GAO, T. M. 2017. An astroglial basis of major depressive disorder? An overview. *Glia,* 65**,** 1227-1250.

WANG, S., WANG, B., SHANG, D., ZHANG, K., YAN, X. & ZHANG, X. 2022. Ion Channel Dysfunction in Astrocytes in Neurodegenerative Diseases. *Front Physiol,* 13**,** 814285.

WANG, X. M., ZENG, P., FANG, Y. Y., ZHANG, T. & TIAN, Q. 2021. Progranulin in neurodegenerative dementia. *J Neurochem,* 158**,** 119-137.

WEBSTER, C. P., SMITH, E. F., BAUER, C. S., MOLLER, A., HAUTBERGUE, G. M., FERRAIUOLO, L., MYSZCZYNSKA, M. A., HIGGINBOTTOM, A., WALSH, M. J., WHITWORTH, A. J., KASPAR, B. K., MEYER, K., SHAW, P. J., GRIERSON, A. J. & DE VOS, K. J. 2016. The C9orf72 protein interacts with Rab1a and the ULK1 complex to regulate initiation of autophagy. *Embo j,* 35**,** 1656-76.

WEBSTER, C. P., SMITH, E. F., SHAW, P. J. & DE VOS, K. J. 2017. Protein Homeostasis in Amyotrophic Lateral Sclerosis: Therapeutic Opportunities? *Front Mol Neurosci,* 10**,** 123.

WESKAMP, K., TANK, E. M., MIGUEZ, R., MCBRIDE, J. P., GÓMEZ, N. B., WHITE, M., LIN, Z., GONZALEZ, C. M., SERIO, A., SREEDHARAN, J. & BARMADA, S. J. 2020. Shortened TDP43 isoforms upregulated by neuronal hyperactivity drive TDP43 pathology in ALS. *J Clin Invest,* 130**,** 1139-1155.

WESTERGARD, T., JENSEN, B. K., WEN, X., CAI, J., KROPF, E., IACOVITTI, L., PASINELLI, P. & TROTTI, D. 2016. Cell-to-cell transmission of dipeptide repeat proteins linked to C9orf72-ALS/FTD. *Cell reports,* 17**,** 645-652.

WESTERGARD, T., MCAVOY, K., RUSSELL, K., WEN, X., PANG, Y., MORRIS, B., PASINELLI, P., TROTTI, D. & HAEUSLER, A. 2019. Repeat-associated non-AUG translation in C9orf72-ALS/FTD is driven by neuronal excitation and stress. *EMBO molecular medicine,* 11**,** e9423.

WHITE, M. A., KIM, E., DUFFY, A., ADALBERT, R., PHILLIPS, B. U., PETERS, O. M., STEPHENSON, J., YANG, S., MASSENZIO, F., LIN, Z., ANDREWS, S., SEGONDS-PICHON, A., METTERVILLE, J., SAKSIDA, L. M., MEAD, R., RIBCHESTER, R. R., BARHOMI, Y., SERRE, T., COLEMAN, M. P., FALLON, J. R., BUSSEY, T. J., BROWN, R. H., JR. & SREEDHARAN, J. 2018. TDP-43 gains function due to perturbed autoregulation in a Tardbp knock-in mouse model of ALS-FTD. *Nat Neurosci,* 21**,** 552-563.

WILLIAMS, K. L., FIFITA, J. A., VUCIC, S., DURNALL, J. C., KIERNAN, M. C., BLAIR, I. P. & NICHOLSON, G. A. 2013. Pathophysiological insights into ALS with C9ORF72 expansions. *J Neurol Neurosurg Psychiatry,* 84**,** 931-5.

WILMUT, I., SCHNIEKE, A. E., MCWHIR, J., KIND, A. J. & CAMPBELL, K. H. S. 1997. Viable offspring derived from fetal and adult mammalian cells. *Nature,* 385**,** 810-813.

WITZIG, V. S., KOMNIG, D. & FALKENBURGER, B. H. 2020. Changes in Striatal Medium Spiny Neuron Morphology Resulting from Dopamine Depletion Are Reversible. *Cells,* 9.

WONG, P. C., PARDO, C. A., BORCHELT, D. R., LEE, M. K., COPELAND, N. G., JENKINS, N. A., SISODIA, S. S., CLEVELAND, D. W. & PRICE, D. L. 1995. An adverse property of a familial ALS-linked SOD1 mutation causes motor neuron disease characterized by vacuolar degeneration of mitochondria. *Neuron,* 14**,** 1105-1116.

WOOLLACOTT, I. O. & ROHRER, J. D. 2016. The clinical spectrum of sporadic and familial forms of frontotemporal dementia. *J Neurochem,* 138 Suppl 1**,** 6-31.

WOOLLEY, J., GORNO-TEMPINI, M.-L., SEELEY, W., RANKIN, K., LEE, S., MATTHEWS, B. & MILLER, B. 2007a. Binge eating is associated with right orbitofrontal-insular-striatal atrophy in frontotemporal dementia. *Neurology,* 69**,** 1424-1433.

WOOLLEY, J. D., WILSON, M. R., HUNG, E., GORNO-TEMPINI, M. L., MILLER, B. L. & SHIM, J. 2007b. Frontotemporal dementia and mania. *Am J Psychiatry,* 164**,** 1811-6.

WU, L. S., CHENG, W. C., CHEN, C. Y., WU, M. C., WANG, Y. C., TSENG, Y. H., CHUANG, T. J. & SHEN, C. J. 2019. Transcriptomopathies of pre- and post-symptomatic frontotemporal dementia-like mice with TDP-43 depletion in forebrain neurons. *Acta Neuropathol Commun,* 7**,** 50.

XI, Z., RAINERO, I., RUBINO, E., PINESSI, L., BRUNI, A. C., MALETTA, R. G., NACMIAS, B., SORBI, S., GALIMBERTI, D. & SURACE, E. I. 2014a. Hypermethylation of the CpG-island near the C9orf72 G4C2-repeat expansion in FTLD patients. *Human molecular genetics,* 23**,** 5630-5637.

XI, Z., YUNUSOVA, Y., VAN BLITTERSWIJK, M., DIB, S., GHANI, M., MORENO, D., SATO, C., LIANG, Y., SINGLETON, A. & ROBERTSON, J. 2014b. Identical twins with the C9orf72 repeat expansion are discordant for ALS. *Neurology,* 83**,** 1476-1478.

XIAO, S., MCKEEVER, P. M., LAU, A. & ROBERTSON, J. 2019. Synaptic localization of C9orf72 regulates post-synaptic glutamate receptor 1 levels. *Acta Neuropathol Commun,* 7**,** 161.

XING, L., YANG, T., CUI, S. & CHEN, G. 2019. Connexin hemichannels in astrocytes: role in CNS disorders. *Frontiers in molecular neuroscience,* 12**,** 23.

XU, L., LIU, T., LIU, L., YAO, X., CHEN, L., FAN, D., ZHAN, S. & WANG, S. 2020. Global variation in prevalence and incidence of amyotrophic lateral sclerosis: a systematic review and meta-analysis. *J Neurol,* 267**,** 944-953.

XU, W. & XU, J. 2018. C9orf72 Dipeptide Repeats Cause Selective Neurodegeneration and Cell-Autonomous Excitotoxicity in Drosophila Glutamatergic Neurons. *The Journal of Neuroscience,* 38**,** 7741-7752.

XU, Z., POIDEVIN, M., LI, X., LI, Y., SHU, L., NELSON, D. L., LI, H., HALES, C. M., GEARING, M., WINGO, T. S. & JIN, P. 2013. Expanded GGGGCC repeat RNA associated with amyotrophic lateral sclerosis and frontotemporal dementia causes neurodegeneration. *Proc Natl Acad Sci U S A,* 110**,** 7778-83.

YAMANAKA, K., CHUN, S. J., BOILLEE, S., FUJIMORI-TONOU, N., YAMASHITA, H., GUTMANN, D. H., TAKAHASHI, R., MISAWA, H. & CLEVELAND, D. W. 2008. Astrocytes as

determinants of disease progression in inherited amyotrophic lateral sclerosis. *Nature Neuroscience,* 11**,** 251-253.

YAMASHITA, S., TAWARA, N., HARA, K. & UEDA, M. 2023. Gender differences in clinical features at the initial examination of late-onset amyotrophic lateral sclerosis. *Journal of the Neurological Sciences,* 451**,** 120697.

YAN, H. & WU, H. 2013. Patch Clamp Measurements On-Chip. *In:* LI, D. (ed.) *Encyclopedia of Microfluidics and Nanofluidics.* Boston, MA: Springer US.

YANG, C., WANG, H., QIAO, T., YANG, B., ALIAGA, L., QIU, L., TAN, W., SALAMEH, J., MCKENNA-YASEK, D. M., SMITH, T., PENG, L., MOORE, M. J., BROWN, R. H., JR., CAI, H. & XU, Z. 2014. Partial loss of TDP-43 function causes phenotypes of amyotrophic lateral sclerosis. *Proc Natl Acad Sci U S A,* 111**,** E1121-9.

YANG, Y., JIAO, J., GAO, R., LE, R., KOU, X., ZHAO, Y., WANG, H., GAO, S. & WANG, Y. 2015. Enhanced Rejuvenation in Induced Pluripotent Stem Cell-Derived Neurons Compared with Directly Converted Neurons from an Aged Mouse. *Stem Cells Dev,* 24**,** 2767-77.

YAZAR, V., KÜHLWEIN, J. K., KNEHR, A., GROZDANOV, V., EKICI, A. B., LUDOLPH, A. C. & DANZER, K. M. 2023. Impaired ATF3 signaling involves SNAP25 in SOD1 mutant ALS patients. *Scientific Reports,* 13**,** 12019.

YI, C., MEI, X., EZAN, P., MATO, S., MATIAS, I., GIAUME, C. & KOULAKOFF, A. 2016. Astroglial connexin43 contributes to neuronal suffering in a mouse model of Alzheimer's disease. *Cell Death Differ,* 23**,** 1691-701.

YOUNG, P. E., KUM JEW, S., BUCKLAND, M. E., PAMPHLETT, R. & SUTER, C. M. 2017. Epigenetic differences between monozygotic twins discordant for amyotrophic lateral sclerosis (ALS) provide clues to disease pathogenesis. *PLoS One,* 12**,** e0182638.

ZACCO, E., KANTELBERG, O., MILANETTI, E., ARMAOS, A., PANEI, F. P., GREGORY, J., JEACOCK, K., CLARKE, D. J., CHANDRAN, S., RUOCCO, G., GUSTINCICH, S., HORROCKS, M. H., PASTORE, A. & TARTAGLIA, G. G. 2022. Probing TDP-43 condensation using an in silico designed aptamer. *Nature Communications,* 13**,** 3306.

ZAGO, S., LORUSSO, L., AIELLO, E. N., UGOLINI, M., POLETTI, B., TICOZZI, N. & SILANI, V. 2022. Cognitive and behavioral involvement in ALS has been known for more than a century. *Neurological Sciences,* 43**,** 6741-6760.

ZANG, D. W. & CHEEMA, S. 2002. Degeneration of corticospinal and bulbospinal systems in the superoxide dismutase 1G93A G1H transgenic mouse model of familial amyotrophic lateral sclerosis. *Neuroscience letters,* 332**,** 99-102.

ZHANG, J., RIQUELME, M. A., HUA, R., ACOSTA, F. M., GU, S. & JIANG, J. X. 2022a. Connexin 43 hemichannels regulate mitochondrial ATP generation, mobilization, and mitochondrial homeostasis against oxidative stress. *eLife,* 11**,** e82206.

ZHANG, K., DONNELLY, C. J., HAEUSLER, A. R., GRIMA, J. C., MACHAMER, J. B., STEINWALD, P., DALEY, E. L., MILLER, S. J., CUNNINGHAM, K. M., VIDENSKY, S., GUPTA, S., THOMAS, M. A., HONG, I., CHIU, S.-L., HUGANIR, R. L., OSTROW, L. W., MATUNIS, M. J., WANG, J., SATTLER, R., LLOYD, T. E. & ROTHSTEIN, J. D. 2015. The C9orf72 repeat expansion disrupts nucleocytoplasmic transport. *Nature,* 525**,** 56-61.

ZHANG, M., XI, Z., GHANI, M., JIA, P., PAL, M., WERYNSKA, K., MORENO, D., SATO, C., LIANG, Y. & ROBERTSON, J. 2016a. Genetic and epigenetic study of ALS-discordant identical twins with double mutations in SOD1 and ARHGEF28. *Journal of Neurology, Neurosurgery & Psychiatry,* 87**,** 1268-1270.

ZHANG, M., XI, Z., SAEZ-ATIENZAR, S., CHIA, R., MORENO, D., SATO, C., MONTAZER HAGHIGHI, M., TRAYNOR, B. J., ZINMAN, L. & ROGAEVA, E. 2021. Combined epigenetic/genetic study identified an ALS age of onset modifier. *Acta Neuropathologica Communications,* 9**,** 75.

ZHANG, S., COOPER-KNOCK, J., WEIMER, A. K., SHI, M., MOLL, T., MARSHALL, J. N. G., HARVEY, C., NEZHAD, H. G., FRANKLIN, J., SOUZA, C. D. S., NING, K., WANG, C., LI, J., DILLIOTT, A. A., FARHAN, S., ELHAIK, E., PASNICEANU, I., LIVESEY, M. R., EITAN, C., HORNSTEIN, E., KENNA, K. P., BLAIR, I., WRAY, N. R., KIERNAN, M., MITNE NETO, M., CHIO, A., CAUCHI, R., ROBBERECHT, W., VAN DAMME, P., CORCIA, P., COURATIER, P., HARDIMAN, O., MCLAUGHIN, R., GOTKINE, M., DRORY, V., TICOZZI, N., SILANI, V., VELDINK, J. H., VAN DEN BERG, L. H., DE CARVALHO, M., MORA PARDINA, J. S., POVEDANO, M., ANDERSEN, P., WEBER, M., BAŞAK, N. A., AL-CHALABI, A., SHAW, C., SHAW, P. J., MORRISON, K. E., LANDERS, J. E., GLASS, J. D., VELDINK, J. H., FERRAIUOLO, L., SHAW, P. J. & SNYDER, M. P. 2022b. Genome-wide identification of the genetic basis of amyotrophic lateral sclerosis. *Neuron,* 110**,** 992-1008.e11.

ZHANG, W., ZHANG, L., LIANG, B., SCHROEDER, D., ZHANG, Z. W., COX, G. A., LI, Y. & LIN, D. T. 2016b. Hyperactive somatostatin interneurons contribute to excitotoxicity in neurodegenerative disorders. *Nat Neurosci,* 19**,** 557-559.

ZHANG, Y.-J., GENDRON, T. F., EBBERT, M. T. W., O'RAW, A. D., YUE, M., JANSEN-WEST, K., ZHANG, X., PRUDENCIO, M., CHEW, J., COOK, C. N., DAUGHRITY, L. M., TONG, J., SONG, Y., PICKLES, S. R., CASTANEDES-CASEY, M., KURTI, A., RADEMAKERS, R., OSKARSSON, B., DICKSON, D. W., HU, W., GITLER, A. D., FRYER, J. D. & PETRUCELLI, L. 2018. Poly(GR) impairs protein translation and stress granule dynamics in C9orf72-associated frontotemporal dementia and amyotrophic lateral sclerosis. *Nature Medicine,* 24**,** 1136-1142.

ZHANG, Z., ALMEIDA, S., LU, Y., NISHIMURA, A. L., PENG, L., SUN, D., WU, B., KARYDAS, A. M., TARTAGLIA, M. C. & FONG, J. C. 2013. Downregulation of microRNA-9 in iPSC-derived neurons of FTD/ALS patients with TDP-43 mutations. *PloS one,* 8**,** e76055.

ZHAO, C., DEVLIN, A. C., CHOUHAN, A. K., SELVARAJ, B. T., STAVROU, M., BURR, K., BRIVIO, V., HE, X., MEHTA, A. R., STORY, D., SHAW, C. E., DANDO, O., HARDINGHAM, G. E., MILES, G. B. & CHANDRAN, S. 2020. Mutant C9orf72 human iPSC-derived astrocytes cause non-cell autonomous motor neuron pathophysiology. *Glia,* 68**,** 1046-1064.

ZHAO, J., WANG, X., HUO, Z., CHEN, Y., LIU, J., ZHAO, Z., MENG, F., SU, Q., BAO, W., ZHANG, L., WEN, S., WANG, X., LIU, H. & ZHOU, S. 2022a. The Impact of Mitochondrial Dysfunction in Amyotrophic Lateral Sclerosis. *Cells,* 11.

ZHAO, X. & MOORE, D. L. 2018. Neural stem cells: developmental mechanisms and disease modeling. *Cell and Tissue Research,* 371**,** 1-6.

ZHAO, Z.-D., HAN, X., CHEN, R., LIU, Y., BHATTACHERJEE, A., CHEN, W. & ZHANG, Y. 2022b. A molecularly defined D1 medium spiny neuron subtype negatively regulates cocaine addiction. *Science Advances,* 8**,** eabn3552.

ZHOU, M., DU, Y., ATEN, S. & TERMAN, D. 2021a. On the electrical passivity of astrocyte potassium conductance. *Journal of Neurophysiology,* 126**,** 1403-1419.

ZHOU, M., DU, Y., ATEN, S. & TERMAN, D. 2021b. On the electrical passivity of astrocyte potassium conductance. *J Neurophysiol,* 126**,** 1403-1419.

ZHOU, M., SCHOOLS, G. P. & KIMELBERG, H. K. 2006. Development of GLAST (+) astrocytes and NG2 (+) glia in rat hippocampus CA1: mature astrocytes are electrophysiologically passive. *Journal of neurophysiology,* 95**,** 134-143.

ZHOU, M., XU, G., XIE, M., ZHANG, X., SCHOOLS, G. P., MA, L., KIMELBERG, H. K. & CHEN, H. 2009. TWIK-1 and TREK-1 are potassium channels contributing significantly to astrocyte passive conductance in rat hippocampal slices. *J Neurosci,* 29**,** 8551-64.

ZHOU, Y. & DANBOLT, N. C. 2013. GABA and Glutamate Transporters in Brain. *Front Endocrinol (Lausanne),* 4**,** 165.

ZHU, L., LI, S., LI, X. J. & YIN, P. 2023. Pathological insights from amyotrophic lateral sclerosis animal models: comparisons, limitations, and challenges. *Transl Neurodegener,* 12**,** 46.

ZOCCOLELLA, S., BEGHI, E., PALAGANO, G., FRADDOSIO, A., GUERRA, V., SAMARELLI, V., LEPORE, V., SIMONE, I. L., LAMBERTI, P., SERLENGA, L. & LOGROSCINO, G. 2007. Riluzole and amyotrophic lateral sclerosis survival: a population-based study in southern Italy. *Eur J Neurol,* 14**,** 262-8.

ZONG, L., ZHU, Y., LIANG, R. & ZHAO, H. B. 2016. Gap junction mediated miRNA intercellular transfer and gene regulation: A novel mechanism for intercellular genetic communication. *Sci Rep,* 6**,** 19884.

ZU, T., LIU, Y., BAÑEZ-CORONEL, M., REID, T., PLETNIKOVA, O., LEWIS, J., MILLER, T. M., HARMS, M. B., FALCHOOK, A. E., SUBRAMONY, S. H., OSTROW, L. W., ROTHSTEIN, J. D., TRONCOSO, J. C. & RANUM, L. P. 2013. RAN proteins and RNA foci from antisense transcripts in C9ORF72 ALS and frontotemporal dementia. *Proc Natl Acad Sci U S A,* 110**,** E4968-77.

8. Appendix

Con-1 SIDAK'S MULTIPLE COMPARISON TEST

	Significance?	Summary	Adjusted P Value
0 pA current injection			
DAY 20 vs. DAY 40	No	ns	>0.9999
DAY 20 vs. DAY 60	No	ns	>0.9999
DAY 40 vs. DAY 60	No	ns	>0.9999
5 pA current injection			
DAY 20 vs. DAY 40	No	ns	0.9942
DAY 20 vs. DAY 60	No	ns	>0.9999
DAY 40 vs. DAY 60	No	ns	0.9956
10 pA current injection			
DAY 20 vs. DAY 40	Yes	**	0.0031
DAY 20 vs. DAY 60	Yes	***	0.0003
DAY 40 vs. DAY 60	No	ns	0.69
15 pA current injection			
DAY 20 vs. DAY 40	Yes	**	0.0057
DAY 20 vs. DAY 60	No	ns	0.9699
DAY 40 vs. DAY 60	Yes	*	0.0383
20 pA current injection			
DAY 20 vs. DAY 40	Yes	***	0.0006
DAY 20 vs. DAY 60	Yes	**	0.0011
DAY 40 vs. DAY 60	Yes	****	<0.0001
25 pA current injection			
DAY 20 vs. DAY 40	No	ns	0.4993
DAY 20 vs. DAY 60	Yes	****	<0.0001
DAY 40 vs. DAY 60	Yes	****	<0.0001
30 pA current injection			
DAY 20 vs. DAY 40	Yes	****	<0.0001
DAY 20 vs. DAY 60	Yes	****	<0.0001
DAY 40 vs. DAY 60	Yes	****	<0.0001
35 pA current injection			
DAY 20 vs. DAY 40	Yes	**	0.0012
DAY 20 vs. DAY 60	Yes	****	<0.0001
DAY 40 vs. DAY 60	Yes	****	<0.0001
40 pA current injection			
DAY 20 vs. DAY 40	Yes	****	<0.0001
DAY 20 vs. DAY 60	Yes	****	<0.0001
DAY 40 vs. DAY 60	Yes	*	0.0306
45 pA current injection			
DAY 20 vs. DAY 40	Yes	****	<0.0001
DAY 20 vs. DAY 60	Yes	****	<0.0001
DAY 40 vs. DAY 60	No	ns	0.5362
50 pA current injection			
DAY 20 vs. DAY 40	Yes	****	<0.0001
DAY 20 vs. DAY 60	Yes	****	<0.0001
DAY 40 vs. DAY 60	No	ns	0.6599

C9-1 SIDAK'S MULTIPLE COMPARISON TEST

	Significance?	Summary	Adjusted P Value
0 pA current injection			
DAY 20 vs. DAY 40	No	ns	>0.9999
DAY 20 vs. DAY 60	No	ns	>0.9999
DAY 40 vs. DAY 60	No	ns	>0.9999
5 pA current injection			
DAY 20 vs. DAY 40	No	ns	>0.9999
DAY 20 vs. DAY 60	No	ns	>0.9999
DAY 40 vs. DAY 60	No	ns	>0.9999
10 pA current injection			
DAY 20 vs. DAY 40	No	ns	0.1594
DAY 20 vs. DAY 60	No	ns	0.9499
DAY 40 vs. DAY 60	Yes	**	0.0015
15 pA current injection			
DAY 20 vs. DAY 40	Yes	****	<0.0001
DAY 20 vs. DAY 60	No	ns	0.9998
DAY 40 vs. DAY 60	Yes	****	<0.0001
20 pA current injection			
DAY 20 vs. DAY 40	No	ns	0.5821
DAY 20 vs. DAY 60	Yes	*	0.0368
DAY 40 vs. DAY 60	Yes	****	<0.0001
25 pA current injection			
DAY 20 vs. DAY 40	No	ns	>0.9999
DAY 20 vs. DAY 60	Yes	****	<0.0001
DAY 40 vs. DAY 60	Yes	****	<0.0001
30 pA current injection			
DAY 20 vs. DAY 40	No	ns	0.76
DAY 20 vs. DAY 60	Yes	****	<0.0001
DAY 40 vs. DAY 60	Yes	****	<0.0001
35 pA current injection			
DAY 20 vs. DAY 40	Yes	****	<0.0001
DAY 20 vs. DAY 60	Yes	****	<0.0001
DAY 40 vs. DAY 60	No	ns	0.2151
40 pA current injection			
DAY 20 vs. DAY 40	Yes	*	0.0238
DAY 20 vs. DAY 60	Yes	****	<0.0001
DAY 40 vs. DAY 60	Yes	*	0.0441
45 pA current injection			
DAY 20 vs. DAY 40	Yes	****	<0.0001
DAY 20 vs. DAY 60	Yes	****	<0.0001
DAY 40 vs. DAY 60	Yes	**	0.0041
50 pA current injection			
DAY 20 vs. DAY 40	Yes	***	0.0002
DAY 20 vs. DAY 60	Yes	****	<0.0001
DAY 40 vs. DAY 60	Yes	****	<0.0001

C9-Δ1 SIDAK'S MULTIPLE COMPARISON TEST

	Significance?	Summary	Adjusted P Value
0 pA current injection			
DAY 20 vs. DAY 40	No	ns	>0.9999
DAY 20 vs. DAY 60	No	ns	>0.9999
DAY 40 vs. DAY 60	No	ns	>0.9999
5 pA current injection			
DAY 20 vs. DAY 40	No	ns	0.993
DAY 20 vs. DAY 60	No	ns	0.995
DAY 40 vs. DAY 60	No	ns	>0.9999
10 pA current injection			
DAY 20 vs. DAY 40	Yes	****	<0.0001
DAY 20 vs. DAY 60	Yes	****	<0.0001
DAY 40 vs. DAY 60	No	ns	0.9686
15 pA current injection			
DAY 20 vs. DAY 40	Yes	****	<0.0001
DAY 20 vs. DAY 60	Yes	*	0.0132
DAY 40 vs. DAY 60	No	ns	0.1447
20 pA current injection			
DAY 20 vs. DAY 40	Yes	***	0.0008
DAY 20 vs. DAY 60	No	ns	0.6414
DAY 40 vs. DAY 60	Yes	****	<0.0001
25 pA current injection			
DAY 20 vs. DAY 40	No	ns	0.3269
DAY 20 vs. DAY 60	Yes	****	<0.0001
DAY 40 vs. DAY 60	Yes	*	0.0227
30 pA current injection			
DAY 20 vs. DAY 40	No	ns	0.0958
DAY 20 vs. DAY 60	Yes	***	0.0008
DAY 40 vs. DAY 60	No	ns	0.2375
35 pA current injection			
DAY 20 vs. DAY 40	Yes	****	<0.0001
DAY 20 vs. DAY 60	Yes	***	0.0003
DAY 40 vs. DAY 60	No	ns	0.3703
40 pA current injection			
DAY 20 vs. DAY 40	Yes	****	<0.0001
DAY 20 vs. DAY 60	Yes	***	0.0004
DAY 40 vs. DAY 60	No	ns	0.999
45 pA current injection			
DAY 20 vs. DAY 40	Yes	****	<0.0001
DAY 20 vs. DAY 60	Yes	****	<0.0001
DAY 40 vs. DAY 60	No	ns	0.2109
50 pA current injection			
DAY 20 vs. DAY 40	Yes	****	<0.0001
DAY 20 vs. DAY 60	Yes	****	<0.0001
DAY 40 vs. DAY 60	No	ns	0.1505

Appendix 1. ***Sidak's multiple comparison test.*** *Following Two-way ANOVA, Sidak's multiple comparison test was employed to evaluate statistical significance observed across time points within each cell line (left, Con-1; middle, C9-1; right, C9-Δ1) at the different current injection steps employed in the protocol. The tables highlight statistical significance and adjusted p-value.*

SIDAK'S MULTIPLE COMPARISON TEST

	Significance?	Summary	Adjusted P Value
0 pA current injection			
Con-1 vs. Con-2	No	ns	>0.9999
Con-1 vs. C9-1	No	ns	>0.9999
Con-1 vs. C9-2	No	ns	>0.9999
Con-1 vs. C9-3	No	ns	>0.9999
Con-2 vs. C9-1	No	ns	>0.9999
Con-2 vs. C9-2	No	ns	>0.9999
Con-2 vs. C9-3	No	ns	>0.9999
C9-1 vs. C9-2	No	ns	>0.9999
C9-1 vs. C9-3	No	ns	>0.9999
C9-2 vs. C9-3	No	ns	>0.9999
5 pA current injection			
Con-1 vs. Con-2	No	ns	0.9972
Con-1 vs. C9-1	No	ns	>0.9999
Con-1 vs. C9-2	No	ns	>0.9999
Con-1 vs. C9-3	No	ns	>0.9999
Con-2 vs. C9-1	No	ns	>0.9999
Con-2 vs. C9-2	No	ns	0.9956
Con-2 vs. C9-3	No	ns	0.9956
C9-1 vs. C9-2	No	ns	>0.9999
C9-1 vs. C9-3	No	ns	>0.9999
C9-2 vs. C9-3	No	ns	>0.9999
10 pA current injection			
Con-1 vs. Con-2	No	ns	0.9359
Con-1 vs. C9-1	No	ns	>0.9999
Con-1 vs. C9-2	No	ns	0.9466
Con-1 vs. C9-3	No	ns	0.9997
Con-2 vs. C9-1	No	ns	0.9936
Con-2 vs. C9-2	No	ns	0.183
Con-2 vs. C9-3	No	ns	0.5212
C9-1 vs. C9-2	No	ns	0.4534
C9-1 vs. C9-3	No	ns	0.9074
C9-2 vs. C9-3	No	ns	0.9997
15 pA current injection			
Con-1 vs. Con-2	No	ns	>0.9999
Con-1 vs. C9-1	Yes	****	<0.0001
Con-1 vs. C9-2	Yes	****	<0.0001
Con-1 vs. C9-3	Yes	****	<0.0001
Con-2 vs. C9-1	Yes	****	<0.0001
Con-2 vs. C9-2	Yes	****	<0.0001
Con-2 vs. C9-3	Yes	****	<0.0001
C9-1 vs. C9-2	No	ns	>0.9999
C9-1 vs. C9-3	No	ns	0.9994
C9-2 vs. C9-3	No	ns	0.9997
20 pA current injection			
Con-1 vs. Con-2	No	ns	0.9033
Con-1 vs. C9-1	Yes	****	<0.0001
Con-1 vs. C9-2	Yes	****	<0.0001
Con-1 vs. C9-3	Yes	****	<0.0001
Con-2 vs. C9-1	Yes	****	<0.0001
Con-2 vs. C9-2	Yes	****	<0.0001
Con-2 vs. C9-3	Yes	****	<0.0001
C9-1 vs. C9-2	No	ns	0.3887
C9-1 vs. C9-3	No	ns	0.5474
C9-2 vs. C9-3	No	ns	>0.9999
25 pA current injection			
Con-1 vs. Con-2	No	ns	0.9769
Con-1 vs. C9-1	Yes	****	<0.0001
Con-1 vs. C9-2	Yes	****	<0.0001
Con-1 vs. C9-3	Yes	****	<0.0001
Con-2 vs. C9-1	Yes	****	<0.0001
Con-2 vs. C9-2	Yes	****	<0.0001
Con-2 vs. C9-3	Yes	****	<0.0001
C9-1 vs. C9-2	No	ns	0.8572
C9-1 vs. C9-3	Yes	*	0.0153
C9-2 vs. C9-3	No	ns	0.5229

	Significance?	Summary	Adjusted P Va
30 pA current injection			
Con-1 vs. Con-2	No	ns	0.6044
Con-1 vs. C9-1	Yes	****	<0.0001
Con-1 vs. C9-2	Yes	****	<0.0001
Con-1 vs. C9-3	Yes	****	<0.0001
Con-2 vs. C9-1	Yes	****	<0.0001
Con-2 vs. C9-2	Yes	****	<0.0001
Con-2 vs. C9-3	Yes	****	<0.0001
C9-1 vs. C9-2	Yes	**	0.0017
C9-1 vs. C9-3	Yes	****	<0.0001
C9-2 vs. C9-3	Yes	**	0.003
35 pA current injection			
Con-1 vs. Con-2	No	ns	>0.9999
Con-1 vs. C9-1	Yes	****	<0.0001
Con-1 vs. C9-2	Yes	****	<0.0001
Con-1 vs. C9-3	Yes	****	<0.0001
Con-2 vs. C9-1	Yes	****	<0.0001
Con-2 vs. C9-2	Yes	****	<0.0001
Con-2 vs. C9-3	Yes	****	<0.0001
C9-1 vs. C9-2	Yes	****	<0.0001
C9-1 vs. C9-3	Yes	****	<0.0001
C9-2 vs. C9-3	Yes	*	0.0469
40 pA current injection			
Con-1 vs. Con-2	No	ns	0.9969
Con-1 vs. C9-1	Yes	****	<0.0001
Con-1 vs. C9-2	Yes	****	<0.0001
Con-1 vs. C9-3	Yes	****	<0.0001
Con-2 vs. C9-1	Yes	****	<0.0001
Con-2 vs. C9-2	Yes	****	<0.0001
Con-2 vs. C9-3	Yes	****	<0.0001
C9-1 vs. C9-2	Yes	*	0.0171
C9-1 vs. C9-3	Yes	****	<0.0001
C9-2 vs. C9-3	Yes	****	<0.0001
45 pA current injection			
Con-1 vs. Con-2	Yes	**	0.0011
Con-1 vs. C9-1	Yes	****	<0.0001
Con-1 vs. C9-2	Yes	****	<0.0001
Con-1 vs. C9-3	Yes	****	<0.0001
Con-2 vs. C9-1	Yes	****	<0.0001
Con-2 vs. C9-2	Yes	****	<0.0001
Con-2 vs. C9-3	Yes	****	<0.0001
C9-1 vs. C9-2	Yes	****	<0.0001
C9-1 vs. C9-3	Yes	****	<0.0001
C9-2 vs. C9-3	Yes	****	<0.0001
0 pA current injection			
Con-1 vs. Con-2	No	ns	0.4802
Con-1 vs. C9-1	Yes	****	<0.0001
Con-1 vs. C9-2	Yes	****	<0.0001
Con-1 vs. C9-3	Yes	****	<0.0001
Con-2 vs. C9-1	Yes	****	<0.0001
Con-2 vs. C9-2	Yes	****	<0.0001
Con-2 vs. C9-3	Yes	****	<0.0001
C9-1 vs. C9-2	Yes	****	<0.0001
C9-1 vs. C9-3	Yes	****	<0.0001
C9-2 vs. C9-3	Yes	****	<0.0001

Appendix 2. ***Sidak's multiple comparison test at day 60.*** *Following Two-way ANOVA, Sidak's multiple comparison test was employed to evaluate pairwise differences between cell lines (Con-1, Con-2, C9-1, C9-2, C9-3) at each current injection step at day 60. The table highlights statistical significance and p-values.*

C9-1 vs. C9-Δ1 SIDAK'S MULTIPLE COMPARISON TEST

	Significance?	Summary	Adjusted P Value
0 pA current injection	No	ns	>0.9999
5 pA current injection	No	ns	0.9998
10 pA current injection	No	ns	0.2025
15 pA current injection	Yes	****	<0.0001
20 pA current injection	Yes	****	<0.0001
25 pA current injection	Yes	****	<0.0001
30 pA current injection	Yes	****	<0.0001
35 pA current injection	Yes	****	<0.0001
40 pA current injection	Yes	****	<0.0001
45 pA current injection	Yes	****	<0.0001
50 pA current injection	Yes	****	<0.0001

Appendix 3. ***Sidak's multiple comparison test at day 60.*** *Following Two-way ANOVA, Sidak's multiple comparison test was employed to evaluate pairwise differences between C9-1 and C9-Δ1 at each current injection step at day 60. The table highlights statistical significance and p-values.*